AD NUMBER

AD351207

CLASSIFICATION CHANGES

TO: unclassified

FROM: confidential

LIMITATION CHANGES

TO:

Approved for public release, distribution unlimited

FROM:

Distribution authorized to U.S. Gov't. agencies and their contractors; Specific Authority; Feb 64. Other requests shall be referred to Air Force Aero Propulsion Lab., Research and Technology Div., Wright-Patterson AFB, OH 45433.

AUTHORITY

DoDD 5200.10; February 1976 IAW Document Markings.; AFWAL ltr., dtd June 9, 1976.

ASD-TDR-63-665, Part II

UNCLASSIFIED

(Unclassified Title)

FEASIBILITY STUDY OF A HIGH CAPACITY DISTILLATION SEPARATOR FOR AN AIR ENRICHMENT SYSTEM

(Design and Fabrication of Boilerplate Air Separator)

TECHNICAL DOCUMENTARY REPORT ASD-TDR-63-665

February, 1964

AIR FORCE AERO PROPULSION LABORATORY
Research and Technology Division
Air Force Systems Command
Wright-Patterson Air Force Base, Ohio

PROJECT NO. 3084, TASK NO. 308403

(Prepared under Contract No. AF 33(657)-8722
by Union Carbide Corporation, Linde Division
Cryogenic Development Laboratory, Tonawanda
New York)

UNCLASSIFIED

[redacted]

NOTICES

When Government drawings, specifications, or other data are used for any purpose other than in connection with a definitely related Government procurement operation, the United States Government thereby incurs no responsibility nor any obligation whatsoever; and the fact that the Government may have formulated, furnished, or in any way supplied the said drawings, specifications, or other data, is not to be regarded by implication or otherwise as in any manner licensing the holder or any other person or corporation, or conveying any rights or permission to manufacture, use, or sell any patented invention that may in any way be related thereto.

This document contains information affecting the National defense of the United States within the meaning of the Espionage Laws, Title 18, U.S.C., Sections 793 and 794. Its transmission or the revelation of its contents in any manner to an unauthorized person is prohibited by law.

Qualified requesters may obtain copies of this report from the Defense Documentation Center (DDC), (formerly ASTIA), Cameron Station, 5010 Duke Street, Alexandria, Virginia, 22314.

Copies of this report should not be returned to the Research and Technology Division unless return is required by security considerations, contractual obligations, or notice on a specific document.

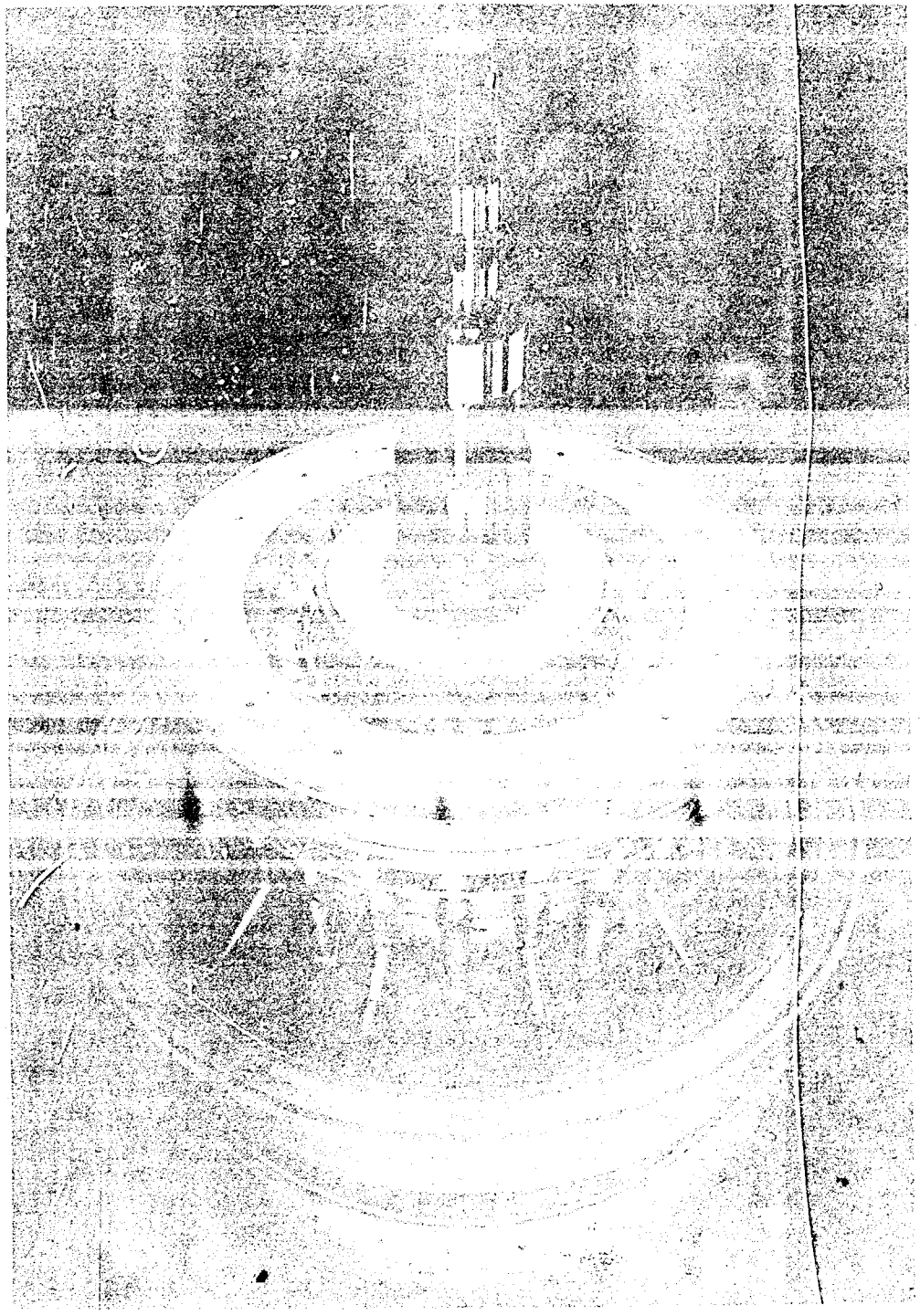

FOREWORD

This report was prepared by Union Carbide Corporation, Linde Division, under USAF Contract No. AF 33(657)-8722. This contract was initiated under Project No. 3084, Task No. 308403. The contract was administered under the direction of the Air Force Aero Propulsion Laboratory, Research and Technology Division with Mr. C. M. Donaldson acting as Project Engineer.

Special acknowledgement is made to Messrs. O. F. Allen; F. W. Bonnet; S. L. Fisher; R. J. Frainier, Project Manager; C. F. Gottzmann; M. O. Johnson; C. J. Linneball; L. C. Matsch; M. Noland; J. Notaro; J. W. Sechler and W. L. Townsend of Union Carbide Corporation, Linde Division for their significant contribution in support of this program.

The associate contractor, General Dynamics/Astronautics, is acknowledged for providing the vehicle oriented information necessary for the performance of this contract.

This report is Part II of a two-part final report and describes design and fabrication phases performed from May 1, 1962 to March 1, 1964.

This report, excluding title, is classified "CONFIDENTIAL" because it contains information on design and performance of components for potential future aerospace systems.

ABSTRACT

Past work conducted under Contracts AF 33(616)-7509 and AF 33(616)-7646 indicated the attractive potential of rotating distillation air separators for future airborne air collection and enrichment systems. Studies made under Contract AF 33(657)-8722 and reported in Part I of this document refined previous concepts on mass transfer, heat transfer, and mechanical areas to the point where general design, weight and volume of future airborne units could be predicted with reasonable confidence and where detailed design of a boilerplate air separator could be undertaken. This report covers design and fabrication of a boilerplate separator completed under Contract AF 33(657)-8722. The major mission of this unit is to demonstrate functional feasibility of the rotary distillation separator concept.

The boilerplate air separator was designed to accept 100 lbs. of saturated air vapor at pressures up to 250 psia and separate this vapor into product oxygen liquid of approximately 90% purity and waste nitrogen vapor of about 98% purity. The unit is representative of future airborne units in radial dimensions and general arrangement of components. It utilizes the double column cycle, the major components of which are a high pressure column, a low pressure column, and a reboiler-condenser. The columns are arranged side by side on a common shaft with the reboiler-condenser located inside the high pressure column. This arrangement was proven to be the optimum since it minimizes fluid transfer problems and promises minimum weight.

The boilerplate unit contains 18 actual trays in the low pressure column and 9 trays in the high pressure column. Predicted tray efficiencies range from 64 to 99%. Predicted average heat flux in the reboiler-condenser is 29,200 Btu/hr.ft.^{2} at a design temperature difference of 10.7°R.

Mechanical construction of the boilerplate separators features a modular approach in that major components as well as individual trays and heat transfer disks can be removed from the unit.

Maximum diameter of the boilerplate rotor is 106 in. and length between bearing supports is 105 in. Design speed is 60 rad./sec. (570 rev./min.).

TABLE OF CONTENTS

TABLE OF CONTENTS (Continued)

TABLE OF CONTENTS (Continued)

(THIS PAGE IS INTENTIONALLY BLANK.)

LIST OF APPENDIXES

(THIS PAGE IS INTENTIONALLY BLANK.)

LIST OF FIGURES

LIST OF FIGURES

LIST OF FIGURES

LIST OF FIGURES

LIST OF TABLES

(THIS PAGE IS INTENTIONALLY BLANK.)

NOMENCLATURE

a	=	Acceleration, Ft./hr.^{2}
A	=	Area, ft.^{2}
Aavg	=	Average total column flow area, ft.^{2}
A_b	=	Boiling side heat transfer area, ft.^{2}
A_B	=	Bellows area for control valve, ft.^{2}
A_c	=	Condensing Side Heat Transfer Area, ft.^{2}
A_{CAS}	=	Surface area of casing, ft.^{2}
A_i	=	Inner total column flow area, ft.^{2}
A_o	=	Outer total column flow area, ft.^{2}
As	=	Active tray area, ft.^{2}
A_t	=	Diffusers throat area (in.^{2})
Ae/At	=	Ratio of diffuser exit area to throat area, dimensionless
A/V	=	Interfacial mass transfer area created per unit volume, ft.$^{-1}$
b	=	Width of tray or weir, ft.
bavg	=	Average column width, in.
b_{dc}	=	Downcomer width (in.)
b_{dt}	=	Wdith diffuser throat (in.)
b_i	=	Column inner width, in.
$b_{i_{LPC}}$	=	Inner width of low pressure column, in.
b_k	=	Width of kettle holdup chamber, ft.
b_o	=	Column outer width, in.

$b_{o_{HPC}}$ = Outer width of high pressure column, in.

$b_{o_{LPC}}$ = Outer width of low pressure column, in.

b_s = Width of kettle separator, in., or width shaft seal (in.)

b_{st} = Width of edge strip on tray (in.)

C, c = Constants, dimensionless

C_2 = Coefficient in Chezy equation and expressed by the Manning Equation, $(lb._m\text{-ft.}/lb._s\text{-sec.})^{1/2}$

$C_3, C_4, C_5, C_6, C_7, C_8, C_9$ = Constants

C_1^o = Constant multiplying factor in equation for calculation of foam height, dimensionless

C_2^o = Constant multiplying factor in equation for calculation of the number of gas phase mass transfer units $(NTU)_g$, dimensionless

C_3^o = Constant multiplying factor in equation for calculation of the number of liquid phase mass transfer units $(NUT)_L$, dimensionless

C_g = Gasket loading constant lb./in.

C_s = Peripheral seal clearance space (in.)

C_{sp} = Specific capacity of bearing or the capacity in lbs. for a life of a million cycles

C_v = Orifice coefficient, dimensionless

C_x = Constant equal to 0.9 and used in equation for calculation of tray frictional pressure drop, eliminating the iteration on foam density, dimensionless

C_Y = Ratio of dry plate pressure drop to hydrostatic pressure drop, dimensionless

d = Diffuser throat diameter, ft.

D_o^1	=	Outer diameter (in.)
D	=	Pipe diameter, ft.
D_{bb}	=	Bearing ball diameter (in.)
D_{bi}	=	Bearing inner contact diameter
D_{bo}	=	Bearing outer contact diameter
dF	=	Differential force, $lb._f$
Dg	=	Gas phase diffusion coefficient, $ft.^2/sec.$
D_L	=	Liquid phase diffusion coefficient, $ft.^2/sec.$
D_m	=	Mean diameter of ball element of ball bearing (in.)
dm	=	Differential element of mass, lbs.
Do	=	Perforation diameter, ft.
Dsi	=	Shaft inner diameter, in.
Dso	=	Shaft outer diameter, in.
D_t	=	Tray diameter
d_t	=	Inside diameter of reboiler-condenser tube, in.
e	=	Natural Logarithm Base, or control system error signal, dimensionless, ft.
E	=	Point efficiency, dimensionless
E^o	=	Tray efficiency after enchancement, dimensionless
E_j	=	Joint efficiency dimensionless
Emv	=	Murphree point efficiency, dimensionless
E_y	=	Youngs modulus psi
f	=	Free area fraction of the tray, dimensionless
fa	=	Active area fraction of tray (dimensionless)

F_b	=	Bearing load - (lbs.)
F_c	=	Static component of force, casing wgt. (lb.)
f_f	=	Friction coefficient (dimensionless)
F_{cs}	=	Circumferential static force (lb./in.)
F_{equ}	=	Equivalent force (lb.)
F_n	=	Normal force (lb.)
f_p	=	Pipe friction factor
F_s	=	Shear force (lb./in.)
F_t	=	Axial tension (lb./in.)
F_u	=	Unbalance force (lb.)
g	=	Normal acceleration of gravity, ft./sec.^{2}
G	=	Molar gas rate, moles/sec.
G_l	=	Mass velocity, lb./ft.^{2}sec.
g_c	=	Newton's conversion factor, $lb._m$-ft./$lb._f$-sec.^{2}
G_D	=	Diffuser fluid flow rate, gal./min.
G_L	=	Seal leakage flow rate, lbs./sec., or liquid flow in two phase tester, lbs./sec.
G_s	=	Shear modulus (psi)
G_T	=	Total exiting flow from periphery, lbs./sec.
h	=	Column shell thickness, in., or heat transfer coefficient Btu/hr.ft.^{2} °R
H,H'	=	Disengagement space or spray height, ft., in.
H_1	=	Distance between inner radius of high pressure column and inner radius of foam on first tray, in.

h_b	=	Boiling side film coefficient, Btu/ft.^{2}hr. °R
h_c, h_c	=	Crest Height, ft., in.
hc_1	=	Condensing side film coefficient, Btu/ft.^{2}hr. °R
$(h_c)_{EXP}$	=	Experimental condensing side film coefficient, Btu/ft.^{2}hr. °R
h_{CM}	=	Calculated condensing side film coefficient for full scale unit, But/ft.^{2}hr. °R
$(h_c)_{THEO}$	=	Theoretical condensing side film coefficient, Btu/ft.^{2}hr. °R
h_{dt}	=	Depth diffuser throat (in.)
h_f, h_f'	=	Foam height, ft., in.
h_{feed}	=	Enthalpy of separator feed, Btu/lb.-mole
h_k	=	Kettle separator shell thickness, in.
h_{K_1}	=	Enthalpy of kettle liquid leaving high pressure column, Btu/lb.-mole
$h_L^o, h_1^{o'}$	=	Constant liquid holdup at kettle periphery of high pressure column, ft., or peripheral column liquid holdup, in.
H_L	=	Liquid enthalpy, Btu/lb.-mole
h_{LC}	=	Enthalpy of high pressure liquid stream leaving reboiler-condenser, Btu/lb.-mole
h_{LK}	=	Kettle separator liquid holdup, in.
$h_L^{(t)}$	=	Liquid level in column as a function of time, ft.
HP_B	=	Bearing friction horsepower loss, hp
HP_F	=	Total fluid acceleration horsepower required, hp
HP_{REQ}	=	Total air separator horsepower requirement, hp

HP_S = Seal fluid horsepower loss, hp

HP_W = Windage horsepower loss, hp

h_{SEAL} = Difference between inner radius of seal fluid and inner radius of column peripheral liquid, ft.

h_{tL} = Liquid holdup at kettle periphery of high pressure column as a time function, ft., or peripheral column liquid holdup, in.

H_v = Vapor enthalpy, Btu/lb.-mole

$h_{v_{RBC}}$ = Enthalpy of high pressure vapor stream entering reboiler-condenser, Btu/lb.-mole

i = Index on evaluation of functions in computer programs, dimensionless

I = Moment of inertia ($in.^4$)

J = Index on evaluation of functions in computer programs, dimensionless

J* = Mechanical equivalent of heat energy $\frac{ft.lb.}{Btu}$

J_P = Polar moment of inertia ($in.^4$)

k = Thermal conductivity, Btu/ft.hr. R, and index on evaluation of functions in computer programs, dimensionless

k_1, k_2, k_3, k_4 = Equations resulting from control valve system analysis, $lb._m/ft.$, $lb._m/ft.^2 sec.$, dimensionless, $ft.^{-1}$

k_b = Bellows constant for control valve, $lb._f/ft.$

k_f = Thermal conductivity of condensate film, Btu/ft.hr.-°R

k_{g_1} = Gas phase mass transfer coefficient, ft./hr.

K_L = Thermal conductivity of liquid, Btu/ft.hr.- °R

K_{L_1} = Liquid phase mass transfer coefficient, ft./hr.

k_m = Thermal conductivity of metal, Btu/ft.-hr. °R

k_p = Thermal conductivity of plastic Btu/ft.-hr. °R

k_s = Spring constant for control valve, $lb._f/ft.$

k_t = Stress concentration factor due to tray perforations, dimensionless

l = Index on evaluation of functions in computer programs, dimensionless

L = Molar liquid rate, moles/sec.

L_1 = Circumferential distance between downcomers on first tray in high pressure column, in.

L° = Length of flow path, ft.

$L^\square, L^{\square'}$ = Liquid flow rate, lb.-moles/lb.-mole feed, lbs./lb. feed

$L^{\square o}$ = Liquid flow rate after enchancement, lb.-moles/lb.-mole feed

L_B = Bolt length (in.)

Lc = Flow rate of high pressure liquid leaving reboiler-condenser lb.-moles/lb.-mole feed

L_{EXT} = Total shaft extension beyond reboiler and reflux condensers, in.

L_g = Length gusset (in.)

LHTA = Length of reboiler-condenser heat transfer area, ft.

$L^\square_{LPC}$ = Flow of liquid leaving low pressure column, lb.-moles/lb.-mole feed

L_m = Liquid flow rate or hydrogen liquid flow through reflux-condenser, lb.-moles/lb.-mole feed

L_N = Bearing life in million of cycles for load F_b

L_R = Length of shaft between reboiler-condenser and reflux condenser, in.

$L^{\square}_{RBC}$ = Flow of liquid leaving reboiler-condenser, lb.-moles/ lb.-mole feed

LRC = Length of reflux condenser, in.

L_S = Length of shaft, in.

l_s = Half length of one side of a square junction (in.)

L/A = Feet of length per square foot of heat transfer area, $ft.^{-1}$

L/V = Liquid to vapor flow ratio, dimensionless

m = Power coefficient in equation,

= $Q_{\Delta T_o} = Q_{10^o} \left(\frac{\Delta T_o}{10}\right)^m$, dimensionless

M = Index on evaluation of functions in computer programs, dimensionless

Ma = Molecular weight of air, lbs./lb.-mole

M_B = Bending moment (in.-lb.)

M_T = Torque (in.-lb.)

n = Roughness factor in Chezy Formula, dimensionless, or power coefficient in general boiling equation, dimensionless

n_1 = Number of tray downcomers, dimensionless

N = Rotational speed, RPM

N_1 = Number of radial segments in two-phase flow computer program, dimensionless

N_{DSI} = Number of diffuser passage blade sides, dimensionless

Ng = Number of gravities $\left(\frac{R\omega^2}{g}\right)$ at superficial rotor speed, dimensionless

NTU = Number of mass transfer units, dimensionless

$(NTU)_g$ = Number of gas phase mass transfer units, dimensionless

$(NTU)_L$	=	Number of liquid phase mass transfer units, dimensionless
$(NTU)_o$	=	Number of overall mass transfer units, dimensionless
P, P'	=	Pressure, $lb._f/ft.^2$, psig or total pressure, $lb._f/ft.^2$, psia
P_{CAS}, P_{CAS}	=	Casing pressure, $lb._f/ft.^2$, psia
P_{COL}	=	Column pressure, $lb._f/ft.^2$
P_{cr}	=	Critical column load (lbs.)
P_{ENV}	=	Environmental pressure surrounding outer casing, psia
p_i	=	Internal pressure psi
p_o	=	External pressure psi
P_P	=	Peripheral pressure minus casing pressure, psia
P^*_{tray}	=	Tray pressure level, psig
P_v, P'_v	=	Vapor pressure, $lb._f/ft.^2$, psia
Q, Q'	=	Heat transfer, Btu/hr., Btu/sec.
$Q_{ELECTRICAL}$	=	Electrical heat input to condensing side of High-G Cryostat, watts
$Q_L, Q_L,$	=	Liquid flow rate, $ft.^3/sec.$, Gal/min.
$\overline{Q_L}$	=	Superificial column liquid rate, $ft.^3/ft.^2$-sec.
Q/A	=	Heat flux, $Btu/ft.^2$-hr.
Q/A_b	=	Boiling side heat flux, $Btu/ft.^2$-hr.
$Q/A_c, (Q/A_c)'$	=	Condensing side heat flux, $Btu/ft.^2$-hr, $Btu/ft.^2$-sec.
r, R, r', R'	=	Radius, ft., in.
R_{avg}	=	Average column radius, in.

R_B	=	Bolt circle radius (in.)
R_c	=	Gas constant, ft.-lb.$_f$/lb.-mole/ °R
R_d	=	Dish radius (in.)
R_D	=	Diffuser passage blade radial depth, in.
R_e	=	Reynolds' number, dimensionless
r_{fic}, r'_{fic}	=	Reboiler-condenser inner radius where tube axis coincides with radius vector, ft., in.
R_i	=	Inner radius, in.
$R_{i_{HPC}}$	=	Inner radius of high pressure column, in.
R_{iC}	=	Inside corner radius (in.)
$r_{i_{seal}}, r'_{i_{seal}}$	=	Inner radius of centrifugal seal fluid, ft., in.
R_k	=	Radius of kettle stream inlet to low pressure column, in.
r_l	=	Inner radius of column liquid holdup, ft.
R_L	=	Volumetric liquid fraction, dimensionless
R_o, R'_o	=	Outer radius of rotor or column, ft., in.
R_{orf}	=	Orifice radius in control valve, ft.
R_p	=	Radius of collector pipe, in.
R_{tray}	=	Tray radius, in.
S, S'	=	Length of reboiler-condenser tube, ft., in.
S_1	=	Stress, psi
S_1, S_2, Sn	=	Stress values 1, 2, n
S_s	=	Shear stress (psi)
t, t'	=	Tray thickness, ft., in.

t_1	=	Time, sec.
T, T'	=	Temperature, °R, °K
T_1	=	Time constant for control valve system analysis, sec.
T_b	=	Boiling temperature, °R
t_c	=	Casing thickness (in.)
T_c	=	Condensing temperature, °R
t_{cas}	=	Thickness of outer casing shroud, in.
t_D	=	Diffuser passage blade wall thickness, in.
t_h	=	Casing head thickness (in.)
T_L	=	Liquid temperature, °R
t_s	=	Column side thickness, in., or shaft wall thickness (in.)
t_{sb}	=	Thickness seal blade (in.)
t_{seal}	=	Seal wall thickness, in.
t_t, t_t'	=	Reboiler-condenser tube wall thickness, in.
T_V	=	Vapor temperature, °R
T_w	=	Wall temperature, °R
U	=	Rotor tangential velocity, ft./sec.
U_o	=	Overall heat transfer coefficient, Btu/ft.^{2}-hr. °R
v	=	Volumetric vapor rate, ft.^{3}/sec., or control system set point, ft.
V, V'	=	Velocity, ft./sec., ft./hr., or velocity imparted to vapor by rotor, ft./sec., or volume (ft.^{3})
V*	=	New fluid velocity for diffuser with change in angle $\phi°$ to $\phi°'$, ft./sec.

V_l	=	Volumetric flow rate, ft.^{3}/sec.
VAS	=	Total air separator volume, ft.^{3}
V_f	=	Froth velocity $(\frac{QL}{bh_f})$, ft./sec.
V_L	=	Superficial liquid velocity or liquid velocity, ft./sec.
V_o	=	Perforation velocity, ft./sec.
V_s	=	Superficial column vapor velocity based upon active tray area, ft./sec.
Vs_{flood}	=	Superficial vapor velocity at the flooding point, ft./sec.
V_{SL}	=	Specific volume of liquid, ft.^{3}/lb.
V_{SV}	=	Specific volume of vapor, ft.^{3}/lb.
V_t	=	Tangential component velocity (ft./sec.)
V_{td}	=	Diffuser throat velocity (ft./sec.)
V_r	=	Radial component of velocity (ft./sec.)
W, W'	=	Stream flow rate, lbs./sec., lbs./min., wgt./lbs.
Wa	=	Separator inlet air flow rate, lbs./sec.
WAS	=	Total air separator weight, lbs.
X	=	Vapor quality, mass fraction
X_1, X_2	=	Mole fraction of more volatile and less volatile component, mole fraction
X_A	=	Liquid Argon purity, mole fraction
X_N	=	Liquid Nitrogen purity, mole fraction
X_O	=	Liquid Oxygen purity, mole fraction
y	=	Thickness of porous condensing surface, ft.
α	=	Volumetric foam density, dimensionless, or coefficient of thermal expansion in./in. °R

αo = Angle between plane normal to tube axis and the radius vector, deg.

$\alpha 1$ = Constant in control valve analysis, dimensionless

αAL = Thermal expansion coefficient for Aluminum in./in. °R

αb = Bearing contact angle (o)

αS = Thermal expansion coefficient for Steel in./in. °R

β = Angle between plane normal to radius vector and the direction of condensate flow, deg.

Y = Angle between radius vector and direction of condensate flow, deg.

Y^* = Activity coefficient, dimensionless

δ = Quantity, $\frac{2\omega}{gh_f}\left(\frac{Q_L}{b}\right)$, dimensionless

Δ = Deflection (in.)

ΔB = Bolt elongation (in.)

Δh_D = Dry plate head loss, ft.

ΔH_T = Turbine enthalpy drop, Btu/lb.

ΔL_S = Shaft elongation (in.)

ΔP = Pressure drop or change, psi or $lb._f/ft.^2$

$\Delta P_D, \Delta P_D'$ = Dry plate pressure drop, $lb._f/ft.^2$, psi

ΔP_{DIFF} = Pressure drop across diffuser, psi

ΔP_f = Tray frictional pressure drop, psi

$\Delta P_H, \Delta P_H'$ = Hydrostatic pressure drop, $lb._f/ft.^2$, psi

ΔP_{LIQ} = Liquid phase pressure drop, psi

ΔP_s = Static pressure change due to gravitational field, psi

ΔP_{SEAL} = Pressure head across centrifugal seal, $lb._f/ft.^2$

ΔP_T = Experimental tray pressure drop, psi

$\Delta P_{TP}, \Delta P'_{TP}$ = Two-phase pressure drop, $lb._f/ft.^2$, psi

ΔP_V = Pressure drop across control valve, $lb._f/ft.^2$

ΔR = Change in radius, in.

ΔS = Shaft deflection (in.)

ΔT = Temperature difference, °R

ΔT_b = Boiling side temperature difference, °R

ΔT_c = Condensing side temperature difference, °R

ΔT_o = Overall reboiler-condenser temperature difference, °R

ΔV_s = Incremental change in superficial vapor velocity for computer program column solutions, ft./sec.

η_d = Diffuser efficiency, percent

η_{db} = Number of diffuser blades

η_g = Composite of vapor phase dynamic mass transfer variables, dimensionless

η_L = Composite of liquid phase dynamic mass transfer variables, dimensionless

η_o = Overall diffuser recovery of theoretical kinetic energy with inclusion of diffuser expansion loss, percent

Θ = Angular direction of reboiler-condenser tubes, rad.

Θ^o = Condensing side temperature difference in theoretical heat transfer model, °R

Θ_D = One half of diffuser divergence angle ($2\Theta_D$), deg.

Θ_s = Condensing side temperature difference in theoretical heat transfer model at point where circumferential temperature gradient is zero, °R - Shaft angular deflection

λ	=	Heat of vaporization, Btu/lb.
μ, μ'	=	Viscosity, lb./ft.-hr., lb./ft.-sec.
$\mu_L \mu'_L$	=	Liquid viscosity, lb./ft.-hr., lb./ft.-sec.
μ_p	=	Poissons ratio (dimensionless)
μ_v	=	Vapor viscosity, lb./ft.-sec.
ρ, ρ_i	=	Density, lb./ft.^{3}, lb./in.^{3}
ρ_L	=	Liquid density, lb./ft.^{3}
ρ_{L_N}	=	Nitrogen liquid density, lb./ft.^{3}
ρ_{L_O}	=	Oxygen liquid density, lb./ft.^{3}
ρ_m	=	Metal density, lb./ft.^{3}
ρ_P	=	Pore density, ft.$^{-2}$
ρ_{TP}	=	Actual two-phase density at radial location (r), lb./ft.^{3}
ρ_v	=	Vapor density, lb./ft.^{3}
ρ_{v_N}	=	Nitrogen vapor density, lb./ft.^{3}
ρ_{v_O}	=	Oxygen vapor density, lb./ft.^{3}
$\bar{\phi}, \bar{\phi}'$	=	Average condensate blanketing angle, rad., deg.
ψ	=	Angle between tube axis and radius vector, deg.
ω, ω'	=	Angular velocity, rad/sec., rad/hr.

(THIS PAGE IS INTENTIONALLY BLANK.)

1.0 INTRODUCTION

Several concepts of future aerospace vehicles employ propulsion systems which require air collection, enrichment, liquefaction and storage for use later in the vehicle mission. During the past few years Union Carbide Corporation, Linde Division, has contributed to the technology required for airborne air enrichment specifically in the area of low temperature distillation. It has been shown that weight and volume of distillation equipment could be compressed substantially by the application of high gravitational fields to mass transfer elements and condenser heat transfer surfaces and that construction of a rotating distillation separator within system imposed weight and volume goals appeared indeed feasible.

The work reported was performed under Contract AF 33(657)-8722 which called for additional studies in the area of mass transfer, heat transfer, preliminary design and analysis of flight weight enrichment systems, mechanical components, and finally design and fabrication of a complete integrated boilerplate separator capable of processing 100 lbs./sec. of air. The results of the studies in the areas of mass transfer, heat transfer, mechanical components, and preliminary design and analysis were reported in ASD-TDR-63-665, Part I. This report constitutes Part II of the subject document and describes design and fabrication of the boilerplate separator. A complete set of manufacturing drawings is available for review at the Air Force Aero Propulsion Laboratory, Wright-Patterson Air Force Base, Ohio.

A detailed review of previous studies as well as of the principles of distillation is given in Section 1, of ASD-TDR-63-665, Part I. The boilerplate separator employs the basic double column cycle presented on Figure 1 and consists of three major elements; a high pressure column, a low pressure column, and a reboiler-condenser. No reflux condenser is required in the boilerplate unit since liquid nitrogen reflux for the low pressure column is supplied externally to the unit.

The various elements of the boilerplate separator were designed on the basis of results from the basic study programs conducted under the contract to yield a machine capable of receiving 100 lbs./sec. of air at pressures up to 250 psia and separating this air into product oxygen of about 90% purity by weight and waste nitrogen of approximately 98% purity by weight. The major mission of the boilerplate unit is to demonstrate functional feasibility of the rotary air separator concept. For this reason the general philosophy employed in the design of the boilerplate model was to produce a unit which is functionally and in general arrangement of components representative of current flight weight separator concepts and at the same time retain sufficient flexibility in exchangeability and operating range of components to satisfy the essential research mission of the apparatus. Since this goal had to be accomplished with limited time and funding, more advanced mechanical design concepts particularly in the areas of light-weight construction had to be subordinated to other requirements.

DOUBLE COLUMN AIR SEPARATOR

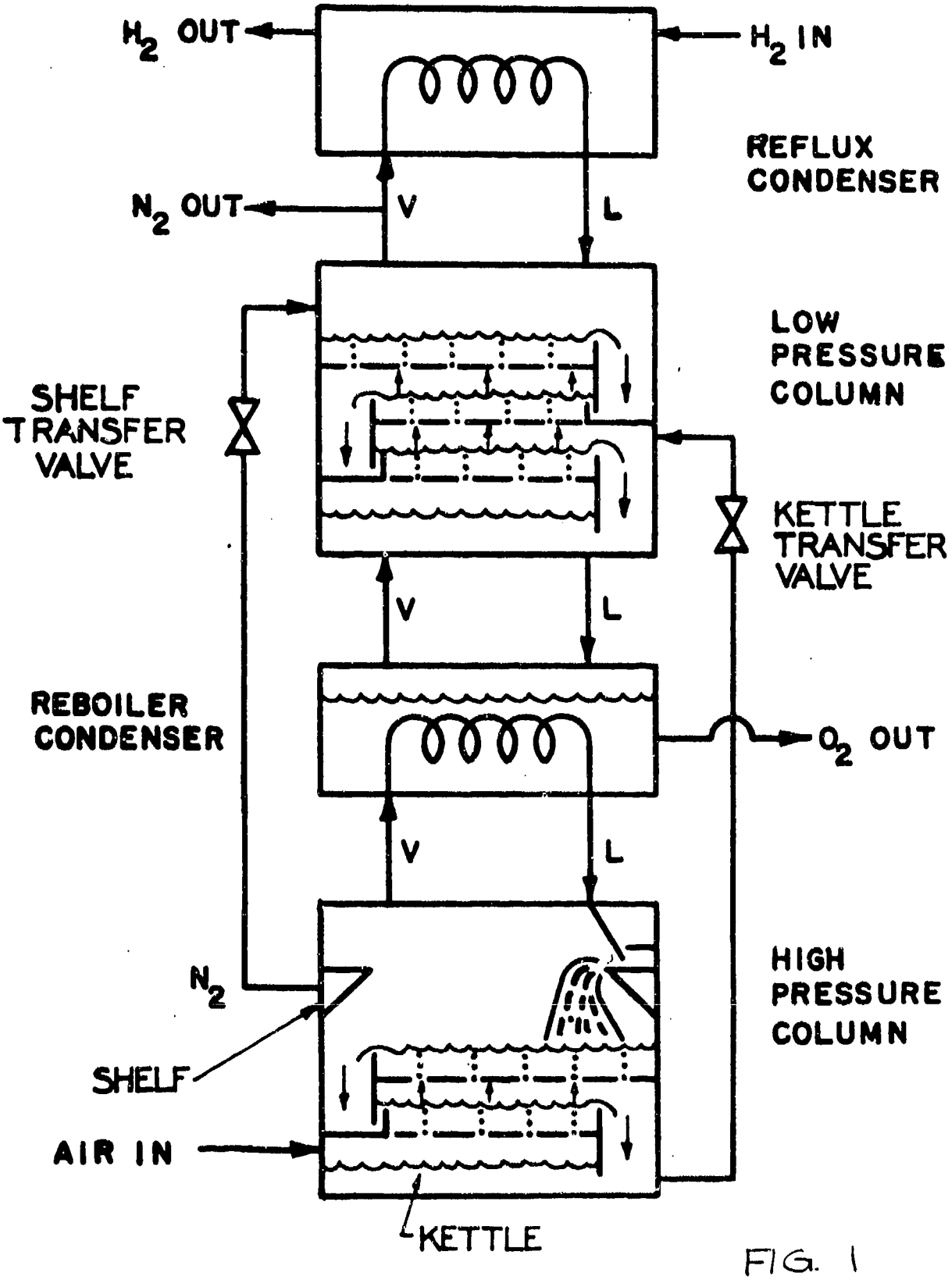

FIG. 1

2.0 SUMMARY

2.1 Conclusions

a. Work performed under the subject contract has demonstrated that the present state of technology in the areas of mass and heat transfer is sufficiently advanced to permit design and construction of a practical rotary distillation separator which in general arrangement of components and radial dimensions is representative of future air borne units. Therefore, the boilerplate unit should be capable of demonstrating functional and in part also mechanical feasibility of the rotary distillation separator concept on a reasonable scale in the test program proposed by Linde Division in response to RFP-6064-NB.

b. The optimum configuration for a rotating distillation separator was proven to be a side by side arrangement (conceived by Linde Division early in 1961) which features high pressure and low pressure columns mounted in tandem on a common shaft with the reboiler-condenser located inside the high pressure column. This arrangement minimizes fluid transfer problems and promises minimum weight in future airborne separators. Therefore, it was also used for the boilerplate model.

c. Predicted performance data for the boilerplate separator at design conditions are as follows:

Air Flow	≈	100 lbs./sec.
Inlet pressure	≈	240 psia
Waste pressure	≈	45 psia
Product Flow	≈	23 lbs./sec.
Product purity	≈	90% oxygen by weight
Waste purity	≈	98% nitrogen by weight
Design speed	≈	570 RPM

The degree to which the predicted performance will be realized hinges largely on the accuracy of correlations used in designing functional elements, particularly the distillation trays. Inaccuracies in the experimentally derived design correlations could result in some variations in boundary pressures and product and waste purities.

The possible operating range for the boilerplate separator covers from about 40 to about 115% of design capacity. Changes in throughput require an approximately proportional change in rotational speed.

d. Mechanical construction of the boilerplate separator features a modular approach in that major components as well as individual trays and heat transfer elements can be removed from the unit.

Maximum diameter of the boilerplate separator rotor is 106 in., length between bearing supports is 105 in. Weight of the rotor is about 9500 lbs. To a great extent the weight is controlled by the many large diameter flanges which were required by the modular approach to the design.

e. The problem of liquid oxygen transfer from the peripheries of the low pressure column and reboiler-condenser was solved by withdrawing liquid through peripheral diffusers and piping it to the shaft where liquid is reintroduced into the rotor. Sealing at the peripheral transfer points is accomplished by centrifugal non-contact type seals which balance pressure differential against centrifugal liquid head.

Controlled transfer of internal liquid streams is attained by specially designed control valves which are actuated directly by pressure differentials resulting from liquid levels in annular liquid hold-up chambers.

f. The columns feature contra-rotational flow downcomer trays (Ref. 1, Section 3.3.4) with spacings from 6 to 12 in. between downcomers. Active tray widths in the low pressure column range from 5-3/4 in. to 32 in. at outer and inner radii respectively. Tray widths in the high pressure column range from 4 in. to 4-5/8 in. These tray widths result in superficial vapor velocities from 7.9 to 8.6 ft./sec. in the low pressure and 4 to 4.6 ft./sec. in the high pressure column. Predicted tray efficiencies are 99% in the high pressure column and range from 64 to 83% in the low pressure column. The predicted pressure drop at design conditions is 30.6 psi for 18 actual trays in the low pressure column and 33.9 psi for 9 actual trays in the high pressure column. Both columns feature windows for observation of froth height on representative trays during operation.

g. At the design point the reboiler-condenser has to transfer 22×10^6 Btu/hr. at a temperature differential of 10.7°R.

The unit consists of a number of disks in parallel. Individual disks are made from 1/4" diameter tubes arranged and brazed to form an annulus between inner and outer radii of

10 in. and 24 in. respectively. A special boiling surface was applied to the outside of the tubes and a porous condensing surface to the inside to maximize heat transfer. An average heat flux of 29,200 Btu/hr.ft.^{2} is predicted for the reboiler-condenser.

2.2 Recommendations

The test program for the boilerplate unit should establish the basic functional feasibility of the rotary distillation separator concept. It is felt that the major breakthrough required to make airborne distillation separators feasible has already been accomplished through the mass and heat transfer advances made by Linde Division in work to date. The transition from the boilerplate unit to a future full-scale airborne separator is believed to be relatively straight forward requiring, primarily, development in mechanical areas plus minor experimental effort for refinement of functional concepts. Consequently it is recommended that the program as envisioned for the immediate future be planned in a way such as to establish final mechanical feasibility of the distillation separator at the earliest possible date and at a minimum total expenditure. With this in mind the following specific program steps are recommended, including what is considered to be a necessary and complementary research effort in several functional areas.

a. Additional research should be conducted on functional design of trays in a test program using complete peripheral trays with cryogenic fluids. The necessary test equipment and facility would be available from previous programs. Purpose of this work would be:

(1) to refine existing design correlations
(2) improve hydraulic characteristics and efficiency of trays and
(3) simplify mechanical construction of trays without sacrificing functional performance.

b. The second item suggested is a modest experimental program in heat transfer, specifically a research effort to optimize the porous condensing surface. Experimental equipment required is available in the high "g" cryostat from previous work. Present indications are that a modest effort should easily yield weight reduction in the reboiler-condenser

c. Additional work is recommended on refinement of two phase flow data in a gravitational field and internal flow transfer

controls. Aim of this work would be to improve or eliminate the internal control valves for the separator. Again equipment available from previous efforts can be used for this task. Work here would substantially improve operational stability of a distillation separator.

d. Another area in which additional effort is recommended is concerned with transport of saturated liquid from the periphery to the center of the device at locations where limited driving force is available. Because of the impact of this problem upon design and reliability, it is proposed to examine analytically and experimentally two competing schemes using stationary diffusers with associated peripheral seals or rotor mounted pumps respectively.

e. Finally it is recommended to design, construct and test, in the facility under construction, a 100 lb./sec. light-weight separator. This unit would represent a slice of a full-scale device in that radial dimensions and construction details would be essentially identical to those of final airborne units. Such a device would bring into focus potential mechanical problem areas and have the capability to demonstrate true potential and final mechanical feasibility of a rotating distillation separator at an early date and a modest expenditure in funds.

3.0 SELECTION OF CONFIGURATION

Since the double column cycle (Figure 1) had been shown to be the most attractive choice for a high throughput distillation separator in previous work (Ref. 2), the first step in the design effort was to find for this cycle the most suitable physical arrangement which promised optimum weight and volumes in future flight weight units while at the same time avoided excessive mechanical complications.

The major components of a double column separator are a low pressure column, a high pressure column, a reboiler-condenser, and a reflux condenser. In the boilerplate separator, reflux nitrogen liquid is supplied externally to the separator and for this reason, no reflux condenser is required. In earlier work (Ref. 2) a configuration was used which featured all components stacked radially. Since this arrangement requires excessive diameters, it was eliminated from further consideration. Basically four different configurations were examined as to suitability in future separators and in the boilerplate model. The four arrangements are shown on Figures 2 through 5.

Arrangement 1 features both columns mounted side by side on a common shaft. The reboiler-condenser is located inside the high pressure column. If a reflux condenser should be required, it would be located inside the low pressure column. Arrangement 2 is essentially identical to Arrangement 1 except that the high pressure column and the reboiler-condenser are mounted on a separate shaft from the low pressure column and both assemblies can rotate at different speeds. Arrangement 3 features a side by side column rotor and a separately rotating reboiler-condenser. Finally, Arrangement 4 employs four separate rotors to house the various separator components. Here the low pressure column is split into two rotors, one accommodating the stripping section and the other, the enriching section.

To judge the merits of various configurations it was necessary to look at possible complications resulting from fluid traffic between separator components and, of course, the possible overall weights of future flight weight separators constructed according to the different schemes.

A particular problem is encountered in rotating separators when a saturated liquid stream has to be removed from the periphery of a component to a point at a smaller radius operating at essentially identical pressure. The reason for this is, of course, that liquid in this case would have to be moved against a large gravitational head, a task which is not possible without substantial pressure drop. Two possible solutions are mounting pumps on the rotors to furnish the necessary head potential to the liquid or withdrawing liquid from the

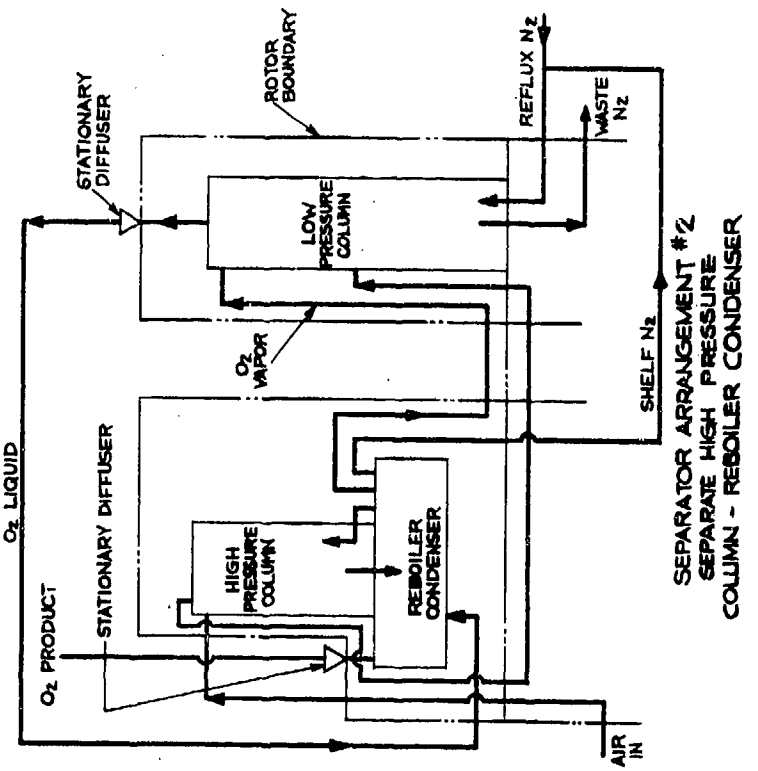

FIG. 3

SEPARATOR ARRANGEMENT #2
SEPARATE HIGH PRESSURE
COLUMN - REBOILER CONDENSER

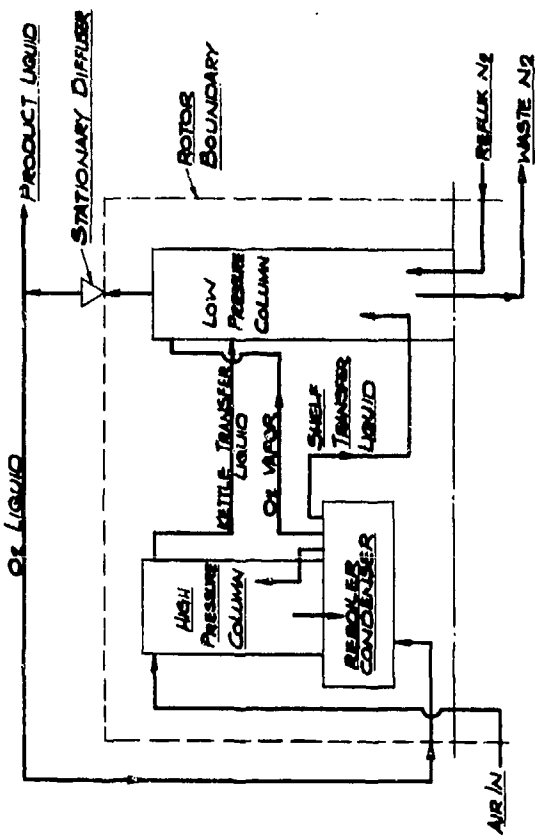

FIG. 2

SEPARATOR ARRANGEMENT #1
ALL COMPONENTS ON ONE ROTOR

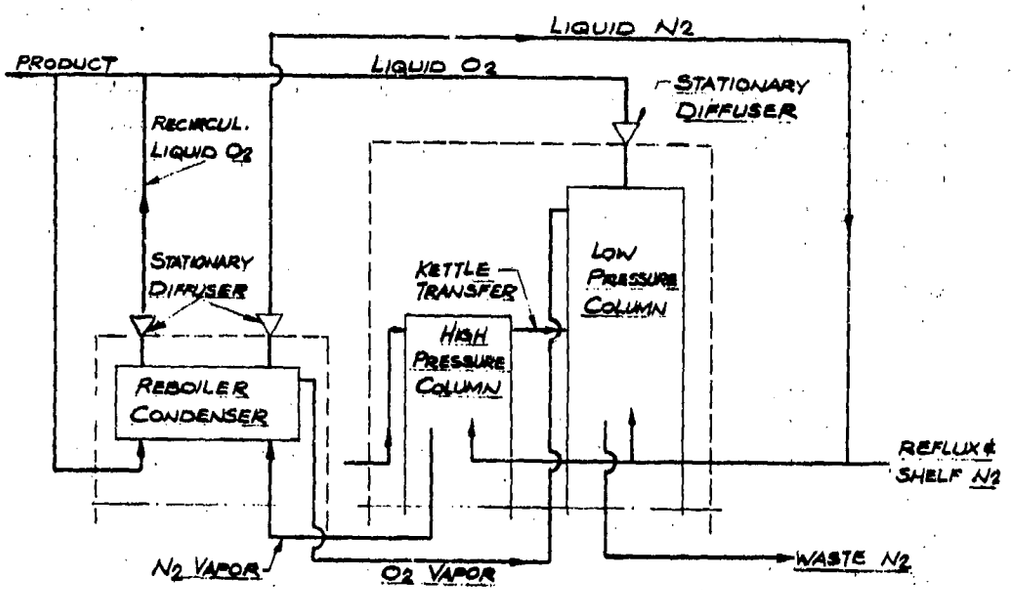

SEPARATOR ARRANGEMENT #4
SEPARATE ROTOR FOR REBOILER CONDENSER

FIG. 4

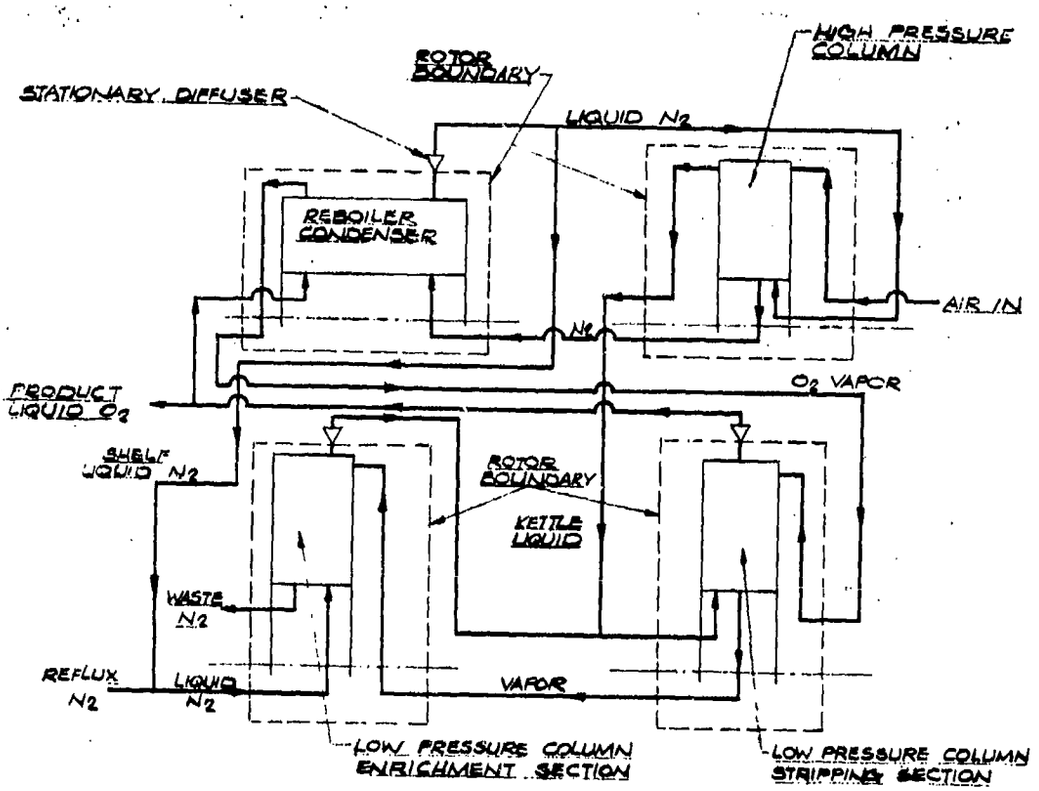

SEPARATOR ARRANGEMENT #3
FOUR SEPARATE ROTORS

FIG 5

rotating equipment through stationary diffusers, which convert the kinetic energy of the liquid into pressure, and reintroducing the liquid back into the rotor through the center shaft. The former approach may have some merit in full scale separators; however, unavailability of suitable pumps and difficulty in driving them made this approach unfeasible for the boilerplate model. For this reason the second approach was selected for the boilerplate model. It is obvious that even in this case considerable complications are encountered in dynamically sealing liquid at large diameters and in building large diameter radial diffusers.

Arrangement 1 can be shown to place the various separator components into their most natural position for the internal traffic of fluid in that liquid within the separator can flow "downhill" or radially outward in most instances. Only one low pressure stream has to be removed from the periphery of the rotor. Kettle and shelf liquid streams can be transferred radially inward because of the driving force furnished by the large difference in operating pressures between the columns.

Arrangement 2 only requires removal of low pressure liquid streams from the periphery of two rotors and for this reason is judged feasible. Naturally, use of two rotors requires a larger number of shaft seals than Arrangement 1.

Arrangements 3 and 4 make necessary removal of liquid streams from the periphery of several components. Particularly disadvantageous is the need for removing a high pressure liquid nitrogen and a low pressure liquid oxygen stream from the periphery of the reboiler-condenser. Since it is not believed possible with the present state-of-the-art to effect a tight seal between the two streams, liquid nitrogen leakage would tend to dilute the product oxygen stream. For this reason both Arrangements 3 and 4 were eliminated from further consideration.

To develop tools for making a choice between the remaining configurations it was necessary to review functional relationships for heat and mass transfer as well as stress-weight relationships for rotating air separators. Even though the mass and heat transfer information available at the time of this work was very preliminary, it was felt that general trends could be established from the information available. As a matter of fact, later work on the basis of UCON data did confirm the original conclusions reached.

It was obvious that an integral separator design imposed certain constraints upon the functional design of heat and mass transfer elements. In general, high condensing and, therefore, heat transfer coefficients, demanded high rotational speeds while the requirements for low column pressure drops favored low radial speeds for the

columns. In an integrated separator the above meant selection of a compromise speed.

On the basis of a simplified stress analysis, a weight expression of the following form was developed for columns. (Ref. 1, Appendix XVII).

$$W_{HPC} \text{ or } W_{LPC} = \left(C_3 \frac{\omega^2}{g_c} + C_4 b_o' P_p'\right)(R_o)^2 \frac{\rho_m}{s_1'} + C_5 b_{avg} R_o \omega^2 \frac{\rho_m}{s_1' g_c} + C_6 R_o^2 b_{avg}' \rho_m \quad (1)$$

Here C_3, C_4, C_5 and C_6 are constants depending upon throughput, fluid densities and design.

From this equation it is evident that column weight is prominently influenced by radial speed and diameter which, of course depends upon the number of trays required and therefore tray efficiency, and tray count, and, to a lesser extent, by superficial vapor velocities which determine width.

For the reboiler-condenser the following weight expression was obtained:

$$W_{RBC} = \frac{C_7}{\omega^{1/2} \Delta T_o^{3/4}} + \frac{\rho_m}{s_1} \left(C_8 \omega^2 + \frac{C_9}{\omega^{1/2} \Delta T_o^{3/4}}\right) \quad (2)$$

Here, C_7, C_8, C_9 are also constants.

The expression was developed for constant radial dimensions of a reboiler-condenser as radii of the reboiler-condenser are fixed by column dimensional requirements.

In general, the weight expression for the reboiler-condenser shows a strong dependence upon unit heat flux which is proportional to $\Delta T^{3/4} \omega^{1/2}$ and the radial speed ω^2. The latter is, of course, an indication of mechanical stresses due to centrifugal forces.

These equations are presented in more detail in Ref. 1, Appendix XVII.

Figures 6, 7, and 8 show the normalized weight for the various components plotted as a function of radial speed. The curves

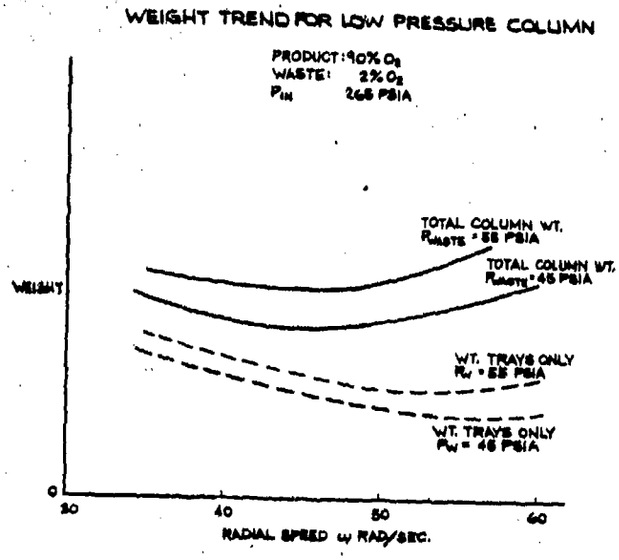

FIG. 6

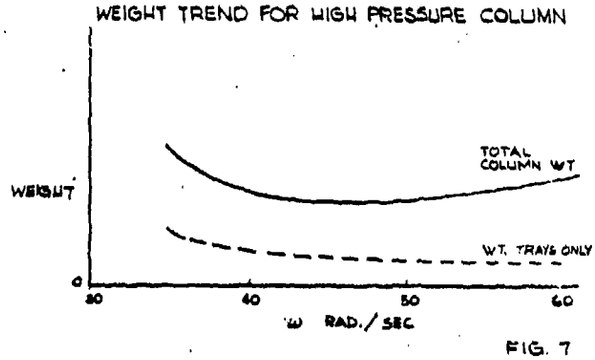

FIG. 7

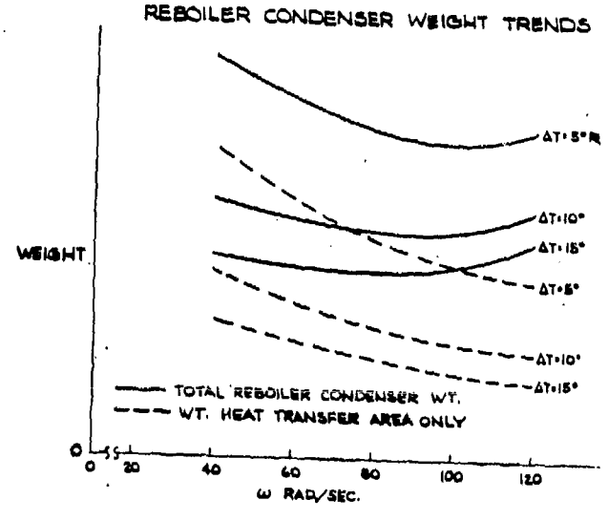

FIG. 8

are plotted on the assumption of constant pressure boundaries for the various components. In this instance, a change in radial speed requires a change in superficial column velocities to stay within the given pressure boundaries.

Most significantly it can be seen that the curves are relatively flat within practical speed ranges even though minimun weight for the reboiler-condenser occurs at a higher speed than for the columns. It should be noted here that the curves were developed from air-water tray dynamics data available at that time. Use of later UCON data should have the effect of shifting the minimum column weight into a higher speed range.

The weight trends presented do not take into account the weight of constant items such as shafts, bearings, seals, bearing pedestals, piping, etc. which are required for each separate rotor. It was found that the weight of these items was substantial and that duplication of these items in the multiple module approach introduced a weight penalty which exceeded the possible weight savings realized in the functional components proper.

Since the investigation had shown the integrated side by side separator arrangement not only to be the mechanically least complicated but also the one promising lowest weight in future flight weight separators, this arrangement was selected for the boilerplate model.

(THIS PAGE IS INTENTIONALLY BLANK)

4.0 FUNCTIONAL DESIGN

4.1 General Considerations

The process and functional design for the boilerplate separator required calculation and assessment of all pertinent performance parameters of separator components such as pressure drop, mass transfer efficiencies, heat transfer coefficients, etc. and some optimization in selection of speed and assignment of pressure drops to the various components. Essentially the work involved application of the results from applied research in mass transfer, heat transfer, and mechanical areas to the design of separator components and integration of these components into a complete separator.

The basic cycle for the boilerplate separator is shown in Figure 9. It can be seen that it is essentially identical to arrangement 1 (Fig. 2) of the preceding section except for a minor variation which provides for product and recirculation oxygen liquid to be withdrawn separately from the reboiler-condenser through a second diffuser instead of being mixed with the low pressure column liquid at the periphery of this column.

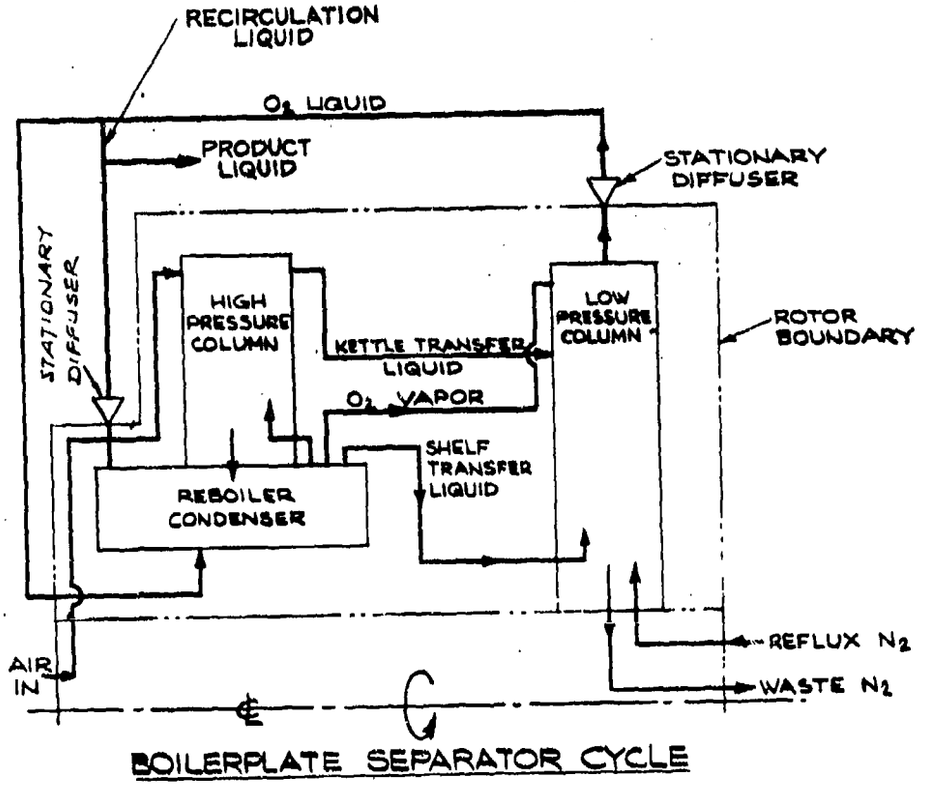

BOILERPLATE SEPARATOR CYCLE

FIG. 9

The reason for the change was that as liquid in the reboiler-condenser boils in equilibrium with the cocurrent vapor it is possible in the modified arrangement to withdraw liquid of the desired product purity from the boiling passage of the reboiler-condenser instead of having to introduce it into the passage at final product purity. As indicated in Figure 10 this results in a substantial increase in ΔT (~1.4°R) across the reboiler-condenser. It is believed that the resulting savings in heat transfer area and weight will more than offset the complications ensuing from the use of an additional diffuser and seal.

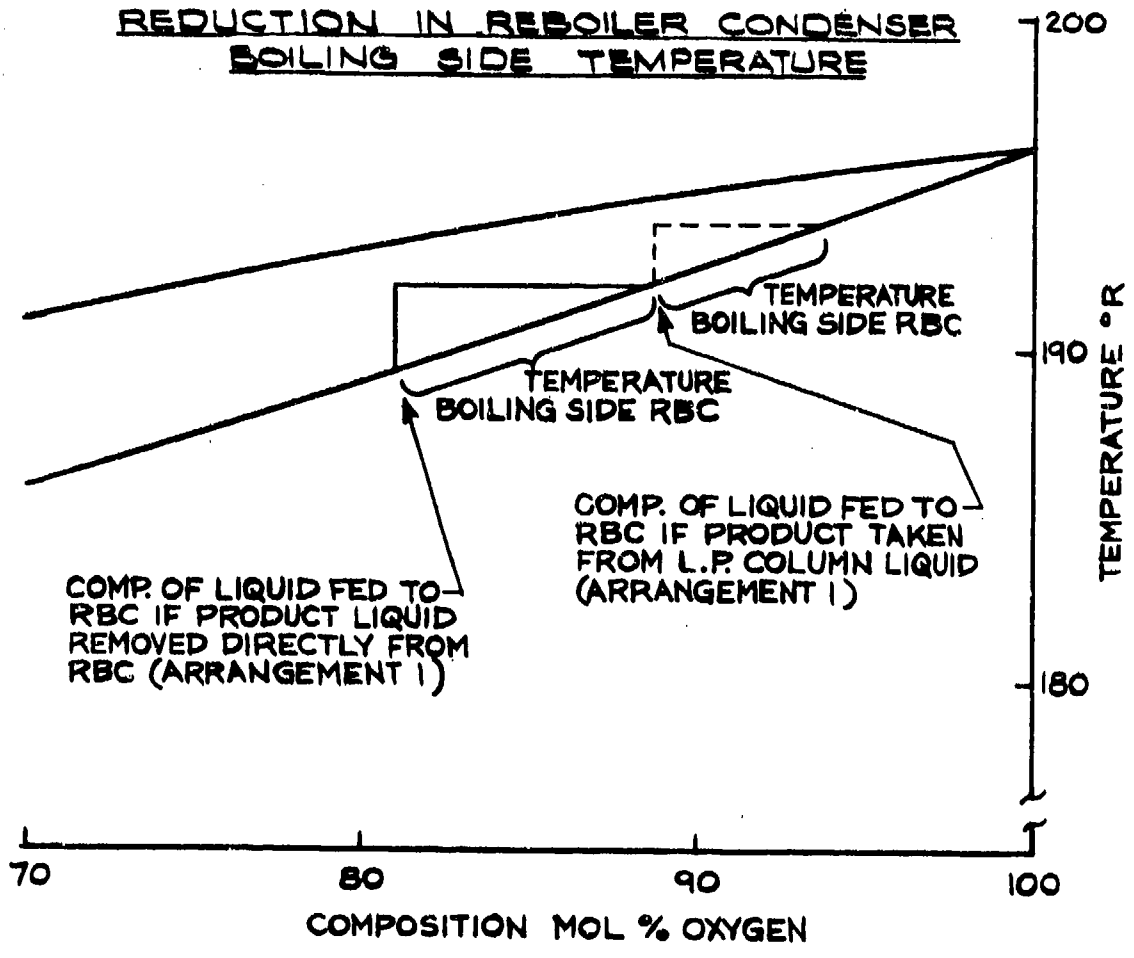

TEMPERATURE COMPOSITION DIAGRAM FOR N_2-O_2 SHOWING TEMPERATURES ON BOILING SIDE OF RBC FOR BOILING SIDE PRESSURE OF 75 PSIA & PRODUCT PURITY OF 90% BY WEIGHT

FIG. 10

4.2 Procedure

Before starting with design work it was necessary to establish some boundary conditions for the separator. Throughput and desired product purities were established by contract specifications. The waste or separator exhaust pressure was more or less arbitrarily fixed at 45 psia. This pressure appeared sufficiently high for rejecting waste gas through reasonable size piping and sufficiently low to permit effective separator operation at high purities. It should be noted here that at higher column pressures, lower relative volatilities require a larger number of trays to effect a given separation.

In the general design procedure, the waste pressure was fixed at 45 psia. To this value, the pressure drop through the low pressure column was added to arrive at the boiling side pressure for the reboiler-condenser. To obtain a reasonably small reboiler-condenser, the ΔT across the heat transfer surface was fixed at about 10°F. This, of course, established the condensing side pressure. Adding to this figure the high pressure column ΔP yielded the required column inlet pressure. In the above procedure pressure changes due to centrifugal effects as well as pipe friction had to be considered, of course.

To develop a feel for possible operating ranges of separator arrangements the initial phase of the general process design work was devoted to parametric studies of various functional relationships developed under previous contracts for rotating distillation trays in air-water tests. The separator was divided into four modules; the reboiler-condenser, the high pressure column, and both sections of the low pressure column (stripping and enriching). These individual components were studied as to variations of efficiency, foam height, liquid capacity, and pressure drop with rotational speed, superficial vapor velocity, and feed and waste pressure. From inspection, apparent optimum design ranges were selcted. This optimization involved choosing conditions that would result in the minimum pressure drop and maximum efficiency at the lowest possible feed pressure and power loss. Thus, a plot of pressure drop/efficiency was constructed at various superficial velocities for a representative Ng range. This indicated that the column should operate as near as possible to the flooding limit. The conclusions reached were only preliminary since they were based on the air-water data. However, the predominant trends were discovered and a first set of design calculations were carried out which gave approximate results.

A number of revisions were necessary when the results from the UCON test series became available. It was found that, in general, the

air-water data predicted higher pressure drops and lower foam heights, than did UCON data and for this reason demanded use of excessively low operating speeds. The UCON data dictated the use of lower superficial velocities and higher speeds to stay within the flooding limit for the innermost tray of the low pressure column and at the same time retain a reasonable separator size. From these preliminary considerations it was found that the separator should be designed for a design speed range from 55 to 65 rad./sec. and that superficial velocities from 8 - 12 ft./sec. in the low pressure column and 4 - 6 ft./sec. in the high pressure column appeared feasible.

Application of the UCON correlations indicated that tray spacings ranging from 1-1/8 to 1-1/2 in. would be adequate. However, to provide some margin for possible errors in the correlations and increase the operating range for the boilerplate separator, it was decided to make the tray spacing 1-3/4 in. in the high pressure column and the stripping section of the low pressure column and from 1-3/4 in. to 2-1/4 in. in the enriching section of the latter.

4.3 Column Design

4.3.1 Tray Counts

Tray counting procedures were complicated by the fact that the number of theoretical trays required to effect a certain separation is a strong function of the pressure level at which the column operates due to the large change in relative volatility with pressure. This, of course, meant that column pressure drops and consequently tray dynamics had a substantial influence upon purities that could be attained with a given number of trays.

The procedure used in the design of the boilerplate model was to run several tray counts for different waste purities and column pressures in the range generally defined by the boundary conditions mentioned (90% oxygen make purity, 45 psia waste pressure) to establish a map of tray counts versus pressure levels. (Fig. 11). From this information and preliminary efficiency data the number of actual trays required was estimated at nine in the high pressure column and eighteen in the low pressure column. After calculating tray dynamics and establishing actual pressure boundaries, a second tray count map was drawn for two waste purities (Fig. 12). Comparing the calculated mass transfer performance of the column to the requirements for various purities yielded a predicted waste purity for the separator.

For the actual tray counts, an available Linde computer program for the ternary Argon-Oxygen-Nitrogen was used. This program was used

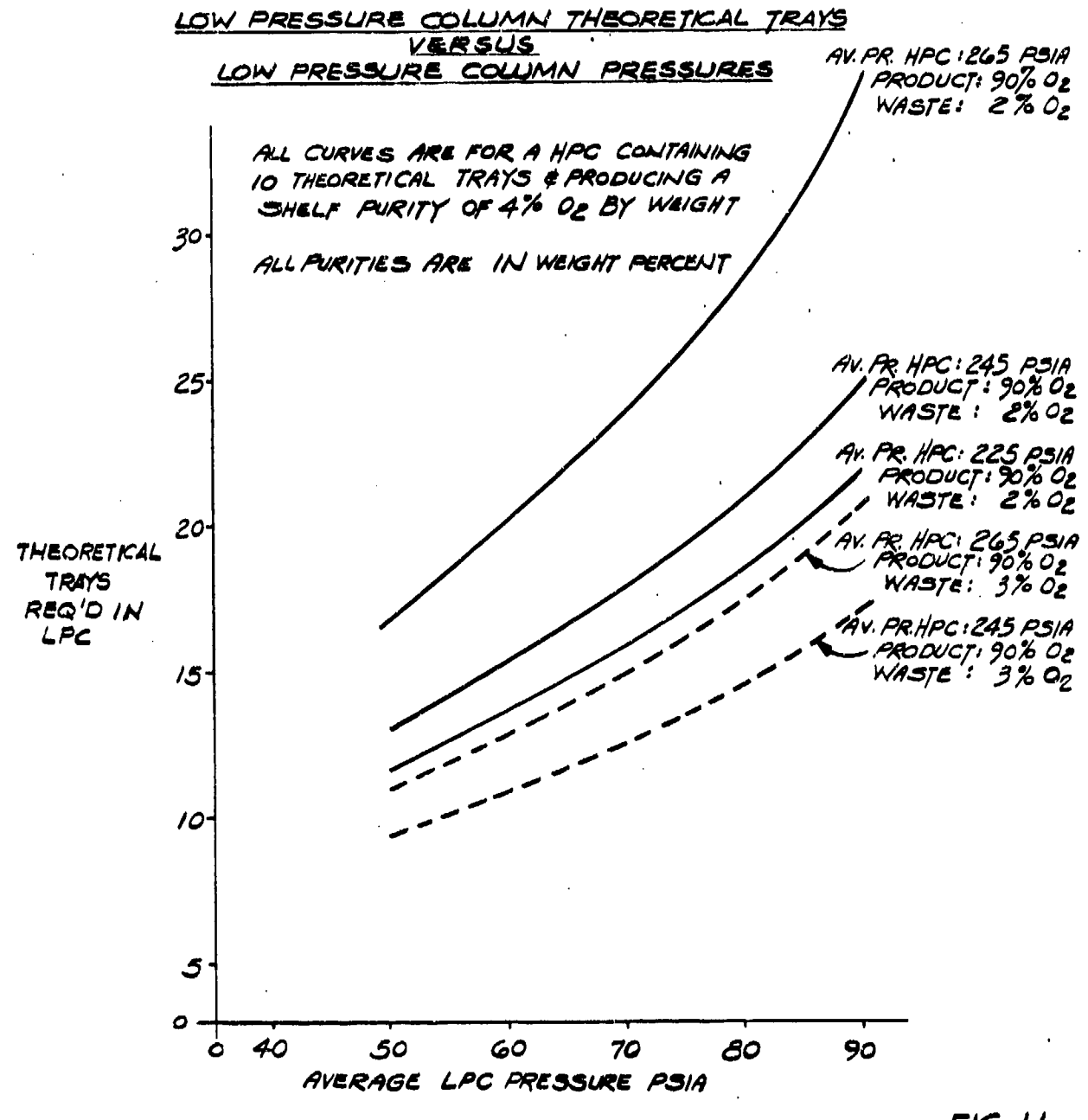
LOW PRESSURE COLUMN THEORETICAL TRAYS
VERSUS
LOW PRESSURE COLUMN PRESSURES
ALL CURVES ARE FOR A HPC CONTAINING 10 THEORETICAL TRAYS & PRODUCING A SHELF PURITY OF 4% O2 BY WEIGHT
ALL PURITIES ARE IN WEIGHT PERCENT
AV. PR. HPC: 265 PSIA PRODUCT: 90% O2 WASTE: 2% O2
AV. PR. HPC: 245 PSIA PRODUCT: 90% O2 WASTE: 2% O2
AV. PR. HPC: 225 PSIA PRODUCT: 90% O2 WASTE: 2% O2
AV. PR. HPC: 265 PSIA PRODUCT: 90% O2 WASTE: 3% O2
AV. PR. HPC: 245 PSIA PRODUCT: 90% O2 WASTE: 3% O2
THEORETICAL TRAYS REQ'D IN LPC
0
5
10
15
20
25
30
0
40
50
60
70
80
90
AVERAGE LPC PRESSURE PSIA

FIG. 11

LOW PRESSURE COLUMN THEORETICAL TRAYS VS HIGH PRESSURE THEORETICAL TRAYS

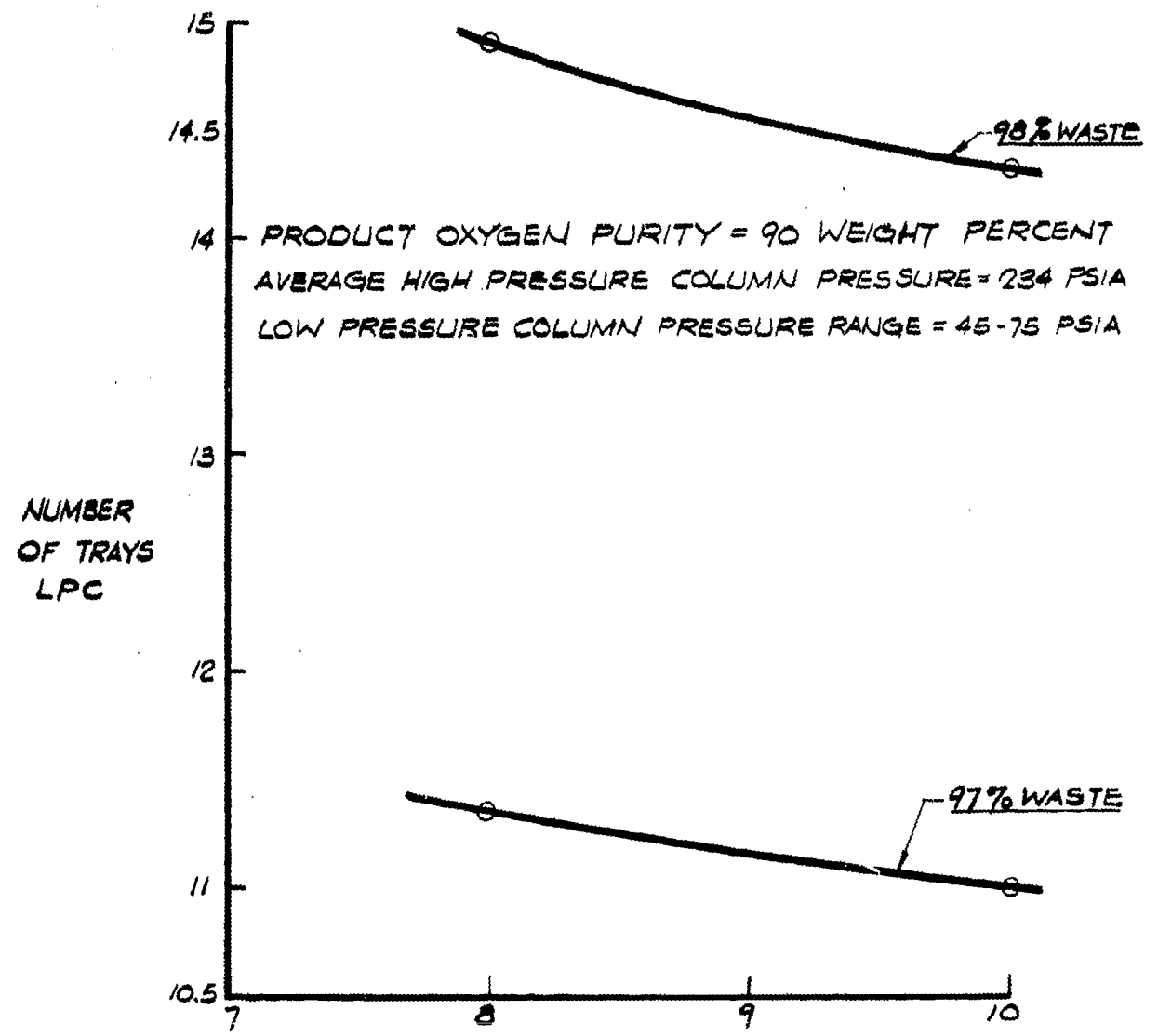

FIG. 12

as it was felt that the influence of Argon upon the tray count was relatively insignificant in the purity ranges under consideration. The program predicts for the given column flows and purities, the minimum number of theoretical trays required in the low pressure column and the kettle liquid feed insertion point. The high pressure column must be specified to run the program. That is, the shelf purity, average high pressure column pressure, and number of theoretical trays in the high pressure column must be specified along with the product purity, waste purity, etc. of the low pressure column.

Since the tray program divides the pressure drop evenly among the trays, a minor inaccuracy is encountered, because in reality the major portion of the pressure drop occurs in the oxygen-rich section, which operates in the high "g" field and is subjected to the highest liquid loading. Therefore, the base case developed was checked graphically on a McCabe-Thiele diagram. This check indicates that the computer tray count is on the conservative side in that actually somewhat fewer trays should affect the predicted separation. Before it was possible to actually predict the expected boilerplate waste purity it was necessary to assess the effect of enhancement upon tray efficiencies.

The efficiency at any point of a tray is defined as the point or local efficiency. It furnishes a direct measure of the enrichment across the tray at that point in terms of the possible enrichment with complete equilibrium. If any concentration gradiant exists on the tray, separation greater than that predicted by point efficiency can be attained with a resultant plate efficiency, which may be greater than 100%.

The degree of enhancement thus possible significantly depends on the assumed concentration gradiant and the length of each tray. A number of representative trays in each column were checked for enhancement using a variety of methods. All methods indicate some enhancement is possible. The enhancement realized hinges mainly on the degree of non-mixing of the liquid that can be maintained. Generally, a fairly long section of tray is necessary for any appreciable enhancement. The 100 lb./sec. unit features a maximum tray length between downcomers of 12 inches which is moderately good for enhancement. Before any valid conclusion can be reached with a high degree of confidence, further research is required. Without enhancement allowance, a waste purity of about 97.5% wt. nitrogen and a product of 90% wt. oxygen is predicted.

4.3.2 Tray Dynamic Design

The correlations used to obtain tray dynamic design were obtained from Ref. 1, Section 3. To establish foam heights, the following expression

was used:

$$h'_f = \frac{48.7 \left(\frac{\bar{Q}_L}{b}\right)^{1/3} V_s^{1.6} \sqrt{\frac{\rho_v}{\rho_L - \rho_v}}}{(N_g)^{.85} (f)^{.13}} \qquad (3)$$

The space allotted for disengagement was,

$$H' = \frac{.05\, V_s^2}{N_g} \qquad (4)$$

Once the approximate foam heights had been established, the flooding limitations and efficiency aspects were examined to further adjust the vapor velocities.

The maximum velocity or flooding velocity was computed from,

$$(V_s)_{FLOOD} = .140 \sqrt{\frac{N_g (\rho_L - \rho_v)}{\rho_v}} \qquad (5)$$

The number of gas phase mass transfer units was calculated from:

$$(NTU)_g = \frac{C (N_g h_f)^{3/4} D_g^{2/3}}{V_s^3} \qquad (6)$$

where C is a constant. Then since the liquid phase resistance is assumed negligible, based on previous work (Ref. 2)

$$E = 1 - e^{-(NTU)_g} \qquad (7)$$

The strong influence of velocity on efficiency was only apparent after the UCON tests and naturally precluded high vapor velocities.

The pressure drop across a tray was composed of three parts, the dry plate pressure drop, the hydrostatic drop (through the foam) and the pressure head resulting from rotation. The static pressure head was computed from:

$$\Delta P_s = \frac{(R_2^2 - R_1^2)\ \omega^2\ \rho_v}{2g_c} \qquad (8)$$

This equation must be integrated if large increments are used since ρ_v will vary. However, between trays the change in ρ_v is small and use of an average ρ_v is justifiable in the static pressure drop computation.

The dry plate portion was computed from:

$$\Delta P_D = \frac{C\ \rho_v\ V_s^2}{g_c} \qquad (9)$$

where:

$$C = \left[1 - \frac{1}{f} + \frac{1}{2\ C_v^2\ f^2} \right] \qquad (10)$$

and C_v is taken as = .88 for the trays used, where the thickness to diameter ratio is ≥ 1.

The hydrostatic head drop was computed from:

$$\Delta P_H = \left(\alpha - \frac{\delta}{N_g} \right) N_g\ h_f\ (\rho_L - \rho_v)\ \frac{g}{g_c} \qquad (11)$$

where:

$$\delta = \frac{2L\ \omega\ \bar{Q}_L}{g\ h_f} \qquad (12)$$

The δ / N_g term is a Coriolis force correction term which generally does not exceed 15% of α. These formulas are explained in more detail in Ref. 1, Section 3.4.2.

The ratio of dry plate pressure drop to the hydrostatic pressure drop was then checked and the free area of the tray adjusted until this ratio was greater than 0.3. This design criteria was established to avoid

dumping through trays.

Following establishment of a feasible design range, a computer program was developed which allowed computation of all pertinent tray hydraulic data and fluid properties on a tray to tray basis. This program is attached as Appendix I. The design was optimized by inspecting computer printouts for various column geometries and making adjustments to the design parameters. The base case developed for the column design is shown in Figure 13 and 14 and Tables 1 and 2. These charts represent the predicted operation at design conditions.

With the required velocities and downcomer spacings established, and the density profiles known, the tray widths were calculated. Since the profile of the enriching section was established earlier from the density profile, this fixed the remaining tray widths in the top section once the eleventh tray width was chosen. In the stripping section and high pressure column, the required tray areas and widths were similarly calculated. However, because straight sided column walls were used for mechanical reasons, the necessary profile was obtained by the use of rings which blocked off tray area.

The selected speed of ω = 60 rad./sec. provided good column performance.

4.4 Process Mass and Heat Balance

With the general column design and performance established and the reboiler-condenser ΔT fixed at 10.7°F it was possible to proceed with the process design for the internal and external separator circuits which consists as shown in Figure 15 of low pressure and high pressure columns, reboiler-condenser, and flash pot. The flash pot provides a holdup tank into which column and recirculation liquid are throttled before being returned to the reboiler-condenser. Since both of these liquids contain the converted kinetic energy imparted to the fluid by the rotors in the form of pressure and heat energy, they flash when pressures are reduced. The amount of vapor to be vented can be computed from knowing the kinetic energy terms.

A rigorous solution would require that the general mass and heat balance for the circuit shown be carried out in conjunction with the tray count and tray dynamic programs since all of these programs are interdependent. However, it was found that the simplified cycle assumptions used in the tray counting procedure adequately describe column flows so that the columns can be assumed as fixed in the general mass and heat balance. Slight changes which do occur in column flows as the result of the particular conditions existing in the actual circuit have

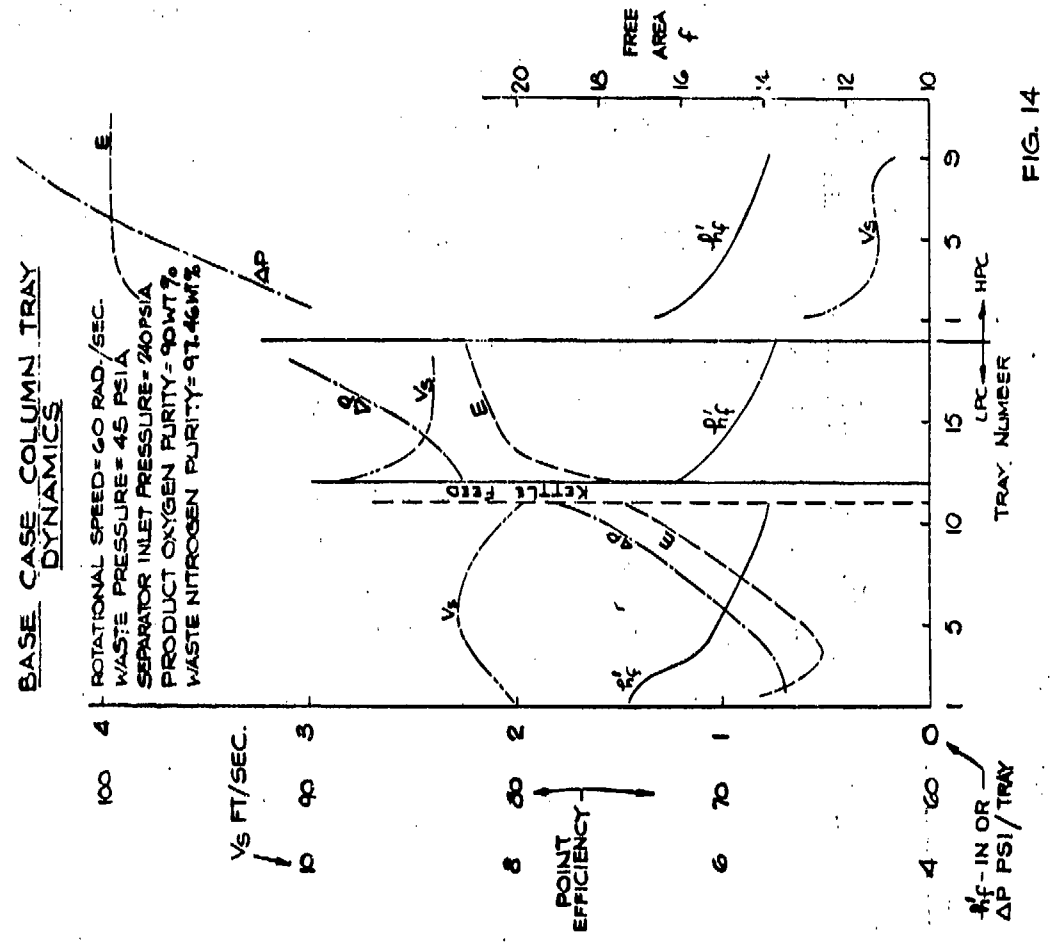
BASE CASE COLUMN TRAY DYNAMICS
ROTATIONAL SPEED = 60 RAD./SEC.
WASTE PRESSURE = 45 PSIA
SEPARATOR INLET PRESSURE = 240PSIA
PRODUCT OXYGEN PURITY = 90WT%
WASTE NITROGEN PURITY = 97.46MT%
ΔP
E
Vs
Ff
Ff'
KETTLE FEED
LPC
HPC
TRAY NUMBER
FREE AREA f
Vs FT/SEC.
POINT EFFICIENCY
Ff' - IN OR ΔP PSI/TRAY

FIG. 14

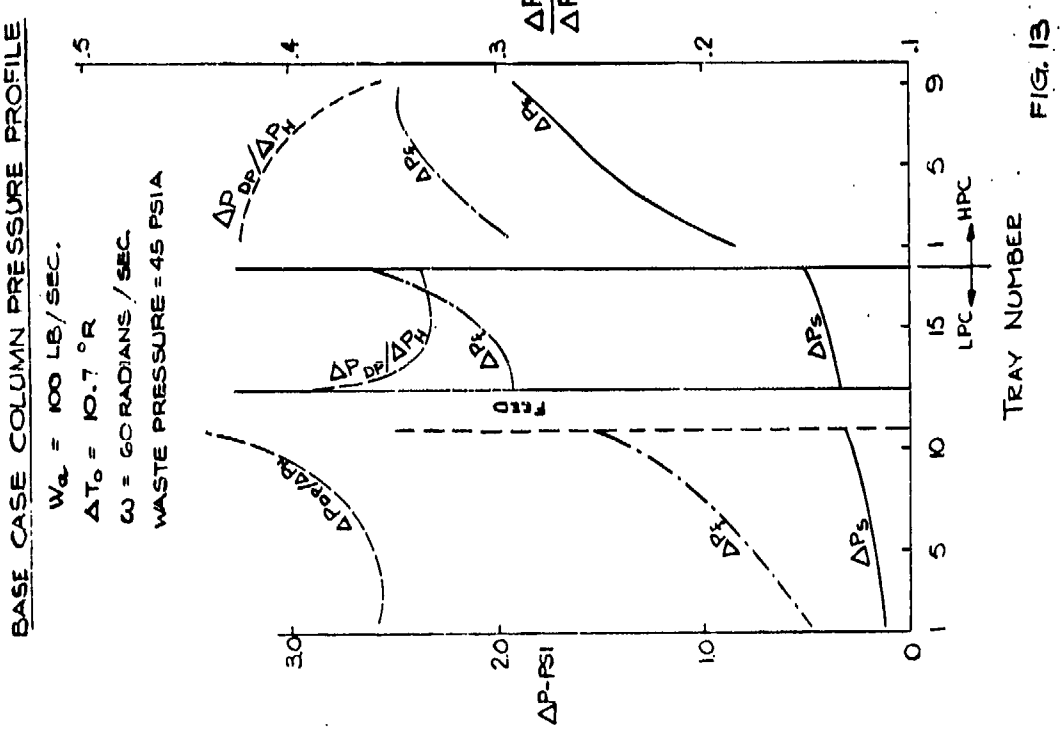
BASE CASE COLUMN PRESSURE PROFILE
Wa = 100 LB/SEC.
ΔTo = 10.7 °R
ω = 60 RADIANS/SEC.
WASTE PRESSURE = 45 PSIA
ΔPD/ΔPH
ΔP DP/ΔPH
ΔPs
ΔPt
FEED
LPC
HPC
TRAY NUMBER
ΔP-PSI

FIG. 13

TABLE I

LOW PRESSURE COLUMN OPERATION - 100 LB./HR. UNIT

ω = 60 rad./sec. X_p = 90% WT.
P_w = 45 psia Y_w = 97.46% WT. (No enhancement Allowance)
ΔT_{RBC} = 10.7°R

ENRICHING SECTION

Tray No.	Press. Psia	Vs / Vmax.	Active Area	Free Area	Tray Section Length/Ft.	Ng	Vs Ft./Sec.	Q_L^* Ft.^{3}/Sec.-D.'C.	h_f (in)	α	$\frac{\Delta P_{DP}}{\Delta P_H}$	ΔP_f (friction)	ΔP_s (static)	ΔP_T (total	Eff.	No. of Dwncmrs.	Tray Spacing (in.)
1	45.81	.712	.8	.20	.785	112	8.05	.132	1.44	.097	.375	.503	.13	.63	.690	8	2.25
2	46.54	.691	.8	.20	.932	133	8.44	.131	1.46	.099	.339	.605	.13	.73	.685	8	2.25
3	47.25	.634	.8	.20	.540	154	8.29	.066	1.05	.101	.375	.551	.16	.73	.650	16	2.0
4	48.0	.624	.8	.20	.604	172	8.58	.065	1.07	.102	.353	.625	.16	.78	.644	16	2.0
5	49.0	.597	.8	.18	.671	191	8.61	.065	1.04	.110	.387	.755	.19	.94	.659	16	2.0
6	50.0	.568	.8	.18	.736	210	8.54	.065	.987	.118	.345	.821	.20	1.02	.672	16	2.0
7	51.2	.543	.8	.16	.801	228	8.49	.064	.952	.128	.389	.981	.22	1.20	.687	16	1.75
8	52.5	.521	.8	.16	.858	244	8.40	.063	.905	.136	.355	1.05	.22	1.26	.698	16	1.75
9	53.8	.499	.8	.16	.916	261	8.30	.062	.859	.144	.325	1.12	.24	1.35	.709	16	1.75
10	55.4	.476	.8	.14	.973	277	8.12	.061	.817	.157	.377	1.31	.27	1.57	.728	16	1.75
11	57.2	.453	.8	.12	1.10	294	7.91	.061	.778	.173	.454	1.56	.28	1.84	.751	16	1.75
											Σ = 9.8		2.2	12.0	7.57		

STRIPPING SECTION

12	59.9	.534	.80	.14	.579	330	9.77	.056	1.19	.135	.390	1.95	.33	2.30	.755	32	1.75
13	62.1	.487	.80	.14	.606	345	8.96	.056	1.02	.157	.326	1.95	.34	2.29	.803	32	1.75
14	64.5	.474	.75	.14	.636	362	8.84	.055	.960	.162	.314	2.01	.39	2.40	.806	32	1.75
15	67.0	.465	.70	.14	.663	378	8.82	.054	.919	.165	.309	2.09	.39	2.48	.801	32	1.75
16	69.8	.455	.65	.13	.693	395	8.82	.052	.885	.169	.350	2.31	.45	2.76	.792	32	1.75
17	72.7	.412	.65	.12	.721	411	8.18	.050	.755	.197	.343	2.48	.48	2.96	.827	32	1.75
18	75.8	.405	.60	.12	.750	427	8.18	.048	.723	.199	.342	2.60	.50	3.10	.818	32	1.75
											Σ = 15.75		2.85	18.6	5.60		

Total Theoretical Trays (Both Sections) = 13.17

TABLE 2

HIGH PRESSURE COLUMN OPERATION 100 LB./SEC. UNIT

Tray No.	Active Area	Free Area	Tray Section Length/Ft.	Ng	Vs Ft/sec.	Q_L° Ft^3/sec. D'C	h_f (in)	α	$\frac{\Delta P_{DP}}{\Delta P_H}$	ΔP_f psi	ΔP_s (static)	ΔP_T (total)	Eff.	Press. psia	Vs / Vmax.
1	.80	.14	.697	298	5.19	.074	1.30	.195	.433	1.97	.90	2.83	.981	230	.70
2	.80	.14	.735	314	4.65	.074	1.08	.231	.358	1.92	1.28	3.02	.993	233.1	.632
3	.80	.12	.775	331	4.37	.074	.955	.265	.413	2.17	1.37	3.5	.996	236.7	.580
4	.75	.12	.813	347	4.40	.074	1.02	.234	.387	2.23	1.43	3.5	.991	240.3	.572
5	.70	.12	.850	363	4.47	.073	.920	.264	.413	2.31	1.50	3.8	.995	244.1	.570
6	.65	.12	.890	380	4.56	.073	.913	.260	.419	2.40	1.70	4.0	.994	248.2	.570
7	.60	.12	.926	396	4.70	.072	.926	.252	.435	2.50	1.65	4.1	.991	252.3	.577
8	.60	.12	.966	413	4.47	.072	.823	.257	.389	2.47	1.83	4.3	.994	256.6	.538
9	.60	.12	1.00	429	4.25	.072	.735	.300	.349	2.44	1.86	4.4	.996	260.9	.503
									Σ =	20.4	13.5	33.9	8.93		

Tray Spacing = 1 3/4"

only a negligible influence upon tray counts. The major effects of substituting the actual flow circuit are a decrease in product flow due to heat input into the oxygen circuit downstream from the low pressure column and a possible slightly higher product purity due to the flash-off removed from the flash chamber before the recirculating liquid is pumped to the reboiler-condenser.

To account for the fact that the separator rotates, work done by or on the various fluid streams due to the action of the centrifugal field has to be included in the overall energy balance. In the case of the kettle and shelf transfer stream an enthalpy change equivalent:

$$\Delta H = \frac{1}{J} \quad \frac{\omega^2}{2 g_c} \quad (R_2^2 - R_1^2) \qquad (13)$$

was assumed.

The enthalpy change in the feed vapor streams to the two columns due to compression was also calculated from Equation (13) above. This, of course, resulted in some vapor superheat at the periphery of the columns. Since the exact thermodynamic path of the superheated vapor and energy changes within the column were difficult to trace two limiting cases were calculated. In (1) the superheat would result in the vaporization of more liquid and in (2) all of the superheat would go into performing turbine work on the rotor. The enthalpy values listed on the process flowsheet assume that half of the superheat goes into turbine work and half into vaporizing more liquid.

With the above assumptions the heat and mass balance for the circuit can be established in a conventional manner. Figure 15 shows the schematized flow diagram used for calculations.

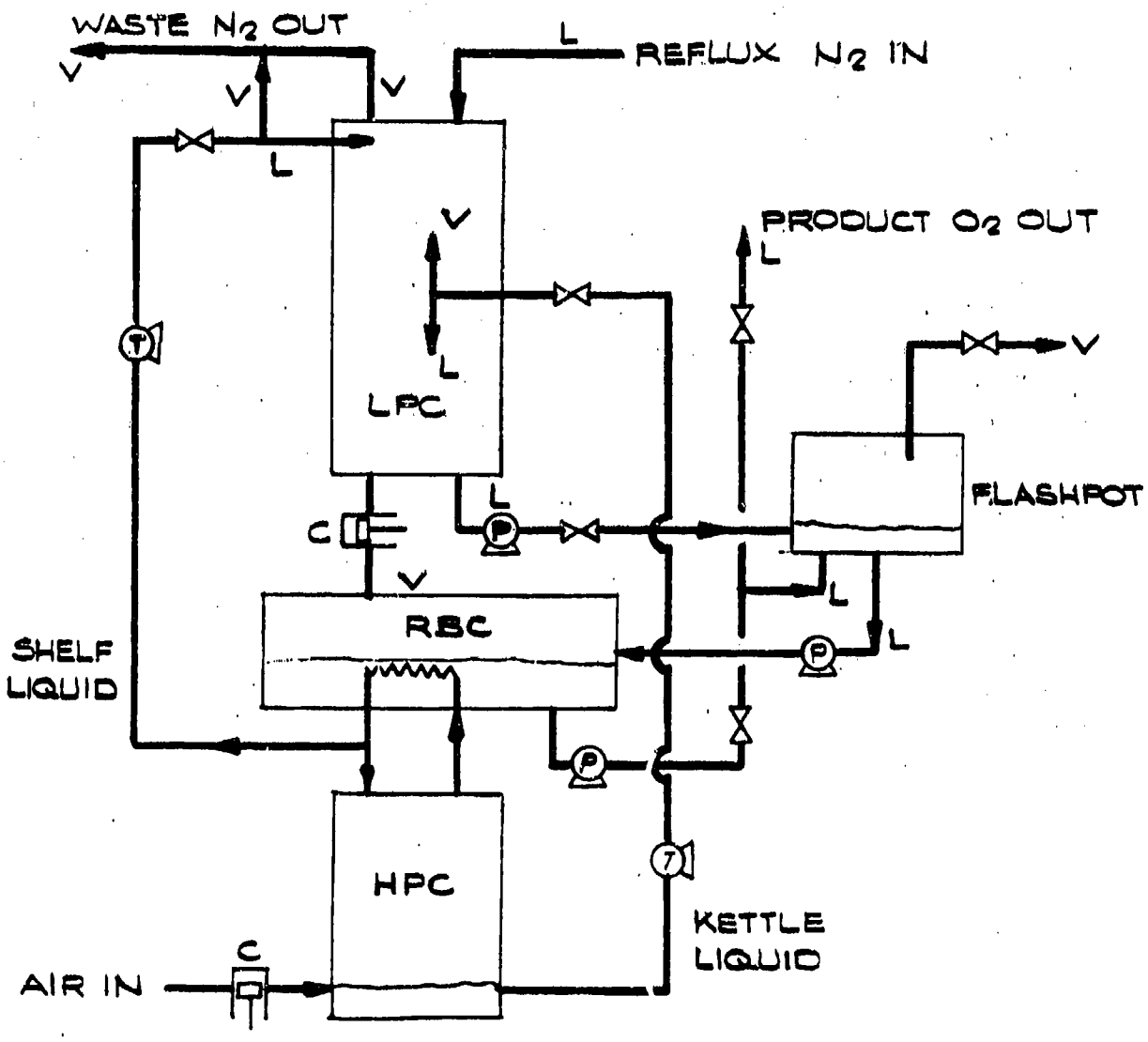

Q_M MECHANICAL HEAT INPUT + HEAT LEAK

C = COMPRESSION
P = PUMP
T = TURBINE-LIKE EXPANSION

V = VAPOR
L = LIQUID

SCHEMATIC FLOW DIAGRAM
BOILERPLATE SEPARATOR

FIG. 15

The flowsheet, Figure 16, lists all the pertinent flow rates, pressures, enthalpies, and compositions prevalent at various points of the boilerplate separator operating at design conditions.

It should be noted that the pressure values listed for the liquid streams downstream from the diffusers were calculated assuming diffuser efficiencies of 20% for the product liquid diffuser and 10% for the low pressure column liquid diffuser. Since in the boilerplate cycle no expansion turbines are used downstream from the diffusers, diffuser efficiency does not affect the cycle balance.

Another point worth mentioning is the pressure profile on the boiling side of the reboiler-condenser. This profile is of considerable importance since it determines the magnitude of the temperature driving force available for heat transfer. For the 100 lb./sec. design it was assumed that some pressure building occurs in the passage as the result of compression of oxygen vapor due to the action of the centrifugal field. Results from the UCON heat transfer tests (Ref. 1, section 4.5.6.4) indicated that above certain flowrates and below certain speeds a pressure rise higher than that calculated from vapor compression was experienced apparently due to the existance of a two-phase flow regime. Comparison of the UCON tester and boilerplate flow conditions indicated that a two-phase flow regime should also exist in the boilerplate model. In the boilerplate design no credit was taken for the additional pressure buildup since it was difficult to accurately estimate the latter and it was also desired to maintain conservative design assumptions. As compression in the boiling passage lowers the required reboiler-condenser liquid inlet pressure, it increases the effective average ΔT along the flow path and is beneficial by reducing either the surface requirements or the high pressure column operating pressure.

4.5 Pressure Drop in Liquid Transfer Lines

Saturated kettle and shelf liquid have to be transfered to the low pressure column against the centrifugal field. The pressure profile for the transfer lines was calculated on the assumption that the friction pressure drop can be neglected and that pressure drop is caused by differences in gravitational head. For the calculation of the profile the correlation and computer program discussed in Ref. 1, section 5 were used. Figures 17 and 18 show the pressure profiles for the two lines. It can be seen that in the kettle transfer lines the major part of the pressure drop is consumed by the transfer line and in the shelf transfer lines the major drop occurs across the valve.

In the calculations performed it was assumed that flow through the lines is isentropic and flow through the valves is isenthalpic.

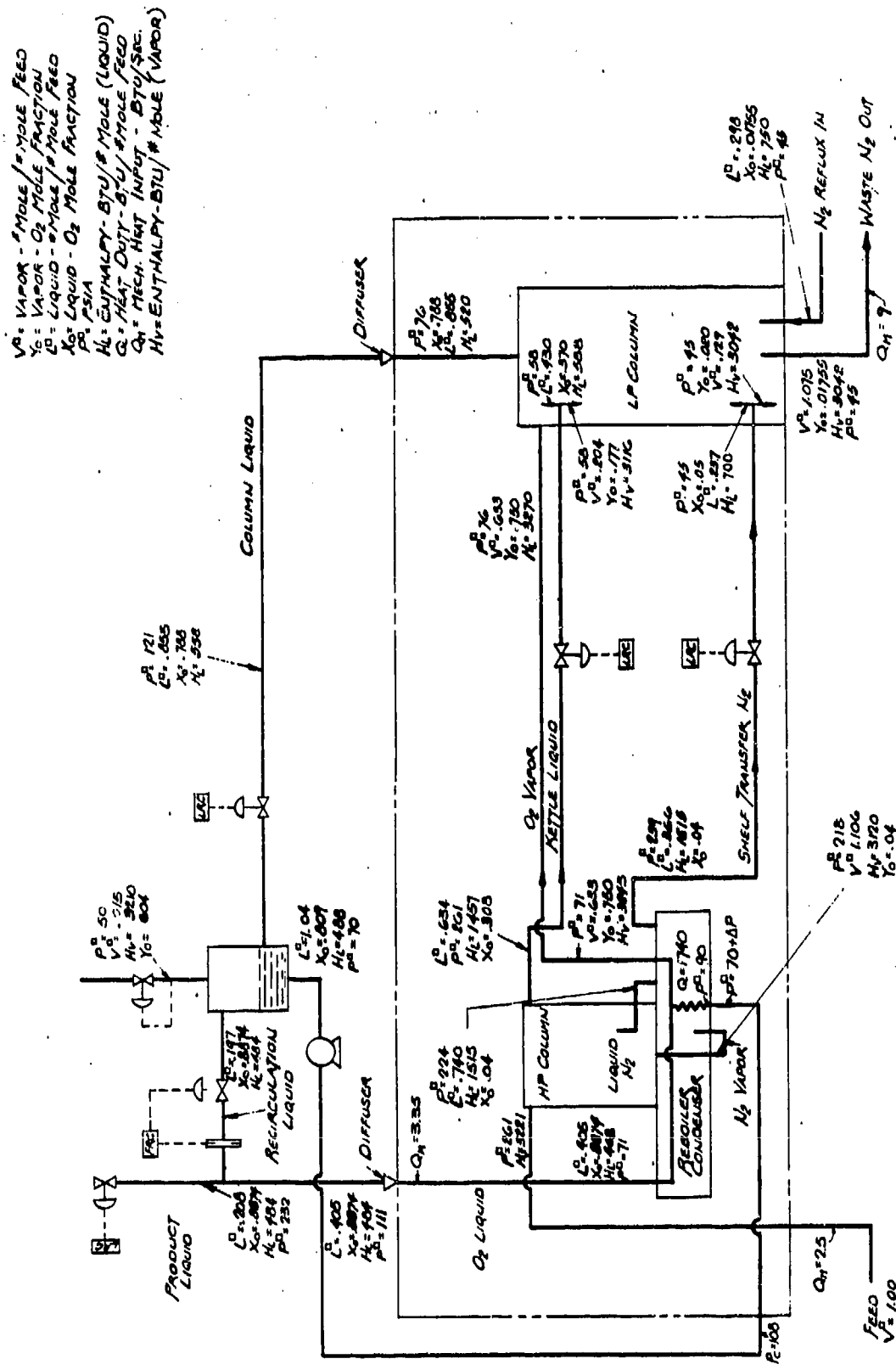

MASS FLOWSHEET - 100 LB/SEC.
SEPARATOR CYCLE

FIG. 16

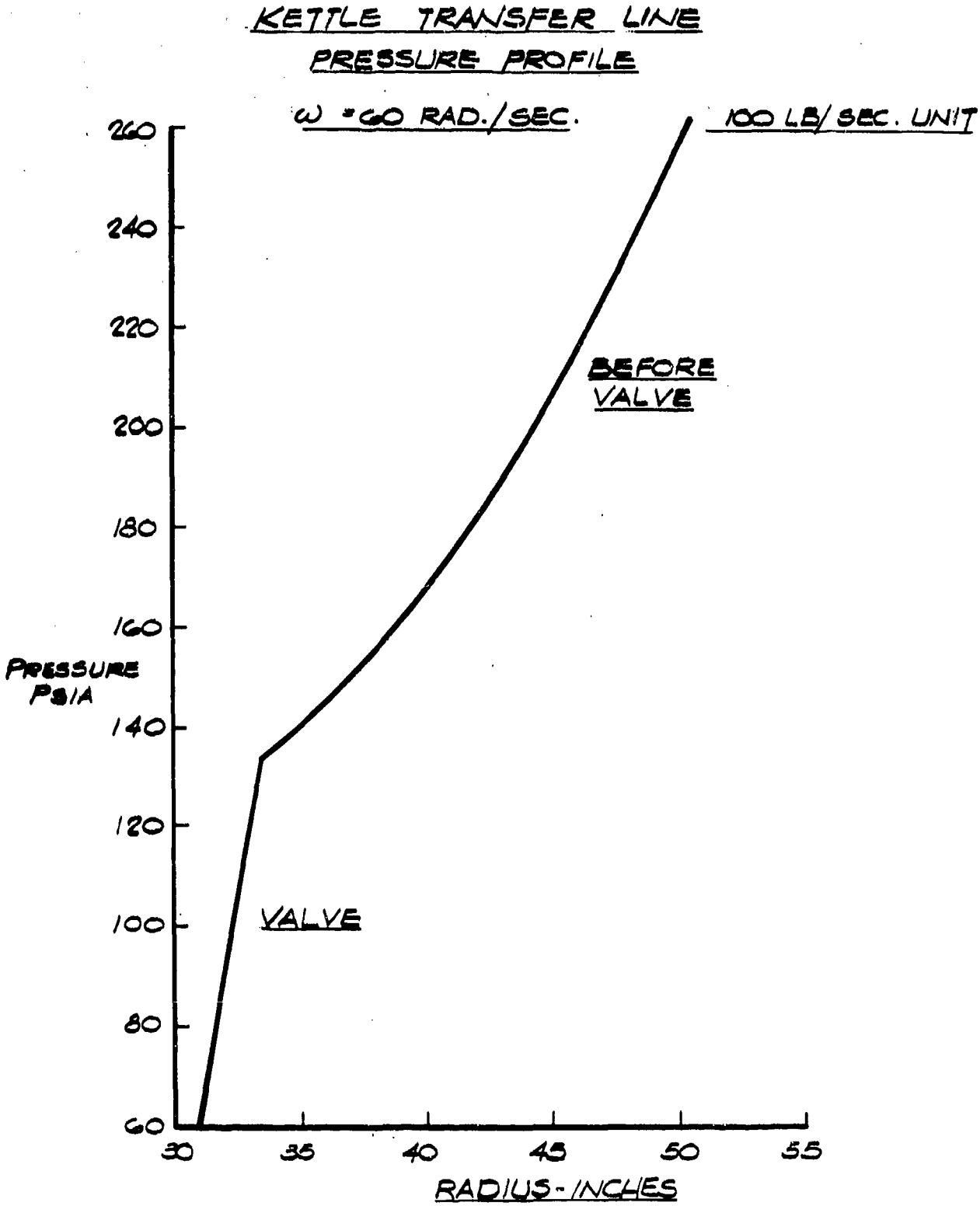
KETTLE TRANSFER LINE
PRESSURE PROFILE
ω = 60 RAD./SEC.
100 LB/SEC. UNIT
260
240
220
200
180
160
140
120
100
80
60
PRESSURE PSIA
BEFORE VALVE
VALVE
30
35
40
45
50
55
RADIUS - INCHES

FIG. 17

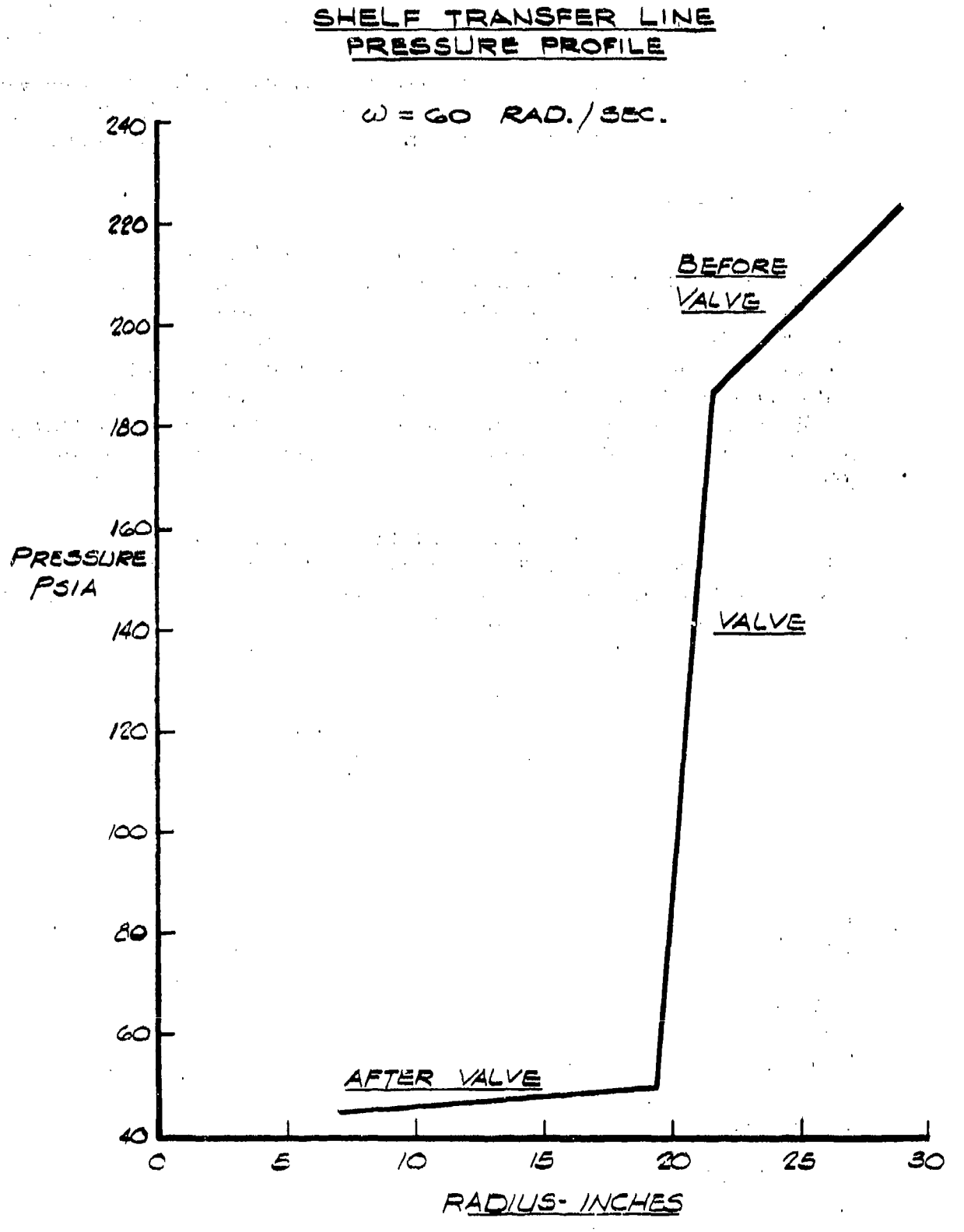
SHELF TRANSFER LINE
PRESSURE PROFILE
ω = 60 RAD./SEC.
240
220
200
180
160
140
120
100
80
60
40
PRESSURE PSIA
BEFORE VALVE
VALVE
AFTER VALVE
0
5
10
15
20
25
30
RADIUS- INCHES

FIG. 18

4.6 Reboiler-Condenser Design

4.6.1 Heat Duty

The reboiler-condenser in the 100 lb./sec. boilerplate separator has the function to transfer 22,000,000 Btu/hr. at a temperature differential of 10.7°F from condensing nitrogen to boiling oxygen.

4.6.2 Geometry

Speed and radial dimensions for the reboiler-condenser were determined from overall separator design considerations. In order to permit effective column operation as well as satisfactory heat transfer performance a compromise speed of 60 rad./sec. (575 rpm) was selected. Radial dimensions were limited by the shaft diameter required for handling fluid quantities of 100 lb./sec. on the one hand and the inner radius of the high pressure column on the other hand. Within these limitations inner radius for the active heat transfer area was fixed at 10 in. and the outer radius at 24 in.

General design of the heat transfer disks followed closely the UCON tester described in Ref. 1, Appendix VIII except for different disk diameters, and in that the starting radius, "r", in the tube geometry equation derived in Ref. 1, Appendix VII,

$$\Theta = \cos^{-1}\left(\frac{r_i}{r}\right) - \sqrt{\left(\frac{r}{r_i}\right)^2 - 1} \qquad (14)$$

was changed to 8.208 inches. This was done because at the time of initial design it was considered desirable to make the exit angle of the tubes 70° with respect to the radial line passing through the point of exit. In later calculations it was found that the exit angle did not materially affect the heat transfer performance of the unit and therefore r_i could have been taken as 10 inches. The general design of the heat transfer disks (before brazing and final machining) can be seen on Figure 19. The exact shape of the curved heat transfer tubes is shown on the attached graph, Figure 20 (in polar coordinates).

The boiling passage width was fixed at 3/16 in. since this width proved adequate in UCON tester experiments and was the smallest that could be easily manufactured.

The tube disks stacked on the shaft to form the appropriate fluid passages are shown schematically in Figure 21.

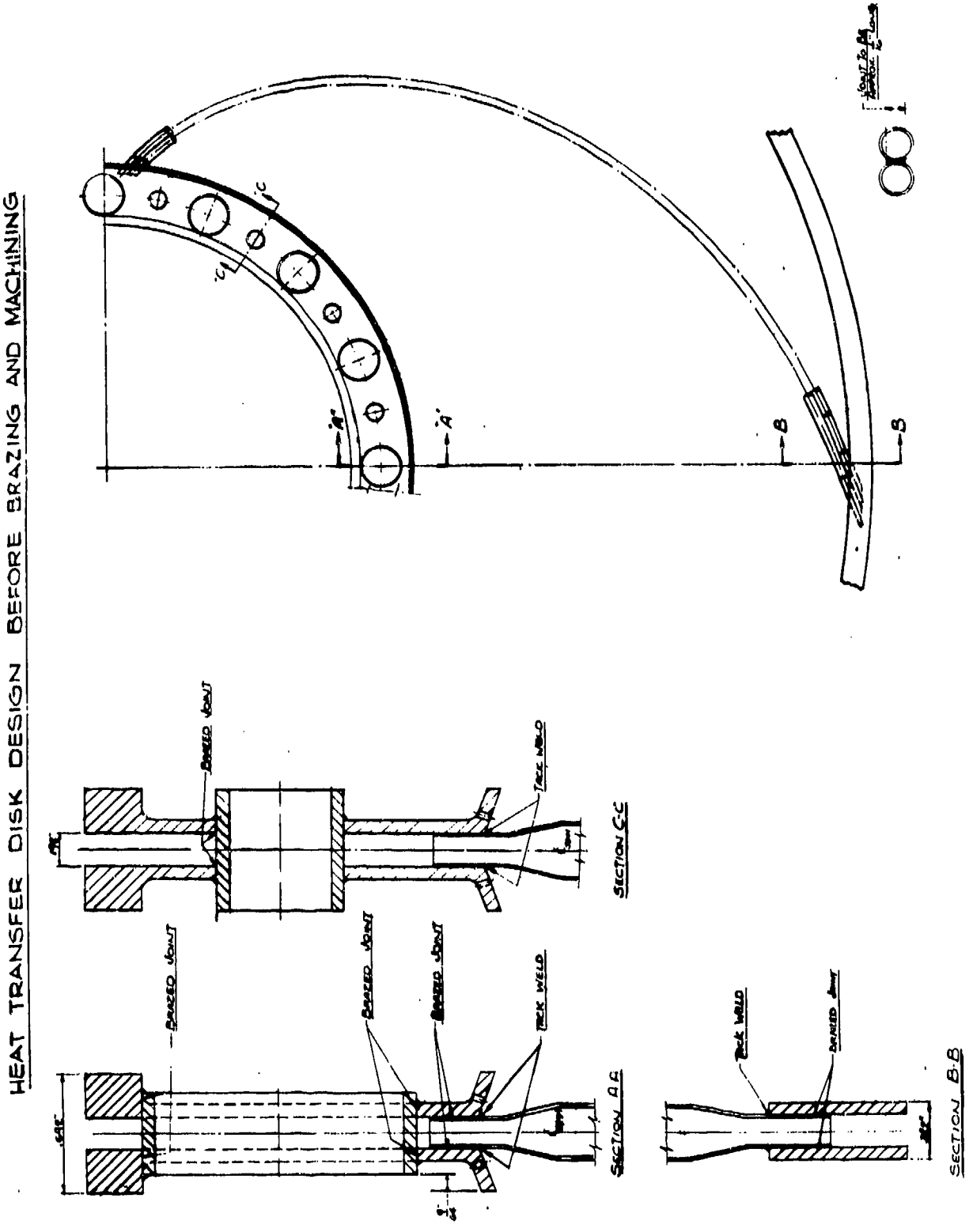
HEAT TRANSFER DISK DESIGN BEFORE BRAZING AND MACHINING
A
A'
B
B
BRAZED JOINT
TACK WELD
SECTION C-C
SECTION A-A
SECTION B-B

FIG. 19

CALCULATED SHAPE OF THE 100 LB/SEC. BOILERPLATE SEPARATOR HEAT TRANSFER TUBES FROM THE GENERAL EQUATION:

$$\theta = \cos^{-1}\left(\frac{r_i}{r}\right) - \sqrt{\left(\frac{r}{r_i}\right)^2 - 1}$$

$r_i = 8.208"$

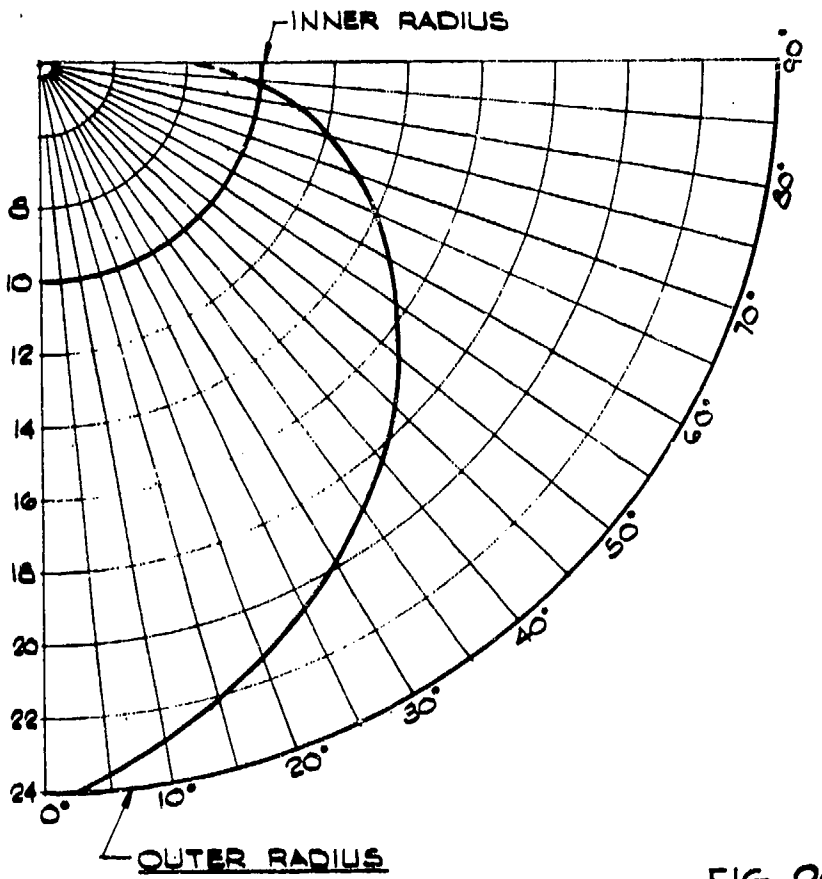

FIG. 20

4.6.3 Analysis

Design for maximum heat transfer requires use of special boiling surfaces and porous condensing surfaces as well as maximum effective heat transfer area. As shown in Table 3, the size of the exchanger can be reduced by 70% by applying a special boiling surface, as was done in the UCON tester. By using a porous condensing surface in addition to a special boiling surface, a reduction in size of 85% can be achieved. (See Table 3).

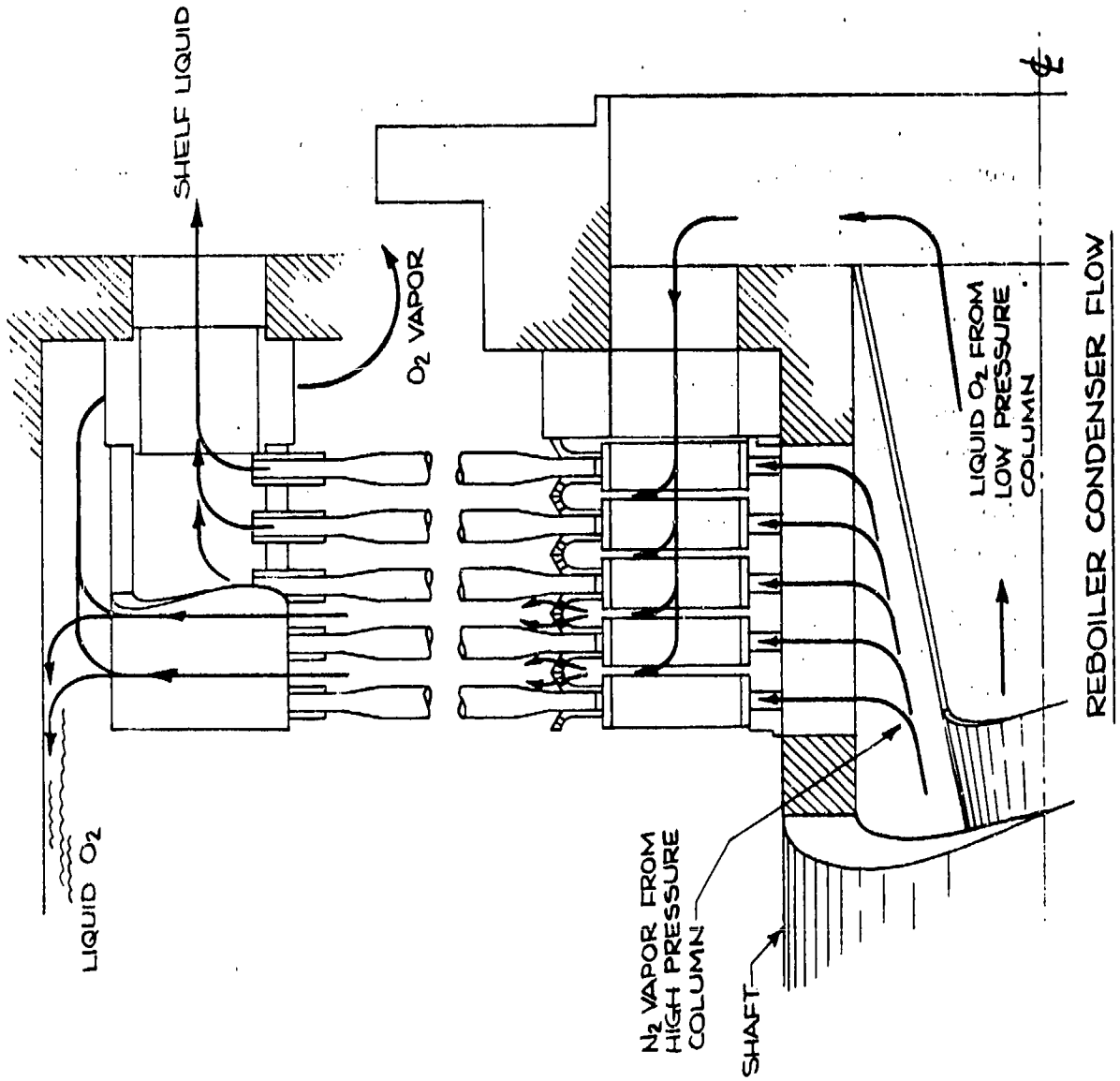
SHELF LIQUID
O2 VAPOR
LIQUID O2 FROM LOW PRESSURE COLUMN
REBOILER CONDENSER FLOW
LIQUID O2
N2 VAPOR FROM HIGH PRESSURE COLUMN
SHAFT

FIG. 21

TABLE 3

Boilerplate Separator

Heat Transfer and Number of Required

Tube Disks for Various Surface Conditions

Surface Conditions	Aver. Overall Heat Transfer Coefficients Btu/ft.^{2}hr./°F	Number of Tube Disks Required in The Heat Exchanger
(1) Smooth Tubes - No special surfaces inside or outside	400	205
(2) Smooth tubes on the boiling side, porous surface on the condensing side	560	145
(3) Special surface on the boiling side	1294	63.25
(4) Special surface on the boiling side and porous surface on condensing side	2730	30.1

The general design of the 100 lb./sec. disks is identical to that of the UCON tester heat transfer disks except the heat transfer characteristics have been changed by applying special surfaces to both sides of the heat exchanger. Even though no experiments were conducted on the performance of porous condensing surfaces in the UCON tester, it was decided to utilize these surfaces because of the potential shown in the "High G Cryostat" tests described in Ref. 1, Section 4.

In the case of the UCON tester disks, heat transfer was controlled by the resistance on the smooth condensing side which is described by the following equation (Nusselt heat transfer equation for filmwise condensation, Ref. 4)

$$h_{c'} = C\left(\frac{K_L^3 \rho_L^2 \lambda}{\mu_L \Delta T_c}\right)^{1/4} \left(\frac{a}{L^o}\right)^{1/4} \qquad (15)$$

In the case of the UCON tester and the 100 lb./sec. unit, with special boiling surfaces, and no condensing surface treatment the total temperature difference between the boiling and condensing streams is a very close approximation of ΔT_c. Calculations indicated that the temperature drop across the tube wall is very small in comparison to ΔT_c.

In the case where a special boiling surface and a porous condensing surface are used the temperature drop in the boiling film and in the tube wall becomes significant and must be described as follows:

$$\Delta T_T = \Delta T_b + \Delta T_W + \Delta T_c = 10.7\,^\circ R \tag{16}$$

The condensing side temperature change can be evaluated by use of equation (17) derived from the correlated data for condensation inside Aluminum tubes with a porous condensing surface as shown in Figure 62 of Ref. 1.

$$\Delta T_c = \frac{Q/A}{h_{c1}} = \frac{(Q/A)^{1.6}}{5160_{\omega}{}^{1.5}} \tag{17}$$

The value of ΔT_W can be found by rearranging the conduction heat transfer formula and applying the design conditions.

$$\Delta T_W = \frac{Q/A}{k/t_t} = \frac{Q/A}{62,400} \tag{18}$$

The value of ΔT_b must be evaluated from emperical evidence. An emperical formula derived from the available data presented in Figures 41 and 42, Ref. 1, is given as equation (19)

$$Q/A = 7,000\ \Delta T_B{}^{1.2} \tag{19}$$

It should be noted that this formula only holds for oxygen boiling at 70 psia. Equation (19) was then rearranged to give ΔT_B as shown in Equation (20).

$$\Delta T_B = \left[\frac{Q/A}{1,320}\right]^{.813} \tag{20}$$

Equations (17), (18) and (20) were then substituted into Equation (16) and rearranged to obtain an overall heat transfer, Equation (21).

$$\omega = \left[12.1 \frac{(Q/A)^{1.6}}{62,400\Delta T_o - 47.5\,[(Q/A)]^{.813} - (Q/A)} \right]^{2/3} \qquad (21)$$

Figure 22 gives a summary of the solution of this equation for various angular velocities and temperature differentials. The design point for the reboiler-condenser lies at ω = 60 rad./sec. and ΔT_o = 10.7°F for which predicted heat flux is approximately 30,000 Btu/nr./sq.ft. Physical properties for use in these equations can be obtained from Ref. (5) and (6).

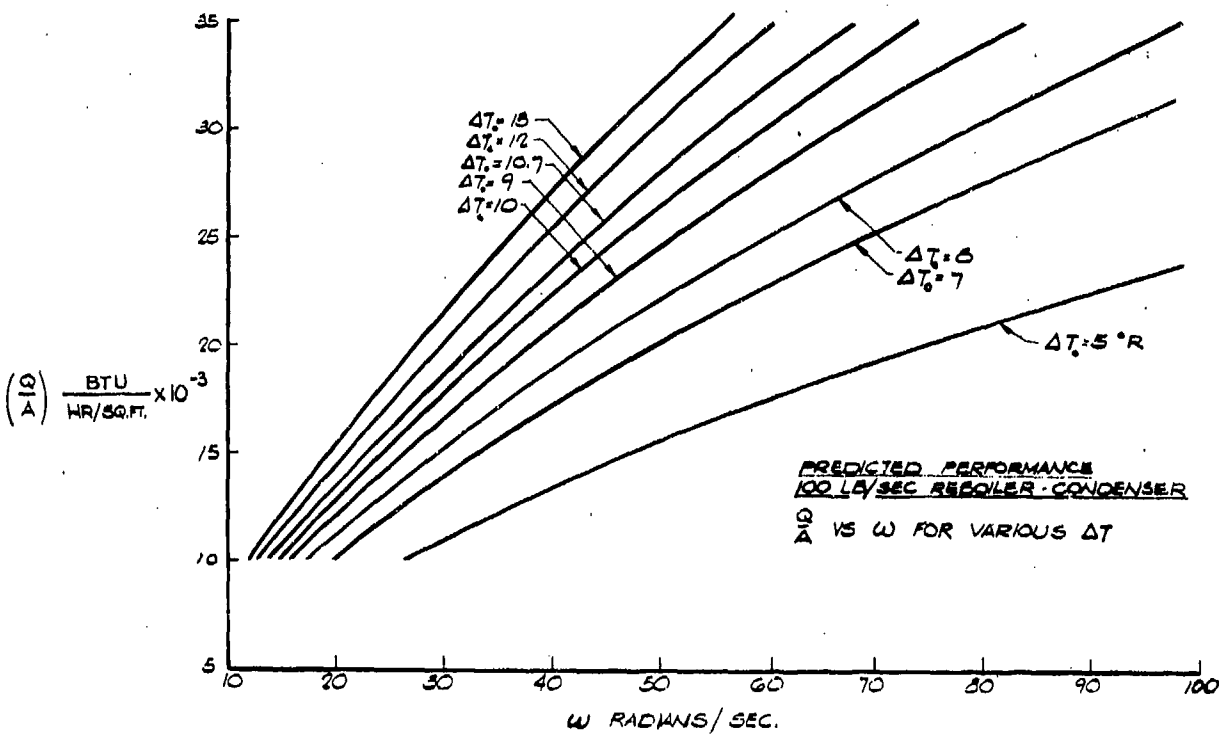

FIG. 22

It should be noted that the above heat fluxes are average for the unblanketed area of the heat exchanger thus neglecting the insulating effect of the condensate on the area it covers as it flows along the bottom of the tube. Equations in Section 4 of Ref. (3) must be used to determine the blanketing angle under the design considerations.

As mentioned earlier, 30 heat transfer disks are required in the boilerplate separator if both boiling and condensing surfaces perform as predicted. Total space available in the unit can accommodate a maximum of 65 disks (the number required to transfer the required amount of heat with smooth condensing surfaces). In view of lack of confirming data on the performance of porous condensing surfaces in a larger scale UCON test, it was decided to initially install 45 heat transfer disks with porous condensing surfaces in the boilerplate separator rather than the calculated number of 30 to make certain that the unit can operate within the given pressure boundaries. Excess disks can be removed from the unit later if not required.

4.7 Operation of Separator at Off-Design Conditions

A study was made of separator operation at off-design conditions in terms of variations of speed and throughput. It was found that the efficient operating range of the separator is limited by the columns. In particular, operation of the unit is limited by flooding of the innermost tray of the enriching section of the low pressure column and dumping of liquid on the outermost trays of both sections of the low pressure column.

The possible operating range for the separator is illustrated on Figure 23. It can be seen that the "operating line" lies roughly halfway between the dumping and flooding lines which define the maximum and minimum speeds at which the separator can be operated with a given throughput. Decreasing throughput requires an approximately proportional reduction in speed to stay within the operating range and vice versa. Increased throughput demands higher speed. It should be noted that the limiting lines denote only flooding or dumping of the most critical trays. Operation beyond these lines should be possible with only a slight decrease in separator efficiency.

Since column pressure drops as well as reboiler-condenser performance depend upon rotational speed and throughput or heat flux, in case of the reboiler-condenser, the reboiler-condenser ΔT and the required separator inlet pressure will vary with changes in speed and throughput. The changes in ΔT and inlet pressure associated with operation along the operation line of Figure 23 are depicted on Figure 24.

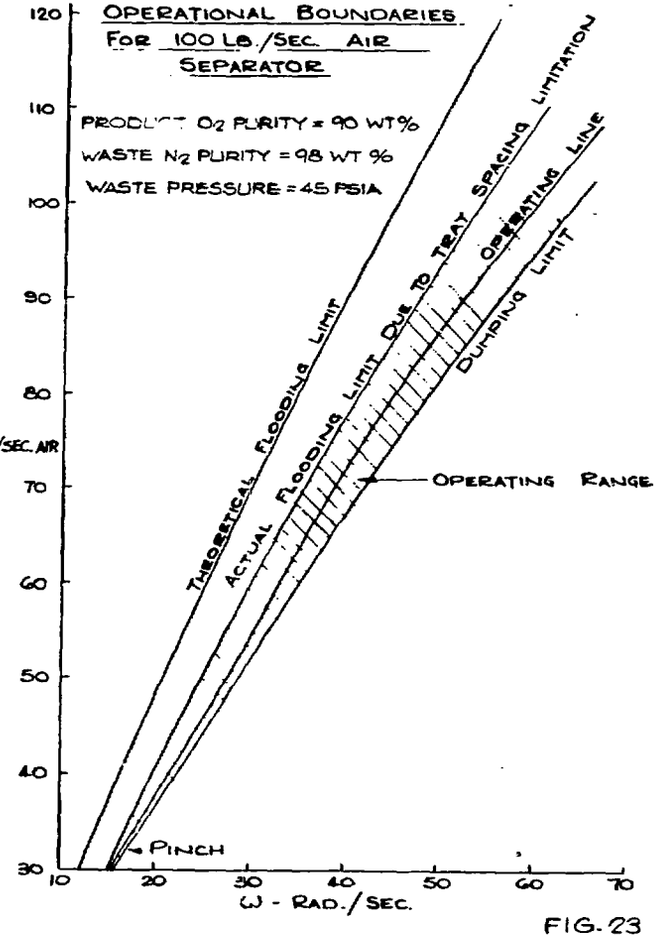
OPERATIONAL BOUNDARIES
FOR 100 LB./SEC. AIR
SEPARATOR
PRODUCT O2 PURITY = 90 WT%
WASTE N2 PURITY = 98 WT %
WASTE PRESSURE = 45 PSIA
THEORETICAL FLOODING LIMIT
ACTUAL FLOODING LIMIT DUE TO TRAY SPACING LIMITATION
OPERATING LINE
DUMPING LIMIT
OPERATING RANGE
PINCH
FEED-LB/SEC. AIR
ω - RAD./SEC.

FIG. 23

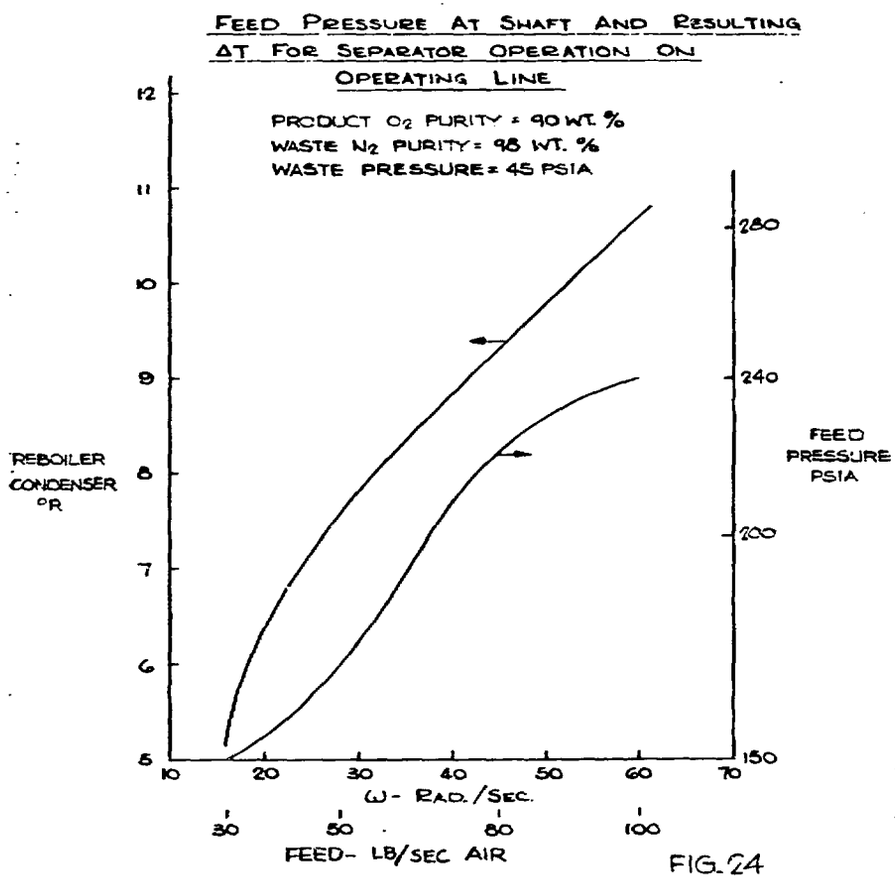
FEED PRESSURE AT SHAFT AND RESULTING
AT FOR SEPARATOR OPERATION ON
OPERATING LINE
PRODUCT O2 PURITY = 90 WT. %
WASTE N2 PURITY = 98 WT. %
WASTE PRESSURE = 45 PSIA
REBOILER CONDENSER °R
FEED PRESSURE PSIA
ω - RAD./SEC.
FEED- LB/SEC AIR

FIG. 24

(THIS PAGE IS INTENTIONALLY BLANK.)

5.0 MECHANICAL DESIGN

5.1 Design Philosophy

As mentioned earlier, general design of the boilerplate model was primarily dictated by functional considerations and the demand for flexibility due to the essential research nature of the apparatus. The latter demand required that the unit be constructed from modules which could be removed and exchanged individually and be sufficiently instrumented to permit adequate interpretation of performance of various separator elements. Accordingly the boilerplate model consists of four basic modules: a reboiler-condenser, a high pressure column, a low pressure column enriching section, and a low pressure column stripping section. To further enhance flexibility within the columns, individual trays are removable and are exchangeable as are heat transfer disks within the reboiler-condenser. Representative tray sections within each column section can be viewed through windows to permit observation of hydraulic behavior of trays. This feature together with strategically placed transducers is intended to establish hydraulic behavior of trays.

Mechanically, the design attempts to create as reliable a unit as possible in that all structural elements were made considerably stiffer than required. In moving elements such as seals and bearings, designs similar to those which could find application in future flightweight separators are utilized to provide opportunity for check on operation of those essential elements in cryogenic service. As mentioned earlier, lightweight construction was subordinated to functional and reliability considerations. To some extent, cost and tight fabrication schedules dictated selection of mechanical design.

5.1.1 General Assembly

Figure 25 shows sections through the assembly of the boilerplate separator. As indicated the selected design features a central shaft (consisting of seven sections) to which the reboiler-condenser casing and the enriching section of the low pressure column are attached by means of bolted flanges. The high pressure column is mounted outside the reboiler-condenser casing and the low pressure column stripping section outside the enriching section. The actual assembly of these units comprising the entire rotating element is shown in figure 26.

All vapor streams are introduced to or discharged from the separator through the 14 to 16 in. diameter hollow shaft which is partitioned and ported to provide the correct flow paths for the various streams. Size of the shaft is governed by the need for reasonable

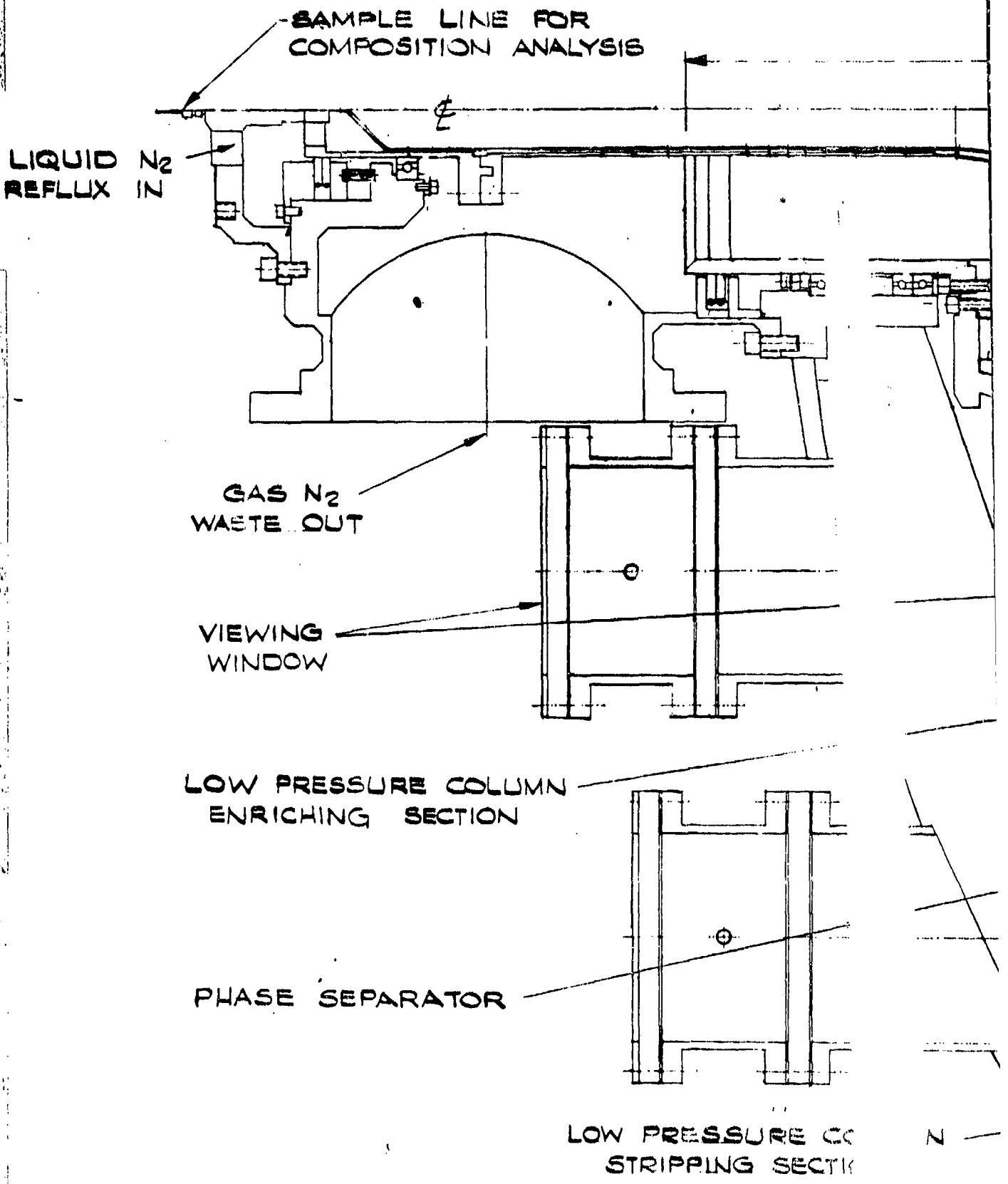

1075

SEAL

STATI ARY D

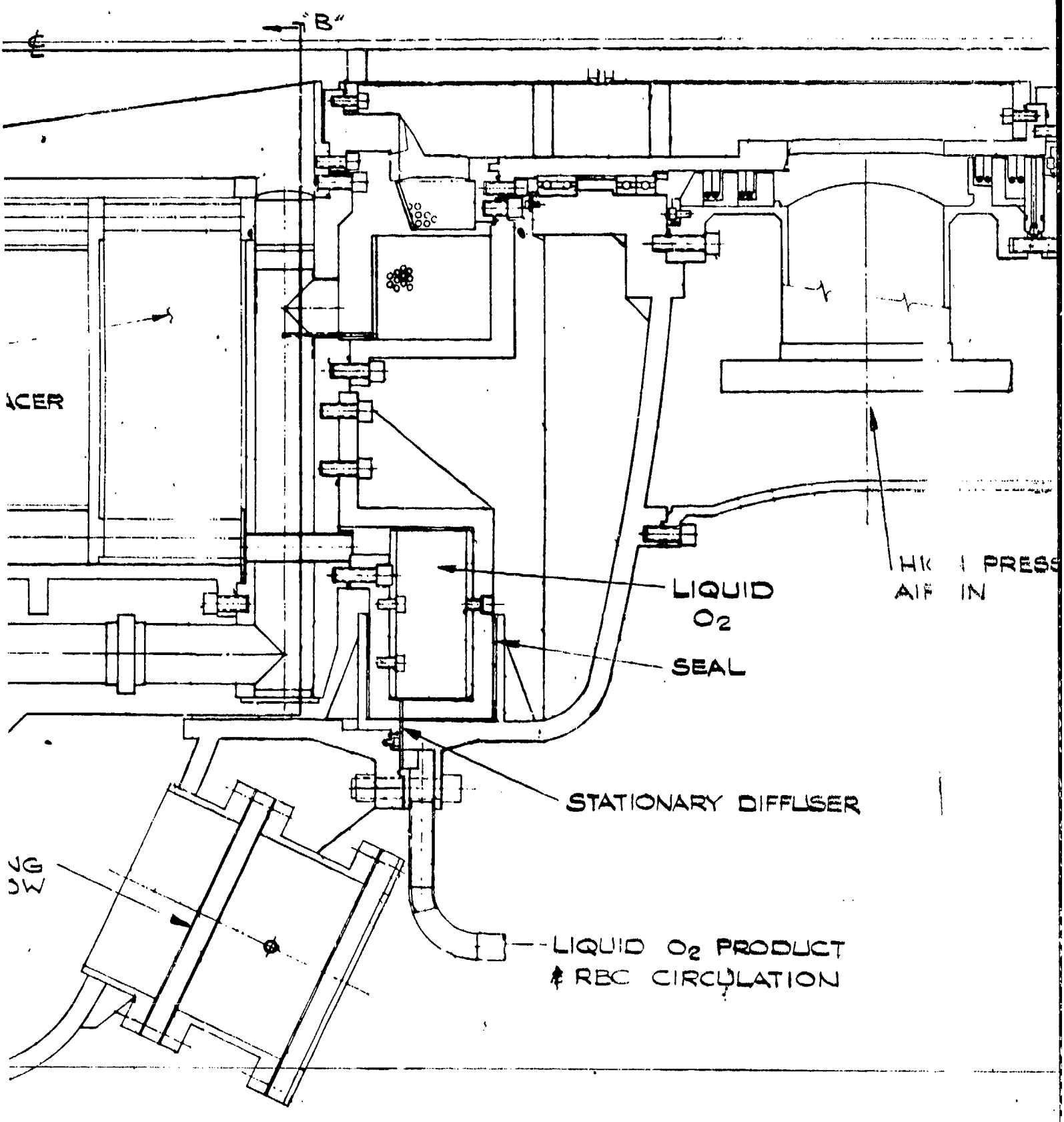
PROX 13'-11½"
"B"
ACER
LIQUID
O2
SEAL
STATIONARY DIFFUSER
LIQUID O2 PRODUCT
& RBC CIRCULATION

ROTOR LENGTH: APPROX

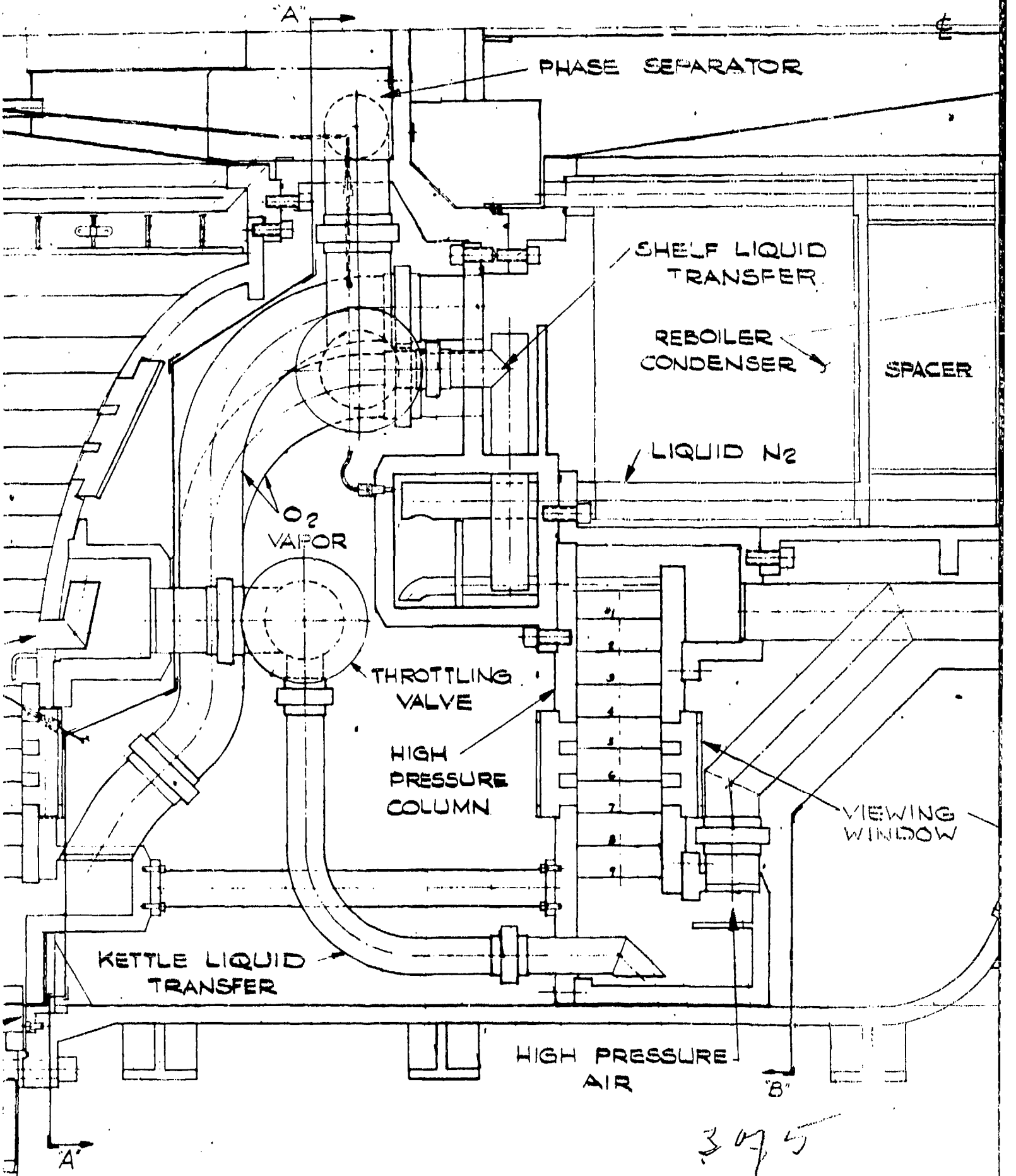

3075

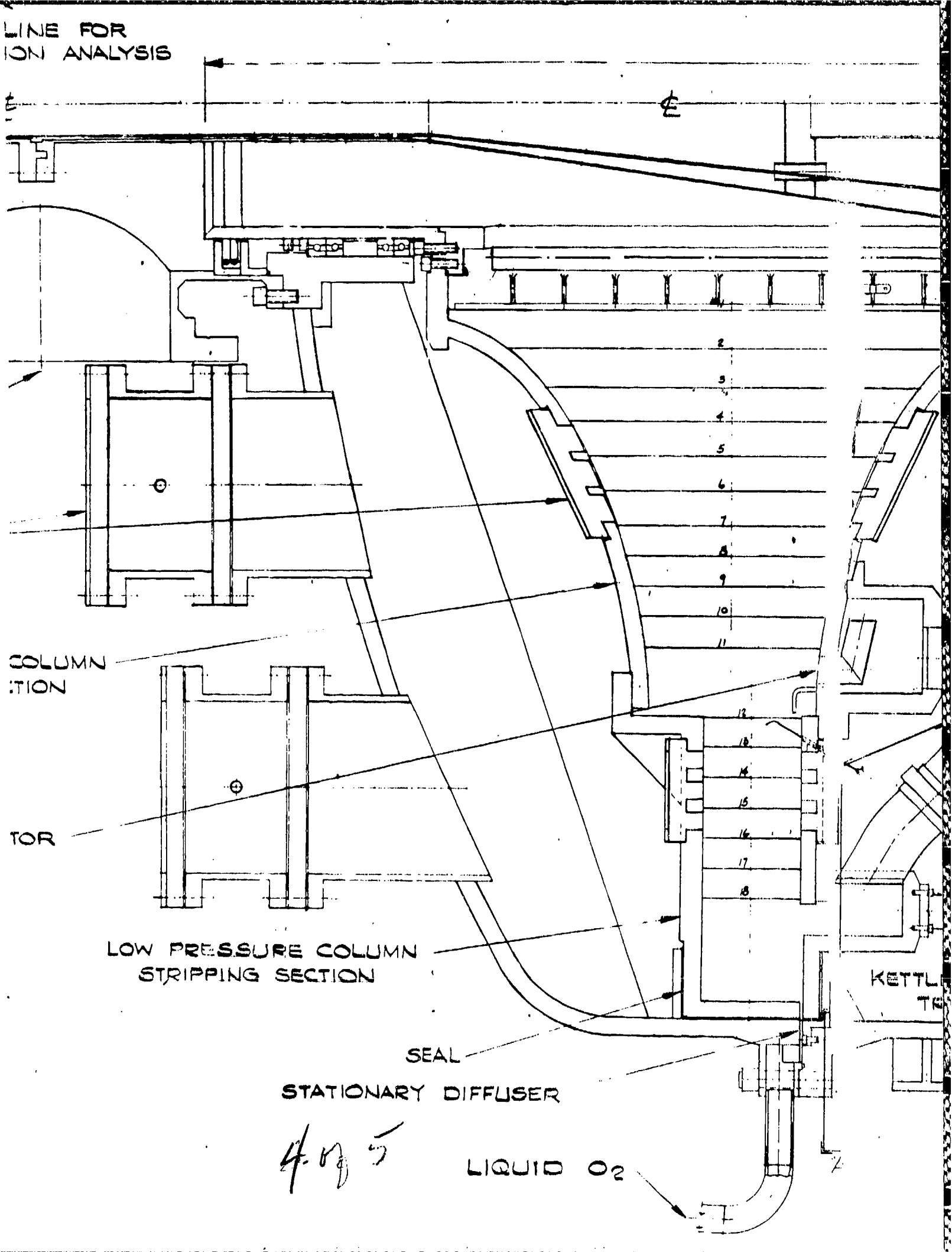
LINE FOR
ION ANALYSIS
COLUMN
:TION
TOR
LOW PRESSURE COLUMN
STRIPPING SECTION
SEAL
STATIONARY DIFFUSER
LIQUID O2
KETTL
TE
2
3
4
5
6
7
8
9
10
11
12
13
14
15
16
17
18

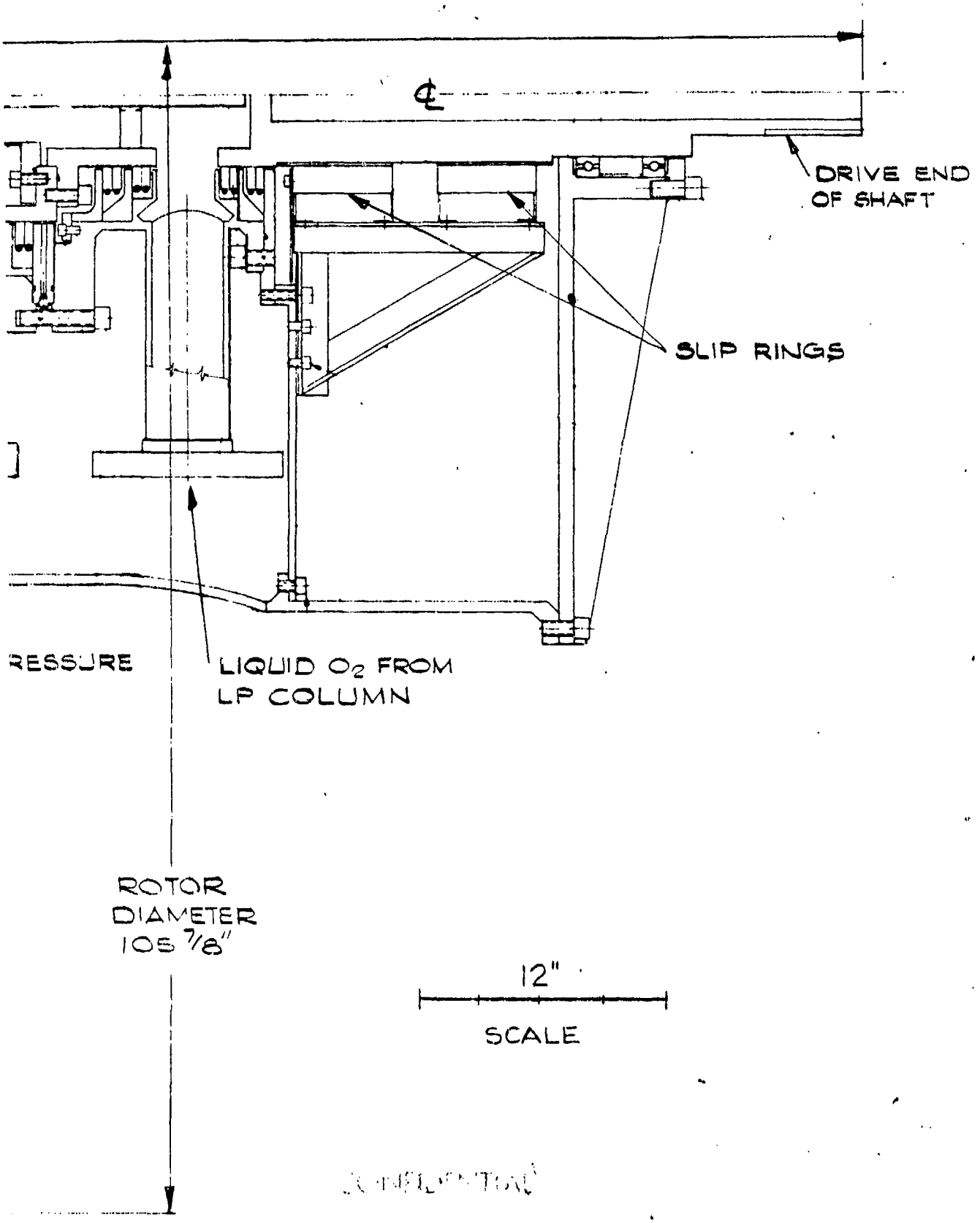

ASSEMBLY - "BOILERPLATE"
AIR SEPARATOR

15 1/3

FIG. 25

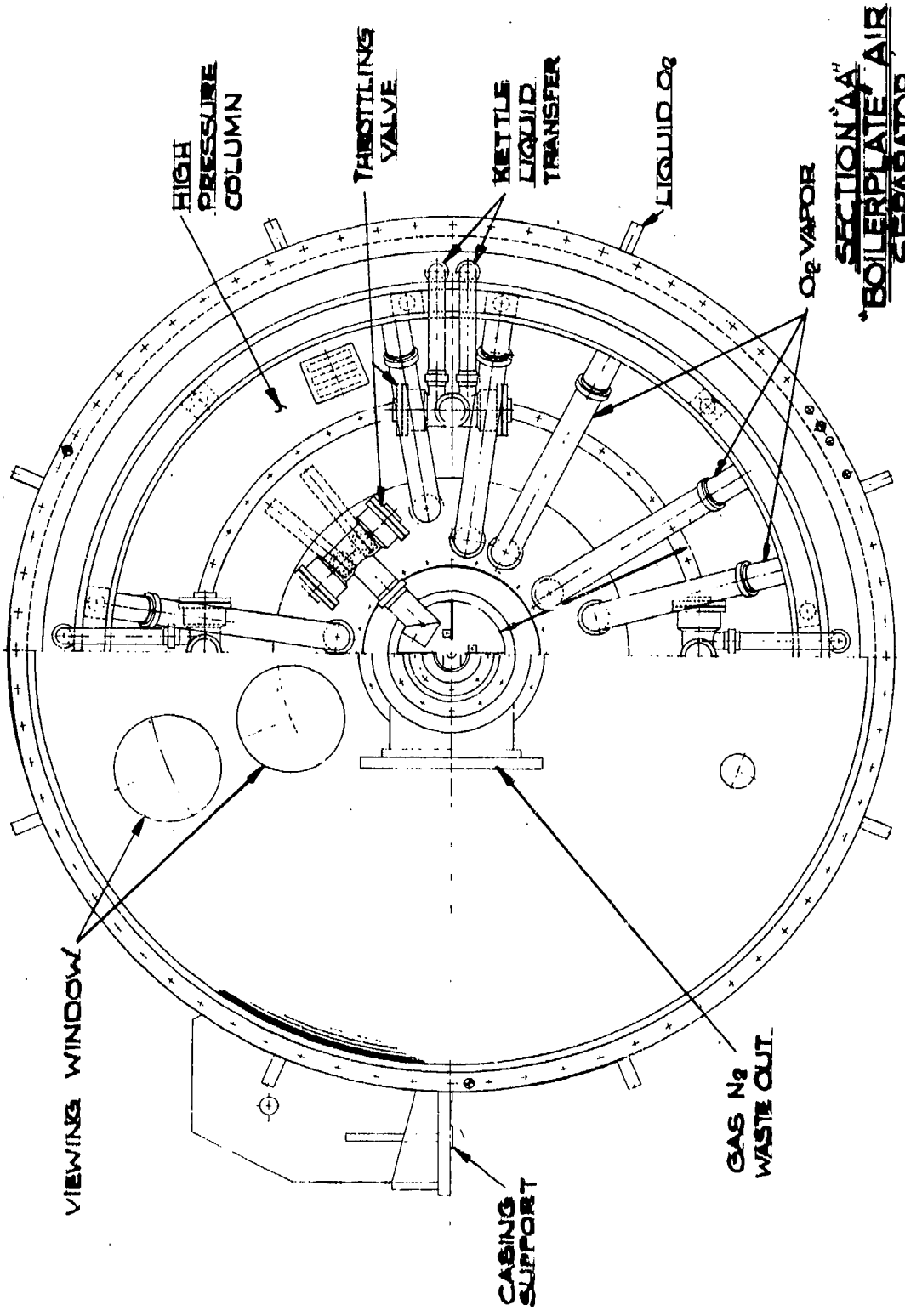
HIGH PRESSURE COLUMN
THROTTLING VALVE
KETTLE LIQUID TRANSFER
LIQUID O2
O2 VAPOR
SECTION "AA" BOILER PLATE AIR SEPARATOR
VIEWING WINDOW
GAS N2 WASTE OUT
CASING SUPPORT

FIG 25a

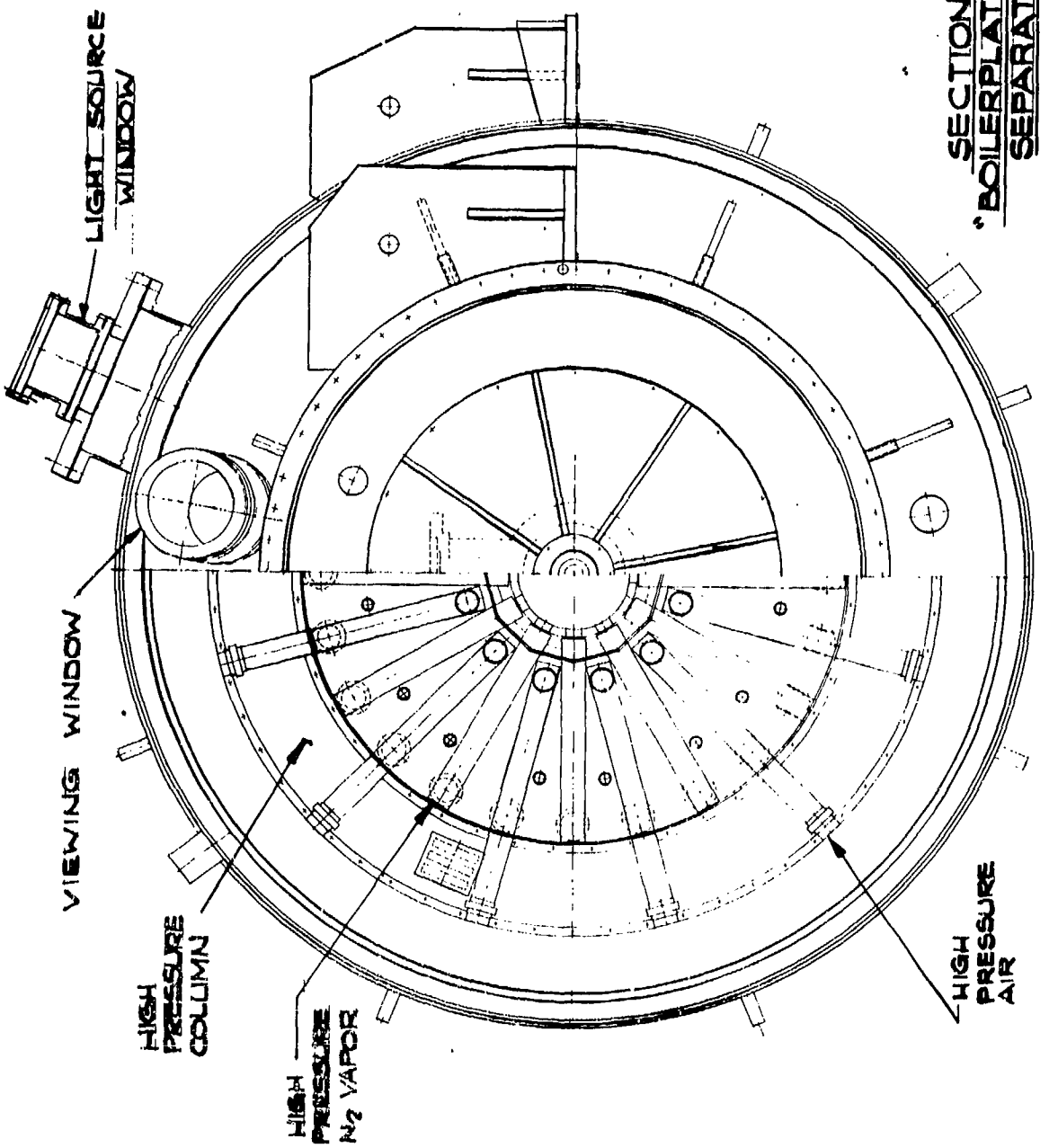
SECTION BB
"BOILERPLATE" AIR
SEPARATOR
LIGHT SOURCE
WINDOW
VIEWING WINDOW
HIGH
PRESSURE
COLUMN
HIGH
PRESSURE
N2 VAPOR
HIGH
PRESSURE
AIR

FIG. 25c

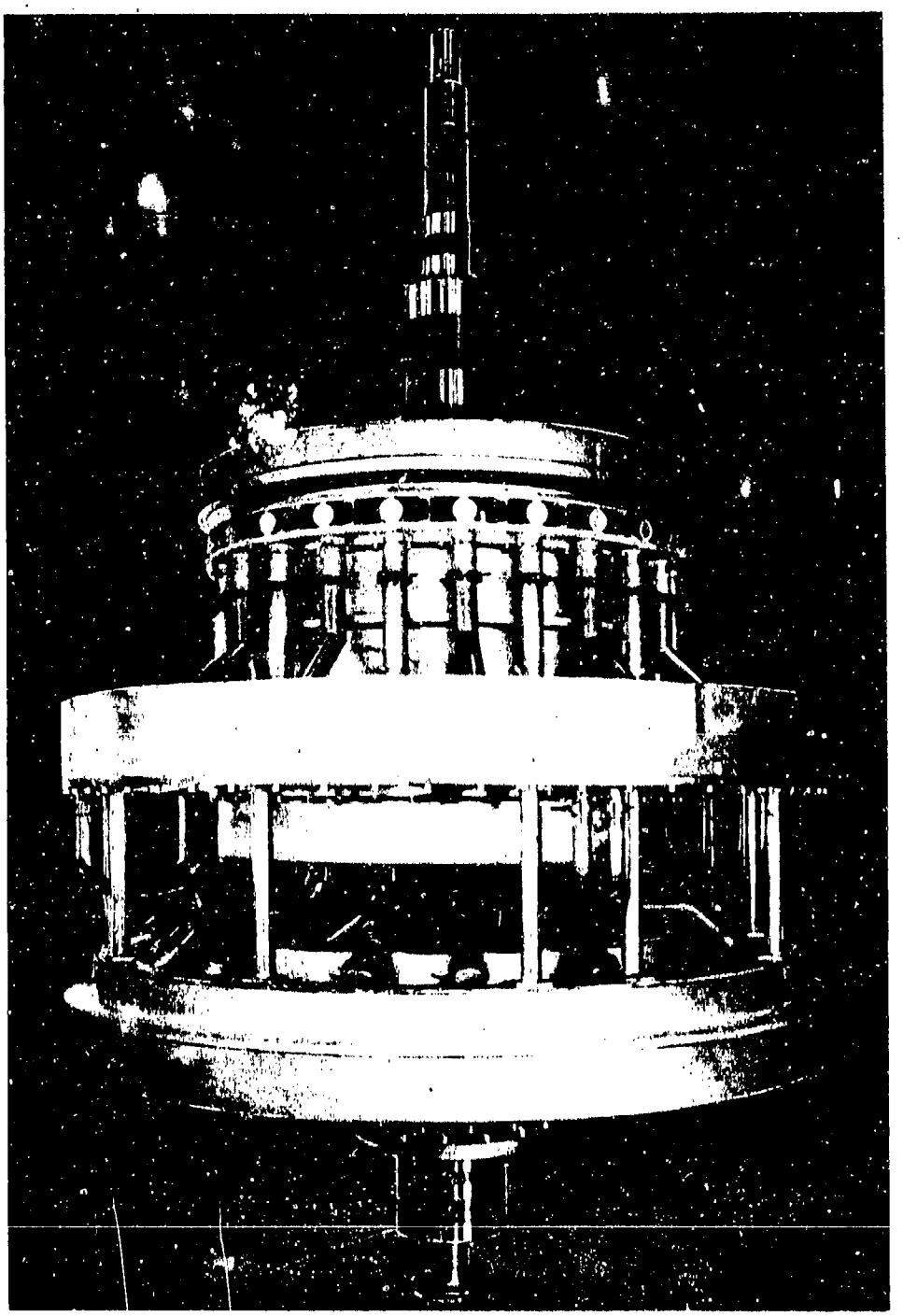

BOILER PLATE SEPARATOR ASSEMBLY

FIG.26

velocities for the high pressure air feed and nitrogen waste streams. Inside the shaft concentric pipes are mounted for the introduction of liquid oxygen to the reboiler-condenser and reflux nitrogen to the low pressure column. The liquid pipes fan out into conical sections to maximize possible internal holdup volumes for the various liquid streams.

Wherever liquid-vapor mixtures are to be introduced into a component such as at the kettle and shelf liquid introduction points to the low pressure column, attempts are made to provide good circumferential fluid distribution by first separating the mixture utilizing the centrifugal field and then introducing the liquid through flow restricting orifices with liquid level in the appropriate holdup chamber providing the driving force for distribution. A similar scheme is utilized at the air inlet to separate entrained liquid from the vapor stream and distribute the liquid uniformly over the various pipes to the high pressure column periphery. Uniform circumferential distribution of liquid is considered essential to avoid excessive radial unbalance.

As mentioned earlier, transfer of shelf and kettle liquid from the high pressure column to the low pressure column are regulated by pneumatic control valves to maintain a constant liquid level in the respective holdup chambers. Liquid collector chambers are designed to provide for a maximum liquid holdup corresponding to from 2-5 sec. of liquid flow.

As indicated, the separator rotor is supported by four sets of angular contact ball bearings which are mounted in the casing hubs. An additional set of bearings supports the overhanging shaft and associated coupling weight at the drive end of the shaft to avoid excessive runout at the slip rings and liquid oxygen shaft seals. At the opposite shaft end, an intricate concentric sealing arrangement utilizing labyrinth seals permits withdrawing samples of shelf nitrogen from the high pressure column and vapor from underneath the kettle feed plate of the low pressure column during separator operation for composition analysis.

The casing housing surrounding the rotor is designed sufficiently heavy to withstand pressures higher than low pressure column operating pressures. This was for reasons of safety in the test installation and to permit operation of the separator even in case of improper performance of the peripheral liquid seals. The casing also houses the peripheral diffusers into which liquid is discharged through slots in the low pressure column and reboiler-condenser casing peripheries.

As can be seen the columns and casing are equipped with windows to permit observation of representative trays during tests. Lighting means for observation are furnished by a strobe light through appropriate mirror arrangements.

Aluminum was uniformly selected as the material for all structural components of the separator. Since use of aluminum was mandatory in the reboiler-condenser from heat transfer, fabrication and weight considerations it was selected for the construction of other components to avoid design complications and stresses arising from the use of different structural materials as the result of differential thermal contraction. At the same time aluminum has the advantage of good low temperature properties (impact, strength and ductility), fairly good strength, ease of fabrication, availability and reasonable cost.

5.2 Detail Design

5.2.1 Casing

5.2.1.1 Introduction

The casing of the 100 lb./sec. boilerplate model air separator is, in essence, a modified pressure vessel which serves two primary functions. First, it supports the shaft with the entire rotating assembly at the bearings and transmits this load to the foundation. Secondly, it contains the peripheral seal leakage fluid and in so doing functions as an unfired pressure vessel. The design of such a vessel depends upon a great many functional considerations dictating many of the dimensions of the vessel as well as the stress levels encountered, which must be determined by a design analysis.

A rigorous analytical analysis for stresses and deflections in machines of this complexity is, of course, impractical and appropriate assumptions and approximations must be employed. For reasons of safety, reliability, and emphasis on the term "boilerplate", a deliberate attempt to over-design was made in areas where a rigorous mathematical analysis is not feasible. Thus, the casing is designed with the generous use of gussets, stiffeners, etc., to compensate for the inaccuracies of the analytical methods.

The individual components of the casing have been designed using the methods of Section VIII of the ASME Boiler and Pressure Vessel Code Ref. 7 (hereafter referred to as the Code) where applicable. Since the loading of the components is not only pressure loading (because of the presence of the rotating internal components), the vessel cannot be classified as a code vessel. The principal shear

stress theory has also been employed, with the necessary assumptions, as a comparison with the ASME code values. Finally, and most important, the composite casing has been analyzed graphically. This last approach is by far the most accurate and most reliable of the methods used. It provides a means for obtaining the deflections and the vibration characteristics of the system. A summary of the pertinent results of each analysis is given in Table 4.

TABLE 4

CASING CHARACTERISTICS

Item	Calculated Value
ASME CODE PRESSURE RATING OF 108" O. D. HEAD	169 PSI
ASME CODE PRESSURE RATING OF 72" O.D HEAD	84 PSI
APPROXIMATE COMBINED STRESS IN 108" CYLINDER SHELL	7100 PSI
MAXIMUM CASING DEFLECTION - FRONT PLANE	.0000279 IN.
MAXIMUM CASING DEFLECTION - SIDE PLANE	.0001439 IN.
COMPOSITE FIRST NATURAL FREQUENCY OF CASING	473/SEC.
106" I. D. FRONT END FLANGE:	
HUB STRESS (MAY BE 1.5 x DESIGN STRESS)	23,600 PSI
TANGENTIAL STRESS	-4,300 PSI
RADIAL STRESS	15,900 PSI
106" I. D. REAR END FLANGE:	
HUB STRESS (MAY BE 1.5 x DESIGN STRESS)	15,750 PSI
TANGENTIAL STRESS	-3,400 PSI
RADIAL STRESS	15,500 PSI
70" I. D. FRONT END FLANGE:	
HUB STRESS (MAY BE 1.5 x DESIGN STRESS)	6,700 PSI
TANGENTIAL STRESS	3,000 PSI
RADIAL STRESS	12,700 PSI
70" I. D. REAR END FLANGE:	
HUB STRESS (MAY BE 1.5 x DESIGN STRESS)	12,100 PSI
TANGENTIAL STRESS	-2,800 PSI
RADIAL STRESS	13,800 PSI

5.2.1.2 General Design Considerations

Design and material selection for the casing of the boilerplate model air separator is dictated by two major factors -- the nature and magnitude of the applied forces and the environment in which the equipment will be required to operate.

Since aluminum had been selected as the material of construction it was necessary to find an alloy of suitable strength, good low temperature properties, and capable of being joined by welding methods. 5083 Aluminum was finally selected. The alloy (magnesium being the principal alloying element) displays excellent low temperature characteristics and good strength properties even in heat affected zones near welds.

The pertinent properties of 5083-0 are shown in Figure 27.

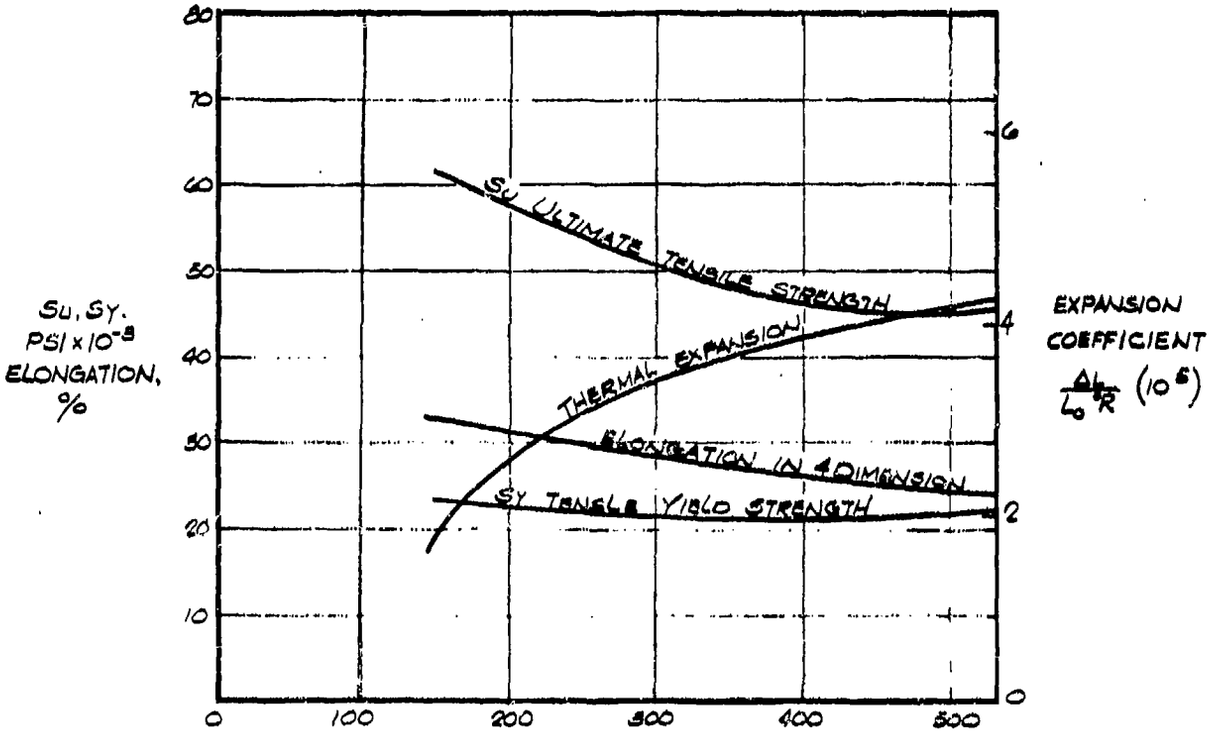

PROPERTIES OF 5083-O ALUMINUM

FIG 27

The Aluminum Company of America (Ref. 8) lists the following wrought properties for this alloy:

	At 75°F	At -320°F
Ultimate Tensile Strength, psi	42,000	60,000
Yield Tensile Strength, psi	21,000	24,000
Endurance Limit at 500 x 10^6 cy, psi	22,000	---

Since the controlling loads and pressures will exist only when the machine is cold and operating, it seems logical that the mechanical properties to be used in the design analysis are the low temperature properties. More specifically, the design is based upon an allowable stress obtained by dividing the yield tensile strength at -320°F by a suitable "factor of safety" or "design factor". The selection of the design factor depends upon the kind of material used, the nature of the loads, the distribution of the stresses, and the safety limitations.

A lower design factor is allowable if the materials used in the design remain ductile under operating conditions than if they become brittle. All of the structural materials used in this machine remain ductile under operating conditions.

Usually a cycling load requires a somewhat larger design factor than a static load. The endurance limit of 5083-0 aluminum, however, is slightly larger than the yield strength. This fact combined with the short design life of the machine tends to reduce the importance of designing for fatigue. Although the component designs incorporate many features which serve as areas of stress concentration, the ductile properties of the materials will allow local yielding and stress redistribution if the stresses become excessive at these points. Another consideration in selecting a design factor is the method used to calculate the principal stress. In general, when a choice of methods was available, the method which resulted in the most conservative value was used.

Based upon these considerations, an allowable design stress of 16,000 psi was selected for 5083-0 aluminum.

This is equivalent to design factors of:

$\frac{24,000}{16,000}$ = 1.5 based upon the yield strength at -320°F

$\frac{21,000}{16,000}$ = 1.3 based upon the yield at 70°F

$\frac{60,000}{16,000}$ = 3.75 based upon the ultimate at -320°F

$\frac{42,000}{16,000}$ = 2.6 based upon the ultimate at 70°F

Both static and dynamic forces exist in this machine. The static forces consist of the weight of each component acting on its supports, and the pressure which must be contained by various members. The nature and magnitude of these forces can be accurately computed. The weights are functions of the dimensions and densities of the materials and the pressures are well known from the performance and flow characteristics. The dynamic forces are inertial forces caused by the rotation of the internal components. They consist of internal centrifugal forces acting on the machine elements, and the unbalance caused by maldistribution of the flowing fluid. The first force can be determined accurately; the latter ones cannot. To arrive at working figures, this study has assumed that a certain fraction of all rotating liquid will be maldistributed. In the absence of experimental evidence it was necessary to assume values for the fraction of liquid maldistributed. The assumed figures are thought to yield somewhat conservative design results.

5.2.1.3 Heads

Three commercially available heads are used in the construction of the casing of the boilerplate model air separator. The front, or waste discharge end of the casing is an ASME flanged and dished head made of 5083-0 aluminum alloy. The dimensions are:

Dish radius	R_d	=	102 in.
Inside corner radius	R_{ic}	=	6-1/2 in.
Thickness	t_h	=	1 inch
Outside diameter	D_o'	=	108 inches

The transition between the 108 in. O.D. cylinderical shell surrounding the columns and the 72 in. O. D. cylindrical shell surrounding the drive end of the reboiler-condenser is also a 5083-0 aluminum ASME flanged and dished head of the same dimensions. The drive end of the casing is a 5083-0 aluminum flanged and shallow-dished head with the following dimensions:

Dish radius	R_d	=	144 in.
Inside corner radius	R_{ic}	=	3 in.
Thickness	t_h	=	1 in.
Outside diameter	D_o'	=	72 in.

If the pressure forces are considered separately, the resulting stresses in an unstayed head may be calculated by the equation of paragraph UA-4 (d) of Section VIII of the Code. Manipulation of the equation gives:

$$S_1 = \frac{P' (R_d M + 0.2_h)}{Et_h} \tag{22}$$

Stresses of 4890 psi for the 108 in head and 9800 psi for the 72 [illegible]ead result. Thus, both types of heads are capable of supporting th[illegible]al pressure of 55 psig without the addition of gussets. The gu[illegible] required to provide support for the bearing loads and to supple[illegible] design to compensate for the inaccuracies of the stress calculations.

Several approximations may be made of the loading. The ASME Code formula as used above assumes that the head supports the pressure alone. The pressure stresses could be superimposed upon those caused by the bearing loads if the bearing support is regarded as a beam. Another method would be to assume that the bearing reactions are supported by the gussets which are approximated by prismatic columns fixed at both ends. This should be a conservative assumption since the head will keep the gusset from buckling. The critical load for such a gusset would be:

$$P_{cr} = \frac{4\pi^2 EI}{L_g^2} = 3.7 \times 10^{10} \text{lb.} \tag{23}$$

which is far greater than any load to which the gusset may be subjected. Thus, the addition of the gussets results in a conservative design.

5.2.1.4 Cylindrical Shell

The cylindrical shell which forms the center section of the casing is also fabricated from 5083-0 aluminum alloy. The casing is supported at this section. This configuration may be closely approximated by a cylindrical shell under internal pressure as described in Paragraph UG-27 of Section VIII of the Code. The equation of UG-27(c) is applicable. Using the allowable stress of 16,000 psi as discussed in Section III and a casing pressure of 70 psia, the required thickness is

$$t_c = \frac{P'Ri}{S_1 E_j - 0.6P'} = 0.443 \text{ inches} \quad (24)$$

Since the remainder of the casing is fabricated from one inch plate and since the non-pressure loading is somewhat unique, the cylindrical shell is also constructed of one inch plate. In addition, T-shaped stiffening rings are provided and the radius transition region is reinforced with triangular-shaped gussets.

The Code values may be compared with an approximate analysis as follows: the axial tension around the circumference of the shell is the flange bolt tension, $F_t \approx 5{,}000$ lb./in. The shear resulting from the static weight and dynamic unbalance is $F_s \approx 50$ lb./in. Distribution of the support forces around the circumference is $F_{cs} \approx 125$ lb./in. The moment resulting from the bearing reactions outside the boundaries of the shell gives rise to tensile forces on the upper half of the shell and compressive forces on the lower portion. This moment is approximately 450,000 in. lb. acting around the circumference of the shell. This may be approximated by a force acting 2/3 of the total distance away from the neutral axis or $F_{equ.} \approx 65{,}000$ lb. For forces other than at the supports:

$$S_2 = \frac{P'(R_i - R_o)}{2\,t_c} = 3740 \text{ lb.in.} \quad (25)$$

$$S_1 = \frac{P'(R_i + R_o)}{4t_c} + \frac{F_t}{\pi\,(R_o^2 - R_i^2)} + \frac{2\,F_{equ.}}{\pi\,(R_o^2 - R_i^2)} \approx 7000 \text{ lb./in.}^2 \quad (26)$$

The load contributed by the supports as given by Roark, Ref. 9, Case 19, Page 160 results in stresses of $S_{ie} \approx 250$ lb./in.^{2} and $S_{se} \approx 90$ lb./in.^{2} Thus, applying the principal shear stress theory:

$$S_1 = \frac{S_1 + S_2}{2} + \left[\left(\frac{S_1 + S_2}{2}\right)^2 + S_s^2\right]^{1/2} \approx 7100 \text{ psi} \quad (27)$$

The maximum shear stress theory and the maximum strain energy theory both yield small values. The above stress value is nearly identical to that which is obtained by solving the Code equation for the stress in a one-inch cylindrical shell. The precautionary additions to the shell result in substantial safety.

5.2.1.5 Casing Flanges

The bolted flange connections for the casing sections are machined 5083-0 aluminum ring forgings. The configuration is shown schematically in Figure 28. Such a flange is regarded by the Code as

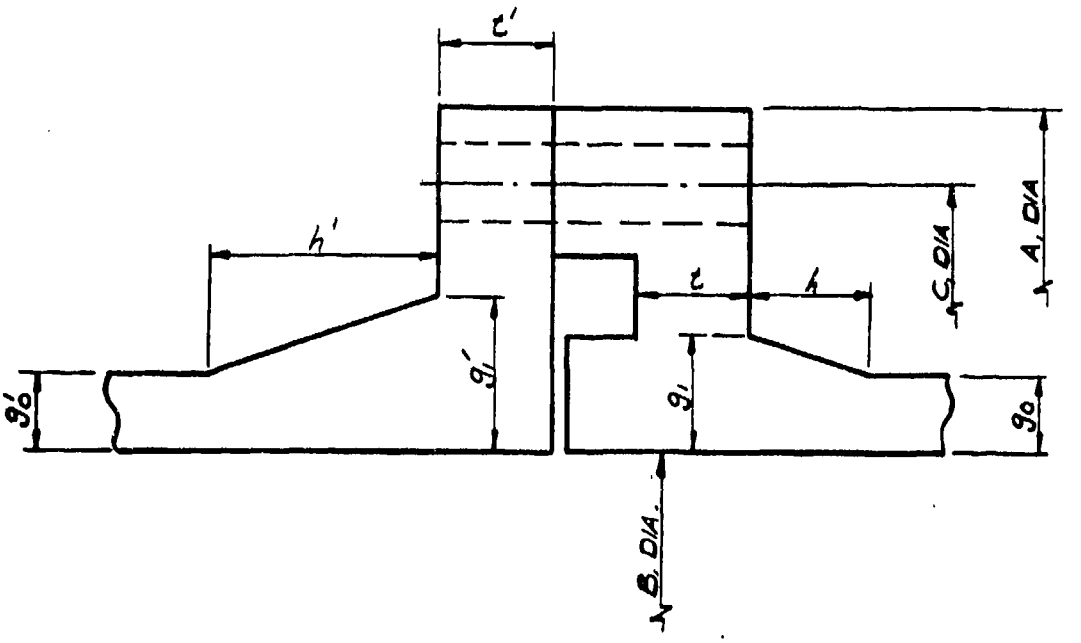

CASING FLANGE CONFIGURATION

FIG. 28

an integral flange. All dimensions with the exception of the flange thickness may be determined from the dimensions of the mating components. The thickness may be determined by applying the methods of Section VII, Appendix II of the Code. The forces acting upon the flange are the internal casing pressure, the post-diffuser collector pressure, and the gasket sealing forces. To minimize the gasket load required, a Teflon*-coated aluminum O-ring is used. The radial, tangential, and hub stresses are plotted against flange thickness for each flange in Figure 29A through Figure 29D.

5.2.1.6 Composite Casing

Since an attempt has been made to provide a sufficient margin of safety in the design of the individual casing components, by far the most important analysis is that of the casing as a composite structure. A schematic diagram of the loading appears in Figure 30. The bearing reaction forces, F(t), vary with time due to the periodic nature of the rotating unbalance and may be expressed as:

$$F(t) = [\, F_u^{\,2} - 2\,(F_s + F_c)\, F_u \sin \omega t_i - (F_s + F_c)^2 \,]^{1/2} \qquad (28)$$

FLANGE STRESS VS. THICKNESS
FOR FRONT-END 106" I.D. FLANGE

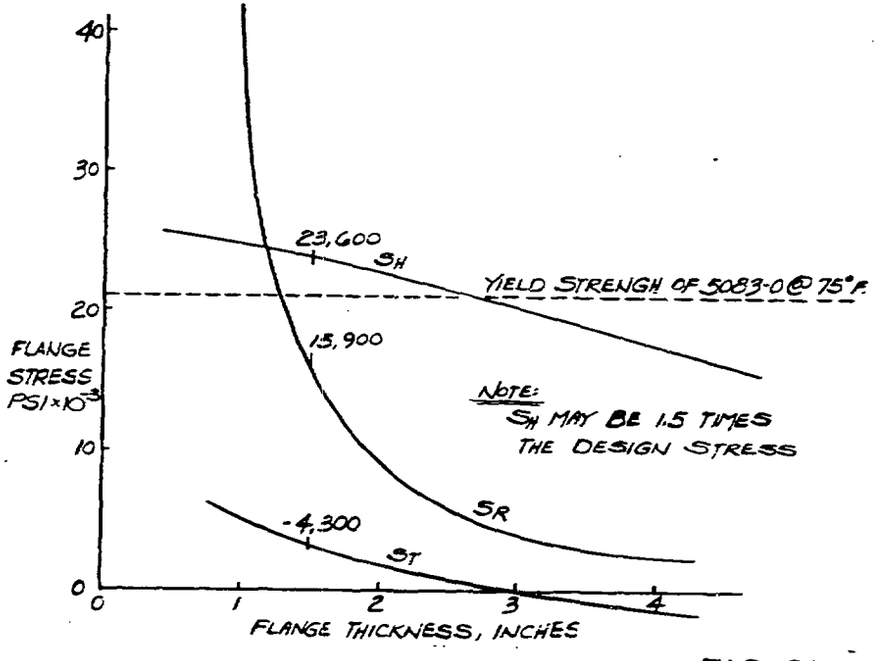

FIG. 29A

FLANGE STRESS VS THICKNESS
FOR REAR-END 106" ID FLANGE

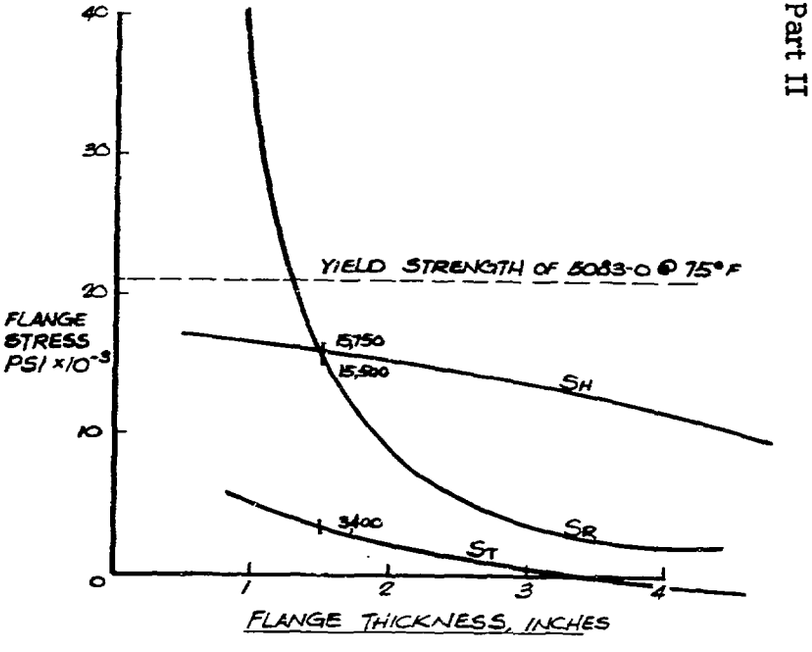

FIG. 29B

FLANGE STRESS VS THICKNESS
FOR FRONT END 70" I.D. FLANGE

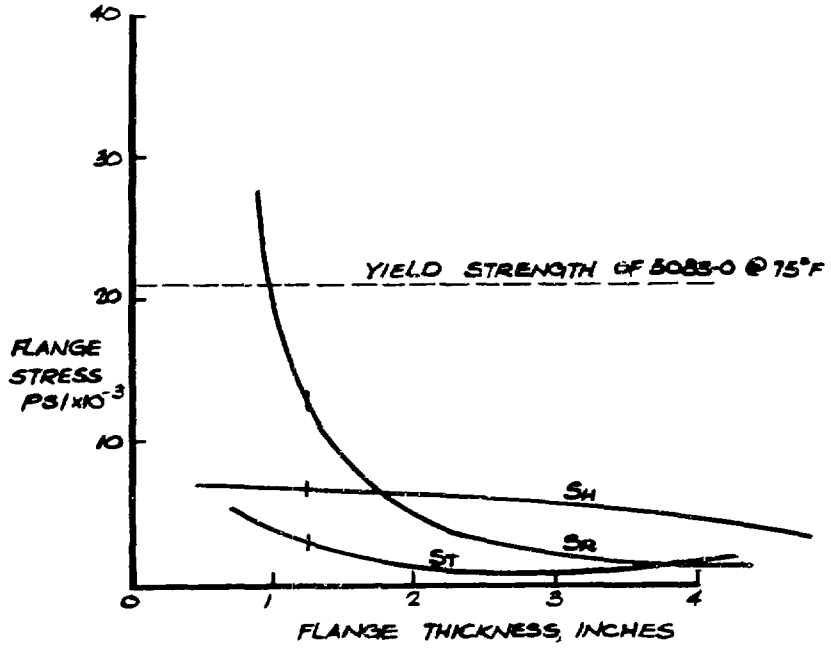

FIG. 29c

FLANGE STRESS VS THICKNESS
FOR REAR END 70" I.D. FLANGE

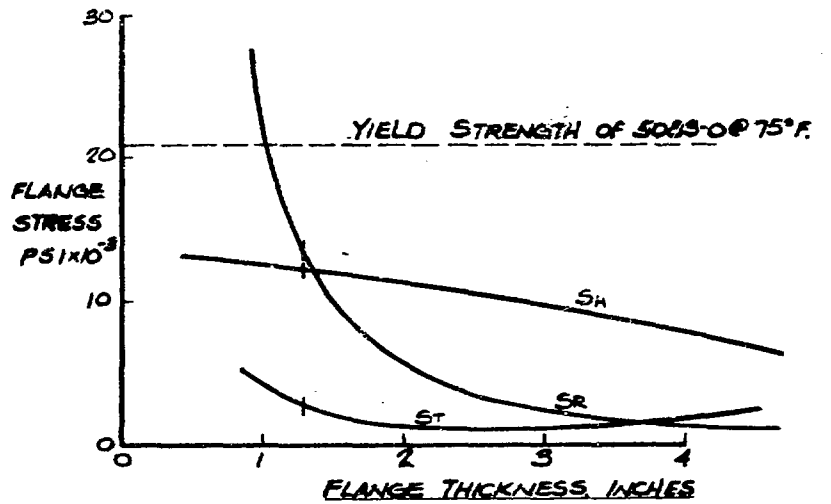

FIG. 29D

CASING FORCE SCHEMATIC

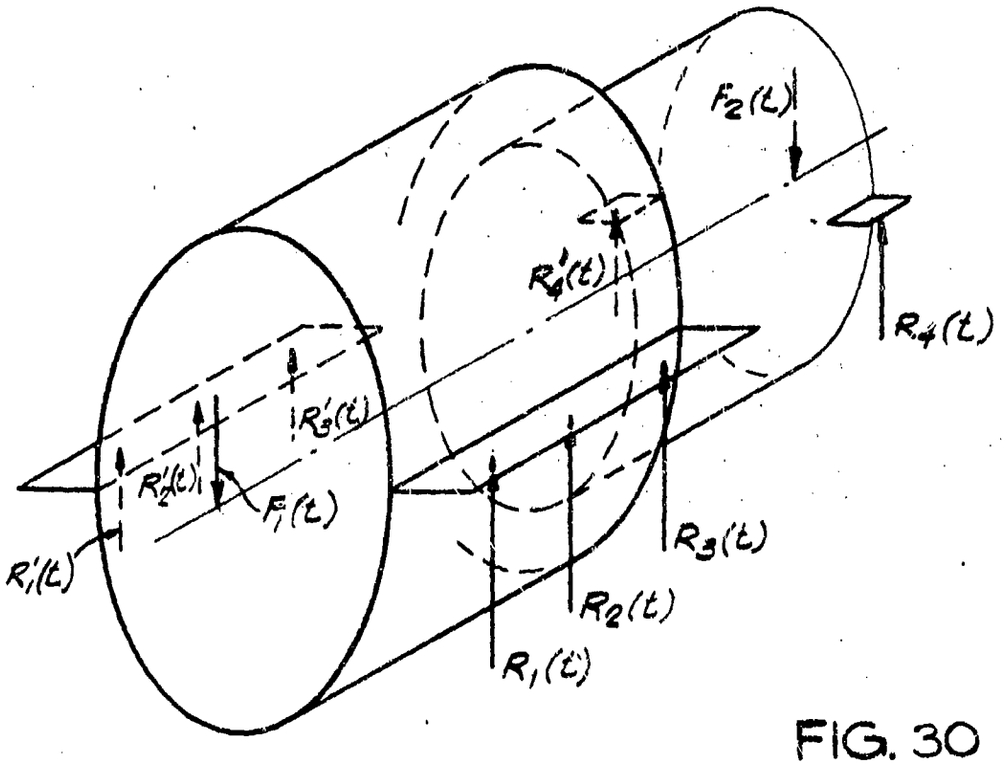

FIG. 30

This force is a maximum when the unbalance is directed vertically downward. Using the force values as computed in Section 3.2.2 a front view of the casing appears as shown in Figures 31A and 31B and a side view appears as shown in Figures 32A and 32B. These sections may be regarded as beams loaded as shown and the deflection curves may be determined graphically. Superposing these deflections yields a composite total maximum deflection of $\Delta = 0.0001439$ in. which occurs at the front end bearings. The resulting stiffness of the structure is 1.68×10^8 lb./in. which is an indication of the design adequacy. The equivalent first natural frequency is $\omega = 473$ rad./sec. If mica-filled phenolic pads are placed beneath the support legs to provide insulation between the machine and the concrete foundation the first natural frequency is reduced to $\omega = 420$ rad./sec.

5.2.1.7 Casing Fabrication

Functionally the casing for the 100 lb./sec. rotary air separator may be compared to the casing of any conventional turbomachine, that is:

a. it serves to enclose and support the rotating element(s) and
b. it houses a diffuser section.

The multifunctional requirements of the assembly required a considerable amount of precision machining on the basic aluminum component weldments. The critical machining areas include the diffuser passages, the stationary faces of the peripheral seals and the bearing housings. In each of the above cases the close dimensional tolerances required for the large diametral dimensions involved, was the biggest factor contributing to the machining difficulties.

Line boring of the bearing housings (14" dia. on the drive end hub and 16" dia. on the opposite hub) on the casing assembly was required to assure concentricity of the bearing supports and shaft parallelism. The overall length of the casing assembly, 115 inches face to face of the extreme hubs, was the complicating factor in the operation. An external view of the assembled casing is shown in Figure 33.

5.2.2 Shaft Assembly

5.2.2.1 Introduction

A shaft is usually defined as a rotating member, transmitting power, but in the case of the boilerplate model air separator it also serves as the principal duct for the transport of fluids. Because of the large fluid

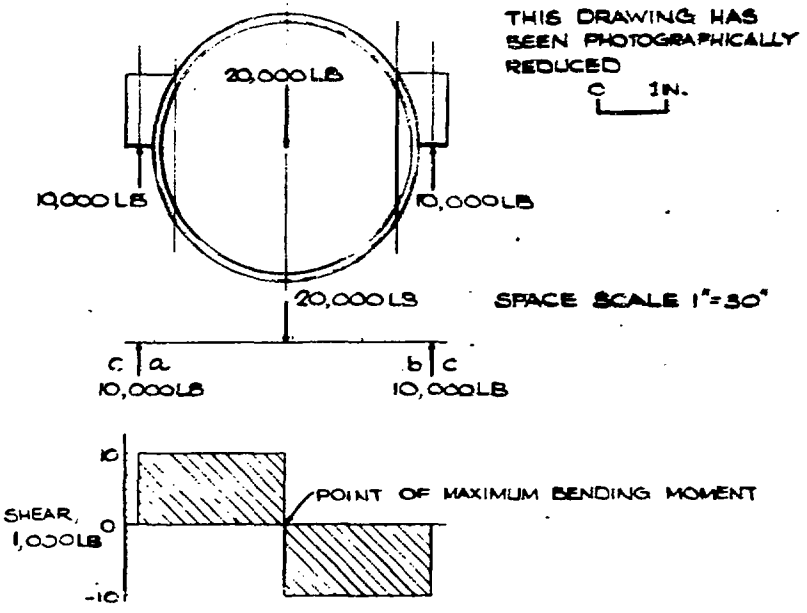

CASING MOMENT DIAGRAM - END VIEW

FIG. 31 A

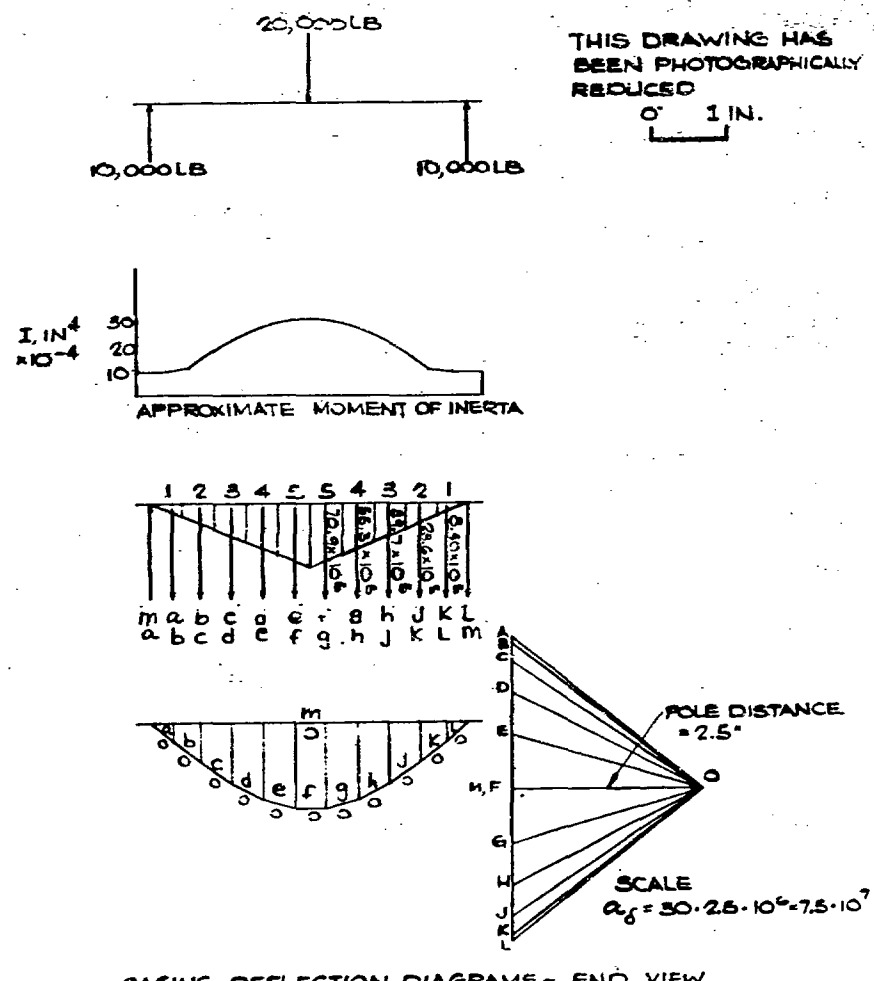

CASING DEFLECTION DIAGRAMS - END VIEW

FIG. 31 B

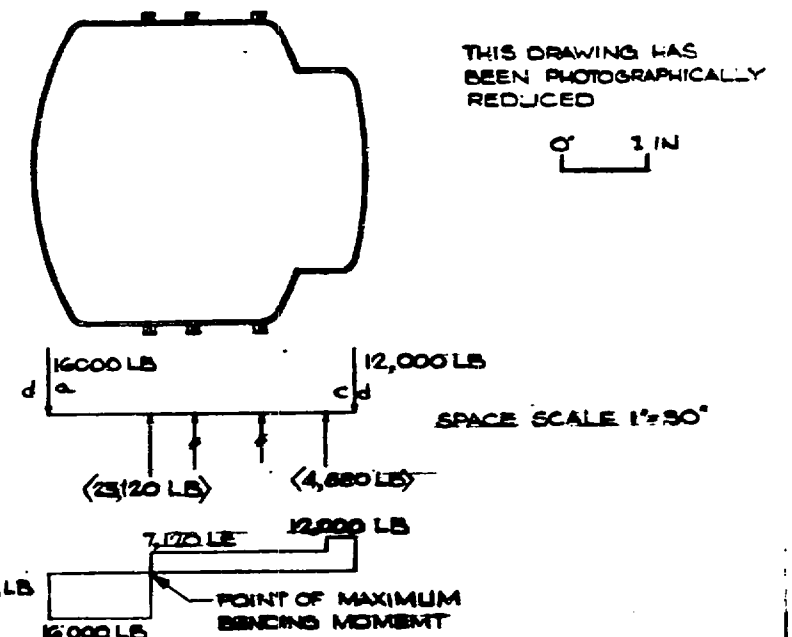

CASING MOMENT DIAGRAMS - SIDE VIEW

FIG. 32A

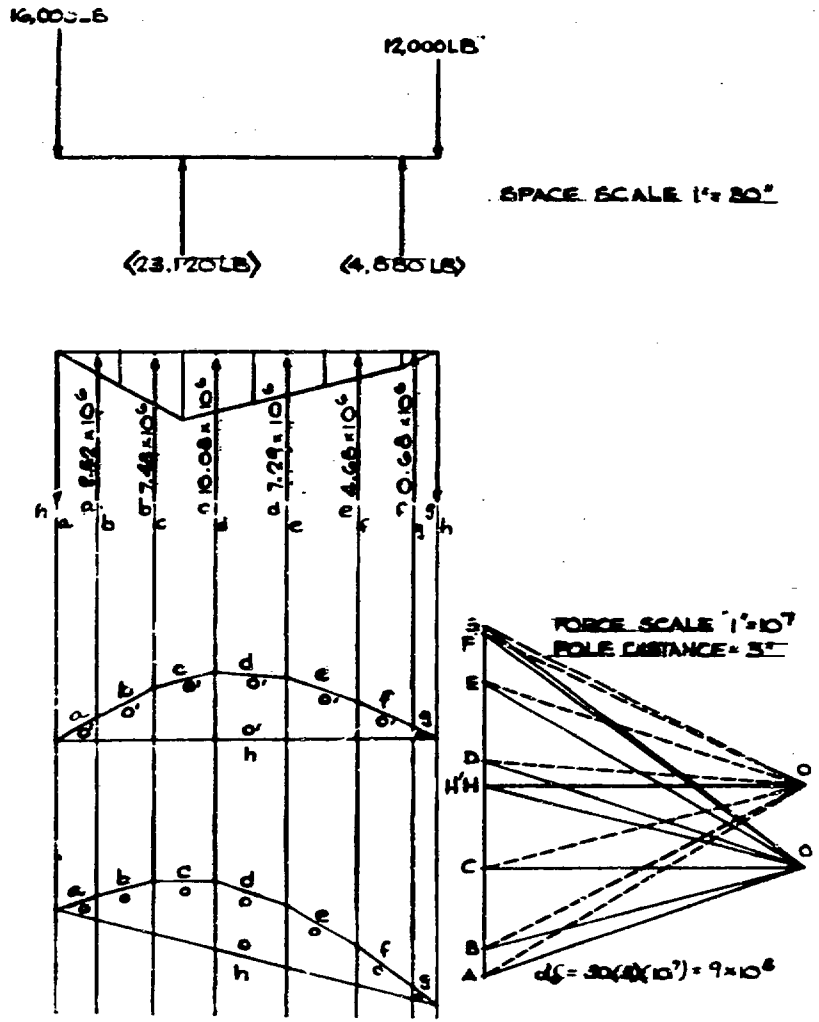

CASING MOMENT DIAGRAMS - SIDE VIEW

FIG. 32B

CASING

FIG 33

flow rates and the resulting flow areas, a large diameter shaft is required. Thus, several considerations are important in the design. First, of course, the shaft must be capable of supporting the transverse loads resulting from the weight of the machine components and the unbalance encountered in the system. Secondly, it must be capable of transmitting the power required to drive the machine. In addition, it must have an inside diameter sufficiently large to provide the required flow areas. It must be rigid enough to allow only very small deflections since a small deflection at the axis of the shaft may be quite critical when an attempt is made to position the column peripheries with small clearances. These deflections are, of course, also critical in controlling the vibrations which occur in the system. The shaft must be of reasonable weight to minimize the loads applied to the bearings.

The shaft wall thickness was initially determined from the combined stresses based upon the maximum shearing stress theory. The maximum shearing stress is considered to be one-half the algebraic difference of the principal stresses, also expressed as:

$$S_{s\ max.} = \left[S_s^2 + \left(\frac{S}{2}\right)^2 \right]^{1/2} \qquad (29)$$

As would be expected, however, in a shaft of this geometry, the wall thickness is not dictated by the combined stresses, but by the amount of radial deflection which can be tolerated. The deflections were analyzed graphically by means of funicular polygons. Such a method is generally more accurate than an analytical approach unless computer methods are employed.

The design analysis and the functional considerations produce a shaft configuration which may be described as follows: a hollow, stepped shaft with a nominal outside diameter of 16 in. and a wall thickness of 3/4 in. or greater throughout. To hold radial deflection to a reasonably small value it is necessary that the two columns be joined near the periphery with at least six tie rods 2-1/2 in. schedule 80 aluminum pipe. This enables the maximum deflection to be reduced to:

$$\Delta_{max} = 0.001 \text{ in.}$$

which occurs at the flange adjacent to the drive-end bearings. Total angular deflection is:

$$\Theta_s = 0.26°$$

The nominal 3/4 in. wall thickness is a conservative figure and a somewhat smaller value may be possible in a more weight-conscious design.

5.2.2.2 Shaft Materials

The general considerations concerning the selection of materials for the shaft are as discussed previously in Section 5.2.1.2. Again the properties of aluminum render it most attractive. Since some edge-welding is required on the fabrication of the internal shaft components an aluminum alloy which displays good welding characteristics and good low temperature welded ductility must be selected. The dimensions and geometry of the shaft further dictated material requirements. The use of specially forged sections was necessary to achieve the final shaft configuration. Availability of 5083-0 forgings made this alloy appear to be the optimum material. Selection of the shaft material was further complicated by the need for a wearing surface for the shaft seals, and the use of steel bearings for the shaft support. Aluminum surfaces, even if anodized, exhibit very poor wear characteristics. The steel bearing aluminum shaft arrangement would require provisions to accommodate the differential thermal contraction and expansion between the bearing races and the shaft. To eliminate both of these problems the shaft sections which support the bearings and those which serve as wear surfaces for the shaft seals were made of nine per cent nickel steel. This material was selected because it matched the thermal contraction of the bearing material, had good low temperature properties, and provided,when hardened,a good wear surface for Teflon in cryogenic service. Both the maraging steels and the series 400 stainless steels were considered but found inferior due to their poor impact properties at low temperatures. The important properties of nine per cent nickel steel are outlined in Figure 34. The nine per cent nickel steel sections were fabricated from forgings, double normalized and chrome plated in the areas where they serve as wear surfaces. The fact that two different materials are used in the shaft and the assembly problems encountered in attaching the columns and reboiler-condenser to the shaft result in a configuration as described below.

5.2.2.3 Shaft Configuration

The shaft is constructed from seven individually machined sections bolted together. The flanged and bolted composite was necessitated by both the use of dissimilar materials in the shaft construction and the boilerplate separator assembly procedures requiring that some of the shaft sections be removed at various stages

TENSILE PROPERTIES NORMALIZED & STRESS RELIEVED, 9% NICKEL STEEL PLATE

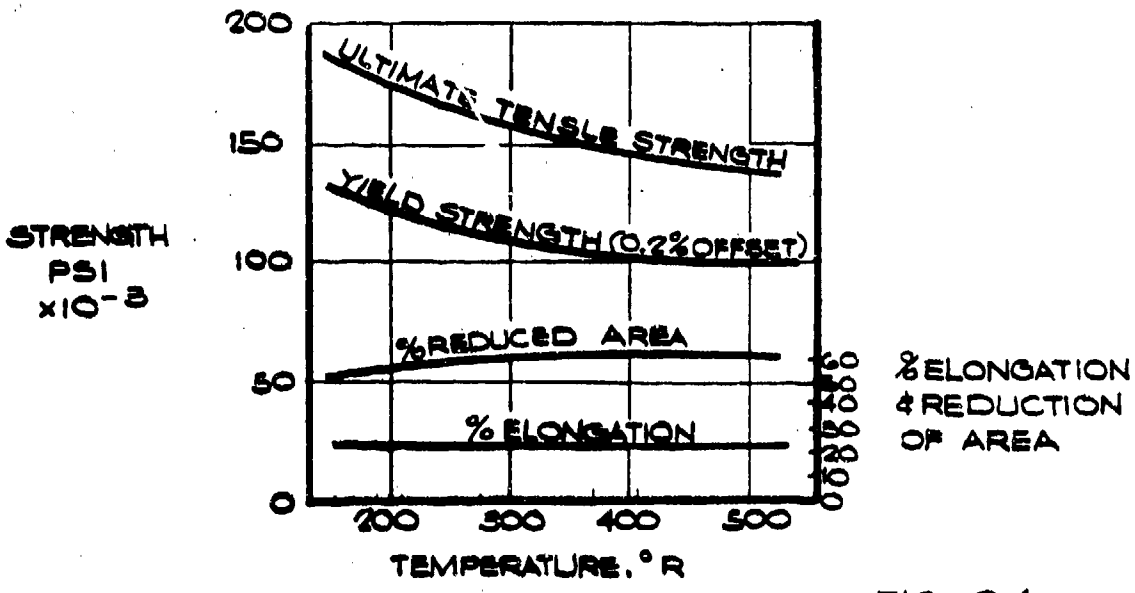

FIG. 34

of assembly. The final shaft configuration is shown in Figure 35. The nine per cent Ni-steel end sections are attached to the aluminum mid-sections by special flange designs. Since use of the conventional single shoulder arrangement for alignment will result in high local bending stresses during cooldown due to the differential thermal contraction at the nine per cent Ni-steel-Aluminum interface (Ref. Appendix II), a double shouldering arrangement is required as shown schematically in Figure 35. One shoulder provides alignment during assembly while the machine is warm and the other shoulder provides alignment during operation while the machine is cold. This means that there is no aligning surface as the shaft cools and this is one reason why the machine cannot operate during cooldown.

The internal ducting is fabricated from the same material as the shaft section in which it is installed with the exception of the drive-end transition between the aluminum section and the nine per cent nickel section. Here the internal duct traverses the flange and a bellows expansion joint is provided to circumvent the differential contraction problem.

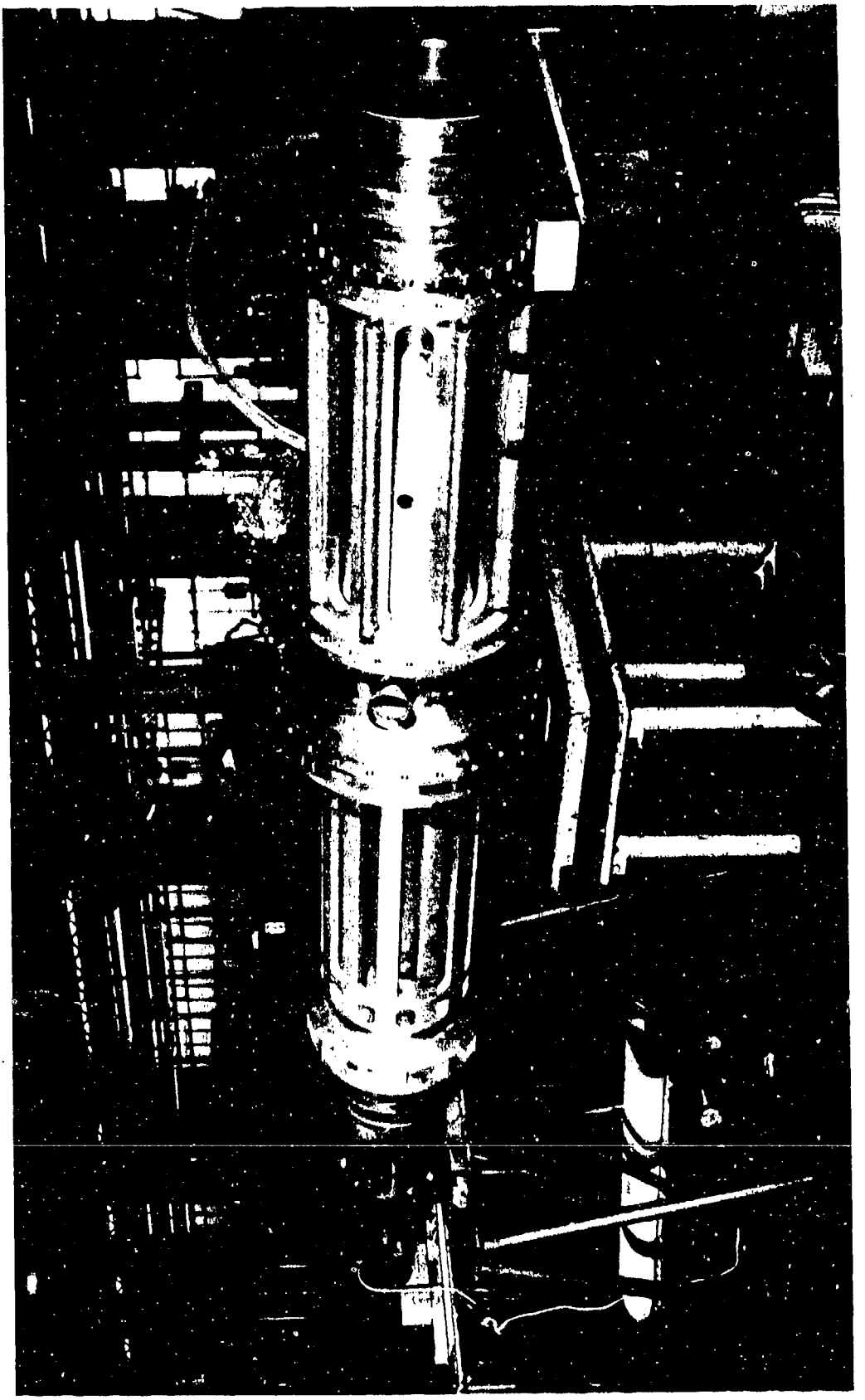

FIG.35

SHAFT

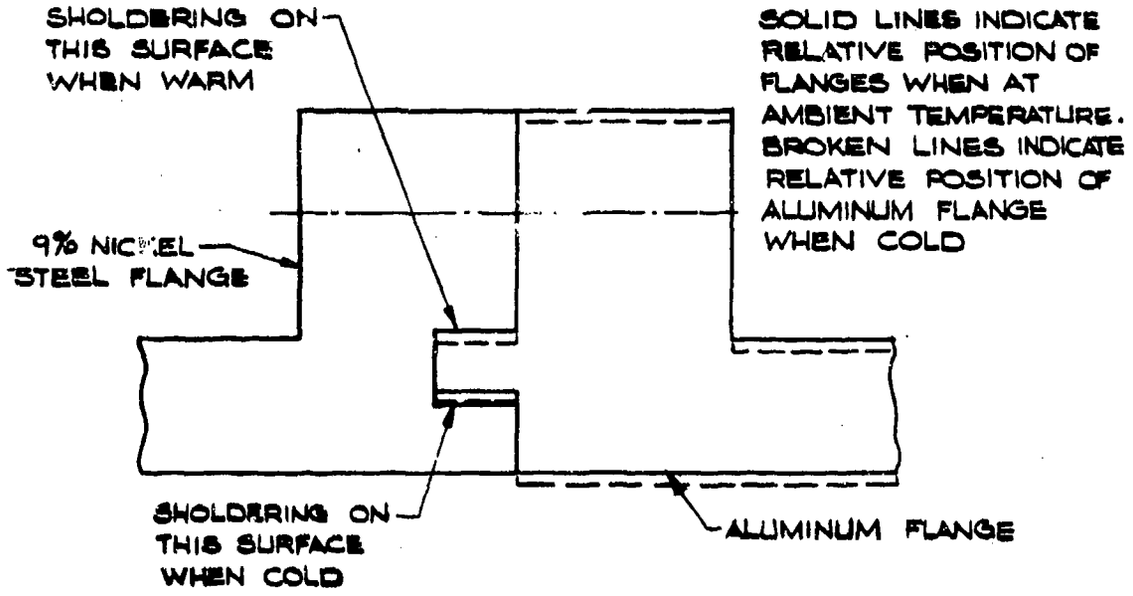

SHAFT FLANGE CONFIGURATION

FIG. 36

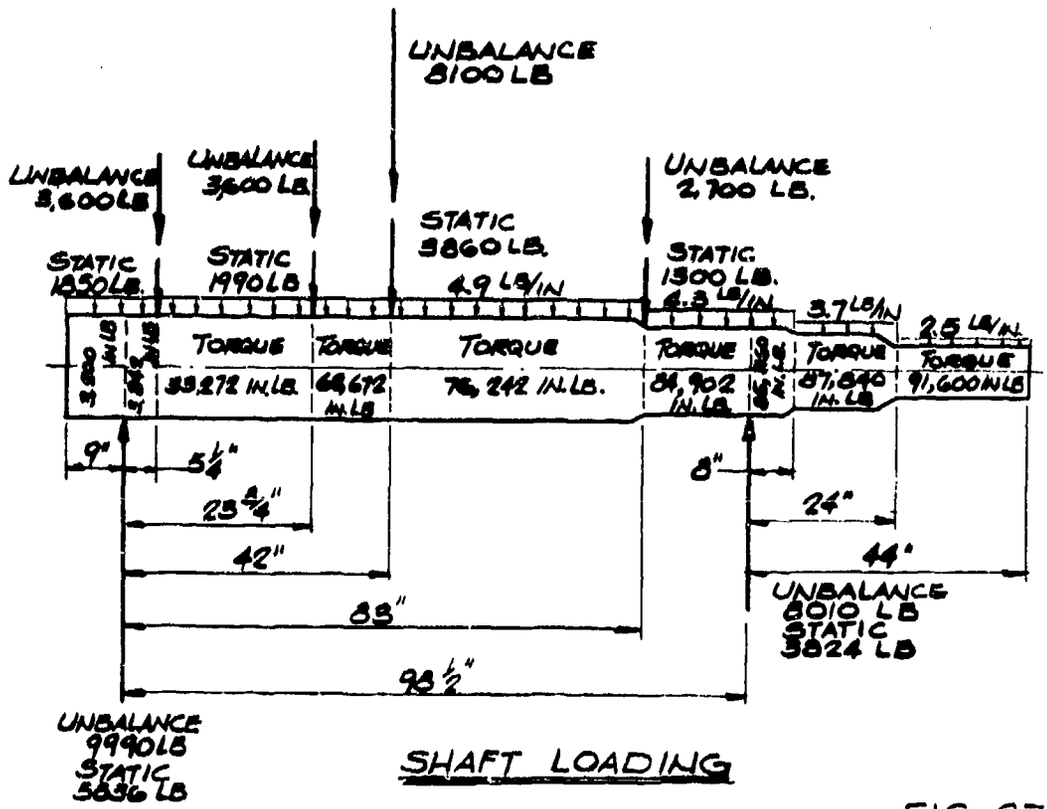

SHAFT LOADING

FIG. 37

5.2.2.4 Design Analysis

5.2.2.4.1 Shaft Loading

The loads which act on the shaft and the resulting bearing reactions are shown in Figure 37. The most obvious shaft load is the weight of the machine. A weight breakdown based on all aluminum construction of the rotors is given in Table 5.

TABLE 5

APPROXIMATE STATIC WEIGHT OF COMPONENTS LESS SHAFT

Item	Approximate Wt. Lb.
Low Pressure Column Side Plates (2)	2560
Low Pressure Column Trays	252
Low Pressure Column Phase Separator	256
Kettle Liquid Transfer Piping	9
Reboiler-Condenser Oxygen Vapor Piping	84
Shelf Liquid Transfer Piping	10
Reboiler-Condenser Rear Plate	198
Reboiler-Condenser Front Plate	227
Reboiler-Condenser Shell	388
Reboiler-Condenser Core	600
Reboiler-Condenser Nitrogen Header	207
Reboiler-Condenser Oxygen Header	86
High Pressure Column Side Plates	1940
High Pressure Column Trays	81
High Pressure Column Header	113
High Pressure Air Intake Header	100
High Pressure Air Intake Piping	76
Reboiler-Condenser Nitrogen Vapor Return Piping	82
Support Tie Rods	8
Control Valves	24
Piping Flanges	37
Shroud, Bolts, Nuts, Misc. Piping, etc.	216
Static Weight of Liquid Holdup	953
Approximate Total	8523 Lb.
Design Value	9000 Lb.

The approximate static weight of the holdup liquid is included. The total static weight which must be supported by the shaft, excluding its own weight, is taken to be 9,000 lbs. The distribution of this weight on the flanges is given in Table 6. The shaft weight is included as the distributed load shown in Figure 37.

TABLE 6

APPROXIMATE STATIC WEIGHT DISTRIBUTION

Flange	% Wt. Carried	Wt. Carried Lb.
#1 Waste N_2 Discharge Side Low Pressure Column Flange	20.6	1850
#2 Drive Side Low Pressure Column Flange	22.1	1990
#4 Low Pressure Column Side Reboiler-Condenser Flange	42.9	3860
#5 Drive Side Reboiler-Condenser Flange	14.4	1300
	100.0%	9000 lb.

The torque transmitted by each section of the shaft is also shown in Figure 37. These torque values are based on a maximum horsepower input of 800 HP which includes a design factor since a 700 HP drive is being provided and a maximum power requirement of 655 HP is expected. Table 7 lists the expected power consumption of each component.

TABLE 7

POWER REQUIREMENTS

@ ω = 60 Rad./Sec. & P_c = 60 Psia

Item	Approximate HP Reqd.	Approximate Torque Reqd.
Low Pressure Column Peripheral Seal	272	29,900 in.lb.
Product Discharge Peripheral Seal	53	5,830
Vapor Windage	19	2,090
Mech. (Bearings, Shaft Seals)	30	3,300
Internal Pumping	232	25,500
TOTAL	606	66,620 in.lb.

(Design Torque = 91,600 in.lb. allowing operation of shaft at higher speeds and/or lower casing pressures.)

The amount of torque withdrawn at each flange is tabulated in Table 8.

TABLE 8

TORQUE DISTRIBUTION

Flange	% Torque	Torque
#1 Waste N_2 Discharge Side Low Pressure Column	32.15	29,430
#2 Drive Side Low Pressure Column	32.10	29,400
#3 Low Pressure Column Side Reboiler-Condenser	14.80	13,570
#4 Drive Side Reboiler-Condenser	9.45	8,660
	88.50*	81,060 In.Lb.

*Remainder Withdrawn @Bearings and Shaft Seals

The liquid unbalance was approximated to be equivalent to 30 lbs. of liquid rotating in a field of 600 Ng (See Appendix III). This creates an unbalance force of:

$$F_u = 30\ (600) = 18,000\ \text{lb.}$$

This unbalance is distributed approximately as shown in Table 9. The shaft will be subjected to maximum loading when the static forces and the unbalance forces are additive.

TABLE 9

UNBALANCE DISTRIBUTION

Flange	% Unbalance	Unbalance Load, Lbs.
#1 Waste N_2 Discharge Side Low Pressure Column	20	3,600
#2 Drive Side Low Pressure Column	20	3,600
#3 Low Pressure Column Side Reboiler-Condenser	45	8,100
#4 Drive Side Reboiler-Condenser	15	2,700
	100%	18,000

5.2.2.4.2 Maximum Bending Moment and Combined Stresses

The maximum bending moment was determined by graphical construction. A vertical shear diagram as shown in Figure 38 located the point of maximum bending moment at the front high-pressure

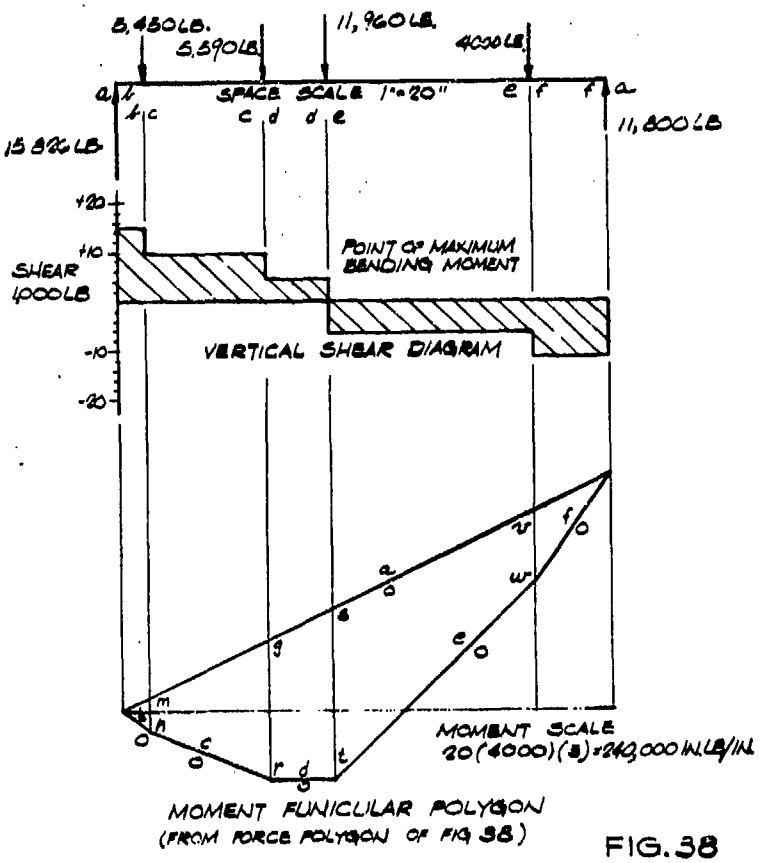

FIG. 38

column flange. By constructing a funicular polygon Fig. 38 and a force polygon as shown in Figure 39 the magnitude of the maximum bending moment was found to be approximately 413,000 in. lb. The bending moments at various locations are given in Table 10.

TABLE 10

BENDING MOMENTS

Location - Fig. 37	Bending Moment In. Lb.
m - n	79,200
g - r	336,000
s - t	413,000
v - w	168,000

FORCE POLYGONS

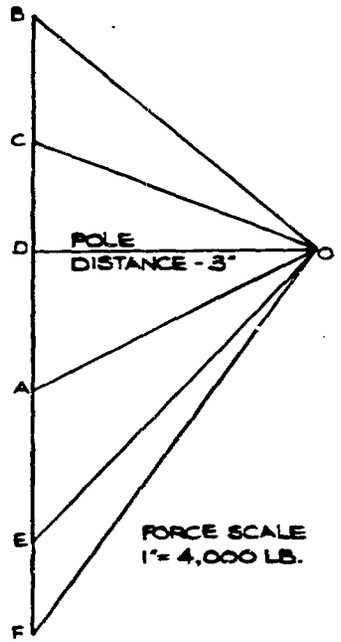

FORCE POLYGON FOR CONSTRUCTION OF MOMENT FUNICULAR POLYGON

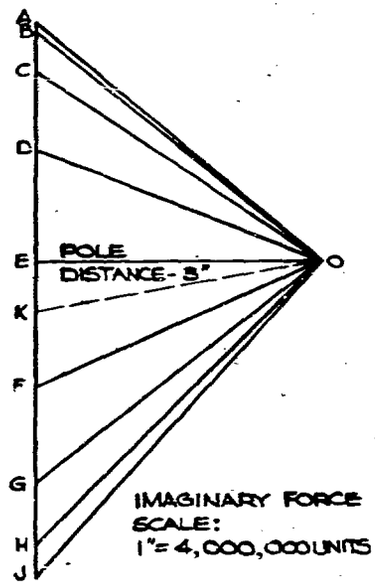

IMAGINARY FORCE POLYGON FOR CONSTRUCTION OF DEFLECTION FUNICULAR POLYGON

FIG. 39

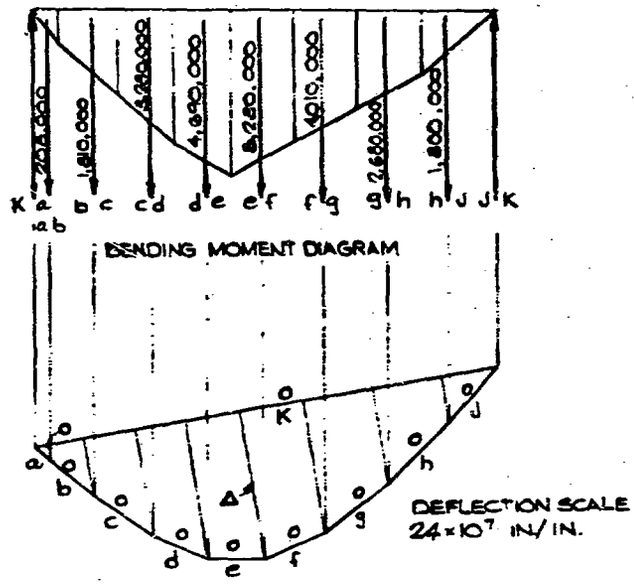

DEFLECTION FUNICULAR POLYGON

FIG. 40

Using the maximum shearing stress theory the following relation may be written:

$$D_{so}^{3} = \frac{16}{\pi S_s \left(1 - \frac{D_{si}^{4}}{D_{so}^{4}}\right)} \left[M_T^2 + M_B^2\right] \qquad (30)$$

When this was applied to the point of maximum bending moment the inside diameter and thickness obtained were:

$$D_{si} \approx 15.79 \text{ in.}, \quad t_s \approx 0.10 \text{ in.}$$

It is immediately obvious that deflections, not the combined stresses, will be controlling for this particular shaft.

5.2.2.4.3 Shaft Deflections

With the bending moment diagram (Figure 40) as a basis a funicular polygon, which is an accurate representation of the shaft deflection, was constructed. The deflection for any given shaft size at any point can be obtained from this polygon. Table 11 lists the deflection at various points for a 3/4 in. thick shaft and a 1 in. thick shaft.

TABLE 11

SHAFT DEFLECTION *

Location Figure 38	Deflection 3/4" Wall Thickness	Deflection 1" Wall Thickness
ab	.00297 in.	.00234 in.
bc	.01370	.0108
cd	.0252	.0199
de	.0332	.0262
ef	.0359	.0283
fg	.0320	.0253
gh	.0228	.0180
hi	.01675	.01322

* Deflection Without Tie Rods Between Columns

Figure 41 shows the maximum radial deflection versus shaft wall thickness. The magnitude of these deflections indicate that additional shaft rigidity is required. This could be achieved by increasing the shaft thickness but a brief look at even a solid shaft yields high deflections. Another method of increasing the effective moments of inertia is to provide supports at some distance removed from the axis of the shaft. This was done by structurally tying the periphery of the two columns together. A moment of inertia of approximately 50,000 in.^{4} would be required to maintain shaft deflections of a reasonable level.

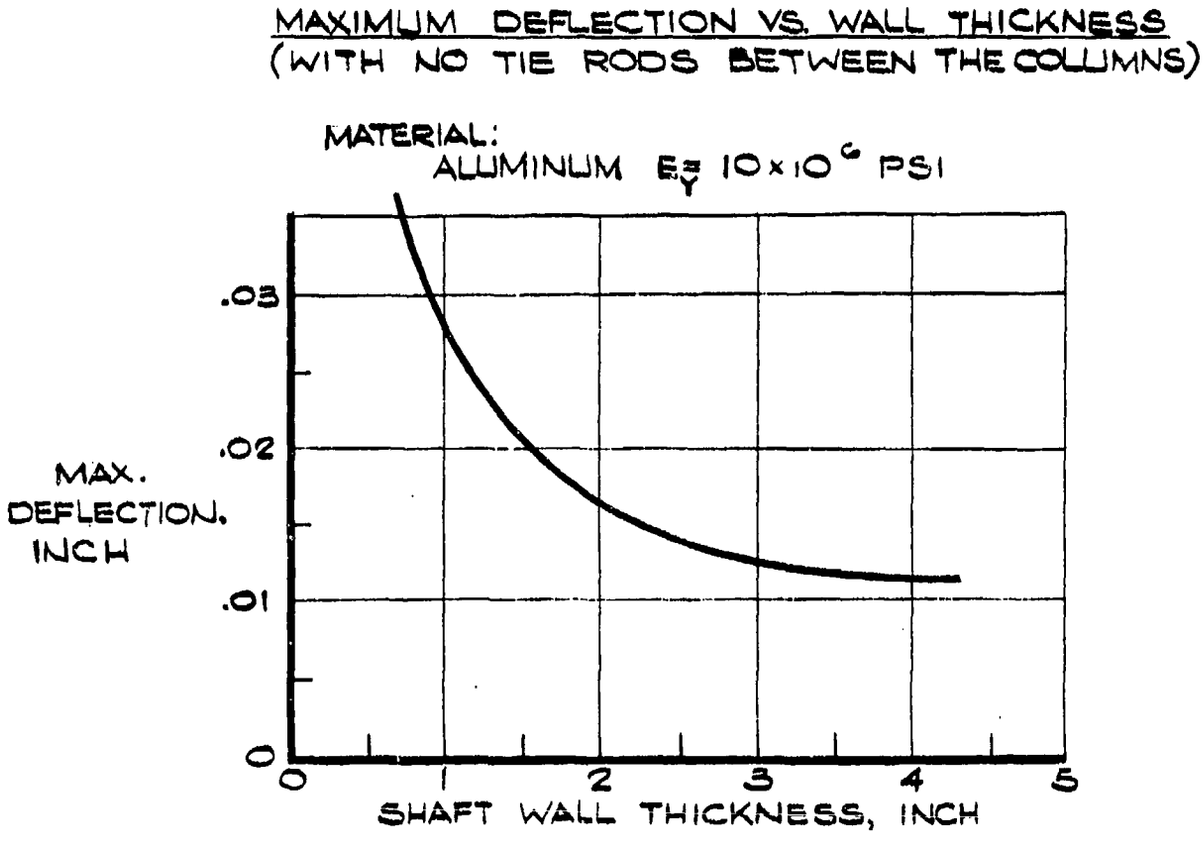

FIG. 41

Table 12 lists the number of various types of tie rods required to give moments of inertia of 75,000 in.^{4} and 50,000 in.^{4}.

TABLE 12

SUPPORTS BETWEEN COLUMNS

Type of Support	No. Req'd to Obtain I = 75,000 In.^{4}	No. Req'd to Obtain I = 50,000 In.^{4}
2" Schedule 40 Aluminum Pipe	22	15
2" Schedule 80 Aluminum Pipe	16	11
2-1/2" Schedule 40 Aluminum Pipe	14	10
2-1/2" Schedule 80 Aluminum Pipe	10	6
3" Schedule 80 Aluminum Pipe	7	5-
2" Schedule 80 Aluminum Pipe	8	5
2" O.D. Solid Aluminum Rod	5	3+
2-1/2" O.D. Solid Aluminum Rod		

Six 2-1/2" schedule 80 aluminum pipe supports will fit conveniently into the hardware of the other components. The Euler critical load of such a rod, acting as a prismatic column, is 270,000 lb., far more than the load to which they are subjected (~5,000 lb.). For such an arrangement the maximum radial deflection occurs at the flange nearest the drive-end bearings and is:

$$\Delta_{max} = 0.001 \text{ in.}$$

Applying the torsion equation:

$$\Theta_s = \frac{M_T \; L_s}{J_p \; G_s} \qquad (31)$$

to each segment of the shaft and summing the results gives a total angular deflection of:

$$\Theta_s = 0.26°$$

Sample calculations for the analysis appear in Appendix IV.

5.2.2.4.4 Shaft Fabrication

Fabrication of the shaft assembly entailed machining operations almost exclusively. A limited amount of welding fabrication was required

in the internal shaft ducting. Since functional and design requirements dictated that the shaft ensemble be made up of seven individual sections, each section had to be processed individually.

Appropriate forgings were specified for each section. Each forging was first rough machined to its approximate final configuration. After this first stage machining operation, the ducting fabrication was performed on each aluminum section. Figures 42, 43, and 44 show some of the rough machined components with the ducting fabrication in progress. Figure 45 shows another aluminum section of the shaft being final machined after welding of appropriate process line connections to it.

The final machining of the individual shaft sections was the most critical operation in the shaft manufacturing process. Since tolerance build-up in the assembly of the seven individual sections could result in considerable shaft eccentricity extremely close tolerances had to be specified on the matching dimensions of adjacent sections. Close dimensional control of the individual sections was necessary to keep total indicated run-out to a minimum for the entire assembly.

Final operation in the shaft manufacture was the surface treating of the bearing and shaft seal contact areas on the 9 per cent Ni-steel end sections after a trial preassembly. These areas were hard chrome coated and ground finished.

5.2.3 Bearings

5.2.3.1 Introduction

Successful operation of rotating machinery depends on the proper design of the shaft support system.

In those cases where high loads have to be carried at moderate speeds and with low bearing friction, use of rolling contact type bearings which can withstand both radial and axial loads becomes mandatory.

Performance of a rolling contact type bearing under normal lubricated conditions has been well established. Manufacturers design data allows the selection of the proper bearing for a particular load and speed application and assures adequate fatigue life for these conditions. In applications where conventional means of ball bearing

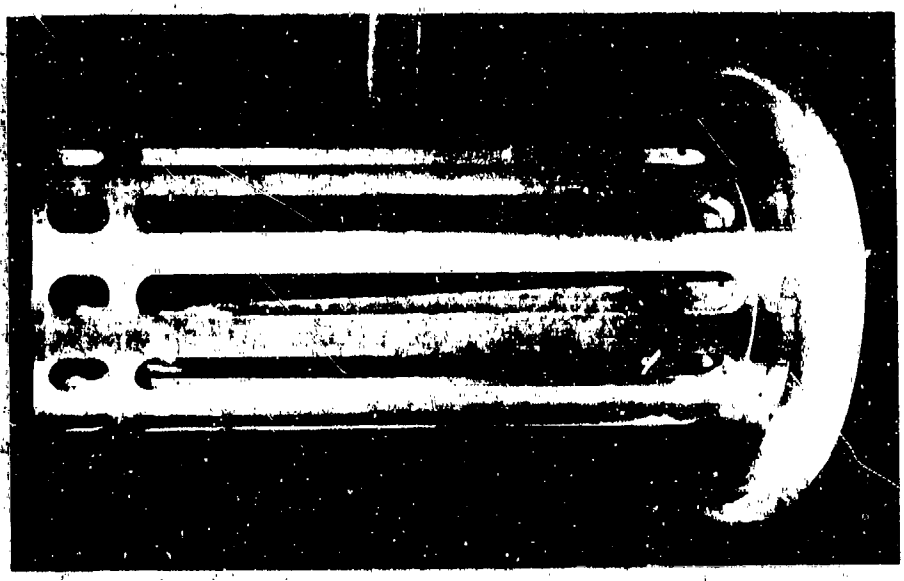

SHAFT FABRICATION SECTION 2
FIG 43

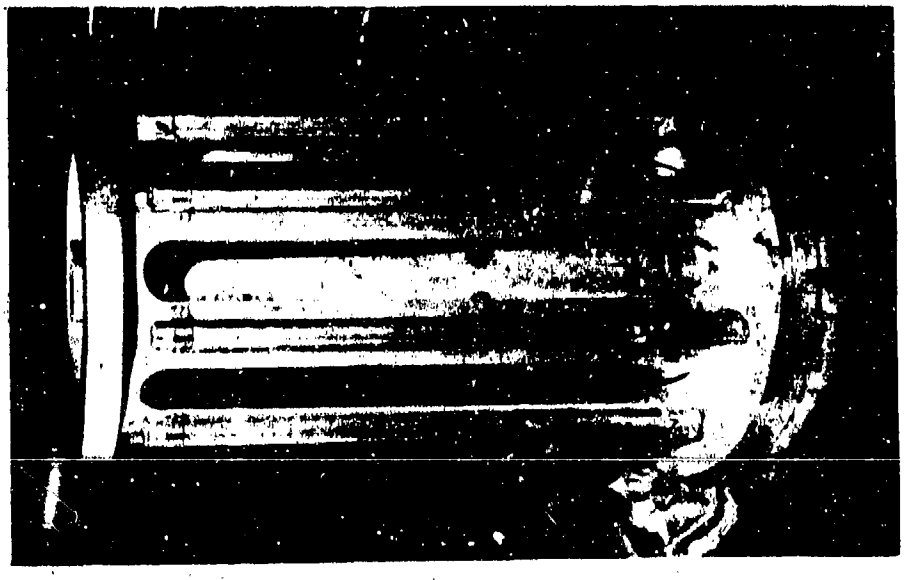

SHAFT FABRICATION SECTION 1
FIG 42

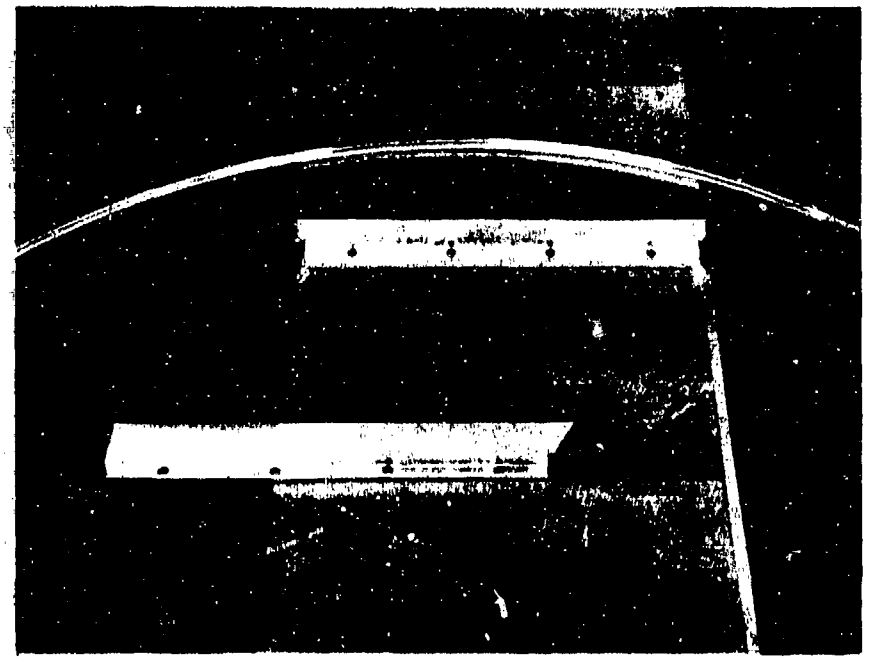

TRAY RING COMPONENTS FIG 44

SHAFT FABRICATION SECTION 4

FIG.45

lubrication (a thin oil film) are not applicable because of bearing environmental conditions, the use of "degreased" standard bearings results in sharp deterioration of bearing life and early failure by wear of components. Almost consistently the bearing ball separator has proven to be the weakest component in the bearing assembly and thus, the source of premature failure, Ref. 10, 11.

Modification of the ball separator has allowed operation of ball bearings in low temperature environments in excess of the rated minimum life. For such operation the ball separators must be free of abrasive material and have a minimum coefficient of friction when rubbing against the ball and race materials.

5.2.3.2 Bearing Selection

5.2.3.2.1 Bearing Motion and Influence on Design

Rolling friction prevails in the operation of a ball bearing. However, some sliding of the ball element will occur since geometrically pure rolling contact cannot be achieved.

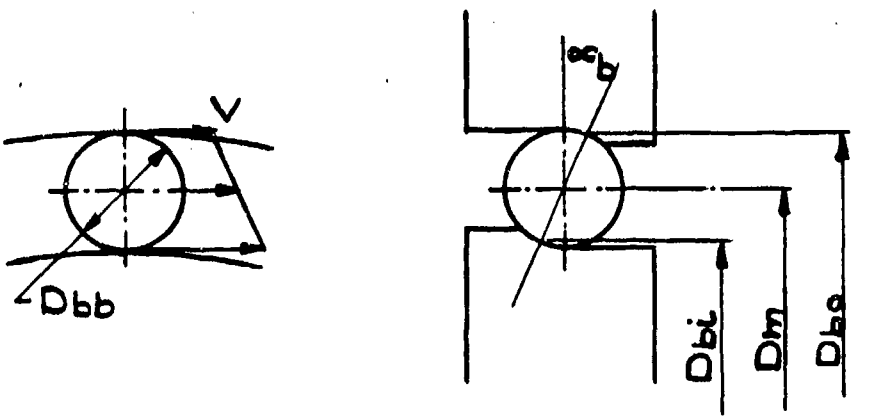

FIG. 46

For a bearing the outer race of which is stationary and the inner race of which rotates at a speed of ω rad./sec., the motion of the ball element for three different types of bearings is: (Ref. 12.)

Radial Bearing	Angular Contact	Thrust Bearing
$\alpha_b = 0 \quad \cos \alpha_b = 1$	$\alpha_b = \alpha_b \quad \cos \alpha_b = x$	$\alpha_b = 90° \quad \cos \alpha_b = 0$
$\omega_m = 1/2\ \omega\left(1 - \frac{D_{bb}}{D_m}\right)$	$1/2\omega\left(1 - \frac{D_{bb}}{D_m}\right)$	$1/2\ \omega$
$\omega_{mi} = 1/2\omega\left(1 + \frac{D_{bb}}{D_m}\right)$	$-1/2\omega\left(1 - \frac{D_{bb}\,x}{D_m}\right)$	$-1/2\omega$
$\omega_b = -1/2\omega \frac{D_m}{D_{bb}}\left(1 - \frac{D_{bb}^2}{D_m^2}\right)$	$-1/2\omega \frac{D_m}{D_{bb}}\left(1 - \frac{D_{bb}^2}{D_m^2}\, x\right)$	$-1/2\omega \frac{D_m}{D_{bb}}$

On the basis of the above relations for radial and angular contact bearings, it is seen that small ball diameters (i.e. $D_m >>$ D_{bb} or $D_{bb}/D_m \rightarrow$ small) will result in relatively high ball rotational speeds but low sliding velocities.

For angular contact bearings the contact angle (ΘC_b) should be as small as practical from thrust load considerations to yield the smallest possible amount of ball sliding.

On the basis of the ball motion alone it is seen that the proper bearing selection should satisfy the following geometrical factors: The ratio $D_{bb}/D_m \rightarrow$ should be small and the contact angle α_b should also be as small as practical.

Small cross section "aircraft" type bearings satisfy these requirements if the loads imposed are within the range of the bearing load carrying ability.

5.2.3.2.2 Bearings Loads and Life Considerations

Fatigue life capacities for bearings are tabulated for a standard speed and an average life expectancy. For different operating conditions capacity corrections must be made according to the empirical load-life correlation:

$$L_N = \left(\frac{C_{sp}}{F_b}\right)^3 \qquad (32)$$

Since from the above, bearing life is very sensitive to the actual bearing load

$$\left(L_N \sim \frac{1}{F_b^3}\right)$$

it can be adversely effected by heavy loading even if of relatively short duration.

In determining the effective load on the bearing it was considered that for a condition of axial balance, the thrust load on the bearing consists mainly of an assembly preload used to fix the shaft with reference to the bearing support (i.e. casing).

The amount of preload is difficult to judge but should be a small fraction of the radial load on the bearing support.

For this reason the equivalent radial load only was used to check the load rating of the bearings selected, Appendix V.

Reduced to the same basis as used in manufacturers bearing rating tables, i.e. a speed of 10.5 rad./sec. and an average life of 3,000 hrs. equivalent to 600 hrs. for 90% of the bearing group, the total bearing loads are:

a. 20,400 lbs. 16" dia. end.
b. 15,500 lbs. 14" dia. end.

Four bearings are to be used at each support with the following rating per bearing:

a. KG-160-AR - 7,140 lbs.
b. KG-140-AR - 6,610 lbs.

As indicated by the above comparison of load ratings and acting loads, the bearings selected provide a considerable margin of safety in the boilerplate.

5.2.3.2.3 Additional Design Considerations

Bearing selection thus far is based on:

a. Bearing elements motion, and
b. prevailing load conditions

Implied is operation of the bearing with adequate lubrication.

Since the operating environment (temperature range -250 to -320°F) for the bearings under consideration excludes the use of conventional oil film lubrication, a modified bearing with an inherent solid film lubricant system must be used. Experience to date shows that a modified ball separator ring made of a low friction, low wear material constitutes an adequate lubrication system for anti-friction bearings operating in low temperature environments, provided that the heat of friction can be adequately dissipated to the cryogenic environment. Because of the relative sliding motion between the balls and the pockets of the ball separator ring a solid film transfer is affected to the ball race contact area.

Proper design of the separator ring hinges on:

1. proper material selection and,
2. geometrical configuration

The ball separator material must have low friction and wear characteristics and adequate strength at operating conditions. Filled Teflon materials meet these requirements and their use has proven successful in similar applications. Low friction characteristics minimize heat generation within the bearing which if excessive would have adverse effects on operating temperature level and bearing internal clearances.

Design of the ball separator ring is guided mainly by the physical properties of the material used. The differential contraction for the ball retainer and the other bearing components will affect the operating clearances of the bearings and thus their performance (i.e., shrinkage of the ball retainer on the balls and/or the inner race must be prevented). Figure 47 shows a ball bearing with a substitute retainer.

To a large extent, control of the bearing dimensions will also be affected by actual bearing operating temperature. An analysis of the heat generating and dissipating abilities of the bearings used, shows that the temperature rise due to the friction work in the bearings is not dangerously high (50°F) so that close control of the operating clearance should be possible.

On the basis of a 50°F temperature rise during operation the relative expansions have been calculated as:

		14" Bore	16"Bore
1.	Inner race - outer race	.002"	.002"
2.	Inner race - ball retainer	.118"	.133"
3.	Ball - retainer	.0005"	.0005"

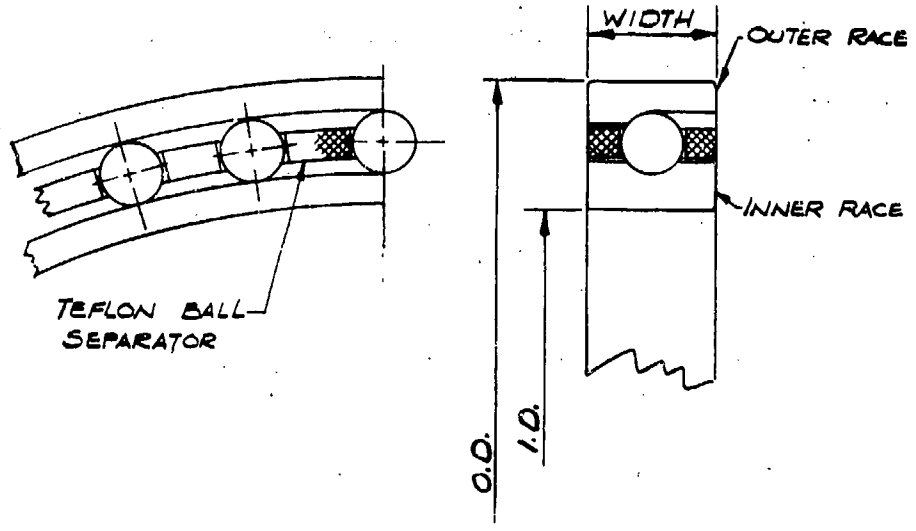

	I.D.	O.D.	WIDTH	BALL DIA.
I	14"	16"	1"	1/2"
II	16"	18"	1"	1/2"

BEARING RETAINER

FIG. 47

As indicated above the standard bearing diametral clearances must be increased by a minimum of .002".

The differential contractions in (2) and (3) are considered representative values only in as much as inconsistencies in the physical properties for different samples of similar Teflon materials have been encountered in past experience. The variation has been found to be a function of the manufacturing process, geometrical configuration, and material heat treatment.

For greater dimensional accuracy these values are checked from data obtained from samples representative of the actual material used for manufacture of the particular ball separators.

5.2.3.3 Bearing Mounting

The bearing mounting arrangement is shown in Figure 48. Two sets of Kaydon KG 140 AR Bearings are used on the drive end of the shaft with two sets of KG 160 AR used on the free end.

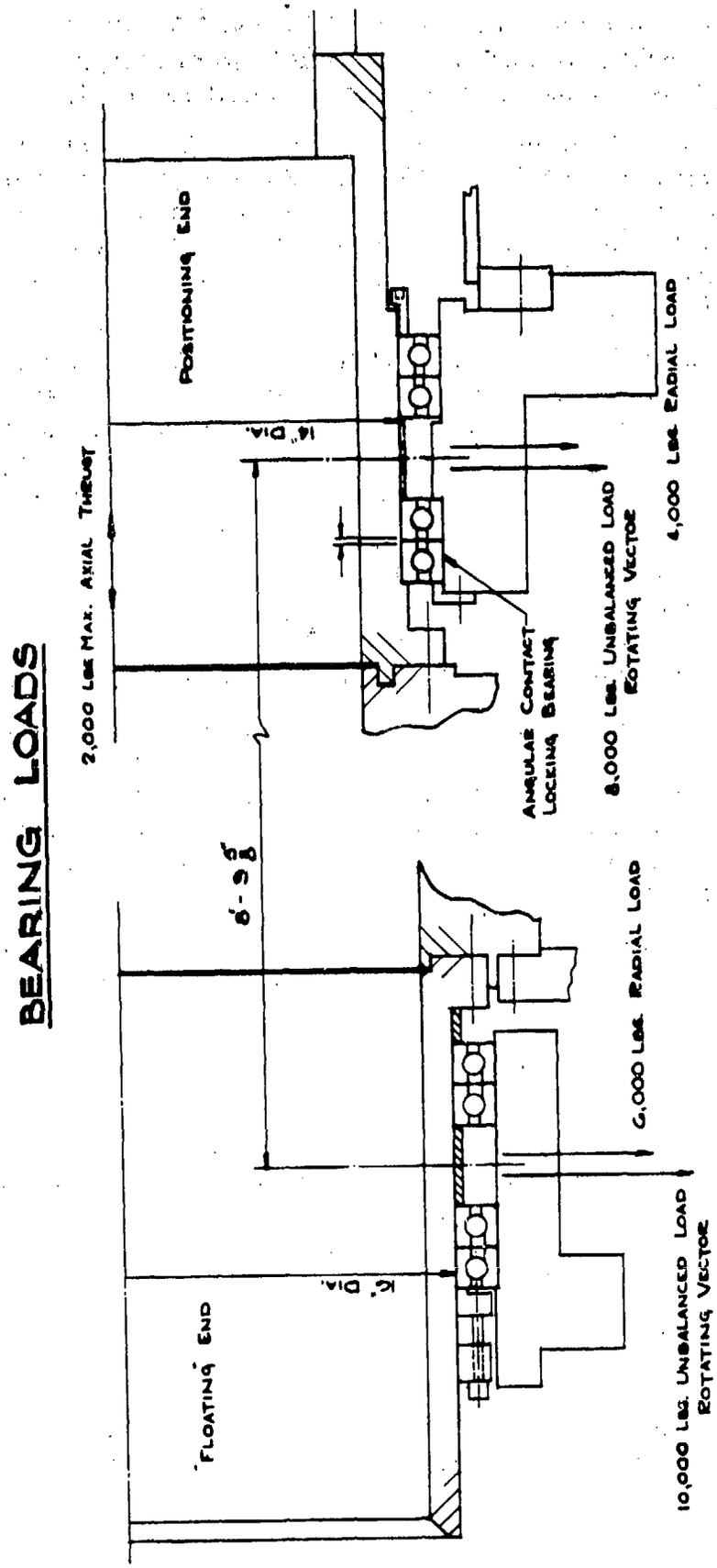
BEARING LOADS
POSITIONING END
FLOATING END
2,000 LBS MAX. AXIAL THRUST
8'-9 5/8"
16" DIA.
16" DIA.
ANGULAR CONTACT LOCKING BEARING
8,000 LBS. UNBALANCED LOAD ROTATING VECTOR
4,000 LBS. RADIAL LOAD
6,000 LBS. RADIAL LOAD
10,000 LBS. UNBALANCED LOAD ROTATING VECTOR

FIG. 48

A back to back mounting is used for the KG-140-AR bearings which are preloaded, making them the axial thrust carrying members. They also establish axial reference for the shaft assembly.

A face to face mounting is used for the "Free-floating" KG-160-AR bearings. KG-14-AR and KG-16-AR are Kaydon designations for 14" and 16" bore light-weight construction angular contact bearings. Although these bearings will have a modified ball retainer for use in a low temperature non-lubricated environment the race material is 52100 bearing steel.

The use of these bearings in an all aluminum construction assembly presents shaft and housing problems, due to differential thermal contractions. The inability to cope with the bearing-aluminum shaft fit resulting at the operating temperatures compounded by the need for a shaft seal wear surface made necessary a material substitution for the shaft sections at the bearing support areas.

9% Ni steel was substituted in three of the seven sections of the bolted shaft assembly. This material has adequate low temperature properties and a coefficient of expansion (contraction) similar to that of the bearing material, thus allowing a conventional shaft-bearing fit.

The all welded casing construction makes a material substitution for the bearing housing impractical. Although the use of a sleeve insert having two locating surfaces (one at ambient temperatures, one at the operating temperature) can be employed, the configuration of the bearing housing (diameter and length) would impose severe limitations on the present design.

For this reason an aluminum bearing housing which results in proper bearing-housing fit at operating temperatures is thought most feasible.

A serious limitation of this design is the inability to rotate until after cooldown of the entire assembly.

Although this does not affect the conduct of the test program it does necessitate the use of temporary modifications during the initial rotor checkout phase. Two possibilities of achieving the correct bearing to housing fit during the warm check-out phase include use of spacers between bearings and housings or localized bearing-housing cooldown.

5.2.4 Shaft Seals

5.2.4.1 Introduction

The transfer of fluid media from a stationary to a moving part of any process equipment requires use of a dynamic seal system so that

leakage loss is minimized at the transfer point. In the 100 lb./sec. rotary air separator where the process equipment is mounted on a hollow shaft which in addition serves the purpose of carrying all of the process streams and is fed from, or discharges into stationary piping a number of fluid transfer points are present:

a. High pressure air inlet (225 psig to (1) atmosphere: (2) casing pressure.)

b. Liquid oxygen (52 psig) to atmosphere

c. Liquid nitrogen reflux (30 psig) to waste nitrogen (30 psig)

d. Gaseous nitrogen waste out (30 psig) to casing pressure.

The seal system at each of the above transfer stations has the dual purpose of:

a. Minimizing leakage.

b. Separating two streams in close proximity to each other.

5.2.4.2 Seal Selection

In general seals can be classified as:

a. Contact-wear type

b. Non-contact or close clearance type

Seals of the second type are of simpler construction consisting basically of a "long" throttling channel which is continuous or interrupted (i.e. labyrinth) in which cases there are a number of throttling steps in series.

Leakage flow in these devices is governed by fluid flow characteristics in the throttling channel.

A simple restriction type seal is more applicable where the pressure drop across the seal and the flow area can be kept

small. In the case of an incompressible fluid, this is readily seen from a simple energy balance:

$$\frac{\Delta P}{\rho} = \text{Friction loss} + \text{Entrance loss} + \text{KE of discharge clearance}$$

$$= f_p \frac{L^\circ}{D} \frac{V^2}{2g_c} + \frac{1}{2} \frac{V^2}{2g_c} + \frac{V^2}{2g_c} = \left(f_p \frac{L^\circ}{D} + 1.5\right) \frac{V^2}{2g_c} \qquad (33)$$

and the continuity equation: $G_L = VA_p$ (34)

A survey of the literature on compressible fluid flow (Ref. 13, 14) also shows that unless the value of the overall pressure ratio is small choking prevails at the last restriction for even a large number of restrictions. Leakage flow then is equal to critical pressure ratio flow for the last restriction.

In the seal systems described above pressure ratios encountered are high.

Moreover, the large shaft diameters for the seal stations (12" diameter and 6.5" diameter) would result in large leakage areas even with the strictest of manufacturing tolerances. For these reasons the use of a contact type mechanical seal is required.

Even where the pressure differences across the seal system are small the need for separation of a liquid stream from a gas stream makes the use of a mechanical seal more desirable.

A mechanical seal constitutes an assembly which forms a rubbing seal between precision finished surfaces, and proper design depends on such factors as:

1. Operating pressures.
2. Operating temperatures.
3. Relative speed between stationary and moving components.
4. Seal materials.
5. Dimensional limitations, etc.

The low friction and wear properties of filled Teflon materials at low temperatures makes these a logical selection for the rubbing component of the mechanical seal used. (Friction coefficient of .1 and low wear are common over a moderate load and speed range.)

Although actual performance data is scanty over a wide range of operating surface speeds, a correlation of load, speed and interface temperature from Ref. 15:

$$\Delta T \text{ surface} = \frac{f_f F_n V}{4.24 \rho_s J^*} \cdot \frac{1}{K_m K_p} \qquad (35)$$

was used as a design criteria.

It should be noted that the above equation does not define the average surface temperature of the contact area but rather maximum local temperatures in the contact area.

Postulating on a limiting surface temperature as the thermal degradation temperature for Teflon, limiting loads were calculated for an operating speed of 67 rad./sec. and typical geometrical conditions (Figure 49).

BASE SPEED - 67 RAD/SEC.
BASE CONTACT WIDTH - $\frac{1}{8}$"
ΔT MAX. 600 - (-270) = 870 °R.

$$\Delta T_{\text{CONT. SURF.}} = \frac{f_f F_n V}{4.24 L_s J^*} \frac{1}{K_m K_p}$$

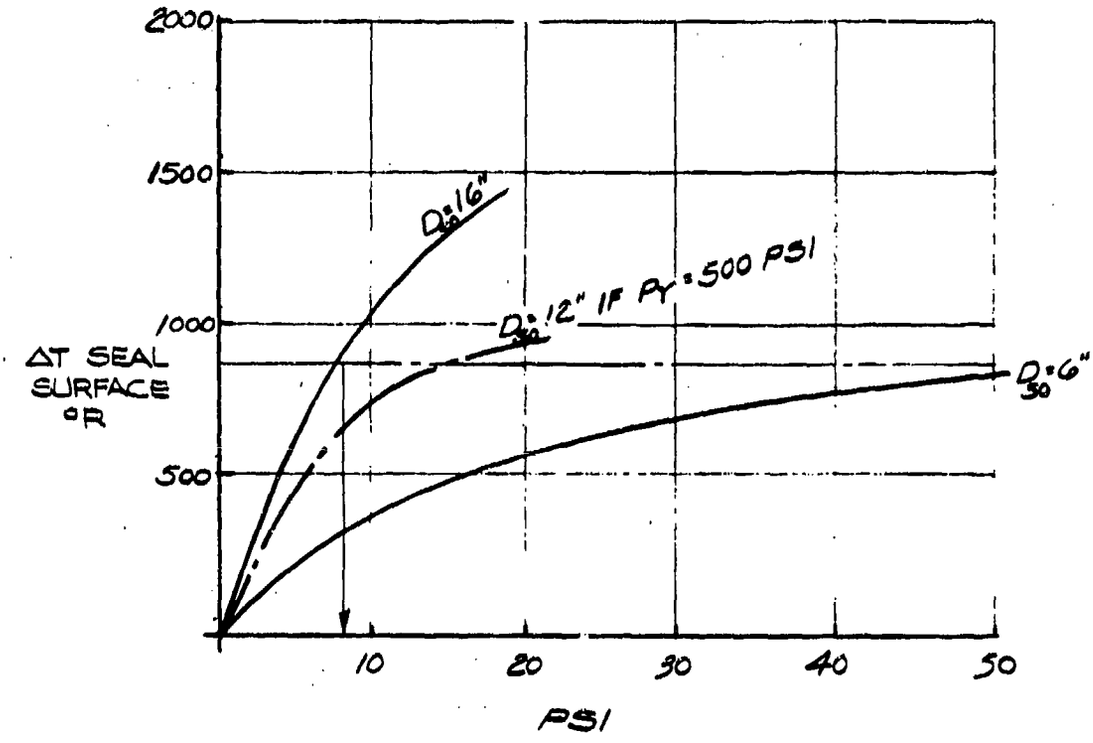

FIG. 49

The numerical values of the limiting loads calculated are at best of marginal accuracy (since average values of friction coefficient and yield strength for Teflon were used in arriving at these).

Of more interest is the fact that the surface temperature is more sensitive to seal diameter (D_{so}) than contact pressure (p) for a given speed. Reducing equation (35), Appendix VI results in the expression:

$$\Delta T_{surface} = C\, D_{so}^{3/2}\, p^{1/2} \qquad (36)$$

For this reason the lowest possible diameter seal should be used. Since the shaft diameter is the lower limit of seal diameter a packing ring type assembly with the inner diameter surface riding on the shaft surface is a logical seal choice.

5.2.4.3 Seal Design

A two-piece ring assembly consisting of a tangentially cut segmental seal ring and a backer ring tangentially or radially cut was selected for the major shaft seals. Fig. 50.

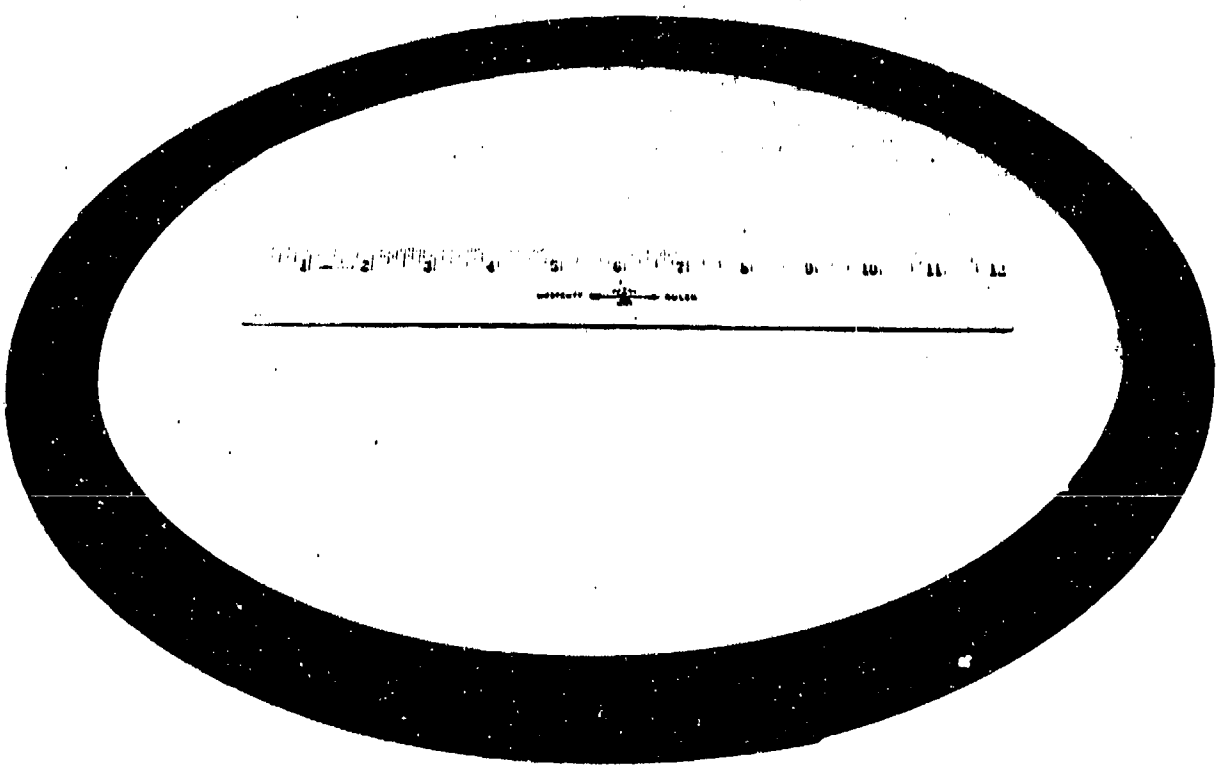

SHAFT SEAL RING

FIG.50

In the two-piece ring assembly, which is stationary with its I.D. surface riding on the shaft surface, radial sealing is accomplished by the tangential cuts in the seal ring while the backer ring provides axial sealing.

The most critical seal area in the entire assembly is at the high pressure air inlet due to both high seal surface velocity (67 ft. per sec.) and high pressure loading (P~221 psi). Using two sets of seal rings and assuming that each set would take equal pressure drop, the contact pressure due to the radial unbalance is approximately 40 psi (based on rings 12 in. I.D. x 3/8 in. x 1-1/2 in. section). To reduce the contact force a ring assembly with balancing grooves cut on the I.D. surface of the rings will be used. 1/8 inch wide grooves cut in the center of each ring would result in 75 per cent reduction in operating contact load.

Grooves of similar design will be used in all other seal areas even though a much more favorable pressure loading situation exists.

In the areas of the high pressure air and liquid oxygen inlets the seal ring assemblies will be free-floating axially although pinned to the housing glands to prevent them from rotating with the shaft. Pressure loading is depended on to form the seal between the ring faces and the ring-gland contact area.

In the area of the liquid nitrogen reflux inlet - waste nitrogen outlet where the pressures on each side of the seal are nearly equal, the sealing performance of a floating ring arrangement may be adversely affected. Pressure fluctuations in either stream may cause axial oscillation of the ring assembly thus an on-off bypassing of fluid around the ring assembly.

To eliminate this the ring assembly can be axially spring loaded in one direction as shown in Figure 57.

In the area of the gaseous nitrogen waste discharge to casing seal pressure unbalance across the seal may be in either direction depending on the pressure level inside the casing. Peripheral seal limitations may require the casing pressure to be maintained at a higher level than the waste nitrogen stream pressure. However, some operation of the separator with casing pressures lower than the waste nitrogen stream pressure may be required. For a two-way seal it is important that the two-piece ring assembly be made up of two identical tangentially cut segmental seal rings. Also, the axial float of the ring assembly should be limited such that a reversal in pressure direction and the accompanying axial movement does not result in disengagement

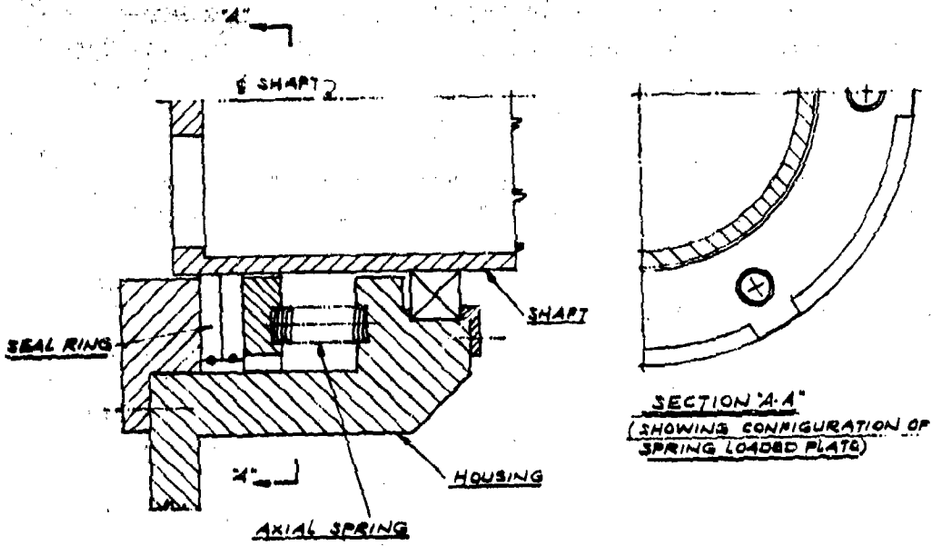

AXIALLY SPRING LOADED ASSEMBLY FIG. 51

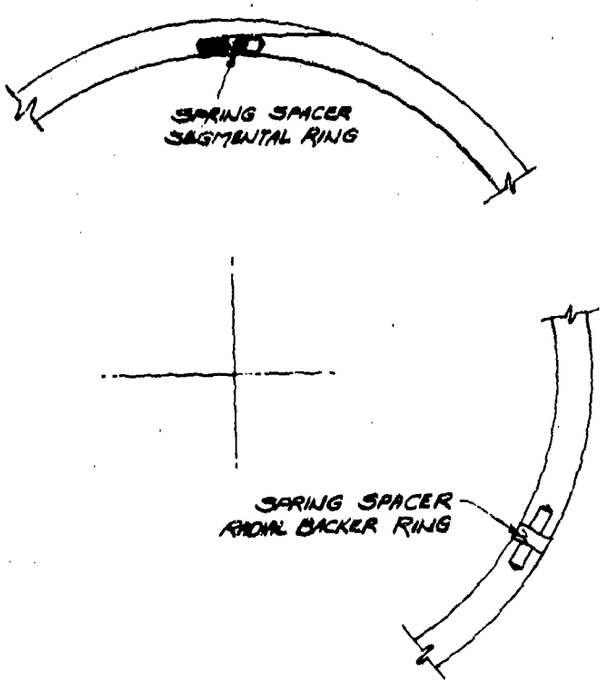

SHAFT SEAL RADIAL SPRING SPACER FIG. 52

of the ring assembly from the pins retaining it against rotation. An alternate to minimizing the ring axial float would be to have the ring assembly pinned on both extreme faces.

Experience with operation of smaller diameter shaft seals of the type described (6 in. I.D.) shows their installation and operation to be satisfactory and stable.

Increasing the diameter of this type seal makes the relative alignment of the rings more difficult probably due to the initial drag on the rings causing the individual segments to "bunch up" at one of the gaps when the rings are conventionally pinned on one segment only.

For this reason better means to maintain relative alignment of the ring assembly are required. Spring loading of the ring segments in the circumferential direction as shown in Figure 52 is used to provide proper ring alignment.

5.2.5 Column Rotor

5.2.5.1 Column Rotor Configuations

Functional design considerations for the rotary air separating plant fix the geometrical configuration of the column rotors. On the basis of a given tray spacing and a given superficial vapor velocity (V_s) at each tray, the axial width is determined by the radial vapor flow as:

$$\frac{V_i}{\rho_v} = \frac{V_s \pi D_t b}{fa} \qquad (37)$$

Because of the tray position (i.e., the small tray diameter) and the amount of vapor flow, it is seen that the enriching section of the low pressure column requires the largest change in axial length for each tray location. A wall profile for this section of the column is shown in Figure 53.

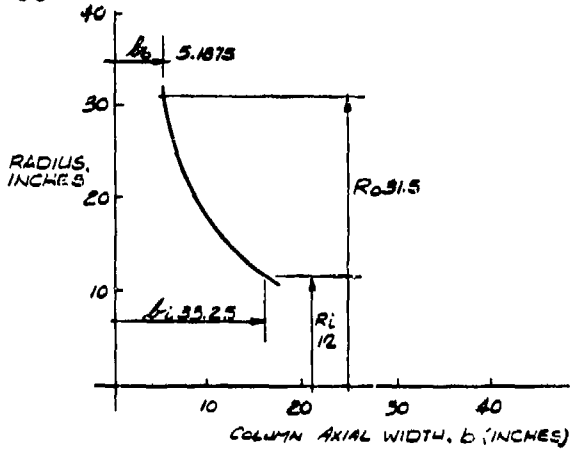

PROFILE LPC
ENRICH SECTION

FIG 53

Contoured walls represented the most feasible approach to effect the required large axial variation in the enrichment section of the low pressure column.

The required wall contour could be approximated by a weldment of a series of conical sections which could then be contour machined, or it could be provided by a properly spun "skirt." The more uniform configuration resulting from a spinning operation providing both a more accurate geometrical section and better material continuity formed the basis for the selection of spun side walls for the enriching section of the low pressure column rotor.

Since only a slight contouring of the walls is required to maintain the desired vapor superficial velocity in both the stripping section of the low pressure column and high pressure column, a spinning operation for the side walls in the above becomes impractical. Instead, the required area can be obtained by controlling the active width of the tray. To do this, the tray edges are blinded by the required amount as shown on Figure 54.

On the basis of a uniform column axial length (b_c) calculations yield:

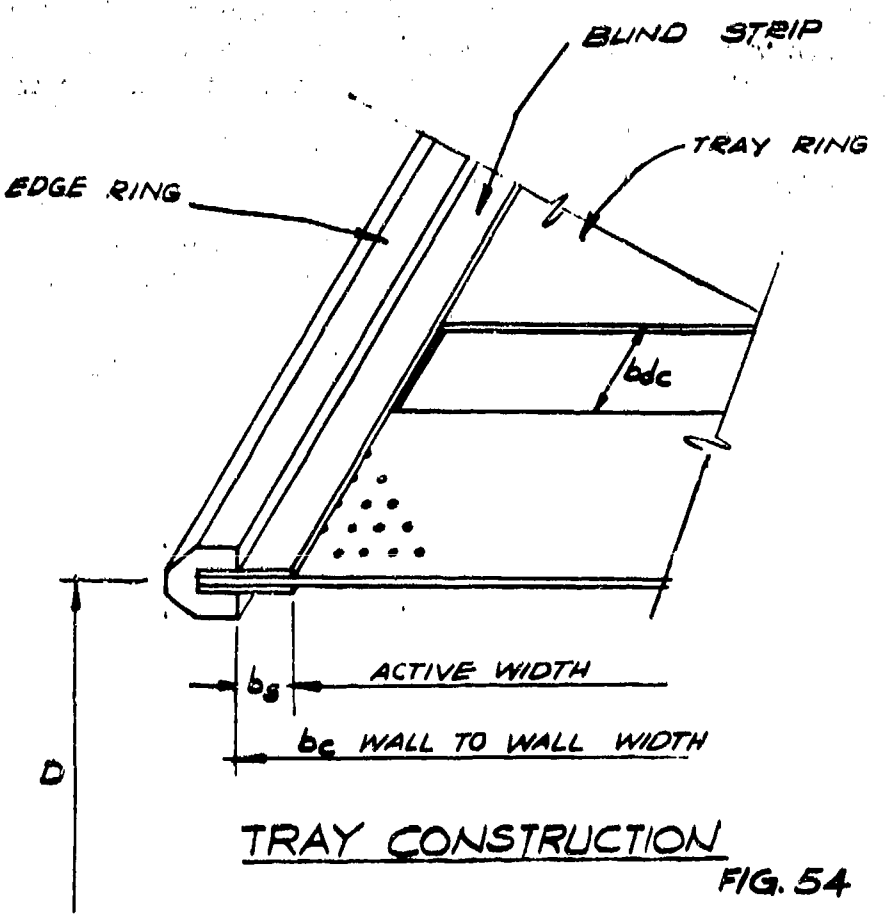

TRAY CONSTRUCTION

FIG. 54

$$\text{Active Area} = \text{Total Area} - \text{Covered Area} \begin{cases} \text{downcomer} \\ \text{inlet} + \text{weir} \\ \text{end} + \text{strips} \end{cases}$$

$$\pi D_t b - b\, b_{dc}\, \eta_l - 2\pi D_t b_{st} + 2 b_{dc} b_{st} \eta_l = f_a \pi D_t b$$

$$b_{st} = \frac{\pi D_t b (1 - f_a) - b\, b_{dc}\, \eta_l}{2 (\pi D_t - b_{dc}\, \eta_l)} \qquad (38)$$

The addition of blind end strips on the tray to control tray active area has the following advantages:

a. It eliminates the spinning operation.

b. It structurally reinforces the tray edges, where maximum stress occurs (refer to stress analysis of tray rings, Appendix VII).

c. The trip application can be integrated into the tray ring construction requiring no additional fabrication.

5.2.5.2 General Mechanical Design

As can be seen, the all-aluminum construction column rotors consist of the concentric tray ring array and the supporting side walls appropriately contoured to provide the required circumferential area at each tray ring. Figures 55 and 56 show the assembly for both the high and low pressure columns. The low pressure column rotor is made up of a stripping section with seven tray rings which bolts to the enriching section having eleven tray rings. The two-section assembly is mounted by appropriate bolting to the shaft. The high pressure column is made up of a single section having nine tray rings. It is bolted to the reboiler-condenser casing. It is easy to see that by proper integration of tray rings into the column walls the trays can be made load-carrying structural members which support axial pressure forces in tension and, therefore, eliminate need for excessively heavy column side walls.

In considering any one of the three sections, it is seen that relative positioning of any tray ring with respect to the adjacent tray ring on either side is critical (i.e., proper alignment of downcomer tubes and inlet or receiver weirs) and proper posi tioning can be accomplished only with one of the side walls not in place.

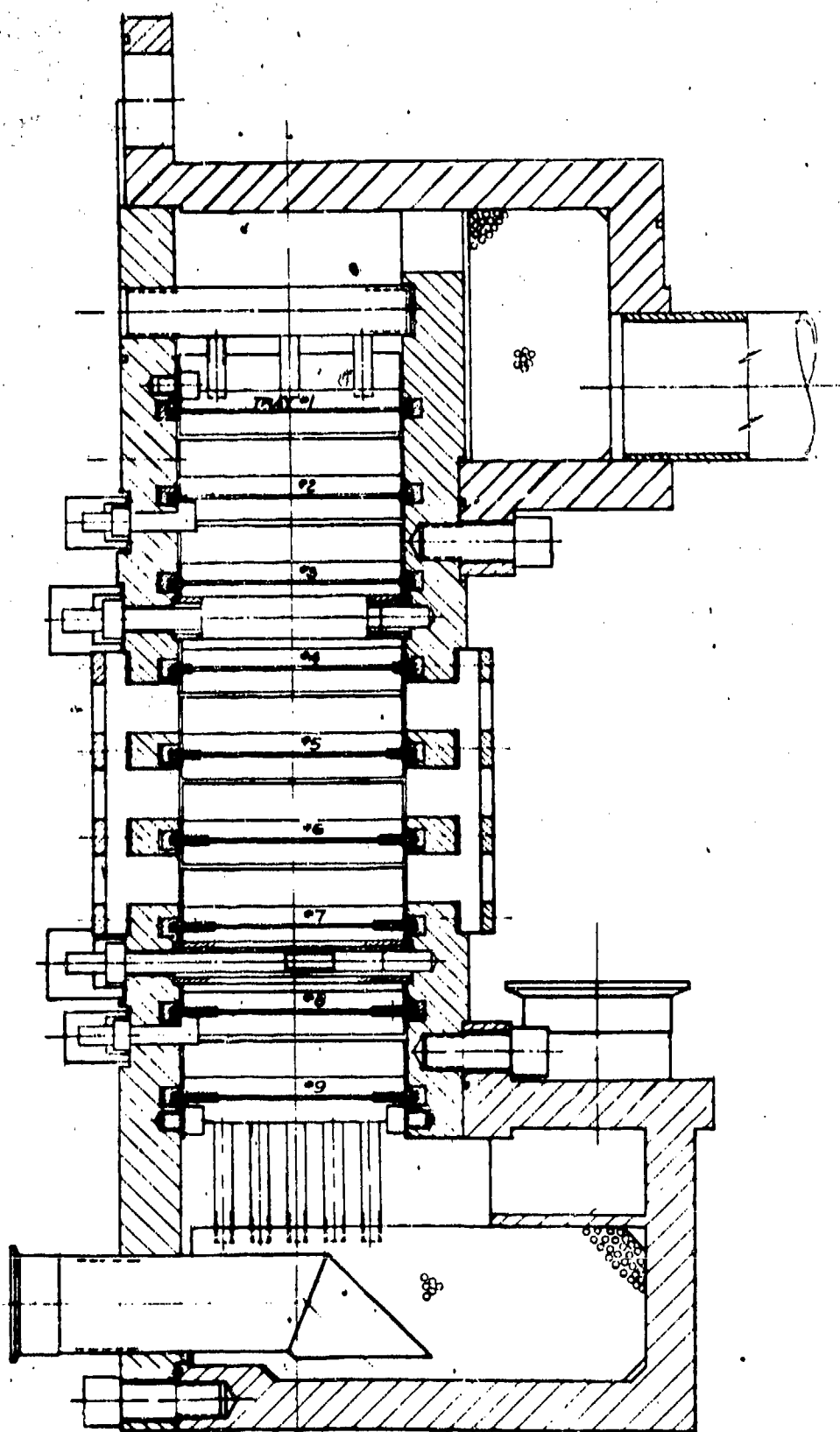

SECTION AA

173

IGH

CONFIDENTIAL

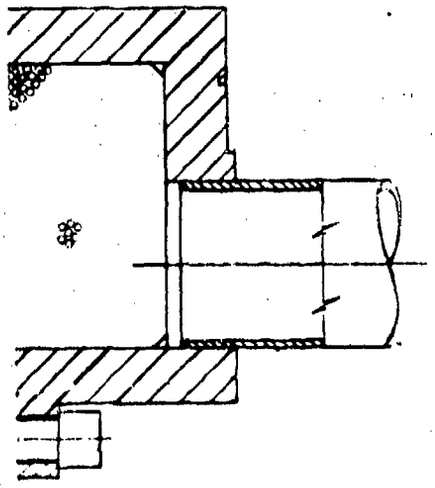

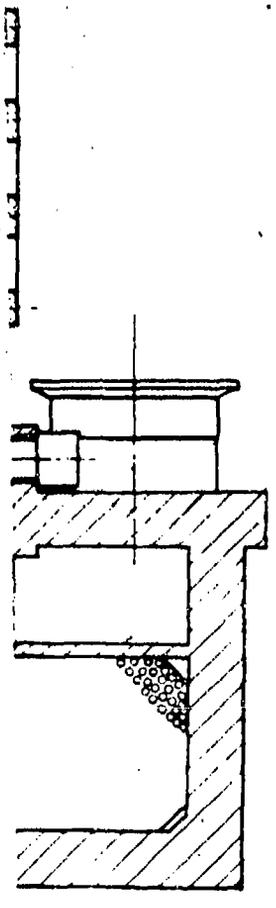

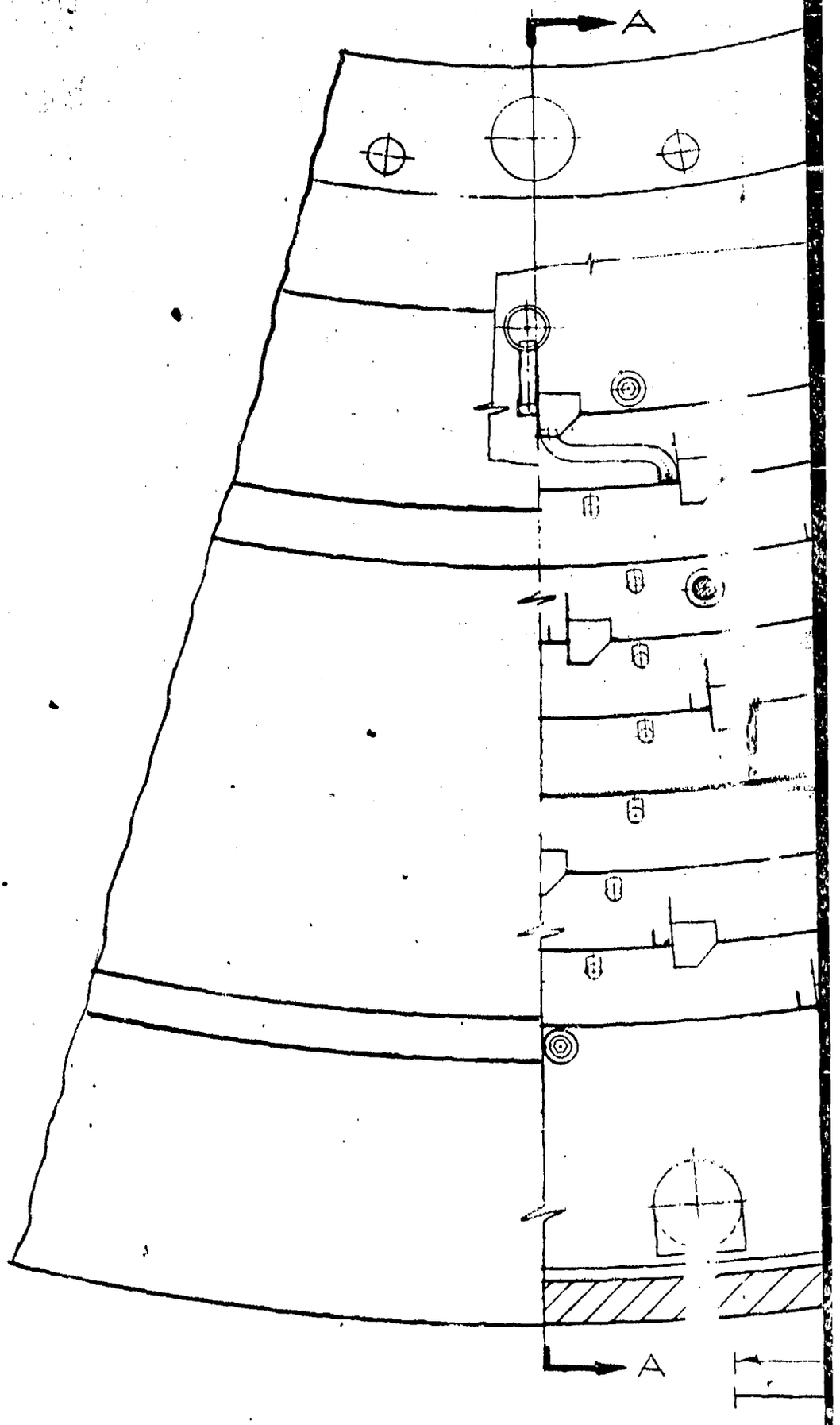

2 of 2

HIGH PRESSURE COLUMN

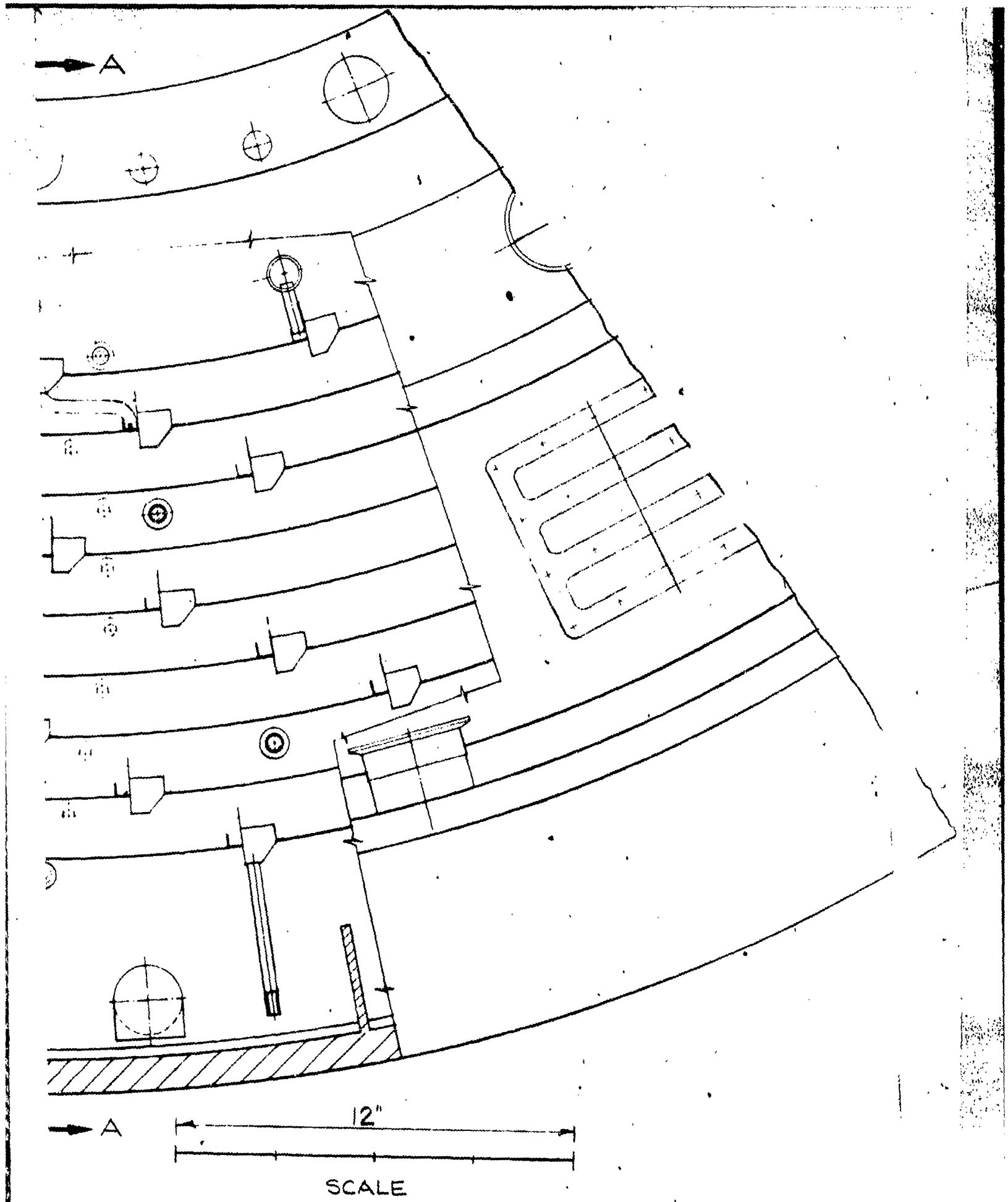

1N

3 of 3

FIG. 5F

C-554424

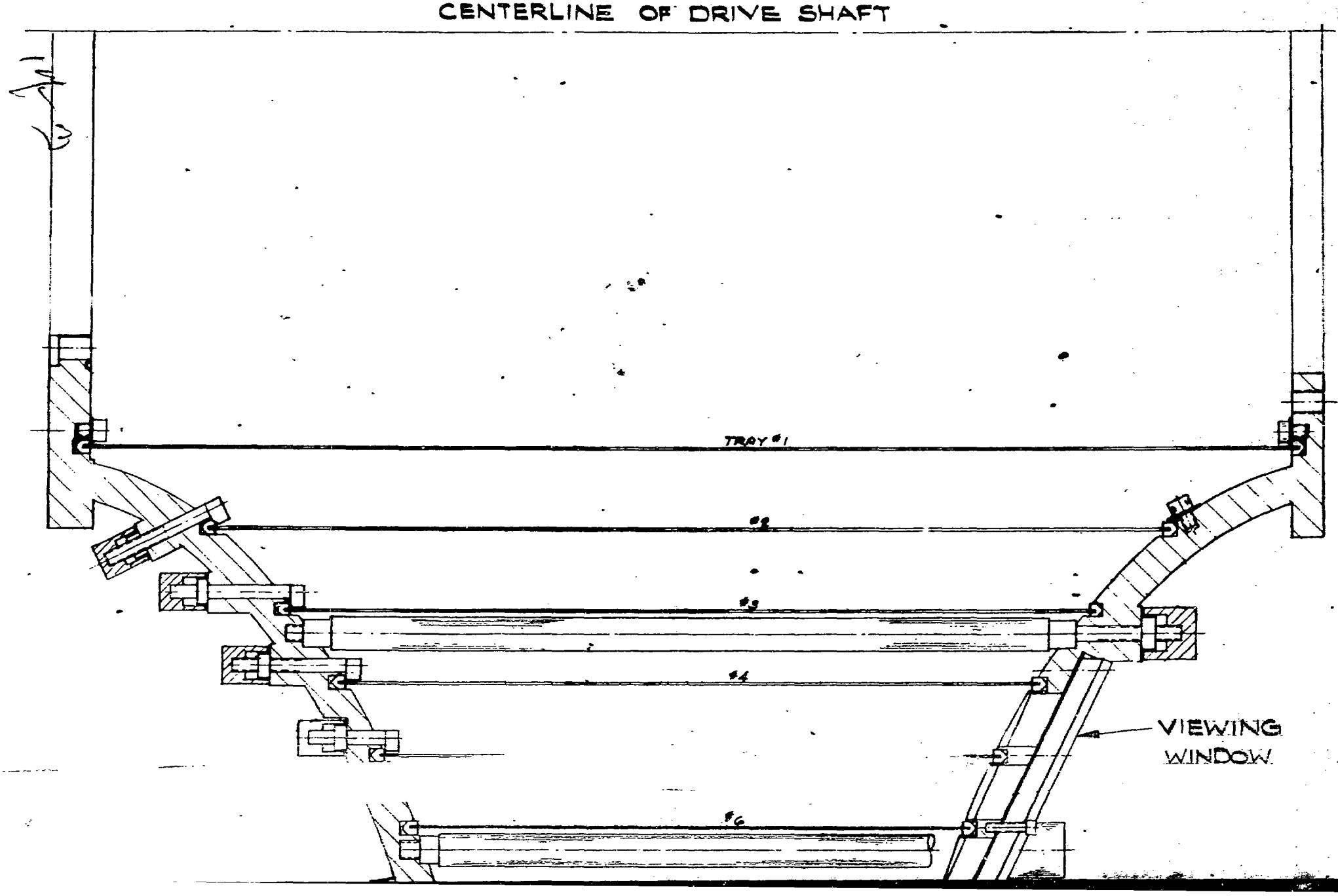

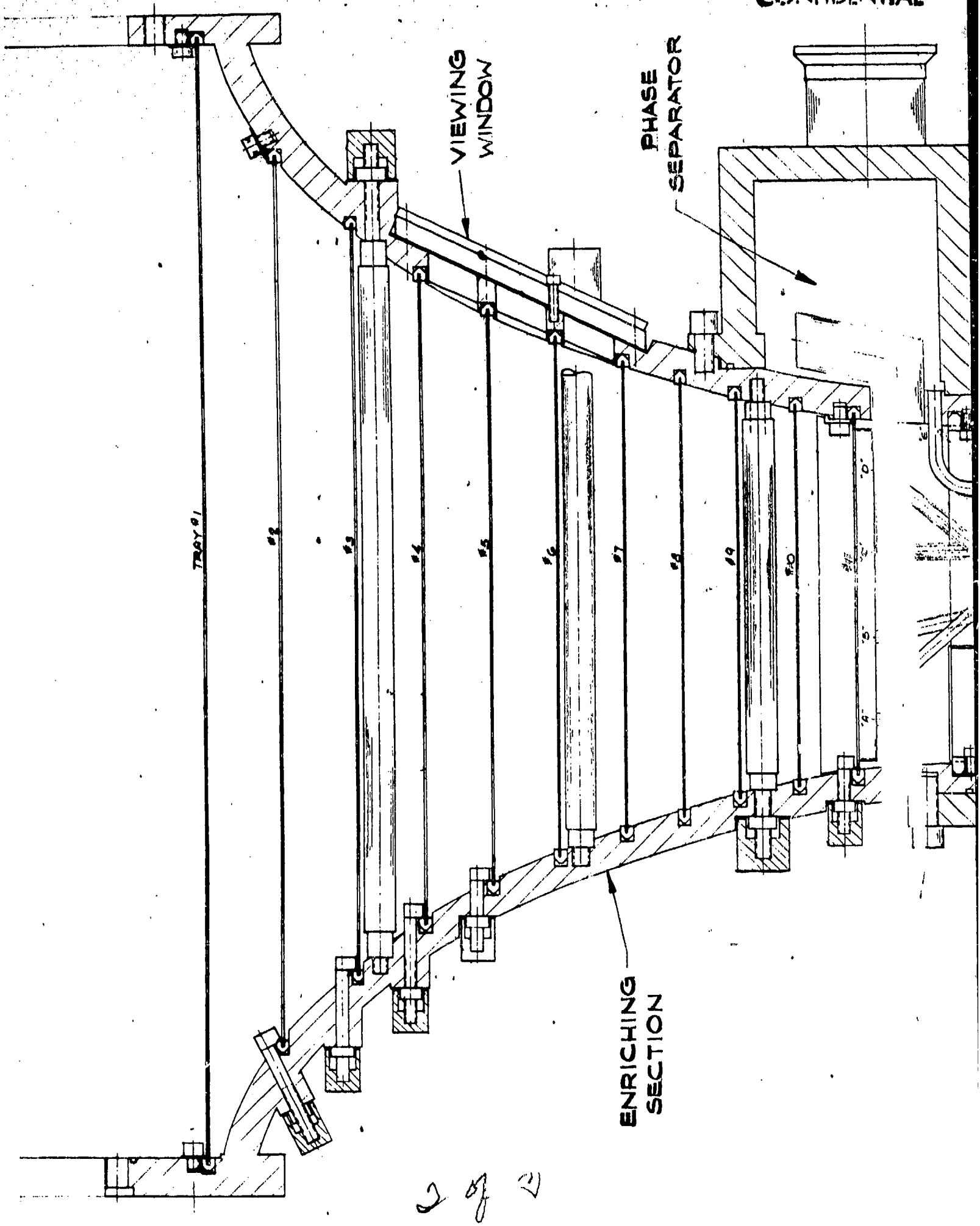
VIEWING WINDOW
PHASE SEPARATOR
TRAY #1
#2
#3
#4
#5
#6
#7
#8
#9
#10
ENRICHING SECTION

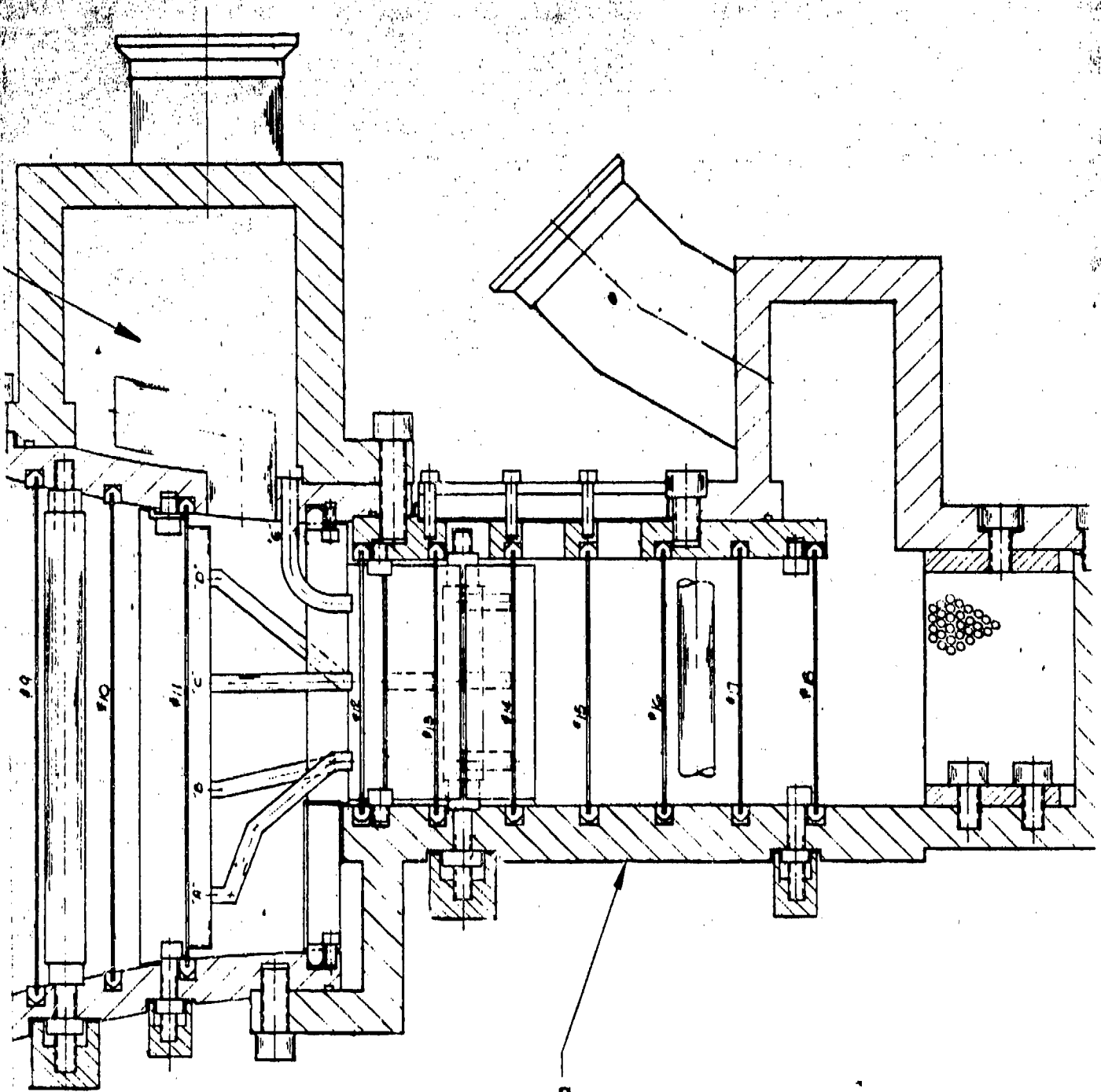

FIG. 5E

In the original design concept, the trays were directly joined to column walls. With this design any modification on trays would have required essentially refabrication of the entire column section. In addition, since trays are inaccessible after being joined to both column walls, the chance of imperfections in tray alignment, or faulty local tray-wall joints, would have increased the risk of having to scrap column assemblies during fabrication.

In order to increase the general flexibility of the apparatus and ease fabrication problems, it was decided to design the columns with individually removable tray ring assemblies similar to the type used in the circumferential tray UCON test rotor (Ref. 1, Appendix V). The trays in this instance are permanently joined to rings which are mounted in grooves in the column walls and secured to the latter by bolts. Aside from increasing the research utility of the apparatus, the separable tray ring provides for flexibility in column assembly and alignment and reduces the scrap risk since trays are individually manufactured.

5.2.5.3 Tray Ring Detail Design

The previous tray ring design used in the UCON tester required two furnace operations to complete fabrication. In the first operation the inlet weir, the downcomer trough, and downcomer tubes were brazed onto the perforated tray strip. In the second operation, the brazed assembly was soldered to thin edge rings or mounting flanges.

Although this fabrication procedure was feasible, the soldering operation was characterized by many troublesome steps. Among these were:

a. Lengthy operation for proper positioning and retention of solder. (The solder wire was positioned in a V-groove and retained by small tie wires which had to be removed after the soldering operation.)

b. Difficulty in control of solder runs which required an additional subsequent cleaning operation.

c. Most detrimentally, pickling of the soldered assembly in the nitric-hydrofluric acid solution required to remove the soldering flux resulted in an increase of the tray open area.

The present tray design is arranged in such a way that the ring assembly can be accomplished in one furnace operation. The solder filler material is replaced by a clad aluminum strip as shown on Figure 54 and the tray is brazed to the edge rings simultaneously with the brazing

of the inlet weir and downcomer to the tray ring. This tray ring design is advantageous since it eliminates one furnace operation and any preparatory setup and cleaning required in the soldering operation. The clad aluminum strip can be varied in width and thus also used to control the tray active area for the straight wall sections of the column rotors. In addition, it reinforces structurally the tray edges where maximum discontinuity stresses occur.

The tray configuration (i.e., tray open area, number of downcomers per tray, etc.) was in part specified by functional design requirements with the general arrangement evolved so as to facilitate fabrication and assembly. For instance, downcomer width was varied only in the enriching section of the low pressure column so that the number of bending dies could be kept at a minimum.

The downcomer tube area was calculated for each tray from:

$$\Delta r \frac{r\omega^2}{g_c} = \frac{\Delta P}{\rho_L} + \left(\frac{V_t}{A}\right)^2 \frac{1}{2 g_c} \qquad (39)$$

The number of downcomer tubes was varied as required on each tray using the same size tube for all trays, thus minimizing the number of bending fixtures and the number of hole sizes required on the downcomer troughs on each tray.

The flanged construction needed for the modular separator design in conjunction with the requirement for observation windows in the column walls led to the specification of heavy wall thicknesses. Since at the same time the tray rings are assumed to carry axial pressure loads in tension, stresses in the walls resulting from centrifugal as well as pressure forces become relatively small.

For this reason, stress analysis work was concentrated upon analysis of the tray ring assemblies which, because of their relatively lightweight construction, become the critical structural members.

The design of the tray rings was carried out on the basis of no axial restraints on the rotor side walls and a casing pressure of 0 psig since this represented the maximum load condition.

On the assumption that each tray ring in the low pressure column and high pressure column rotors behaves like a cylindrical shell with fixed edges under the action of internal pressure, an analysis was carried out to determine the maximum stresses developed (which occur at the fixed edges). (See Appendix VII)

This is plotted as a function of radial position on the basis of a tray ring thickness t = 0.04" for the low pressure column and t = 0.06" for the high pressure column in Figure 57.

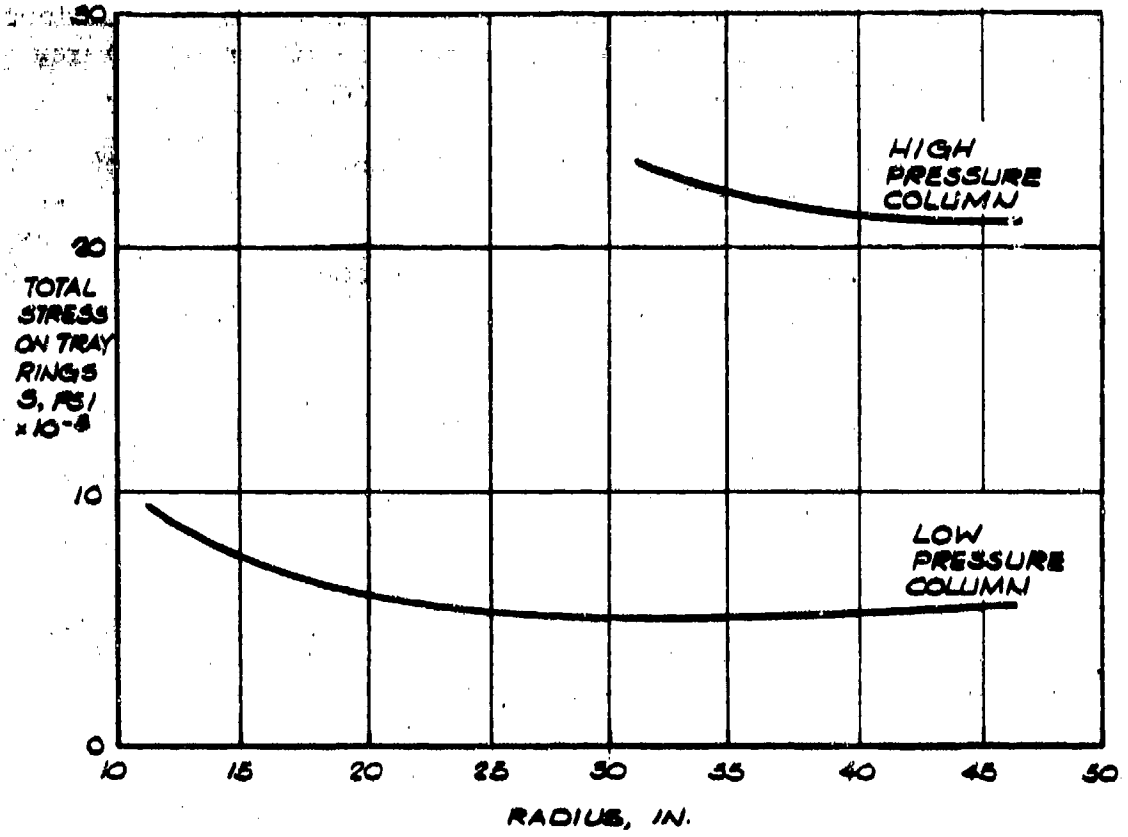

DISCONTINUITY STRESS IN TRAYS

FIG. 57

The stress levels in the low pressure column tray rings (8,500 psi maximum at inner tray ring) are within the range of allowable stresses for 3003 aluminum alloy. For the high pressure column tray rings a 5083-0 or 6061 T6 aluminum alloy is required. Poor brazeability of 5083 aluminum makes the use of 6061 T6 aluminum necessary.

It must be again emphasized that the stress analysis for the high pressure column and low pressure column tray rings neglects the effects of axial restraints on the rotor sides, i.e., bolting to shaft flanges which would tend to reduce the axial tension on the tray rings. The increased rigidity of the tray rings due to the brazed downcomer troughs has also been ommitted from the analysis.

In addition to the trays, a number of 7/16 inch diameter tie rods with their tubular spacers have been provided with the following distribution to rigidize the column rotor side walls:

	No. Rows	No. Rods/Row
Low pressure column enrichment section	3	8
Low pressure column stripping section	2	8
High pressure column	2	8

Furthermore, the casing pressure will have a countering effect on the internal rotor pressure and, depending on its level, it may result in a complete balance or even a reversal of pressure loading in the case of the low pressure column.

5.2.5.4 Tray Ring Fabrication

The tray ring consists of a brazed assembly of three basic and single components as shown in Figure 58. The most basic element of the tray ring assembly is the perforated strip on which are mounted the inlet weir and the downcomer trough. Edge rings border the tray strip and serve the same function as that of mounting flanges.

The downcomer troughs and inlet weirs were formed from clad aluminum sheet on a 24" box and pan brake. Due to unusual bending operations modified end fingers were required for the brake. To insure more positive positioning of these individual components on the tray and to achieve a more uniform brazed joint rivetting was used for preassembly as shown in Figure 59.

The downcomer tubes leading from the downcomer trough of one tray to the incoming weir of the adjacent tray were bent to the specified S-shape by means of a specially adapted fixture shown in Figure 60. Since the tray spacing necessitated the use of small radius bends special techniques had to be adapted to prevent collapse of the tube during the bending operation.

The size of the tray rings required ranges from 24" diameter minimum to 96" diameter maximum. Handling this size range for the brazing operation in the available equipment (furnace) presented a serious problem. The brazing operation used in the fabrication of the tray rings requires preheating of the furnace to the brazing temperatures so that the work piece can be raised to brazing temperature almost instantaneously to have the flux remain active. This implies a small drop in furnace temperature while the work piece was being introduced. Availability of large furnaces capable of the above heat duty cycle is limited. For this reason it was decided to fabricate the tray in sections,

SHAFT FABRICATION SECTION 3 FIG. 58

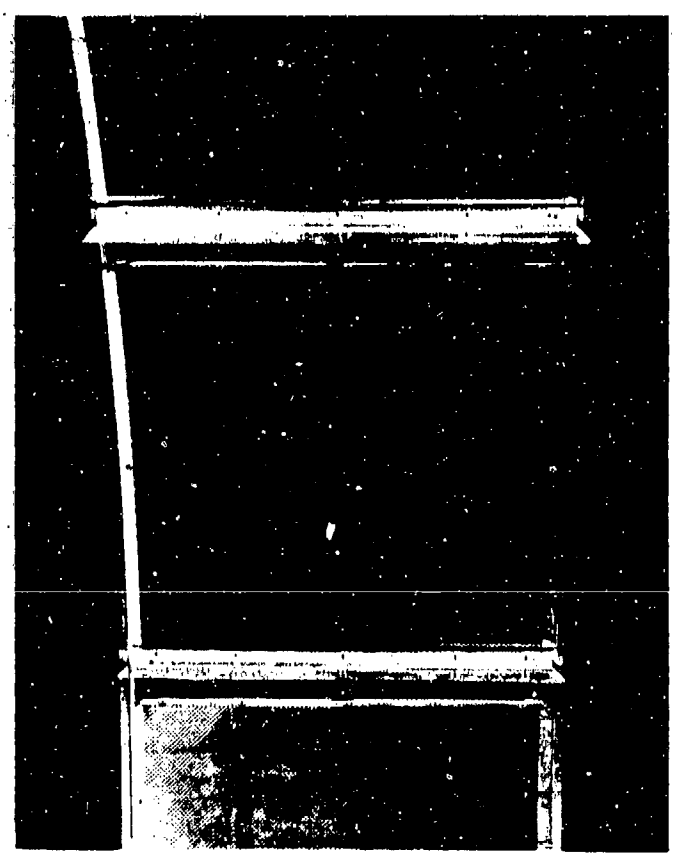

TRAY RING ASSEMBLY

FIG. 59

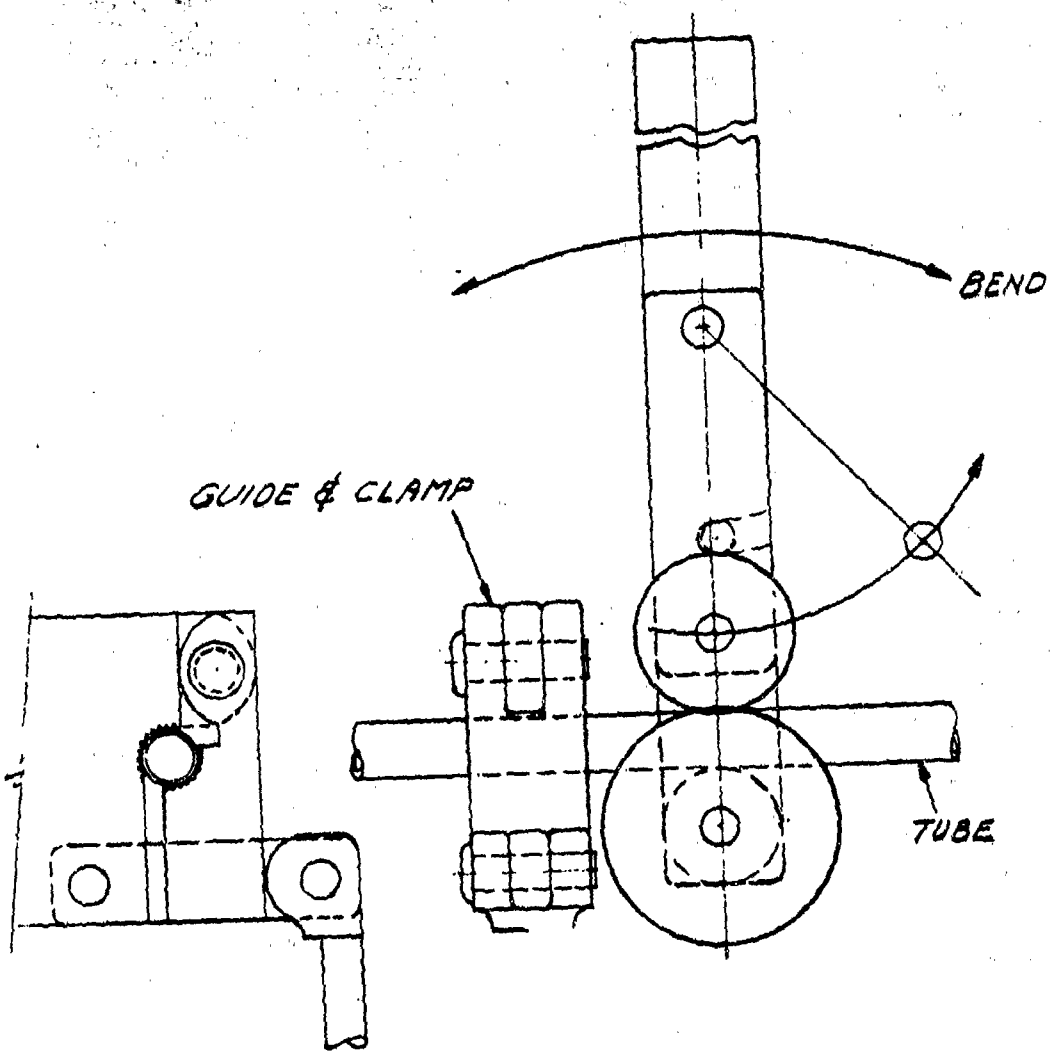

DOWNCOMER TUBE BENDER

FIG. 60

(Fig. 61 and 62), later joined to form continuous rings. Figure 63 shows one-half tray ring being removed from the furnace after brazing.

The brazing heat cycle is depicted in Figure 64. It is noted that since the tray rings were inserted into the furnace cold the furnace was preheated well above the brazing temperature range (1100-1140°F) so that the tray rings could be brought up to temperature in three to five minutes, that is, before the flux became inactive. The flux used was Alcoa No. 30 principally used in furnace brazing operations.

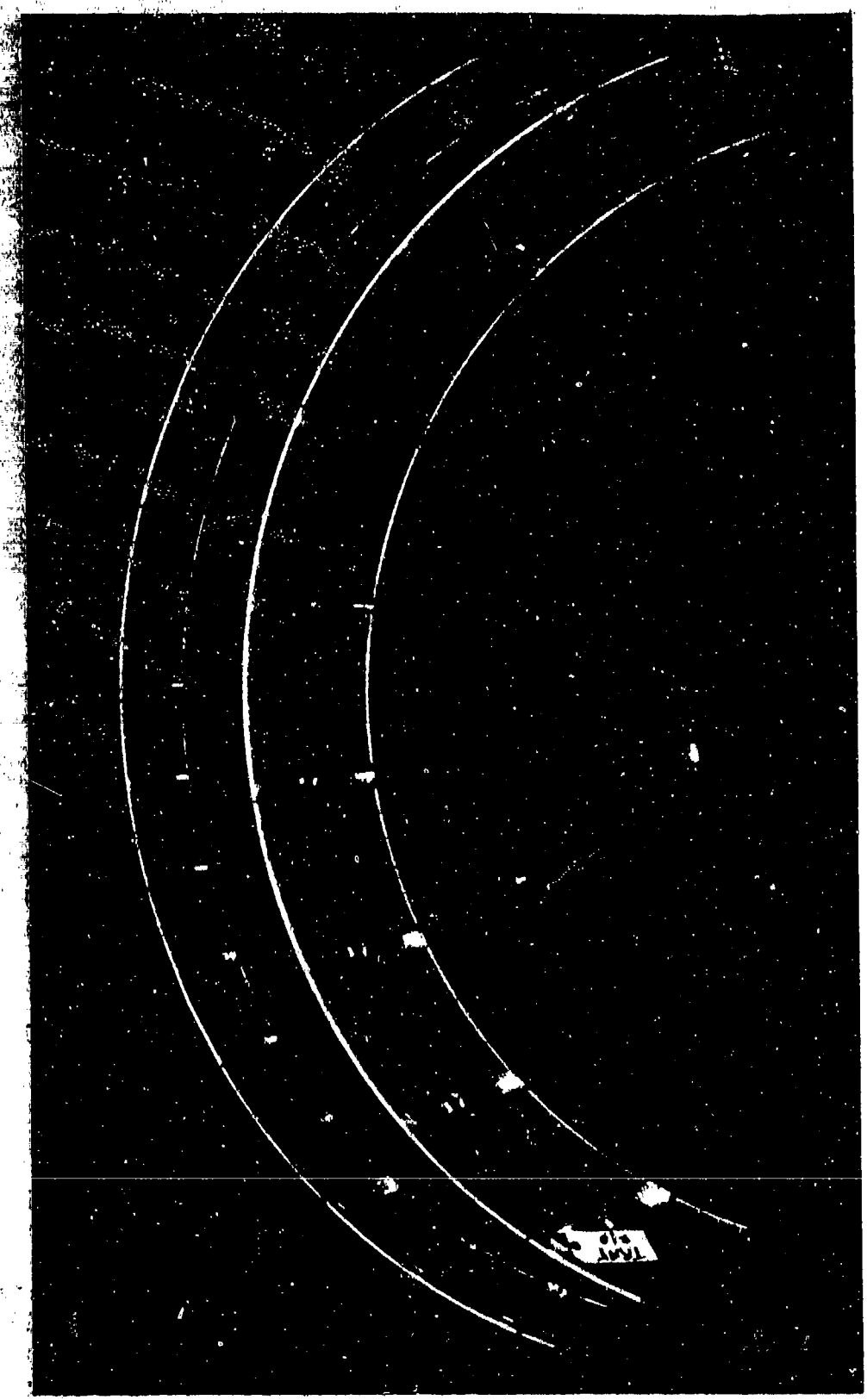

TRAY SECTION PRIOR TO BRAZING

FIG. 61

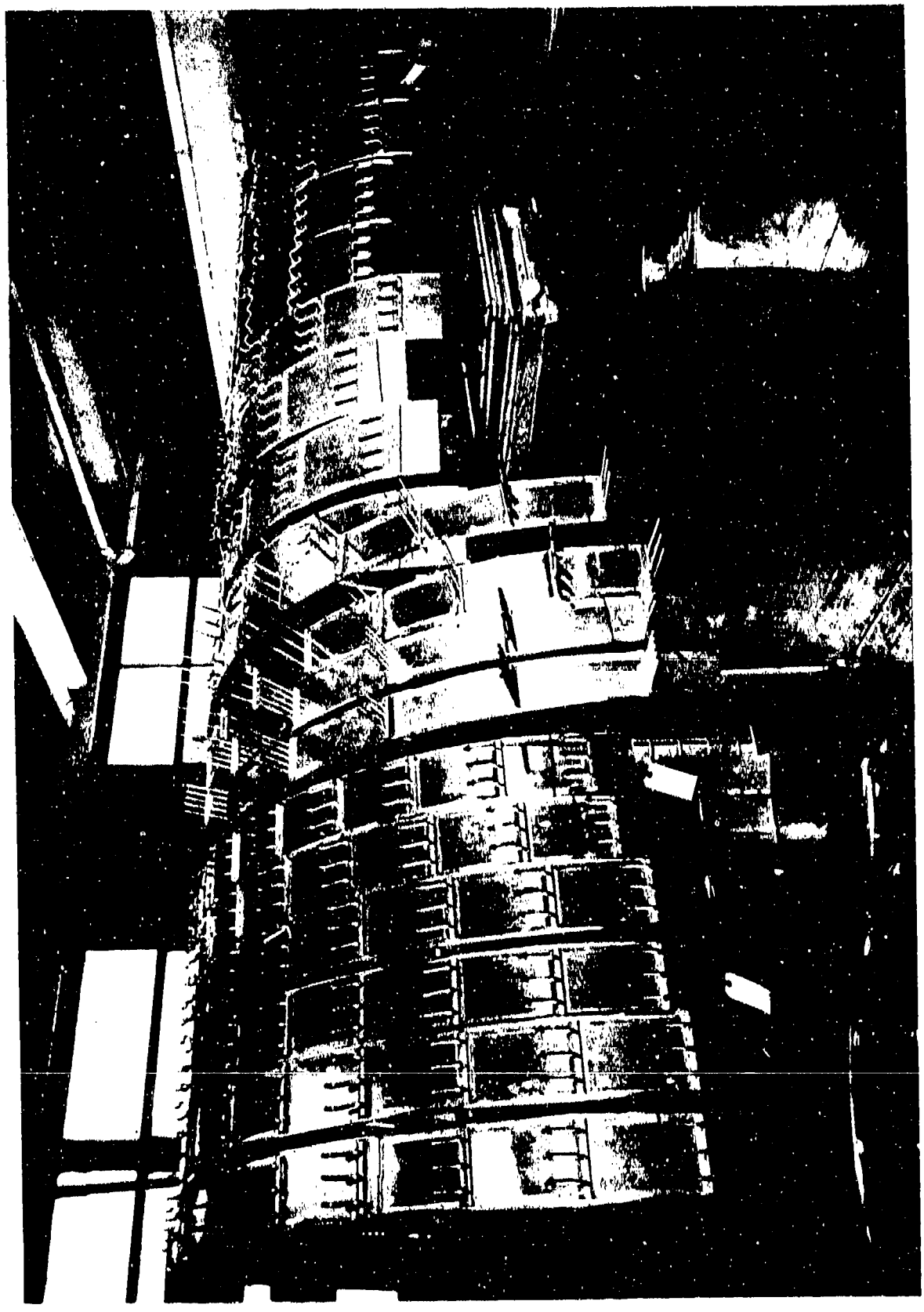

TRAY SECTION AFTER BRAZING

FIG. 62

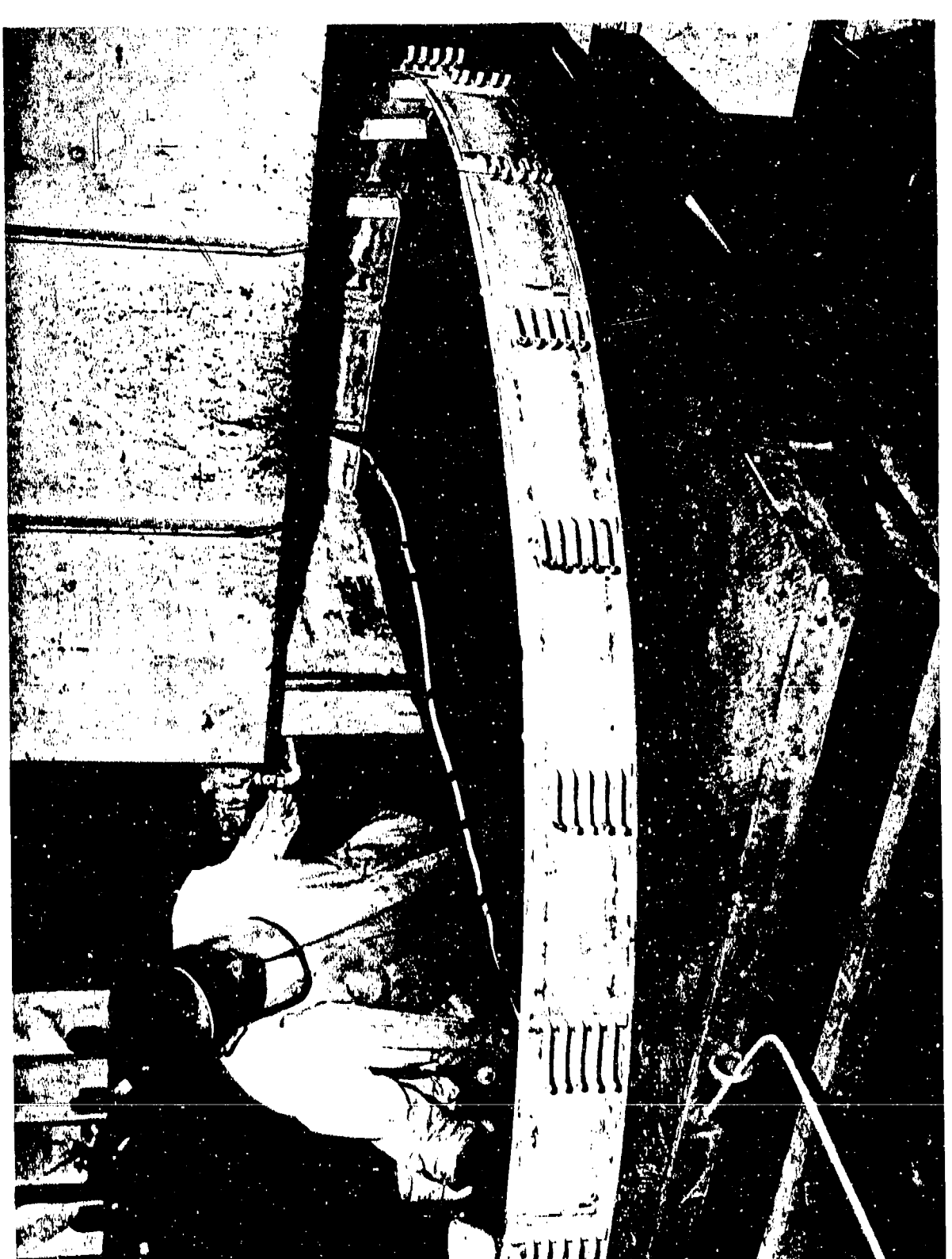

FIG.63 TRAY SECTION AFTER BRAZING

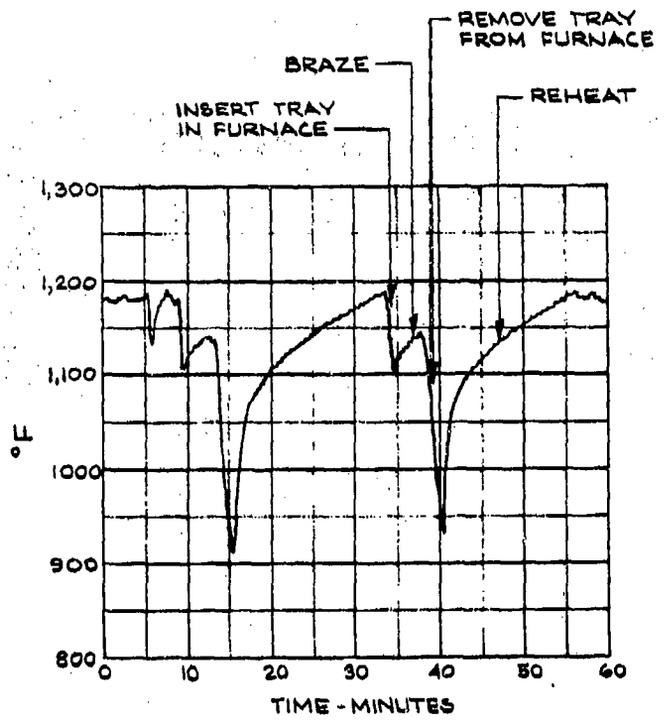

TRAY BRAZING HEAT CYCLE

FIG. 64

In the case of trays No. 1, 2, and 3 of the low pressure column although their diameter was not limiting, their width was larger than the furnace head clearance and prevented brazing of the tray ring in an upright position. Since fixturing of sections of the rings in any other position was difficult, torch brazing methods had to be used for these tray rings.

The as-brazed tray rings required only a moderate amount of work such as cleaning excess brazing material, straightening of distorted sections, etc. prior to their installation on the appropriate groove on the column walls. A fair amount of hand fitting was required during installation.

A number of assembled tray rings are pictured on Figures 65 and 66. Figure 65 shows the tray array for the two sections of the low pressure column assembled on one side wall and bolted to the appropriate shaft section. Figure 66 shows the tray subassembly of the high pressure column.

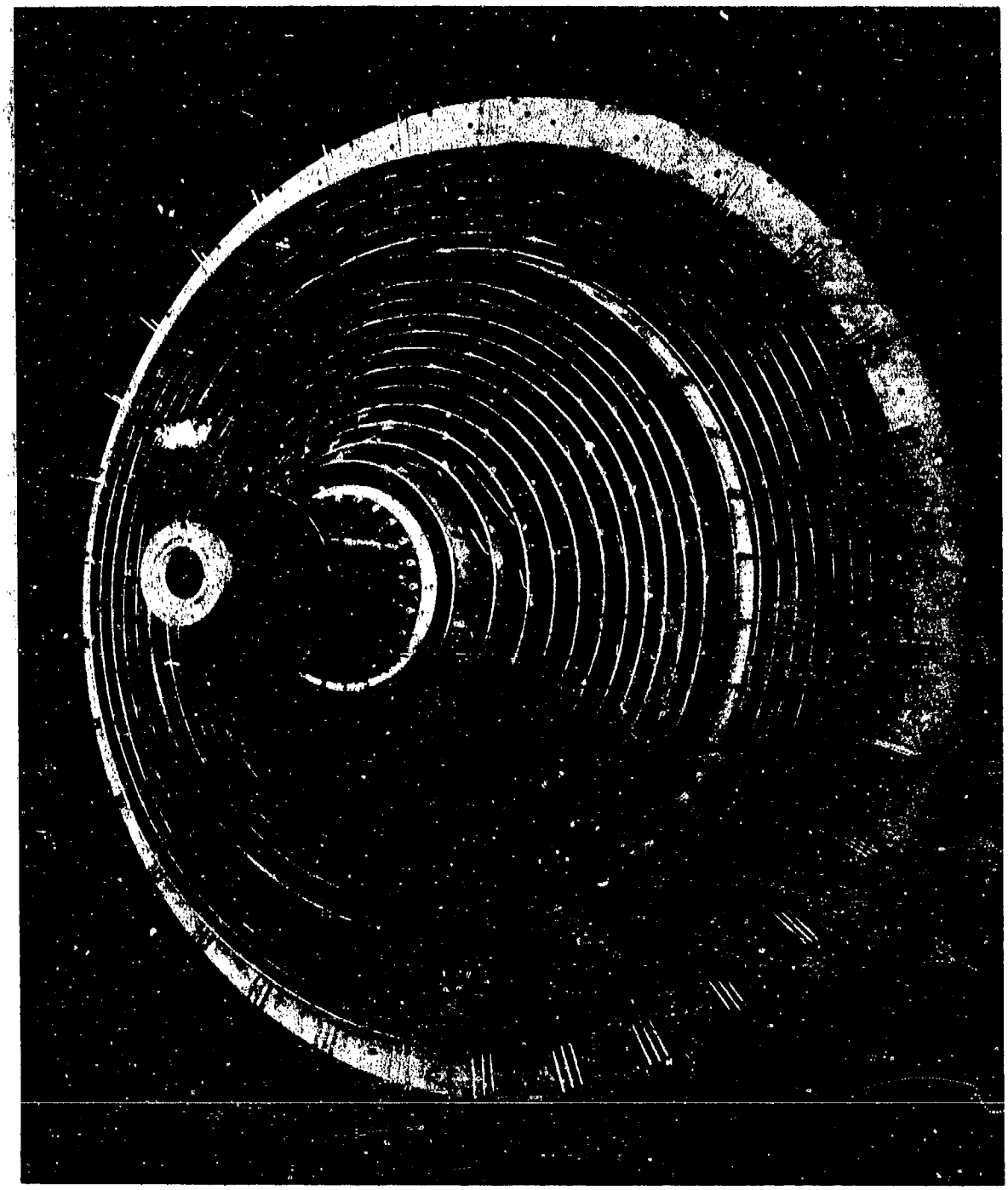

LOW PRESSURE COLUMN

FIG.65

HIGH PRESSURE COLUMN FIG.66

5.2.5.5 Column Rotor Assembly

Satisfactory column rotor assembly depends at least in part on the accessibility of the trays for proper alignment of downcomer and downcomer tubes with respect to incoming weirs on adjacent trays.

Because of this the rotor assembly design provides for installation of the tray rings in concentric circumferential retaining grooves on the inner face of one rotor wall first. After relative alignment of the tray rings bolting of same to the rotor wall would be accomplished from the inside face. Assembly of the entire rotor would be completed by "dropping" the second side wall into position. This die will have the same concentric groove arrangement to retain the other edge of the tray ring. Bolting of the tray rings on this side of the rotor will be done from the external surface by means of specially designed J-bolts. Figure 67.

The bolting of the tray rings within the low pressure column rotor walls is not critical and the bolting arrangement is principally selected to result in a rigid unitized assembly.

In the case of the high pressure column on the basis of no other axial restraints on the rotor walls the axial pull on the tray rings is:

$$F_t = P \cdot s_t \quad \frac{\text{lb}}{\text{inch of circumference}}$$

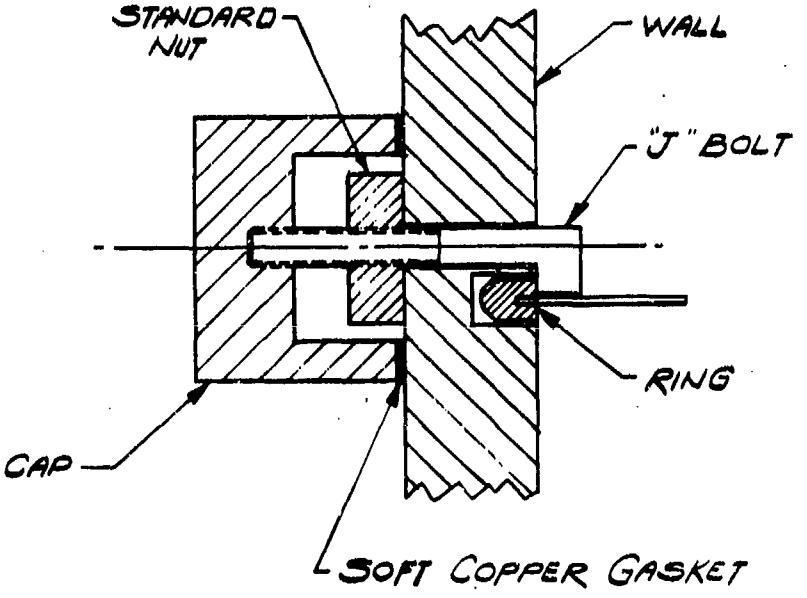

"J" BOLT SEAL

FIG. 67

For a net pressure (P) on the rotor walls as high as 200 psi and tray spacing (s_t) of 1.75 in., the axial pull on the tray would be 350 lb./inch of circumference. With this loading use of 3/8" bolts spaced 4" apart would result in a bolt tensile load and a bolt-tray ring contact stress of 20,000 psi requiring use of 2024-T6 Al which has a yield strength of 68,000 psi at -320°F.

Since blind bolting is used to assemble the tray rings on one side wall no sealing problem is encountered here. On the second side wall the through type J-bolts must be sealed on the external surface of the rotor wall. In previous similar situations a STAT-O-SEAL washer (i.e. a washer with a built-in rubber O-ring gasket on the ID) was used. The unavailability of such compact fastener seals for low temperature applications and the limited applicability of other commercially available low temperature seals led to the use of cap nut-soft gasket seals. (Figure 67)

In the side-by-side arrangement of low pressure column and high pressure column rotors on the same shaft the section of the shaft between the two rotors has the least flexural resistance. Axial rods connecting the peripheries of the rotors were provided to increase the rigidity of this section as discussed under "shaft design".

The resulting effect on the rotor wall edges was considered by estimating the strain of the axial rods due to the bending of the shaft if the axis of the column rotors remained plane.

This strain results in a maximum load on the edge of the column side wall of 750 lb.

In assessing the effect of this loading condition on the rotor side wall it was taken that the rigidity of the central section of the column rotors (i.e. tray-rotor sides assembly) is much larger than the rigidity of the cantilevered edge at the periphery (in the ratio of 100/1 min.) so that it was considered that the cantilevered edge was critical.

On this basis bending stresses in the order of 1000 psi are obtained. It is felt that these results are of such a magnitude as not to warrant a more rigid approach.

5.2.5.6 Process Stream Manifolding

A number of manifolds are attached to the columns. Of particular importance are the ones from which liquid has to be distributed to the columns. These are:

a. Manifold for receiving kettle liquid transfer from high pressure column to stripping section of low pressure column

b. Manifoldreceiving shelf liquid transfer from reboiler-condenser enriching section of low pressure column, and

c. Manifold receiving condensate from reboiler-condenser for distribution to high pressure column.

In the first two cases the stream manifold must act as a centrifugal phase separator for liquid-vapor streams, and at the same time act as liquid reservoirs or surge volumes stabilizing internal flows in the separator.

In order to maintain a predetermined liquid level and adequate liquid distribution in the manifold rings, a flow distributing resistance has to be introduced into the liquid flow path downstream from the manifolds. This is accomplished easiest through the use of orifices with liquid level as the driving force.

Liquid withdrawal from the manifold rings is dictated by the tray ring onto which the liquid is discharged. That is, for uniform liquid distribution the number of liquid headers from the manifolds must be the same as the number of inlet weirs on the receiver tray.

The kettle liquid is discharged onto Tray No. 12 of the low pressure column with 32 inlet weirs, while the shelf transfer liquid and the nitrogen reflux discharges onto Tray No. 1 of the low pressure column with 8 inlet weirs.

The kettle liquid transfer to Tray No. 12 is arranged with 32-7/16 inch tube headers equally spaced on the manifold annulus side wall and bent into the close end of a corresponding inlet weir on the tray ring. The tubes themselves furnish the flow distributing restrictions. A liquid head of 16 psi or 2 inches of liquid in the manifold is required. The holdup volume available in the manifold is approximately twice the normal operating level.

The vapor is directed to the midsection of the low pressure column by means of sixteen 1-1/2 inch diameter tube headers.

The shelf and reflux liquid nitrogen is transferred to Tray No.1 using eight main headers leading from the outer surface of the separating manifold chamber housed within the shaft section of the low pressure column. The headers protrude through the shaft surface and run parallel to the shaft for the length of the low pressure column Ten 3/16-inch orifices on each main header gives an even liquid distribution over the entire length of the inlet weirs on Tray No. 1. A liquid

head of 7.2 psi or 4.5 in. is required at the orifices. The reduced diameter of the shelf-reflux liquid manifold limited the amount of liquid "holdup" at this point. To increase the volume of the reservoir, the long conical design was adapted.

The vapor from the shelf-reflux manifold is directed through a center tube to a radial chamber discharging to the waste nitrogen annular chamber.

The manifolding at the discharge of the condensing side of the reboiler-condenser includes no phase separation. The liquid nitrogen stream is, however, discharged into two separate compartments within the manifold. One side of the manifold (approximately two-thirds of the liquid) is transferred by 24 one-inch headers each containing three 3/8-inch downcomer tubes to the inlet weirs of Tray No. 1 of the high pressure column. This headering system is also based on a two-inch liquid level in the manifold chamber.

The other side of the manifold (approximately one-third) handles the shelf transfer liquid through a system of radial pipes.

5.2.6 Reboiler-Condenser Design

5.2.6.1 General Design

The reboiler-condenser (Figure 68) for the boilerplate unit consists of a variable number of tube disks arranged in parallel and housed in a pressure casing. The disks are arranged in permanent modules of 5, 3, or 2 disks. The modules are manifolded by means of suitable gaskets and held together by tie rods running the complete length of the assembly. Nitrogen vapor condenses within the tubes of the disks while oxygen vapor boils on the outside of the tubes.

Liquid is distributed to the boiling passages through orifices at the inner circumference of the boiling passage. To obtain uniform axial and circumferential liquid distribution, one hundred and twenty orifices per passage are used to introduce the liquid. A driving potential of 20 psi is required. To assure the desired split between shelf liquid and high pressure column reflux liquid, condensate from about two-thirds of the disks is discharged in the high pressure column liquid distributor and the remaining condensate is discharged into the shelf liquid collector space. The split is accomplished by inserting a spacer at the desired location between the two reboiler-condenser sections. This spacer guides condensate from the outside disks into the column liquid collector. Position of the spacer and consequently the liquid split can be changed as desired.

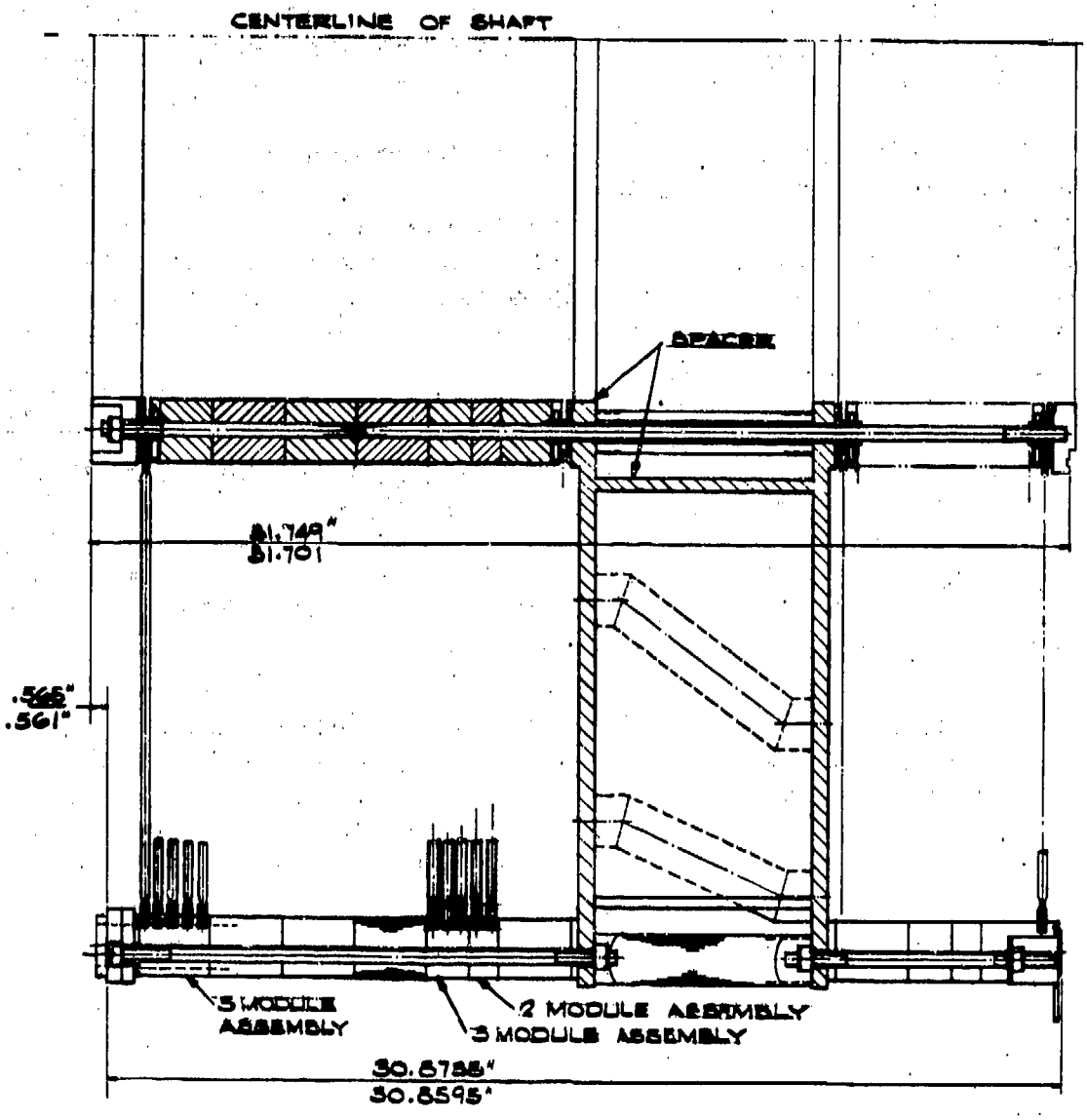

MODULE ASSEMBLY
REBOILER CONDENSER

FIG. 68

5.2.6.2 Tube Disks Design

The basic mechanical design of the reboiler-condenser heat transfer tube disks as seen from Figure 69 is in many respects similar to the design of the UCON test heat transfer disks (Ref. 1 Appendix VIII). The geometry and its basis for the tube disks was discussed in section 4.6.2.

To obtain a disk with a 20 in. inner diameter and a 48 in. outer diameter, 183 - .250 in. I.D. x .016 in. wall tubes were required. The tubing used for the disk fabrication was selected on the basis that it represented the least expensive and most readily obtainable thin wall tubing in the quantities required. The headering arrangement for the disk assemblies is shown on Figure 70. Inlet headering was integrated into the disks' inner flange design.

Experience with the UCON test disks had indicated that headering of the condensing passages at the disks periphery by means of integrally designed header blocks on the individual disks presents difficult problems. For this reason the tube disk stack for the reboiler-condenser was designed so that modular subassemblies of two, three and five disks can be used as shown in Figure 68. Matching pipe crossheaders as shown in Figure 70 were used on adjacent disk modules. This cross headering arrangement reduced the number of seals required (O-ring seals) and simplified final machining of individual disks.

5.2.6.3 Tube Disk Fabrication Procedure

The reboiler-condenser tube disks are basically an assembly of curved tubes placed adjacent to each other and in lateral contact all along their length with circumferential flanges retaining the tube sheets at the inner and outer peripheries. For improved heat transfer characteristics, application of a special boiling surface and a porous condensing surface was required.

Fabrication of the described assemblies can logically be broken up into the following operations:

a. Subassembly of the side-by side tube arrangement on a flat plane.

b. Joining the adjacent tube array along the tube line of contact to form a rigid circular tube sheet.

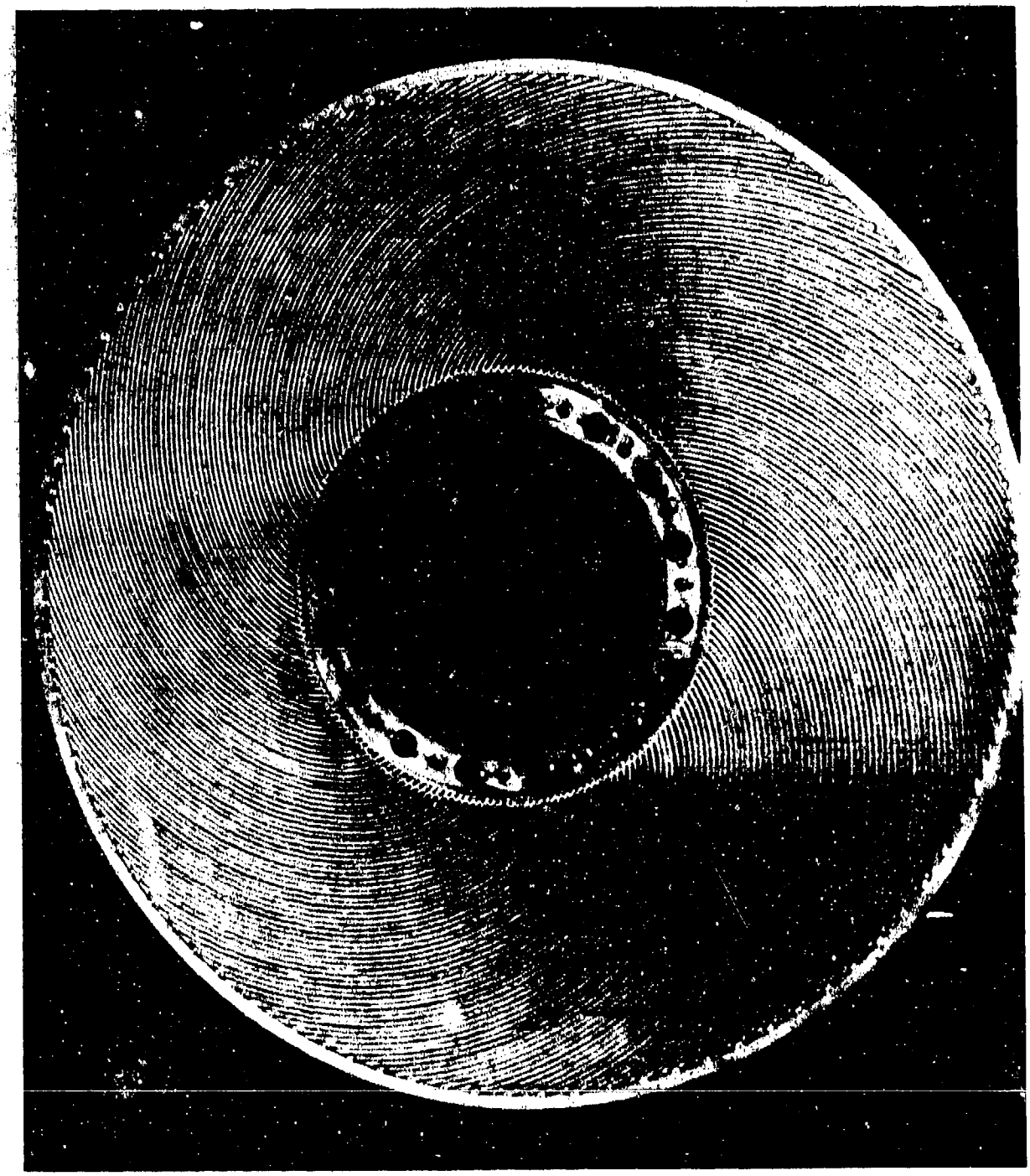

TUBE DISK

FIG. 69

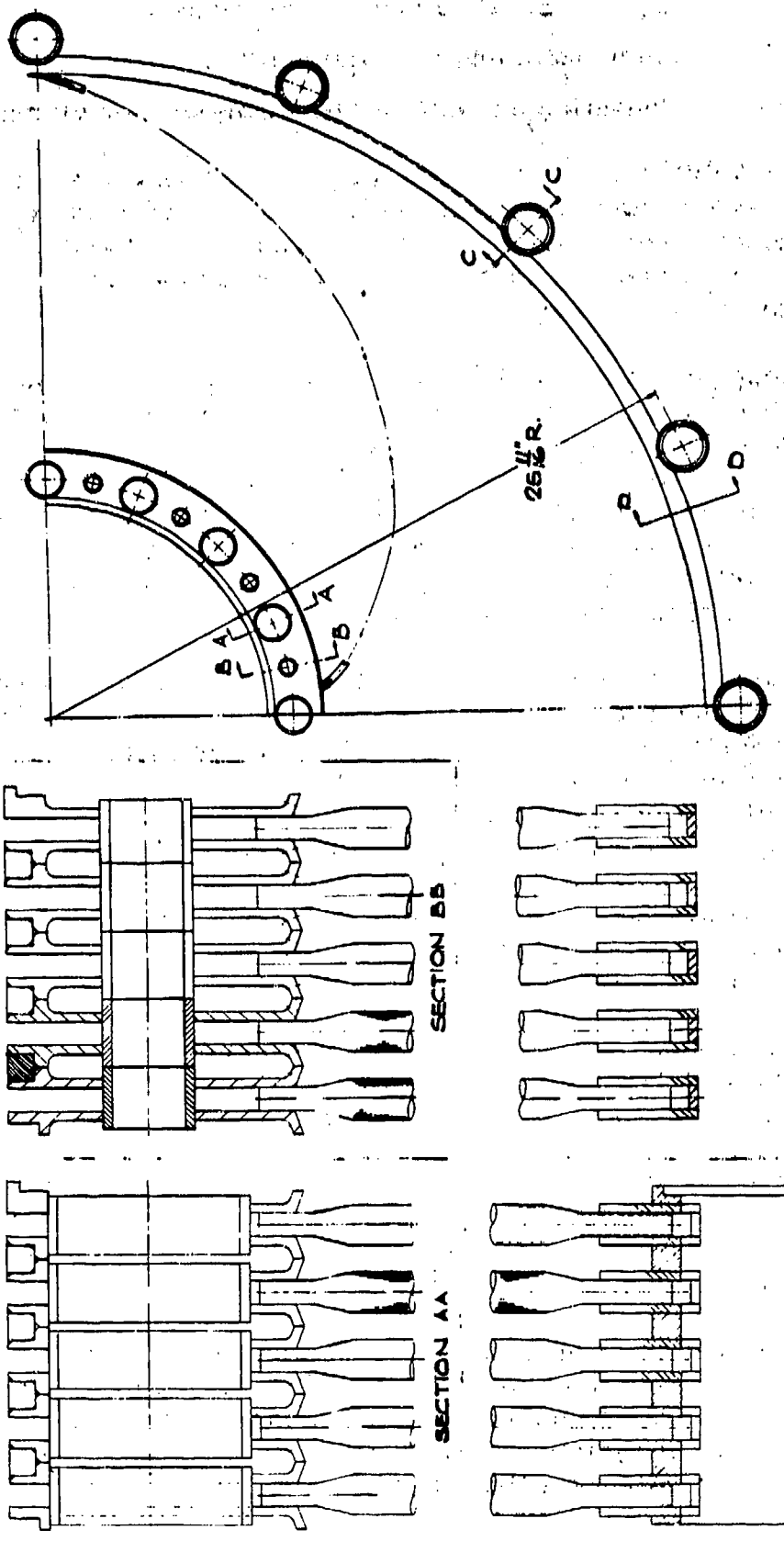

MODULE ASSEMBLY
REBOILER CONDENSER

FIG. 70

c. Application of the surface treatments.

d. Final machining of individual tube disks.

e. Headering and modular assembly of tube disks.

A satisfactory flat pattern layout of the tube disks would result only from an accurate and uniform preparation of the individual curved tubes. Since a large number of identical tubes were required (183 per disk), accuracy and uniformity was preserved by the use of a number of special tools and fixtures.

Bending of the individual tubes to the desired configuration was accomplished on an appropriately developed cam profile. The bending force was applied by a spring loaded rotating roller follower. The bending sequence is illustrated in Figures 71, 72, and 73. The tube bending machine not only provided for uniformity in the tube contour, but it eliminated the lengthy and tedious hand bending operation. The ability to bend tubes at the rate of 20 per minute resulted in a considerable time saving in the tube disk assembly operation.

Flat flanges were provided at the inner and outer peripheries on each side of the circular tube spread to form circumferential inlet and outlet channels. For leak tight channels after the flange application (by brazing) the tube ends needed to be flattened. For close control of the flattened dimension a special flattening apparatus was constructed essentially consisting of a pneumatically operated press and die set. The tube ends flattening sequence is shown in Figure 74, 75, and 76. Figure 77 shows one of the last steps in the processing of the individual tubes, trimming of the tube ends to proper form. Deburring of the edges completes the process.

The processed tubes are assembled into a side-by-side array to form a circular tube sheet on a plane, rigid fixture and positioned by tack welding as shown on Figure 78 in preparation for the brazing operation.

Structural integrity of the tube sheets is achieved in a dip brazing operation where joining of the adjacent tubes along the line of contact takes place. In the same operation the circumferential flanges are joined to the disks.

The tube sheet of Figure 78 is shown in the brazing fixture in Figure 79. A ribbed plate holds the disk flat and a series of rings and weight bars are used to hold the Alcoa 718 brazing alloy filler wire in position at the tube joints. Clamps are used to position the brazing wire at the inner and outer peripheral headers.

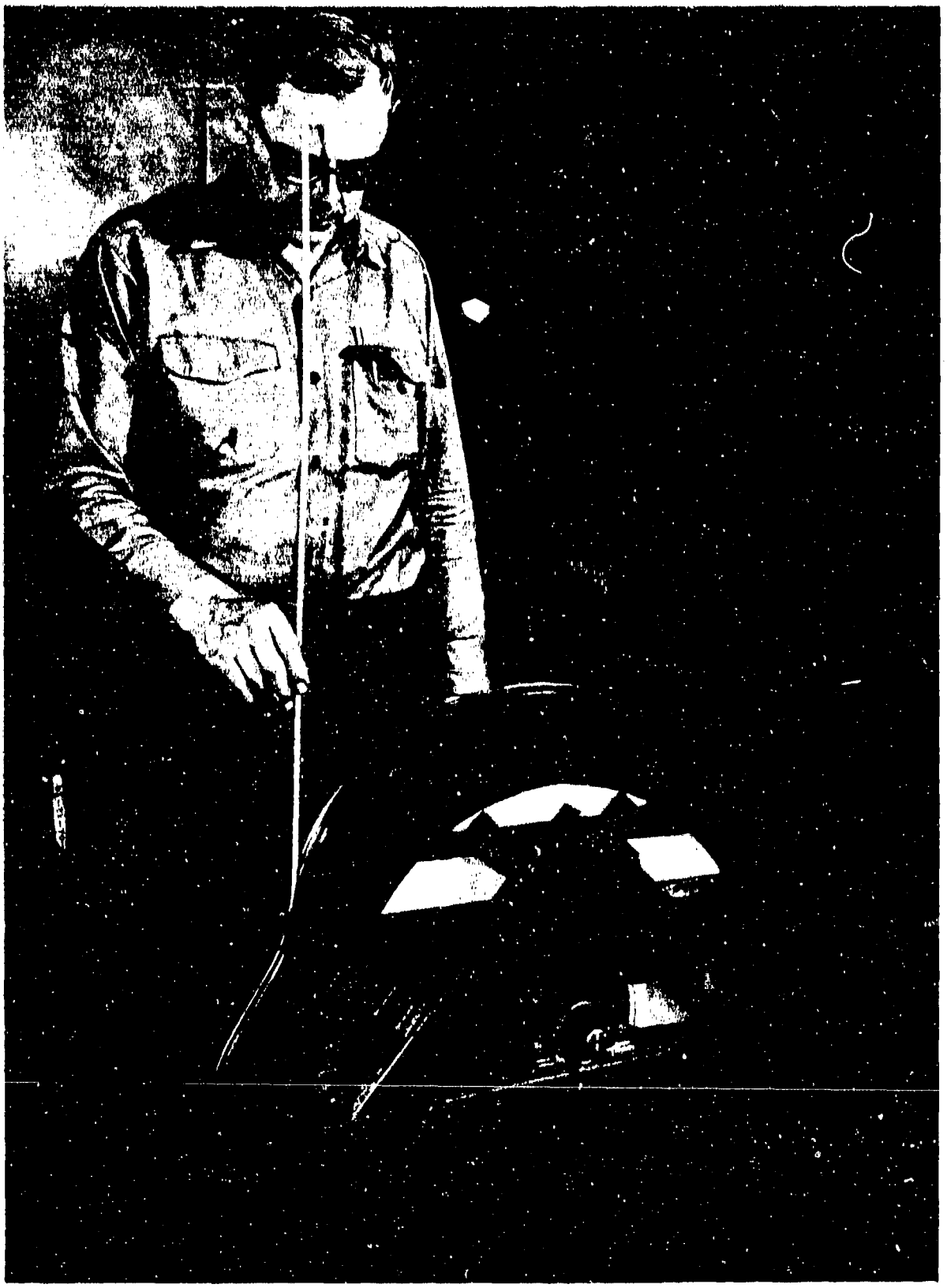

TUBE BENDING SEQUENCE FIG. 71

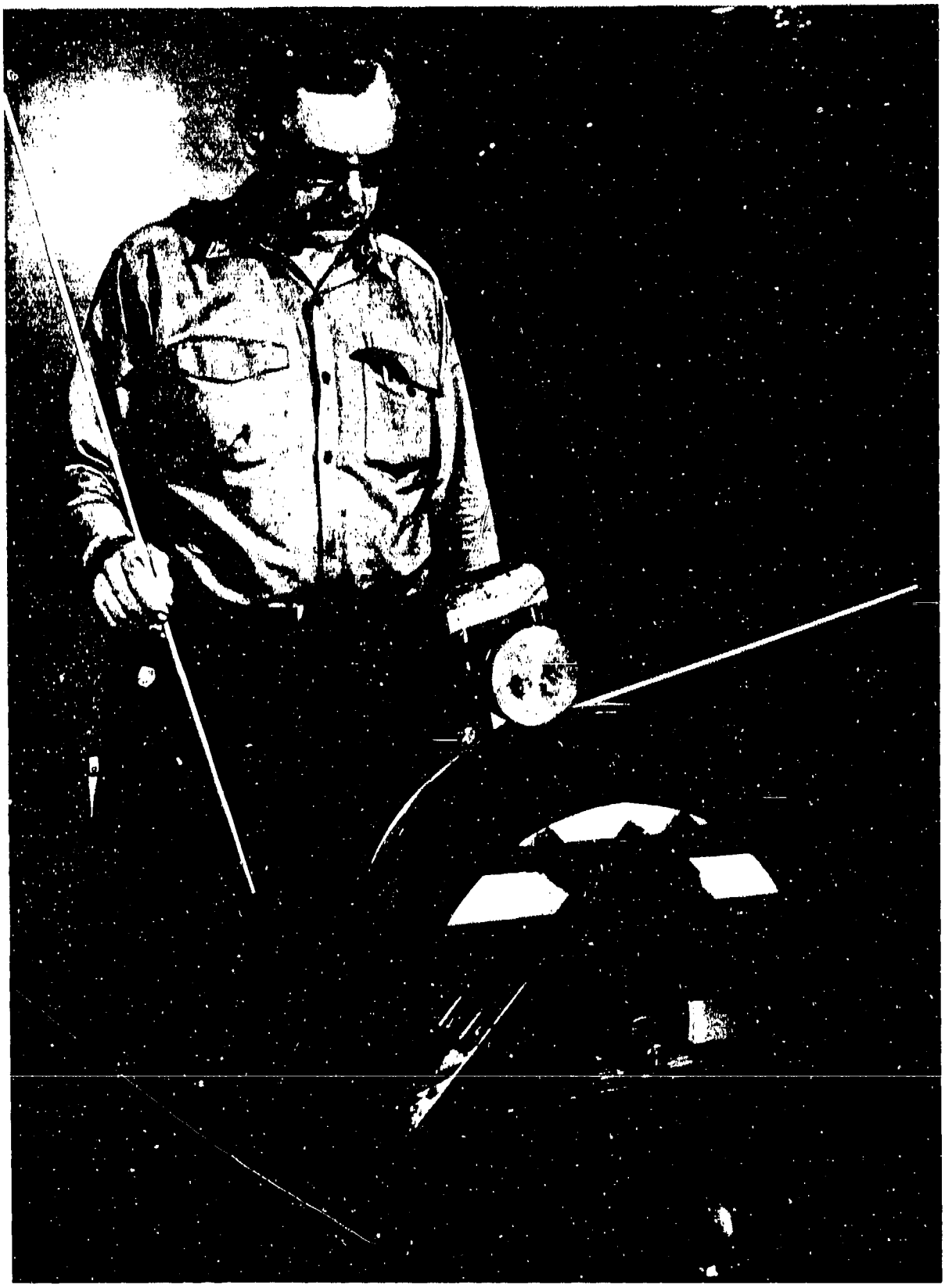

TUBE BENDING SEQUENCE FIG. 72

TUBE BENDING SEQUENCE FIG. 73

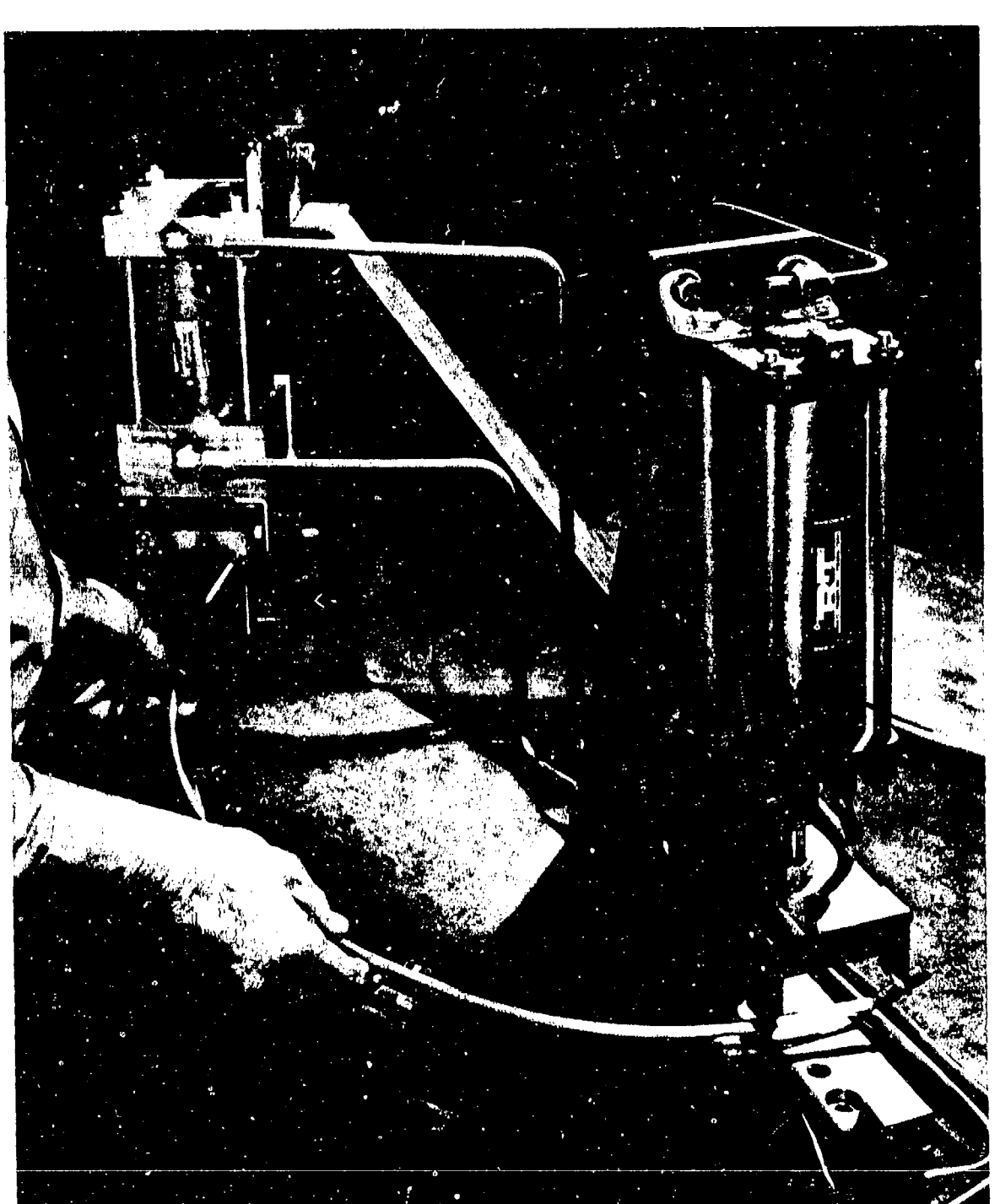

TUBE END FLATTENING SEQUENCE

FIG. 74

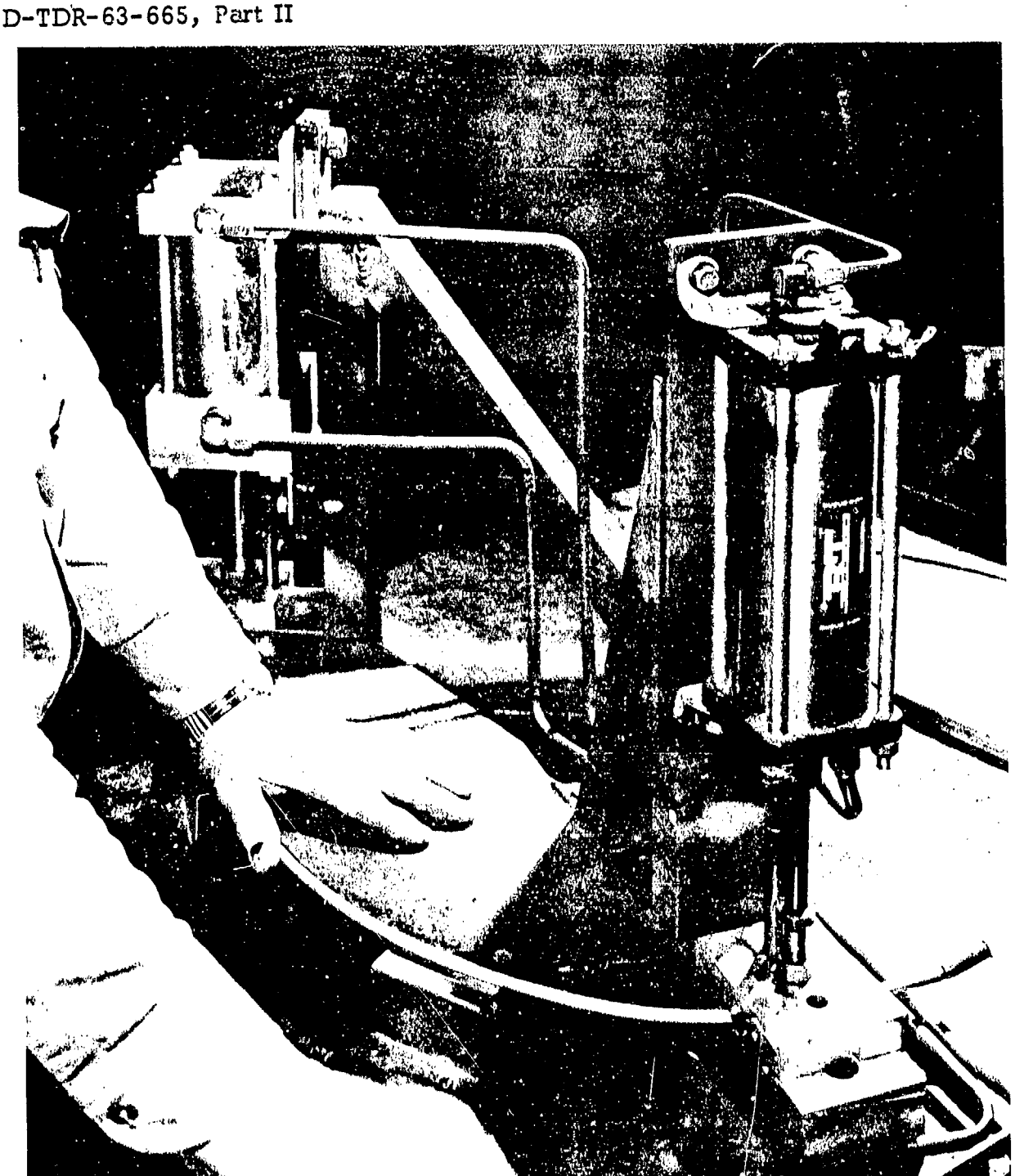

TUBE END FLATTENING SEQUENCE

FIG. 15

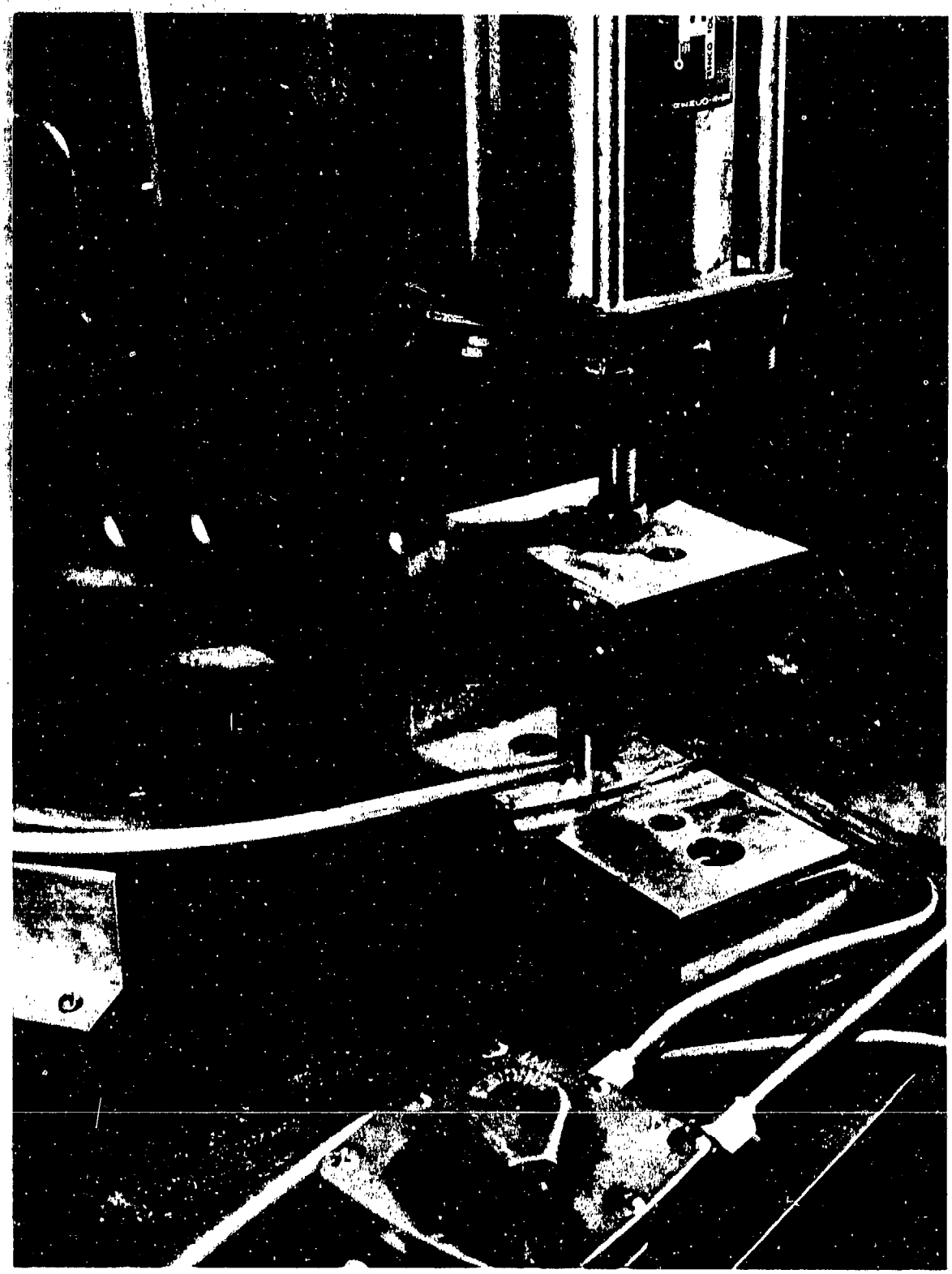

TUBE END FLATTENING SEQUENCE

FIG. 76

TUBE END TRIMMING FIG.77

TUBE DISK FIXTURED

FIG.78

The degreased and acid cleaned disks (dipped in a 10% solution HNO_3) were brought to brazing temperature in two steps. They were preheated to 1050°F, slightly below the melting range of the 718 filler wire (1070 - 1080°F) for approximately 45 minutes. The preheated disks were then dipped in a flux bath maintained at 1100°F for about 4 minutes. The flux used was Alcoa No. 33 principally used in dip brazing operations.

The brazed disks were immersed in a boiling water bath to dissolve residual flux salts prior to any further processing.

The next operation was the application of the special boiling surface and the porous condensing surface to the rigidized (brazed) tube disks.

The porous condensing surface on the inner area of the tube disks diagrammatically shown in Figure 80 is characterized by the following properties:

Average surface thickness	- .010 in.
Porosity	- 40%
Average pore size	- .002 to .005 in.

The surface treated disks represent an essentially finished product. Final machining of the inner diameter flanges for matched stacking of disks into modules was required. The unique construction

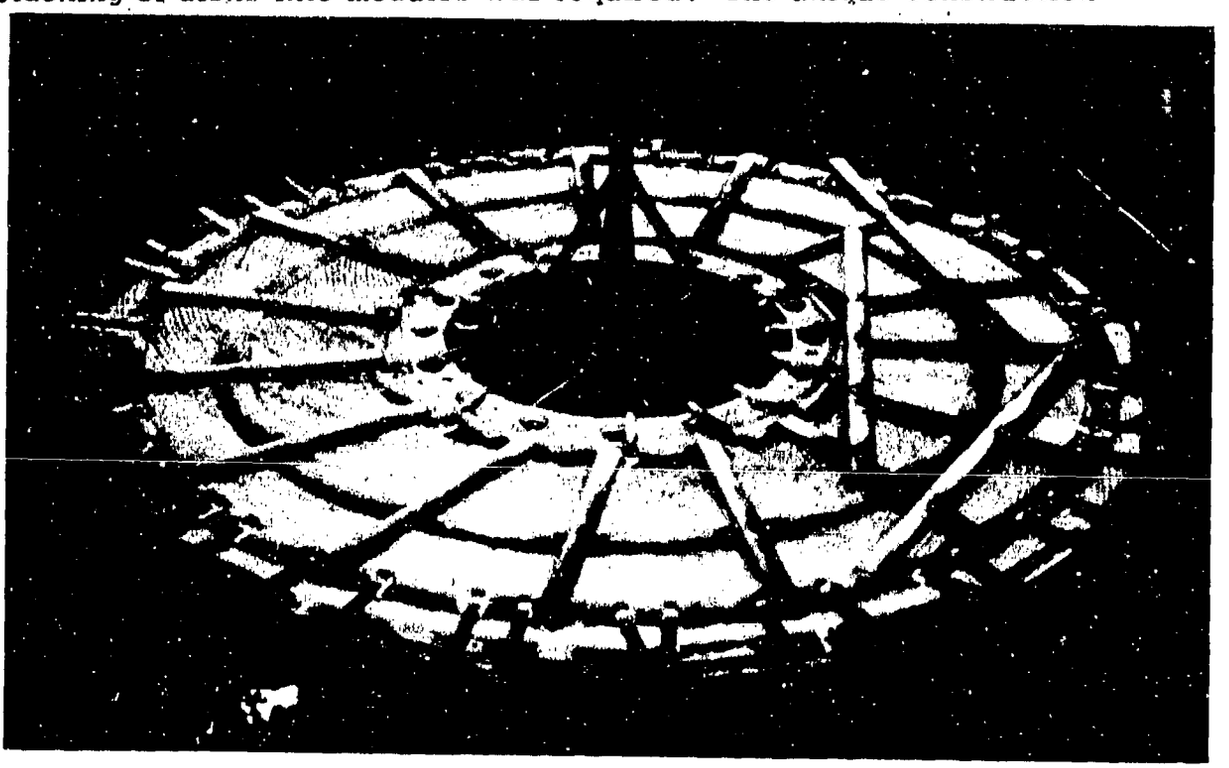

TUBE DISK BRAZING FIXTURE FIG.79

of the tube disks, complicated by various processes to which the disks were subjected to during fabrication, made the final machining operation to close tolerances an exacting and time-consuming process.

The modular assembly of the finished disks was characterized mainly by unusual sealing problems in two areas, namely the mating of contacting surfaces on the inner flanges of adjacent disks and the intersections of the cross headers on the disks' outer periphery. Sealing of these inaccessible areas was possible only by using sealants with adequate low temperature properties. The assembled reboiler-condenser package is shown in Figure 81.

5.2.6.4 Reboiler-Condenser Casing

5.2.6.4.1 General Design

The casing of the reboiler-condenser performs two principal functions:

a. It serves as a manifolding shell for the heat transfer tube disk stack and

b. It acts as a hub on which the high pressure column rotor is supported by bolting.

In addition, the casing supports two liquid manifolds, namely the oxygen product discharge manifold bolted on one end face; and the shelf liquid manifold integrated into the other.

Although the casing takes the basic form of a cylindrical pressure vessel its multifunctional design results in a complex assembly. Analysis of the casing was approached by considering strains due to static forces such as pressure and strains due to centrifugal forces.

The flanged sections on the casing to which the column rotor mounts represent areas of maximum stress. Stresses due to inertia forces were evaluated from the following expressions for rotating disks (Ref. 16).

$$(S_r)_1 = \frac{3 + \mu_p}{8\,(1-\mu_p^2)}\, NE_y \left(R_i^2 + R_o^2 - r^2 - \frac{R_i^2 R_o^2}{r^2}\right) \qquad (40)$$

$$(S_t)_1 = \frac{3 + \mu_p}{8(1-\mu_p^2)}\, NE_y \left(R_i^2 + R_o^2 - \frac{1 + 3\mu_p}{3 + \mu_p} + r^2 + \frac{R_i^2 R_o^2}{r^2}\right) \qquad (41)$$

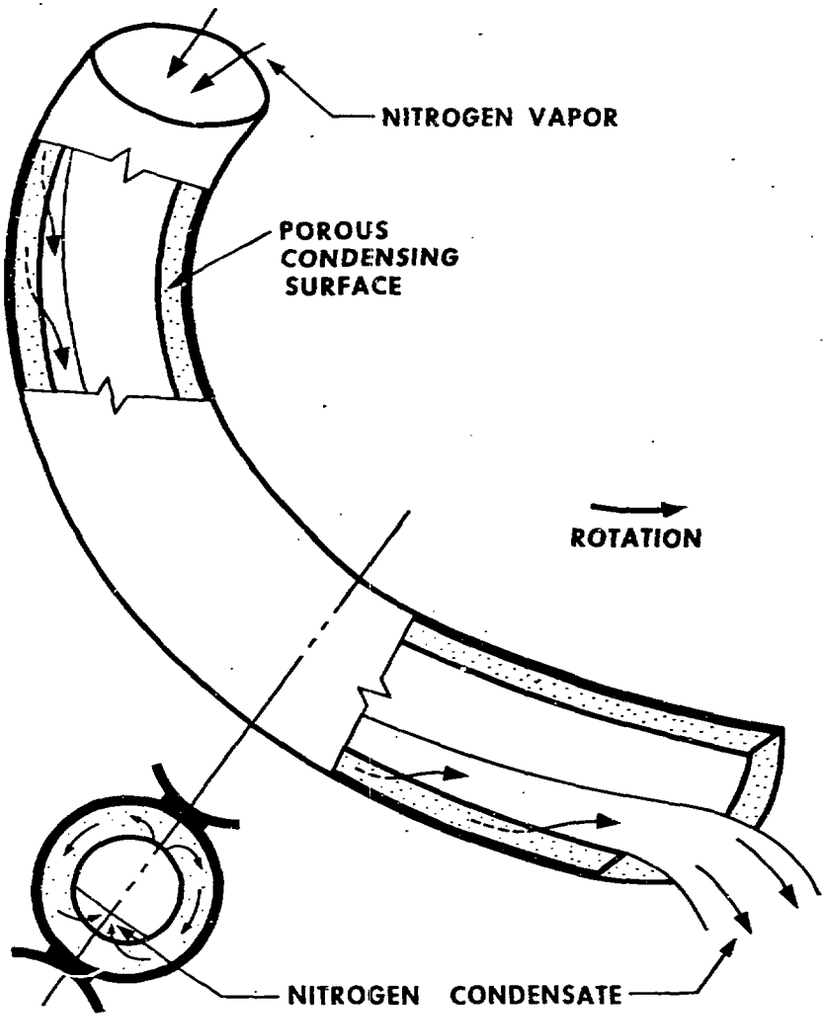

ROTATING REBOILER–CONDENSER DISK

FIG.80

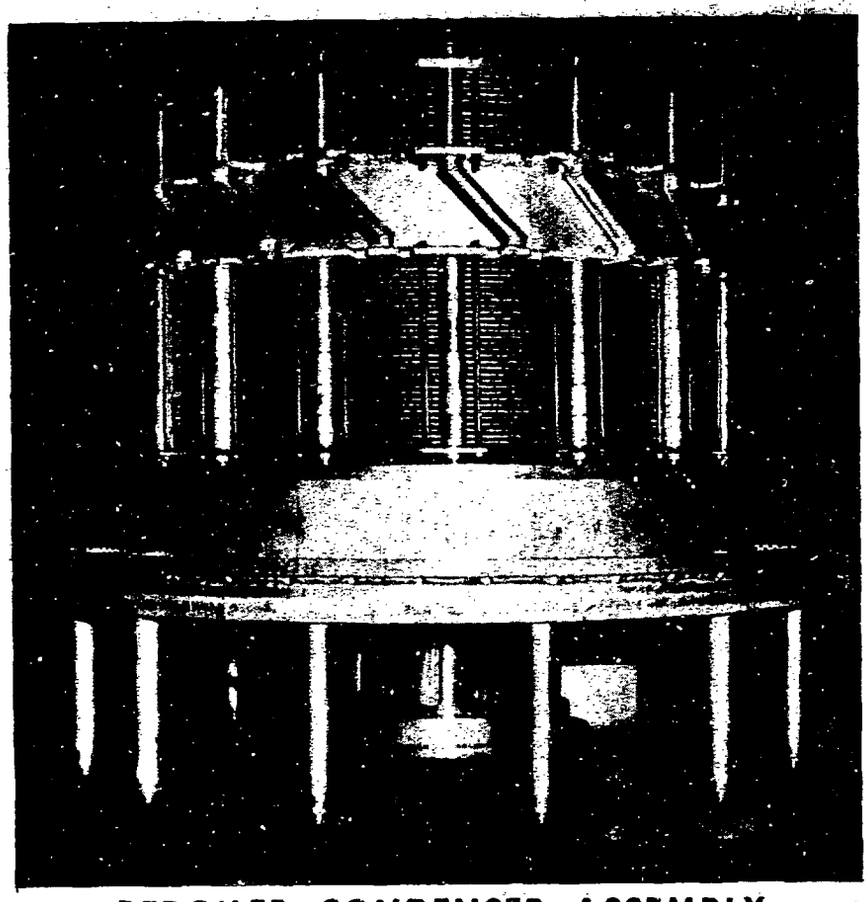

REBOILER CONDENSER ASSEMBLY FIG.81

where:

$$N = (1-\mu_p^2)\ \frac{\rho\omega^2}{g_c E_y} \qquad (42)$$

The stresses due to internally and/or externally acting pressures were evaluated by use of the following expressions for thick walled pressure vessels:

$$(S_r)_2 = \frac{R_i^2 p_i - R_o^2 p_o}{R_o^2 - R_i^2} - \frac{(p_i - p_o) R_i^2 R_o^2}{r^2 (R_o^2 - R_i^2)} \qquad (43)$$

$$(S_t)_2 = \frac{R_i^2 p_i - R_o^2 p_o}{R_o^2 - R_i^2} + \frac{(p_i - p_o) R_i^2 R_o^2}{r^2 (R_o^2 - R_i^2)} \qquad (44)$$

Superposition of these two components is shown on Figure 82 for the end plate in close proximity to the high pressure column rotor. The low values

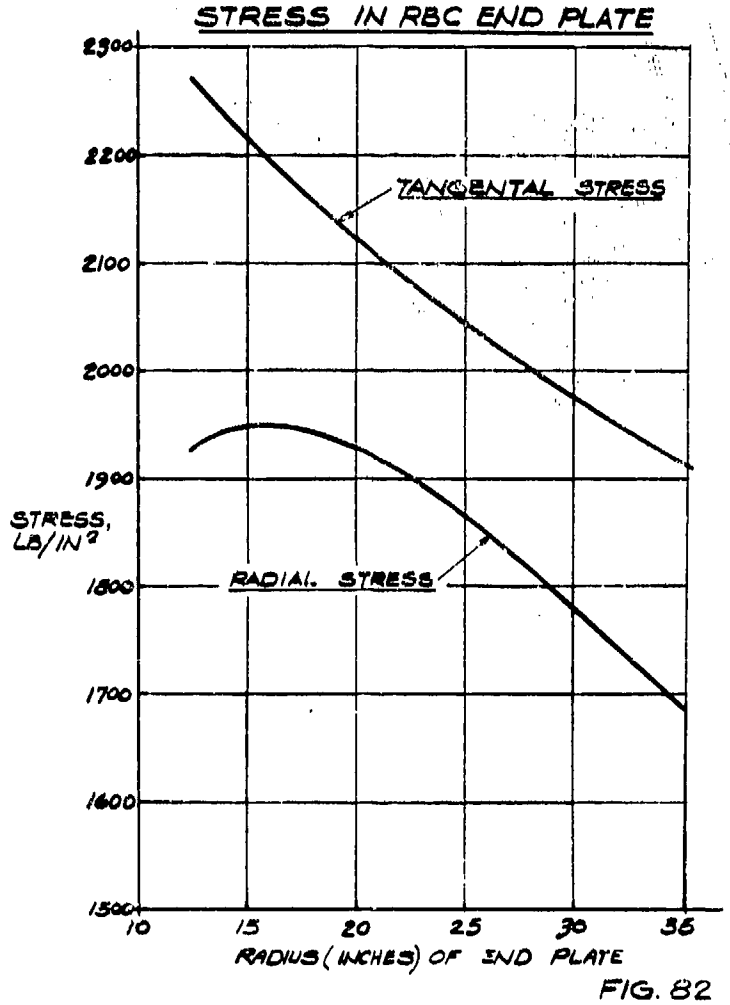

FIG. 82

of stresses obtained are indicative of the conservative design of the reboiler-condenser casing. A rigidized type design consisting of two circular plates reinforced by a channel spacer between the two plates was used for both ends of the reboiler-condenser casing. In addition to stiffening end plates this design also encloses the radial array of piping webbing each end of the casing. Transverse bending of the casing end plates was checked by considering a radial segment with a uniform (pressure) load and assuming it fixed at inner and outer arc length. Even though this method yields conservative results, since no restraining effects are considered on two sides of the typical segment, very small deflections and stresses were obtained by the analysis.

5.2.6.4.2 Casing Fabrication

Fabrication of the reboiler-condenser casing required two separate weldments which form the cylindrical barrel and two circular weldments, one for each end. The end plate weldments because of their rigidized design, presented some fabrication problems not typical of other components used in the rotary air separator. For instance, welding of thin wall tubing midway on 2" plate was required. Machining of the end plate weldments was accomplished with relative ease even though some warpage resulted from the extensive welding inherent in the rigidized design.

5.2.7 Peripheral Diffuser

5.2.7.1 Diffuser Design

Peripheral diffusers were utilized at low pressure column discharge and at the product-recirculation stream discharge manifold to convert the liquid kinetic energy into static head.

The design of the peripheral diffusing passages for the boilerplate model rotary air separator was based on information obtained from tests conducted with water as described in Section 5.4.2 (Ref. 1). Data from these tests, indicated that better diffusing performance and rangeability would result if the angle $\emptyset^{o}$ between the diffuser passage throat axis and the tangent to the rotor exceed that obtained by calculation using the rotor tip speed and pertinent liquid flow rates. The calculated value is near 1°. A value of 5° was selected for the boilerplate peripheral diffusers. This value was selected as a compromise between the practical limitations dictated by the flange dimensions and slip assumptions obtained from the water tests.

The throat width was selected using continuity relations to obtain a throat velocity nearly equal to the velocity calculated from

representative slip values. The diffuser width was selected to be slightly larger than the rotor orifice slot width to accommodate the free stream flow conditions.

Blades are attached at the rotor orifice to accelerate the fluid through the high loss region and minimize slip.

With the diffusers operating at the overall calculated recovery efficiencies of 33.4 and 53.9%, the downstream system pressures for a speed of 63 rad./sec. would be:

Low pressure column	P = 240-260 psia
Product discharge	P = 200-210 psia

It might be assumed that some performance enhancement could occur due to a reduction in slip provided by radial blades within the orifice slot. Any such reduction would increase the incidence mismatch, but the greater amount of available kinetic head should more than offset any incidence losses.

5.2.7.2 Diffuser Ring Specifications

Design of both, low pressure column and product discharge diffuser rings, is specified below:

Parameter	Low Pres. Column Diffuser	Product Discharge Diffuser
Throad width	b_{dt} = 5/32"	1/8"
Diffuser depth	h_{dt} = 5/32"	5/32"
Number of blades	n_{db} = 60	36
Inside diameter of annulus	D_i = 106"	70"
Outside diameter of annulus	D_o = 109"	73"
Divergence angle	$2\Theta_D$ = 6°	6°
Aspect Angle	$\emptyset$ ° = 5°	5°
Area ratio	A_e/A_t = 5.2	5.5
Length-to-throat-width ratio	L/b_{dt} = 50	50
Fluid flow rate	W = 100 lb./sec.	40 lb./sec.
Fluid density	ρ_L = 60 lb./ft.^{3}	60 lb./ft.^{3}

From these specified parameters and using values for the low pressure column diffuser the total throat area is:

$$A_t = \frac{N_{db}\, b_{dt}\, h_{dt}}{144} = 0.01017 \text{ ft.}^2 \qquad (45)$$

This results in a velocity in the diffuser throat of

$$V_{td} = W/A_t \; \rho_L = 164 \text{ ft./sec.} \qquad (46)$$

and the available kinetic head is:

$$\frac{\rho_L V_{td}^2}{2g_c} = 174 \text{ psi} \qquad (47)$$

Comparing this to Figure 83A shows that the throat continuity conditions match a slip value of 41 per cent. The angle formed by the fluid velocity components is:

$$\omega^\circ = \tan^{-1} \frac{V_r}{V_{td}} = \tan^{-1} \frac{5.76}{164} = 2.016^\circ \qquad (48)$$

For the design expansion ratio, the optimum diffuser efficiency would be:

$$\eta_d = 1 - \left(\frac{A_t}{A_e}\right)^2 = 96.3\% \qquad (49)$$

The overall recovery for such a diffuser geometry would be:

$$\eta_o = \left[1 - \left(\frac{A_t}{A_e}\right)^2\right] \frac{V_{td}^2}{V_t^2} = 33.4\% \qquad (50)$$

Comparison of ω° with φ_{act} shows a mismatch of three degrees.

A section of diffuser blade layout is shown on Figure 84A.

Using the same relations above for the product discharge diffuser results in the following:

$$A_t = .00488 \text{ ft.}^2$$

$$V_t = 136.8 \text{ ft./sec.}$$

$$\frac{\rho_L V_{td}^2}{2g_c} = 121 \text{ psi}$$

$$\varphi = 5^\circ$$

$$\eta = 96.7\%$$

The slip imposed by continuity conditions is 25% as illustrated in Figure 83B. This results in a diffuser with an optimum overall recovery of $\eta_o = 53.9\%$ and an aspect angle mismatch of 3°.

A section of the diffuser blade layout is shown in Figure 84B.

5.2.7.3 Diffuser Ring Assembly

The two dimensional diffusing passages, in both the case of the low pressure column and the product stream discharge, are formed by spacing the appropriate number of guide vanes is the annular space between two flat face flanges also used to house the liquid collect channel. Proper spacing of the guide vanes is affected by retaining the contoured guide vanes on one of the flanges. Figure 85A shows the assembled diffuser ring for the product discharge stream. Figure 85B shows a close detail of a diffusing passage.

5.2.8 Peripheral Seal

5.2.8.1 Introduction

Peripheral liquid seals are required at the peripheries of the low pressure column and the reboiler-condenser casing where liquid is discharged from the rotating elements into stationary collectors. In selection and design of the peripheral seals the experience gained in air-water tests (Ref. 1, section 5.3.3) was utilized. In this work it was shown that contact type seals were unsuitable for large diameter, high velocity applications and that a bladed centrifugal type seal promised to provide the most suitable design for the boilerplate separator. A centrifugal seal balances pressure differential by liquid head.

5.2.8.2 Seal Design

The centrifugal seal pressure capability is expressed by:

$$\Delta P = \frac{\omega^2}{2 g_c} \rho_L \left(R_o^2 - r_{i\,seal}^2\right) = \omega^2 \frac{\rho_L}{2 g_c} \left(1 - \frac{r_i^2}{R_o^2}\right) \qquad (51)$$

From the above expression it is evident that effective operation of this type seal depends on two factors:

a. The velocity imparted to the leakage fluid in the clearance space between the rotor face and the stationary wall and

b. The radial length of the seal blades or in terms of the above expression the ratio $\frac{r_{i\,seal}}{R_o}$.

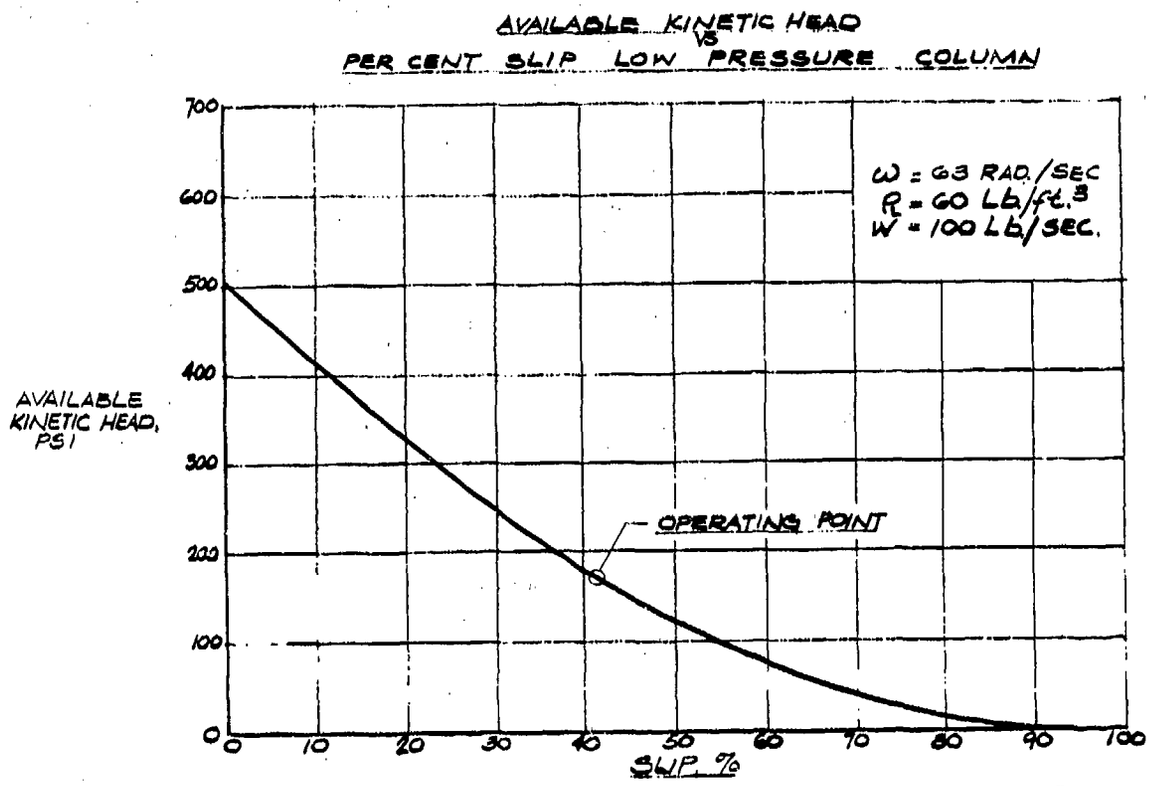

FIG. 83 A

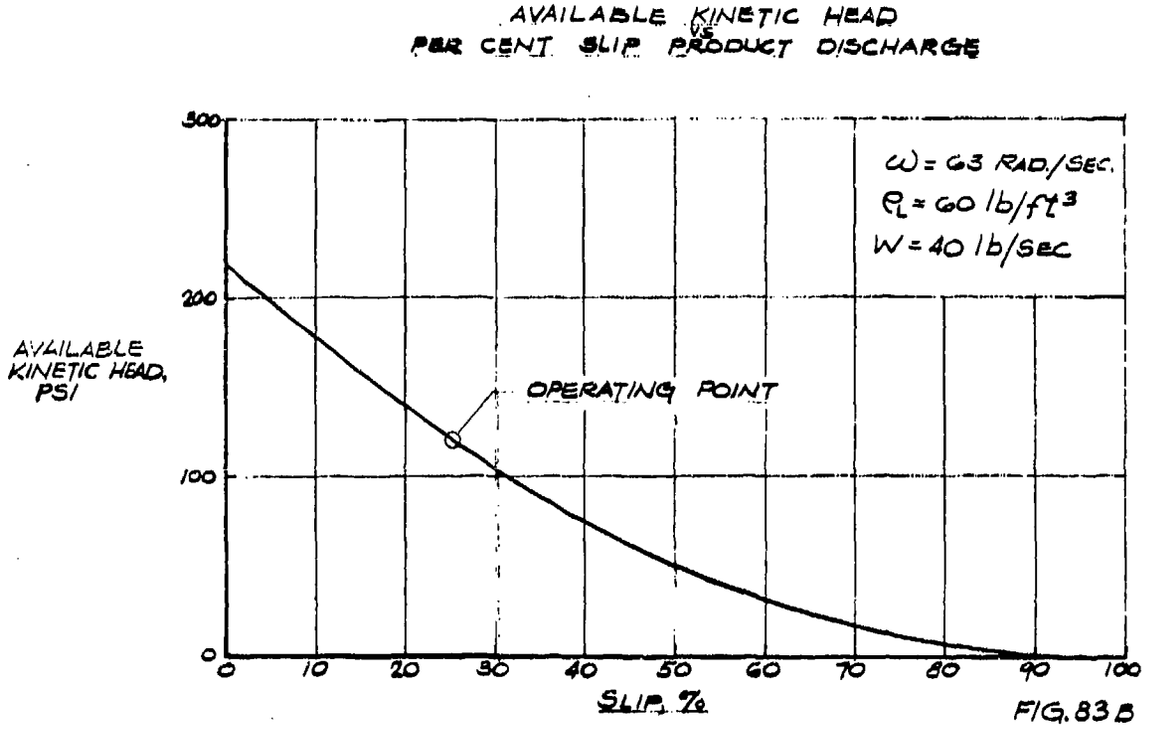

FIG. 83 B

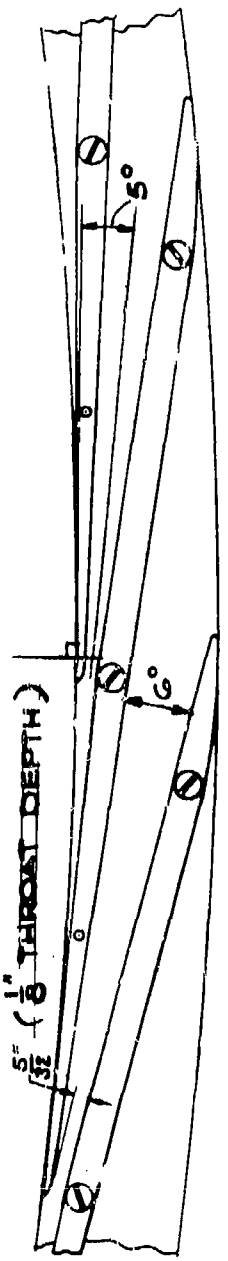

FIG. 84 A

LOW PRESSURE COLUMN DIFFUSER

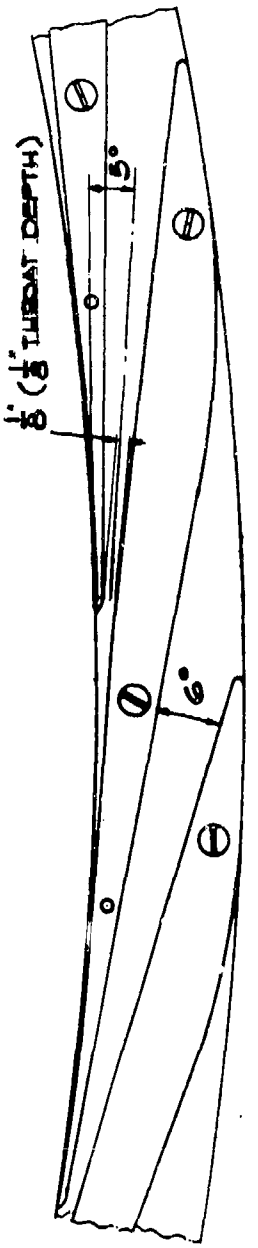

FIG. 84 B

PRODUCT DISCHARGE DIFFUSER

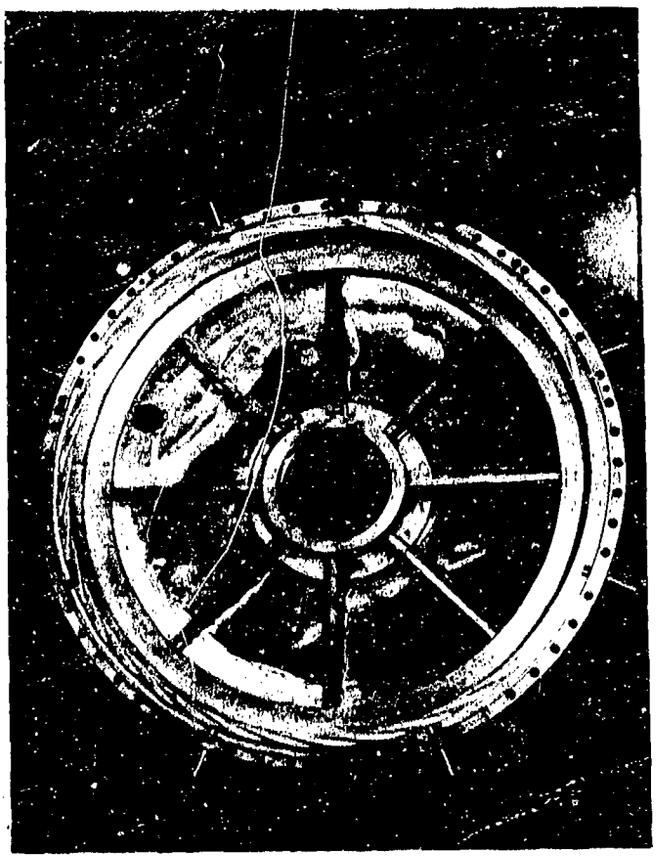

DIFFUSING PASSAGE

FIG.85A

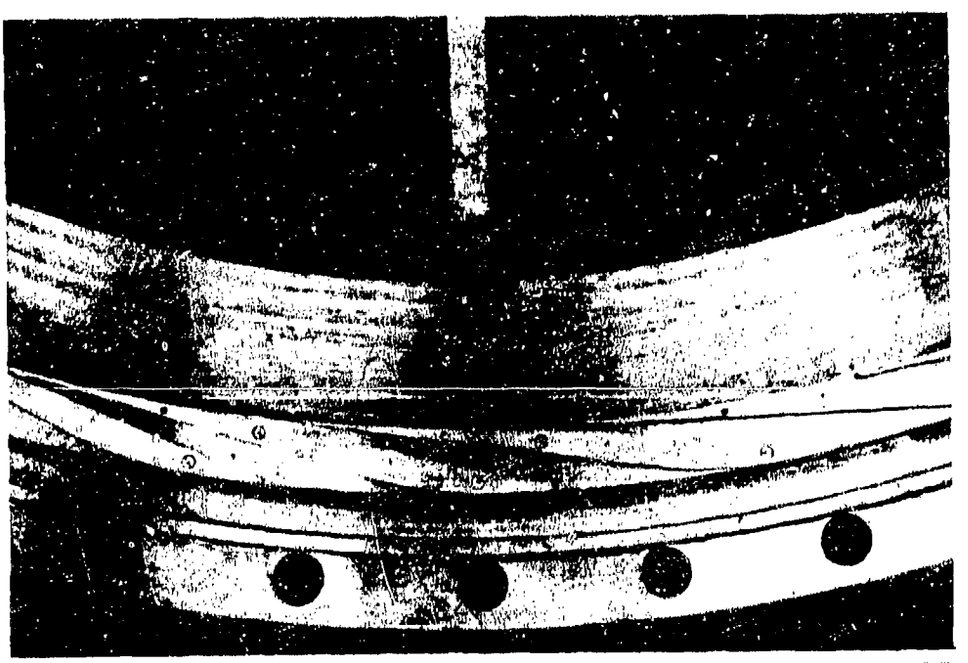

DIFFUSING PASSAGE FIG.85B

Power consumption considerations (Section 5.2.13) dictate as short a radial wetted section (seal section) as possible or as large a ratio $r_{i\,seal}/R_o$ as possible.

In the case where the leakage fluid is located in an open space between a rotating and a stationary plane the average fluid velocity is one-half the angular velocity of the rotating element or $\omega' = \omega/2$.

A more fully developed rotation of the enclosed fluid can be affected by providing retaining "blades". Thus (Ref. 21)

$$\omega' = \frac{\omega}{2}\left(1 + \frac{t_{sb}}{C_s}\right) \qquad (52)$$

and in the limit where: $t \approx c$, $\omega' = \omega$

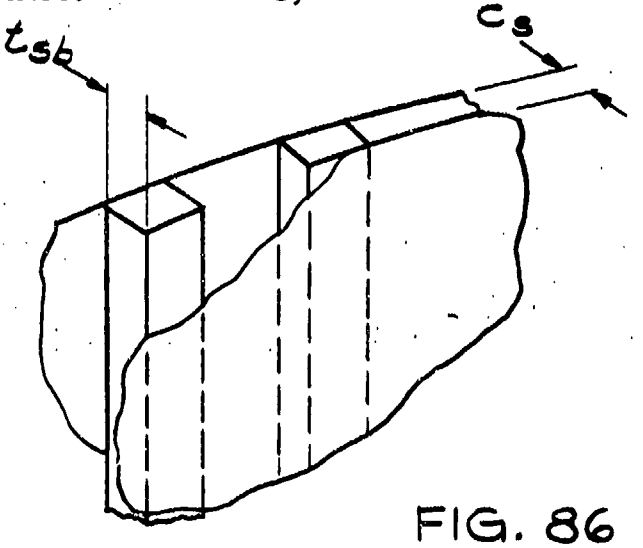

FIG. 86

In this arrangement reasonable values of t_{sb}/C_s result in at least 90% rotation of leakage fluid thus allowing use of the shortest possible radial wetted area to develop the required ΔP.

5.2.8.3 Seal Specifications

In the 100 lb./sec. rotary air separation device liquid oxygen is extracted from the periphery of a rotating element into a stationary collector at two separate points:

a. at the low pressure column periphery - 53" R

b. at the reboiler-condenser periphery - 35" R

A centrifugal type peripheral seal is provided at each location.

Figures 87A and 87B show the radial depth of seal required for these separate cases of ΔP across the seal and an operating speed range of 50 to 65 rad./sec. for a set fluid pressures. The pressure across the seal varies depending on the degree of casing pressurization.

Setting the design point at a rotational speed of 60 rad./sec. and 30 psia casing pressure the required seal dimensions are:

ω	P_{casing}	ΔP seal		Blade Length Total In.		Blade Length effective	
		Low Press. Col.	Reboiler Condenser	Low Press. Col.	Reboiler Condenser	Low Press. Col.	Reboiler Condenser
60 rad/sec	30 psi	46 psi	41 psi	4-1/2"	6"	2-1/2	4

It is noted that a decrease in speed will decrease the effectiveness of the seal which must be countered by increasing pressurization of the casing.

The seal is self compensating to an increase in both speed and casing pressure. This is, an increase in speed increases the pressure capacity of the seal or decreases the seal depth required. Similarly, increasing the casing pressure decreases the pressure difference across the seal resulting in a self adjustment of the seal depth.

The centrifugal seal arrangement lends itself to simple construction. The seal components consist of the radial retaining blades and a retaining continous ring at the blades inner ring, Figure 88.

If these components can be made of a material with low friction and wear characteristics, axial clearances can be maintained at a minimum resulting in t_{sb}/C_s approaching unity.

No set criteria other than some experience gained in air-water tests are available for determining blade thickness, width and spacing. It is reasoned, however, that small pockets between blades would cut down internal circulation, thus reduce seal losses.

The use of small pockets between blades means thin, narrow seal blades. These can be made from materials such as:

PERIPHERAL SEAL
LOW PRESSURE COLUMN

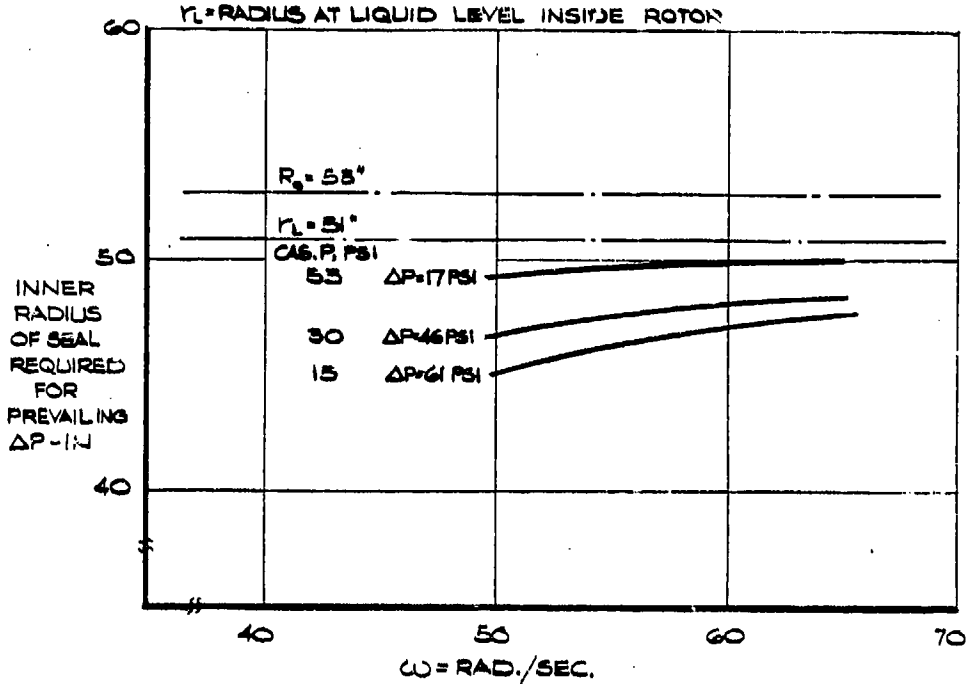

FIG. 87A

PERIPHERAL SEAL PRODUCT DISCHARGE

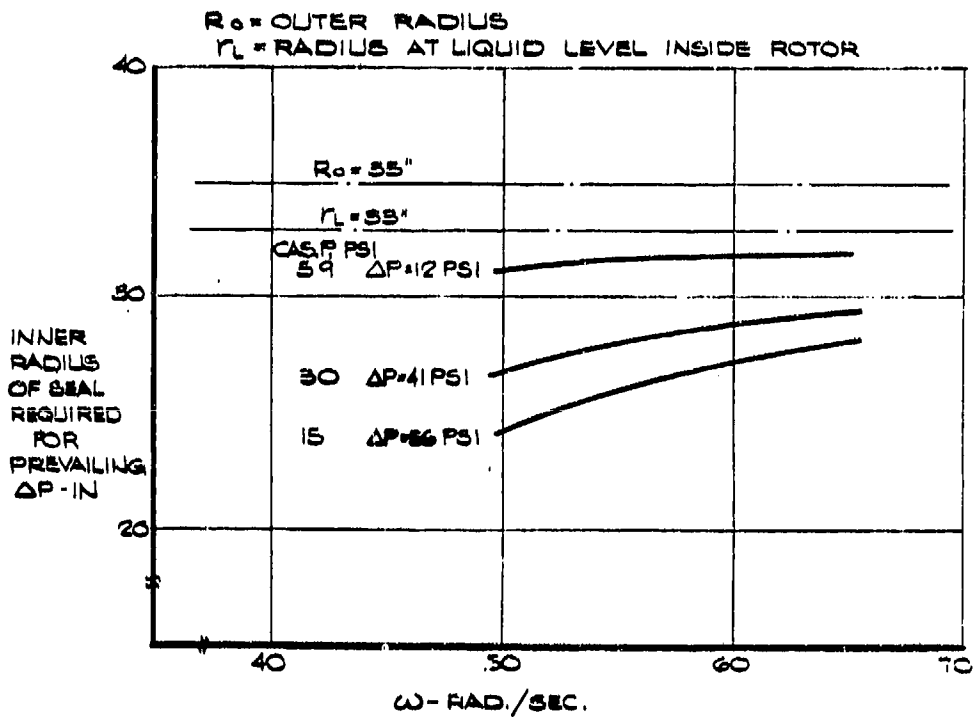

FIG. 87B

PERIPHERAL SEALS

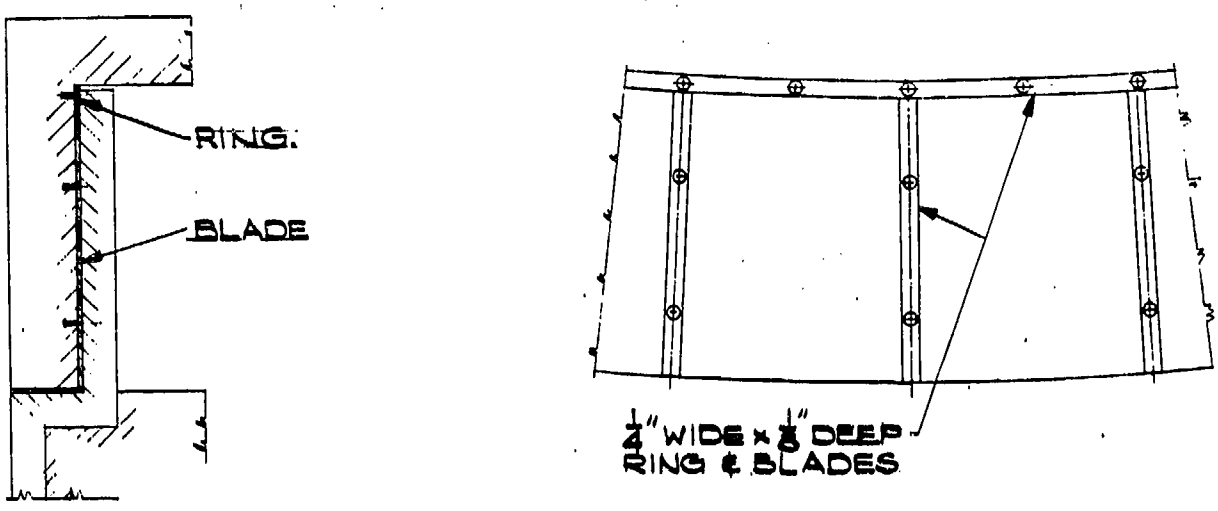

DETAIL OF SEAL

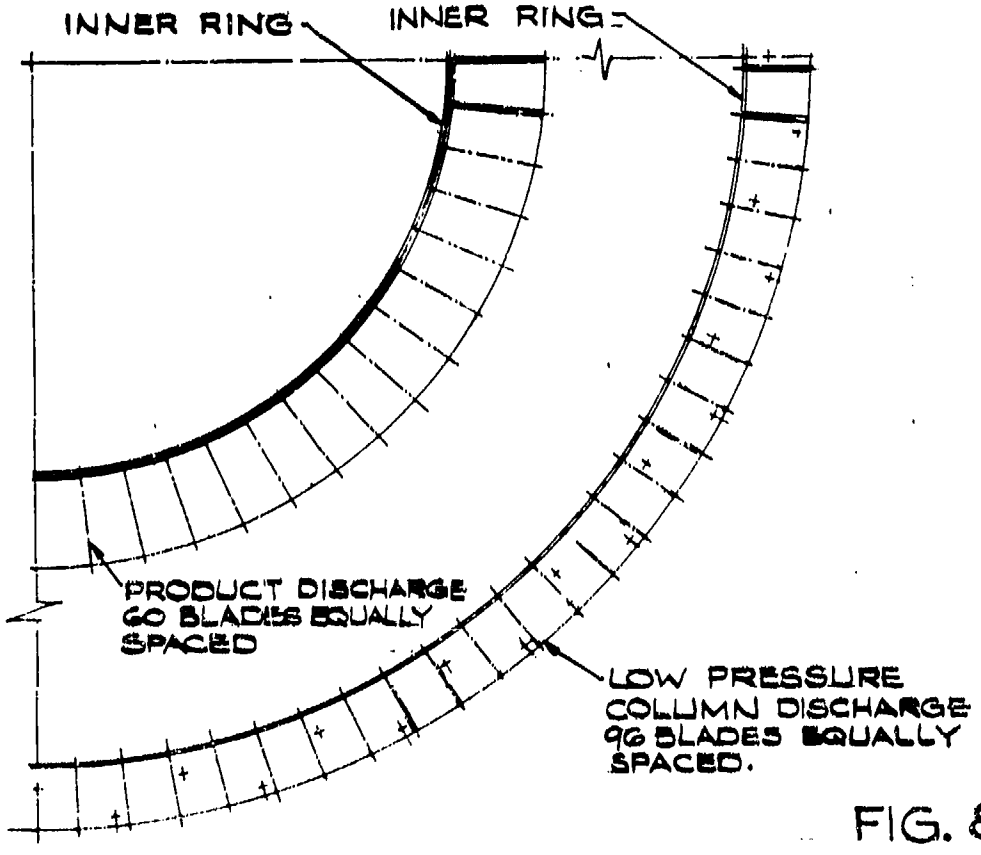

FIG. 88

a. Filled Teflon sheet

b. Glacier DU material, a metallic backing, porous bronze surface impregnated with Teflon

c. Teflon molded perforated metal sheet

d. Teflon bonded on metallic backing

The last three of the above materials are the most desirable since they would facilitate assembly on the rotor faces. For the 100 lb./sec. unit use of Teflon molded 1/8" thick perforated metal has been specified.

5.2.8.4 Peripheral Seal Assembly

The selection of Teflon molded perforated aluminum strips 1/4" wide x 1/8" thick was made on the basis that it provided the most workable material with as much of non-metallic wear surface as possible. The close running clearances of this seal arrangement requires adequate rigidity in the seal blade material so that even and smooth surfaces would result after assembly. At the same time some flexibility was required in the strips to permit forming of the retaining segments at the inner tip of the blades. Above all, a low friction wear surface was required in case of misalignment or run out of the rotating elements on which the seal configuration is mounted.

The material obtained in sheet form was cut to the required sizes and mounted on the machined rotor peripheries with self-tapping screws to develop the seal configuration. Figures 89 and 90 show the seal assembly on the external face of the product discharge manifold.

5.2.9 Internal Controls

5.2.9.1 Introduction

The internal control systems have to function to control liquid level in the high pressure column kettle and in the shelf liquid collector. In principle the control system is identical to the prototype system which was tested in a UCON test rotor (Ref. 1, section 5.6.2). Basically the system consists of a bellows operated piston valve with the control signal furnished directly by the pressure differential due to the liquid level in the respective collector spaces. (Figure 91.)

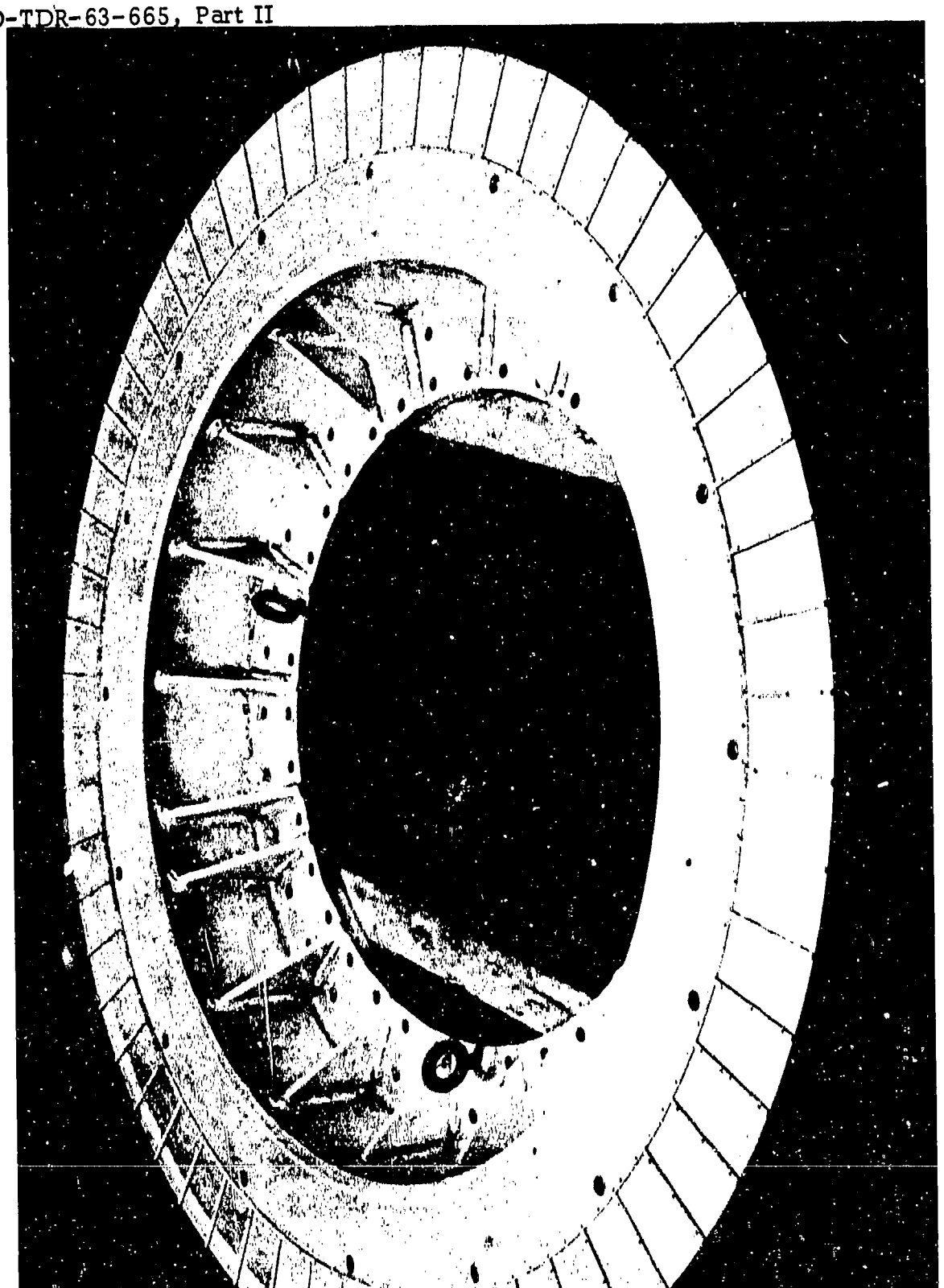

FIG.89 PERIPHERIAL SEAL

FIG.90 PERIPHERIAL SEAL

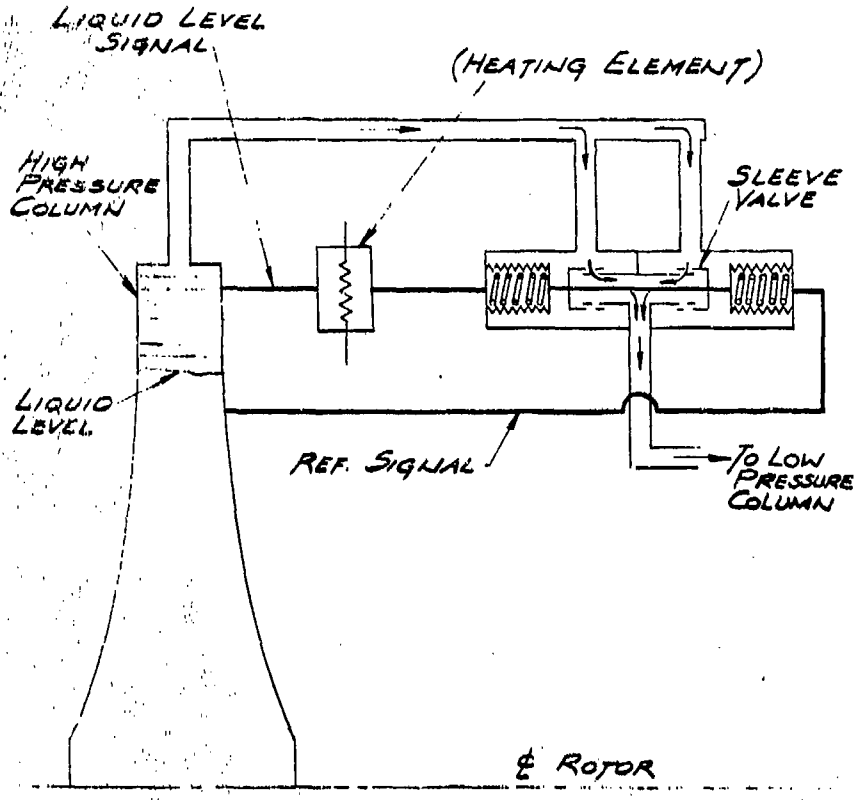

SCHEMATIC CONTROL ACTUATOR

FIG. 91

5.2.9.2 Control Valve Design

It was found that to keep valve size within reasonable limits 4 valves in parallel are required for the kettle liquid transfer stream and 2 valves in parallel for the shelf liquid transfer stream. The basic valve design (Figure 92) selected is similar to the one used in the prototype system. The design features a balanced piston arrangement with two inlet ports and a common outlet. The hollow valve piston contains two orifices which engage two inlet orifices in the valve body. The hollowed piston section aligns with the discharge port on the valve body. The piston position relative to the valve body and thus the size of the inlet flow orifices is determined by the differential pressure control signal fed to the opposing bellows. The pressure signal is opposed by the spring action of the bellows and additional springs which can be adjusted to change the set point for the valve.

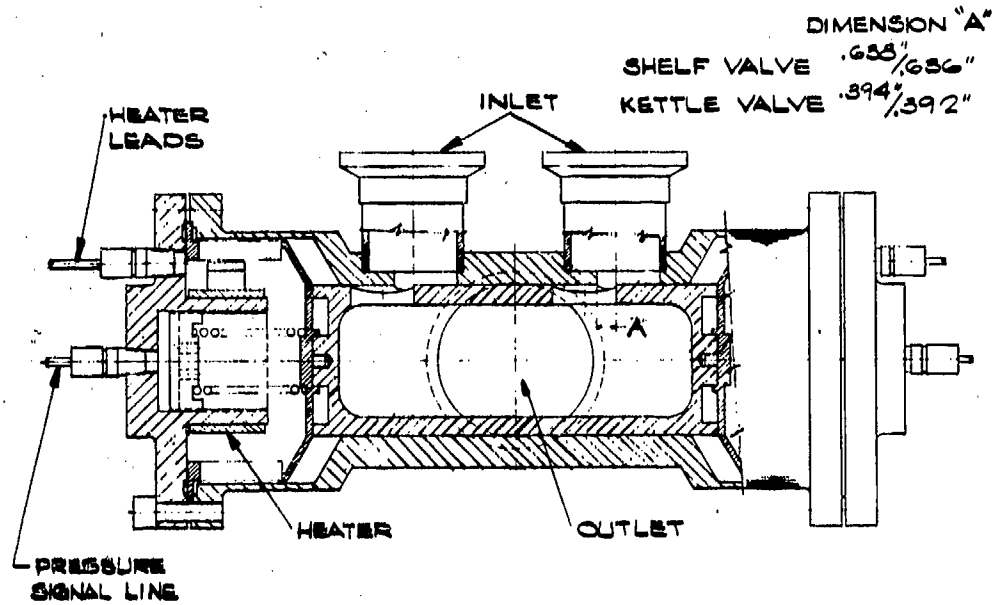

BASIC CONTROL VALVE DESIGN

FIG. 92

In order to reduce hysteris effects resulting from friction, the bellows size has been made as large as practical and piston weight as light as possible. The bellows selected feature an outer diameter of 4-3/4" and an inner diameter of 4".

The required orifice area was calculated using Hoopes' correlation for two-phase flow (Ref. 17) for a design condition of 100 lb./sec. throughput, a speed of 60 rad./sec. and pressure drops of 90 psi for the kettle transfer valves and 140 psi for the shelf transfer valves. The pressure drops across the valves were determined from the pressure conditions on the process flowsheet and the two-phase flow correlation (Ref. 1, Section 5.5.2). The areas required for the valve orifices (2 orifices per valve) at design condition were calculated at 0.605 $in.^2$ for the kettle transfer valves and 0.8 $in.^2$ for the shelf transfer valves. The required valve openings are obtained by appropriate overlap of the 1.25 in. diameter holes in the valve body and piston. The kettle and shelf transfer valves are identical except for position of the orifices on the pistons.

The combined spring constant of bellows and springs is 706 lb./in. Figures 93A and 93B show the variations in orifice area with valve travel and Figures 94A and 94B show the valve area as a function of signal level for both the shelf and the kettle transfer valves. The system is designed to permit separator operation between 30% and 115% throughput. Variations expected in liquid levels for variations in throughput and, therefore, also radial speed are shown on Figures 95A and 95B.

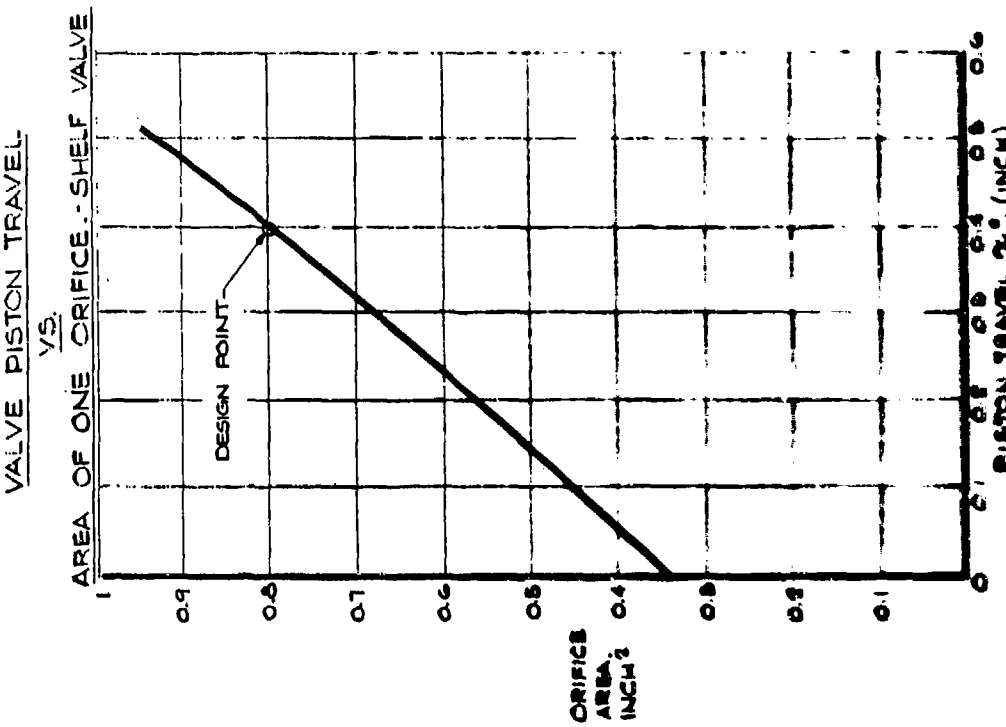

FIG. 93 B

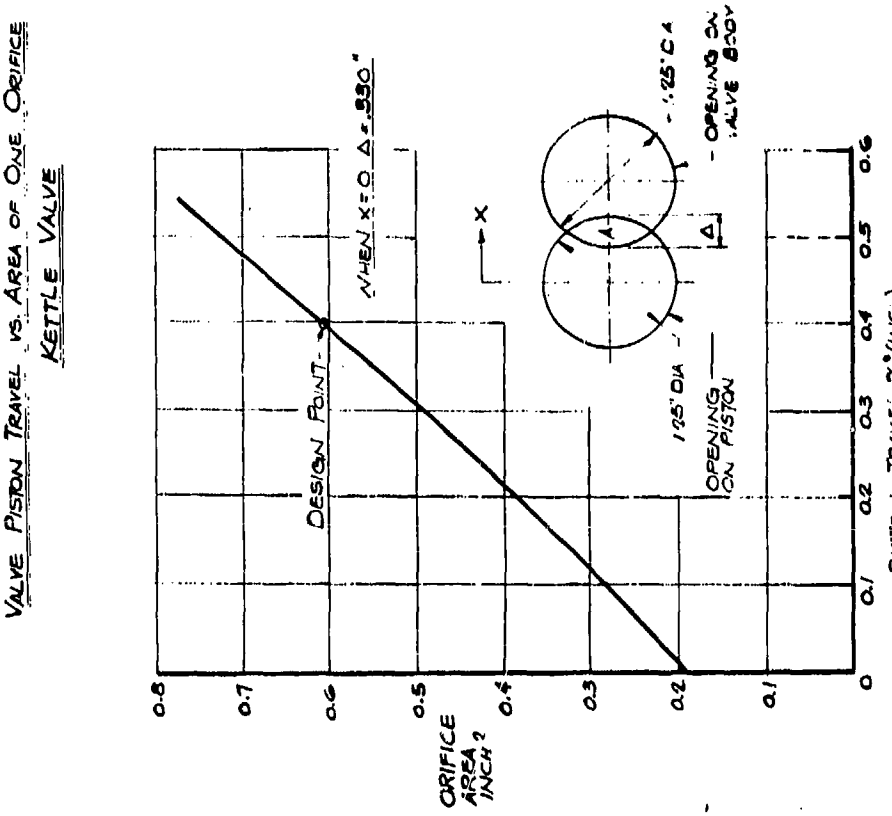

FIG 93 A

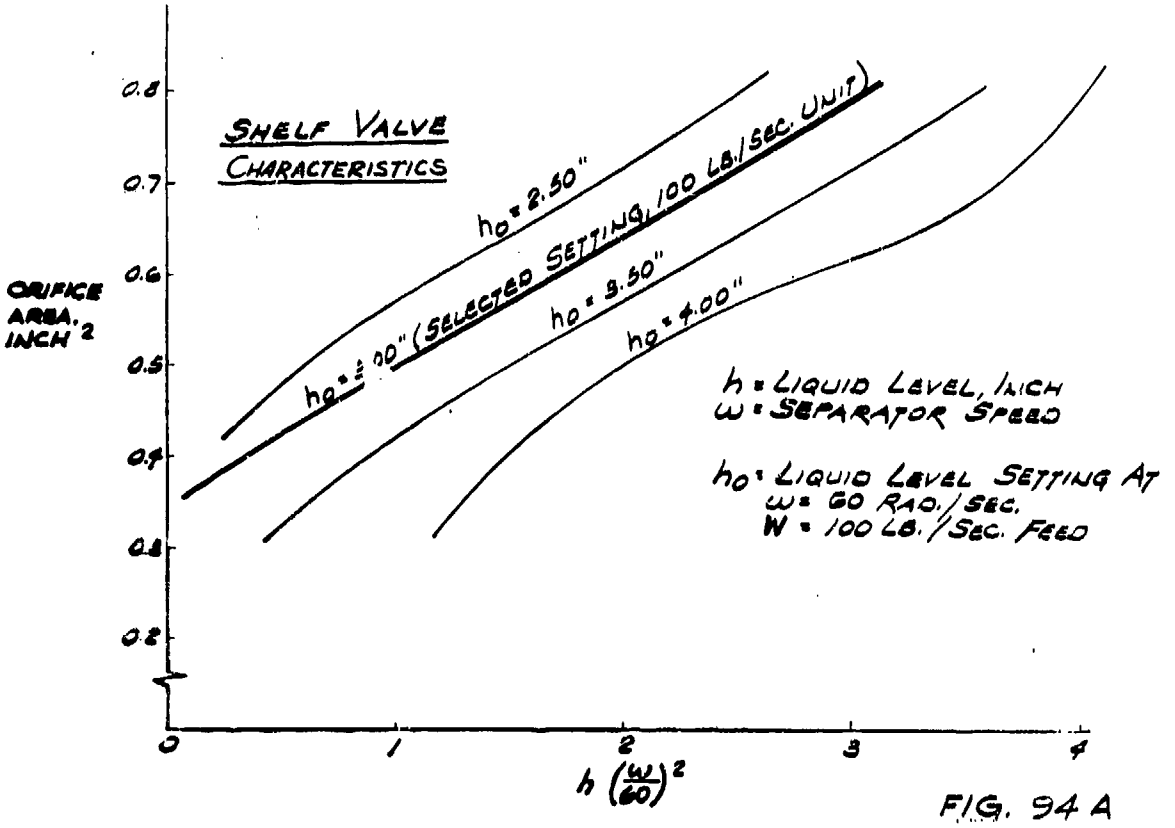

FIG. 94 A

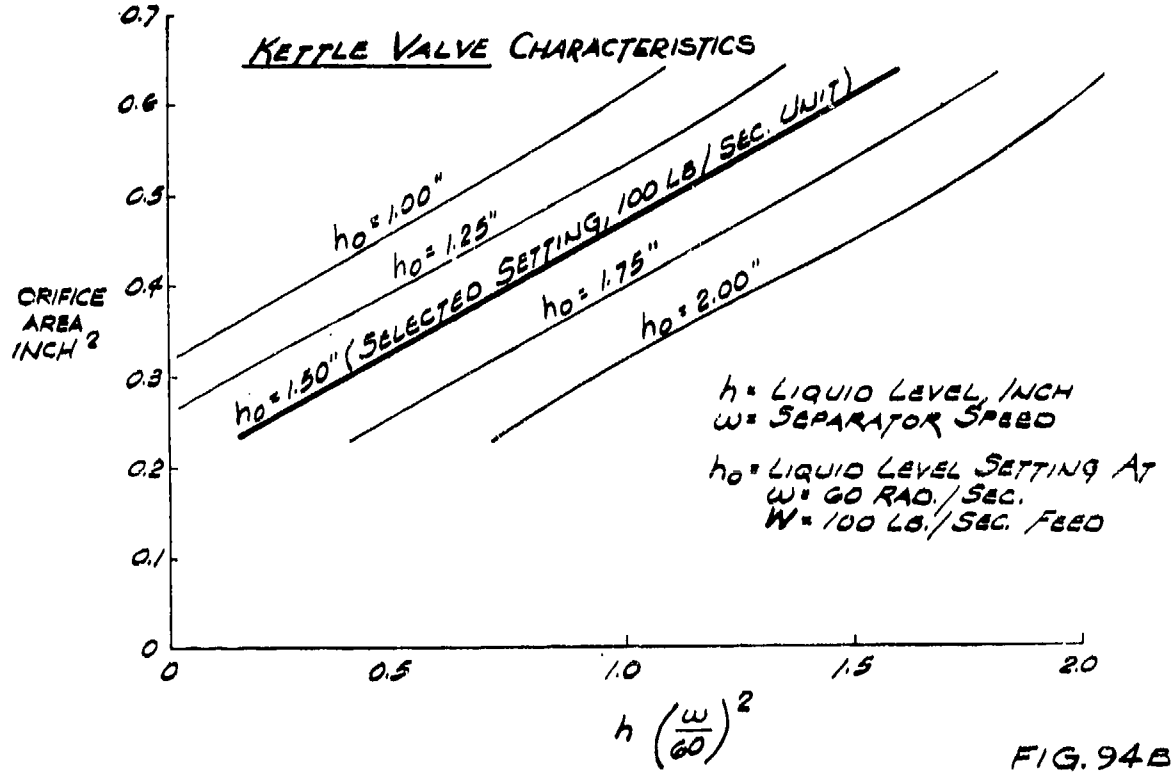

FIG. 94B

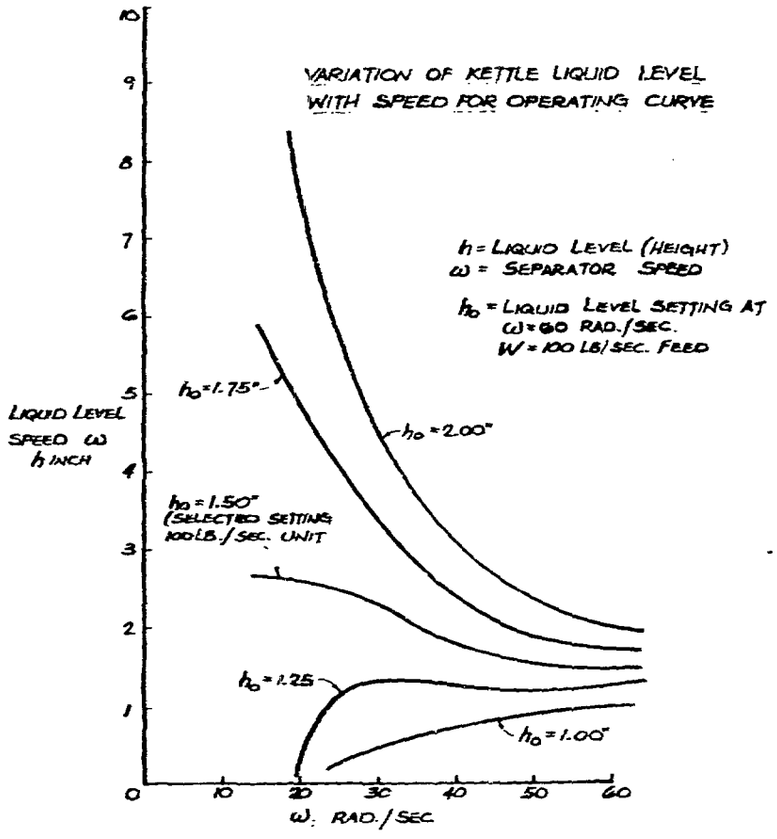

FIG. 95A

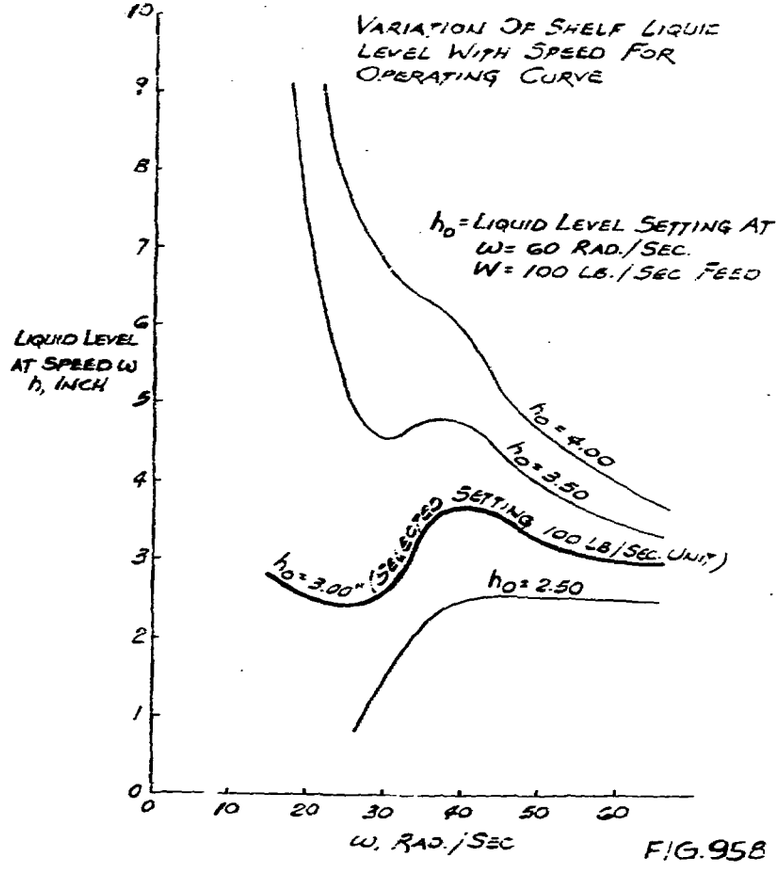

FIG. 95B

5.2.9.3 Signal System

The opposing operating bellows of the valves are connected to vapor and liquid taps respectively. To insure a differential pressure signal at the bellows it is necessary to feed sufficient heat to the liquid sample tap to maintain fluid at this location in the vapor phase. In the boilerplate model this is accomplished by using a small chamber (Figure 96) which is connected to the liquid reservoir through a small orifice at the periphery of the liquid collector space. Liquid introduced into the chamber is vaporized by an electric heater located within the chamber. Capacity of the heater has to be sufficiently large to provide instant response with the expected sudden variations of flow into the liquid reservoir.

In the boilerplate model two (500 watt) heaters, one for two valves, furnish the signal vapor for the kettle transfer valves while one 500 watt heater furnishes the signal vapor for the shelf transfer valves. The heaters were sized from the considerations of Appendix VIII.

The heater consists of a small cartridge which is inserted into the heater chamber wall. Figure 96 shows details of the heater installation.

Ring heaters are also mounted inside the bellows to prevent condensation of signal vapor within this space as a result of heat transfer to the colder process stream.

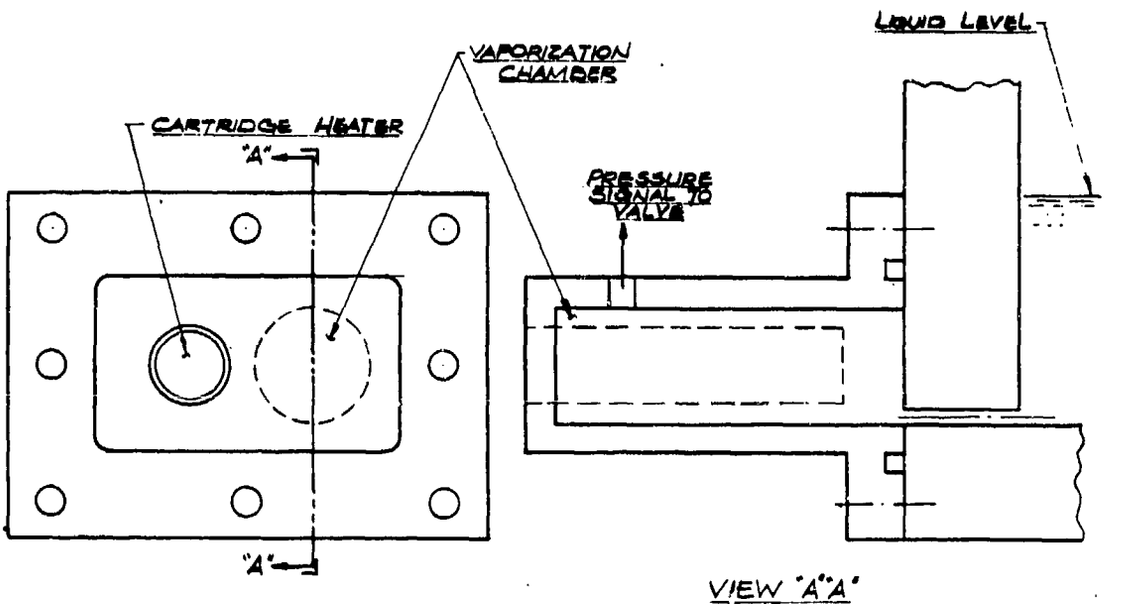

HEATER FOR VALVE PRESSURE SIGNAL SYSTEM

FIG. 96

5.2.9.4 Valve Assembly

A bellows operated piston housed within a cylindrical body with appropriate inlet and outlet parts comprises the basic control valve assembly. Except for the bellows and their associated flanges materials of construction are aluminum throughout. The welded stainless steel bellows assemblies are mounted on each end of the aluminum piston by a simple threaded connection.

The piston and the mating cylindrical surface of the housing have been treated with an ELECTROFILM solid film lubricant to eliminate metal to metal contact and thus minimize friction during operation.

An exploded view of the valve is shown in Figure 97.

5.2.10 Internal Piping

5.2.10.1 General Design

The low pressure column, and high pressure column and reboiler-condenser mounted on a common shaft are interconnected by a rigid piping system.

The internal piping consists of the following branches:

a. Feed air inlet to O.D. of high pressure column.

b. Nitrogen vapor from high pressure column to reboiler-condenser.

c. Kettle liquid transfer from O. D. of high pressure column to low pressure column.

d. Oxygen vapor from O. D. of reboiler-condenser to low pressure column.

Each piping branch is made up of a number of radially spoked ducts which transport fluid between two circumferential manifolds or reservoirs. The number of parallel (radial) lines in each branch and their size was determined from flow considerations while their general arrangement and method of connection was evolved from fabrication and assembly considerations and the loading on the piping due to the energy transfer through it.

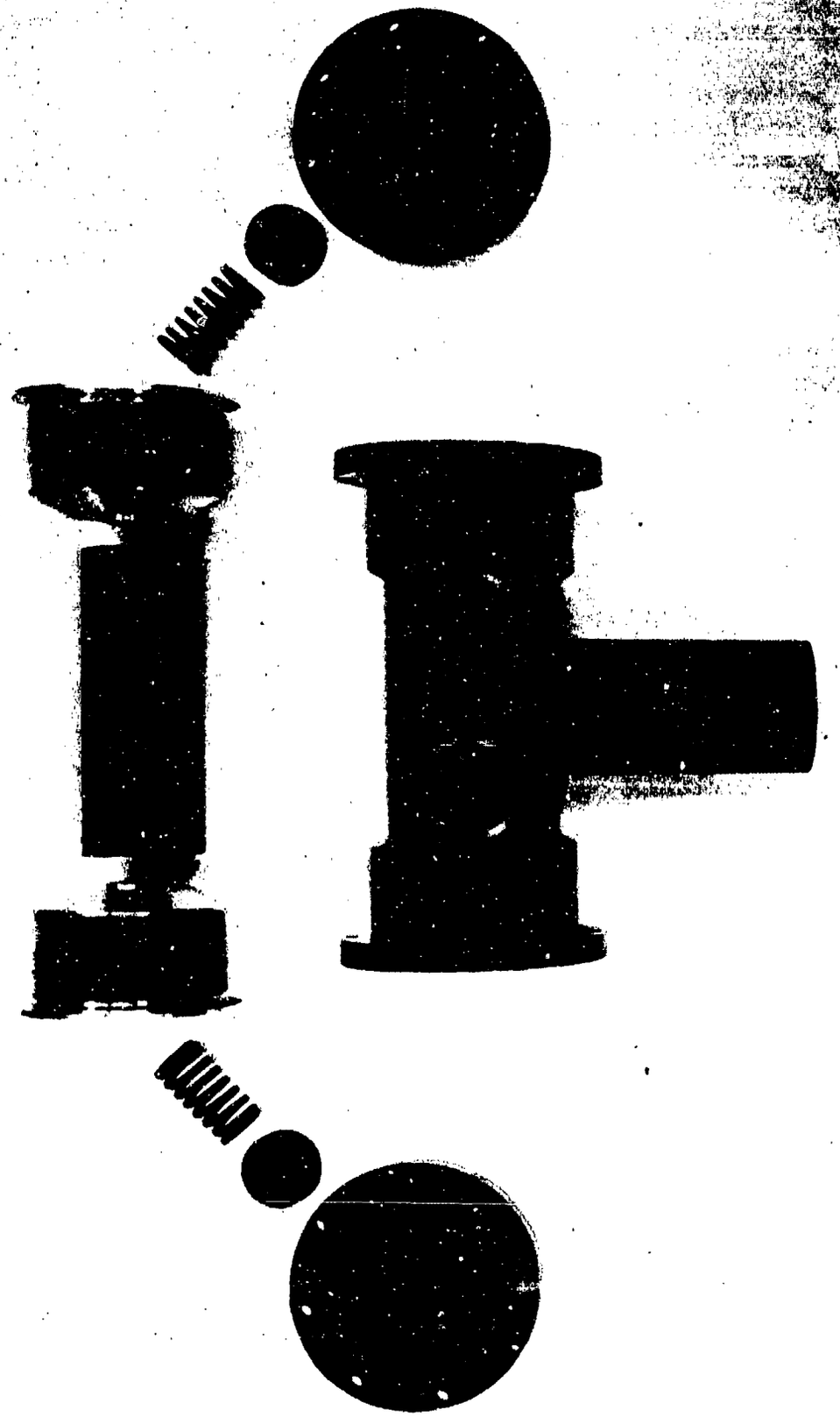

EXPLODED VIEW CONTROL VALVE FIG. 97

5.2.10.2 Feed Air Inlet

The feed air is introduced into the rotary separator through an annular chamber in the hollow shaft on the drive end. This chamber guides the air to a circumferential phase separator. 12-3" O. D. tubes connect the separator with the O. D. of the high pressure column. The location of the high pressure column on the far end (from inlet air manifold) of the reboiler-condenser casing requires a double bend traverse for the inlet feed lines. The full traverse is designed in two sections. The one leg leading from the inlet manifold is fabricated into the reboiler-condenser casing end wall and a spacer leg with two flanged connections completes the run to the O. D. of the high pressure column.

This piping arrangement results in a fluid stream velocity of 59 ft./sec. with a total frictional loss of 8 psi between air inlet and high pressure column periphery.

5.2.10.3 Nitrogen Vapor to Condensing Side of Reboiler-Condenser

This piping branch is in essence parallel to the feed air inlet system. It leads from a circumferential vapor manifold on the I.D. of the high pressure column to an annular chamber in the hollow shaft adjacent to the inlet air manifold. The quantities of nitrogen vapor handled (0.8 mole/lb. mole feed) result in the same number and size of lines as required in the air inlet feed system and the terminal points of the piping branch facilitate the use of a similar fabrication arrangement. Since the nitrogen vapor lines consist of a single bend traverse only one flange connection is required.

5.2.10.4 Kettle and Shelf Liquid Transfer

The transfer piping for these two streams makes up part of the "internal control system" for the liquid levels in the kettle and the shelf and to that extent, it is discussed separately. The mechanical design only is considered here.

Since four control valves with dual inlet ports are used to control kettle liquid flow eight transfer lines are required to the valves. The design of the valve and its mounting has been arranged such that a single 90° bend spacer type section with flanged ends comprises the transfer line between the O. D. of the high pressure column and the valve inlet ports. The eight kettle liquid transfer sections are 2" in diameter resulting in an inlet velocity of 12 ft./sec. The velocity and pressure at any point in the lines is a function of the flashing stream quality.

Two-phase flow correlations yield a pressure drop in the kettle transfer lines upstream of the valve of 115 psi.

Each of the four valves discharges through a single port into a circumferential separator on the wall of the low pressure column rotor.

With the use of two control valves to handle the shelf transfer stream, four lines are required to the valves from the shelf liquid circumferential reservoir on the O.D. of the reboiler-condenser casing. The four lines, two pairs - one to each valve - spaced 180° apart, are fabricated into the reboiler-condenser casing end wall with flanged end connections for attachment to the valves. The two valves have a single 3" diameter discharge to an annular reservoir in the hollow shaft leading to the first tray of the low pressure column. The transfer lines upstream of the valves are 2 in. in diameter resulting in an inlet velocity of 11 ft./sec. Two-phase pressure drop for the same section has been estimated at 50 psi.

5.2.10.5 Oxygen Vapor to Low Pressure Column

The oxygen vapor from the boiling side of the reboiler-condenser collects in a radial space between the tube disk assembly and the housing end wall where it is manifolded into twelve 3-1/2" diameter lines leading to the O.D. of the low pressure column. Each of the twelve lines consists of an S-type spacer section with flanged ends for connection to mating flanges on the reboiler-condenser casing and the low pressure column walls. This piping arrangement results in a fluid stream velocity in the lines of 90 ft./sec. and a total friction pressure drop of 1.5 psi.

5.2.10.6 Piping Connections

To minimize heat joining and bolting in the final rotor assembly steps, all internal piping sections have been provided with a "Conoseal" joint. This consists of a male and female flange, a conical seal gasket and a V-retainer coupling tensioned by a single bolt.

This type joint can be assembled with relative ease and because of its design it affects a leak tight seal even with small degrees of flange looseness. This condition is inherent to the design because of the differential contraction between the aluminum flanges and the stainless steel U-coupling at the operating temperatures.

5.2.10.7 Piping Loads

Since the internal piping system constitutes a rotating assembly the added inertia loads on the pipe sections had to be considered. For a rotating member, forces acting in the radial direction are:

$$dF_r = Adr \frac{\rho_r \omega^2}{g_c} \quad (53)$$

and those acting in the tangential direction:

$$dF_t = 2\omega\ Vdm = 2\omega\ V\rho\ Adr \quad (54)$$

where dF_r represents a direct pull on the pipe and dF_t, a uniform load over the pipe span giving rise to bending moments on the fixed ends. These effects would be largest on the liquid carrying pipes because of larger fluid density.

With the spans involved maximum moments of 70 in. lbs. were calculated for the kettle transfer lines. These moments have a negligible effect upon stress levels.

Piping loads due to temperature gradients have not been considered. These would occur during initial cooldown only. The cooldown procedure for the unit is specified to minimize these effects, as shown in Appendix IX.

Additional forces on the kettle and shelf transfer lines due to the mass of the control valves have also been omitted from considerations on the basis that each valve will be supported separately.

5.2.11 Optical System

As mentioned earlier it is desired to observe the operation of representative trays in each column section during separator tests. For this purpose a viewing system is provided as part of the rotor assembly. This consists of Plexiglas windows appropriately provided on the column walls. Two windows diametrically apart are provided on the stripping section of the low pressure column, the enriching section of the low pressure column and the high pressure column respectively. These windows can be viewed when in line with radially matching windows on the casing walls. The latter consist of two Plexiglas disks separated by a stainless steel spacer. The chamber between the disks can be evacuated or pressurized slightly with a dry gas. Heating around the outer end of the stainless steel spacer insert will prevent condensation of moisture on the outer casing window.

A strobotac lamp mounted on top of the casing and suitably triggered by an electronic switching device constitutes the light source

for tray observation. The light beam enters the casing through a double window and is reflected to the column windows by suitably oriented mirrors mounted on the rotating column walls. The latter consist of highly polished aluminum surfaces.

The stepped casing construction requires that the casing window for observation of the high pressure column trays be oriented at an angle with respect to the casing axis. For proper observation of these trays it is necessary to bend the light image from the column by means of two prisms mounted in front of the windows. The optical installation including windows, mirrors, and prisms is shown in Figure 98.

This system is in essence similar to that used in the UCON circumferential tray test rotor which allowed a view of the tray flow characteristics as shown in figure 15 of Ref. 1. In the UCON rotor optical system the light source was introduced through a window in line with the viewing window inasmuch as only one rotor was involved. In the case of the 100 lb./sec. unit where the same strobotac lamp is used as the light source for two in-line rotors reflection of the light beam, entering in a direction normal to the axis of the rotors, by suitably oriented mirrors was necessitated. Undoubtedly the indirect path of the light beam will somewhat reduce the effectiveness of the optical system.

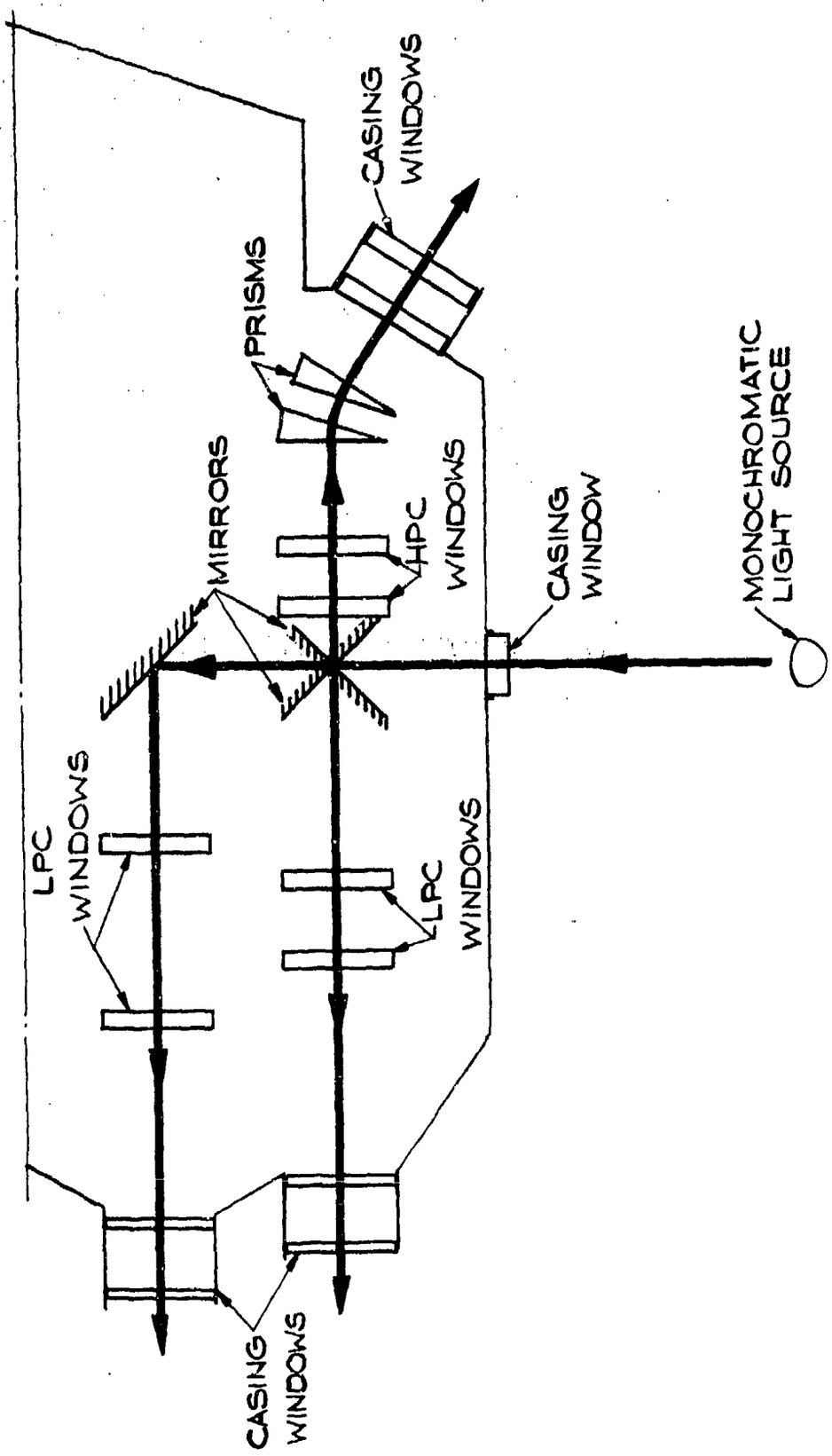

FIG. 98

OPTICAL SYSTEM

(THIS PAGE IS INTENTIONALLY BLANK.)

5.2.12 Instrumentation

Operation and performance of the 100 lb./sec. boilerplate model air separator will be controlled and monitored by measuring liquid levels, pressure drops, dynamic unbalance and by examining fluid samples withdrawn from various internal fluid chambers. Figure 99 shows the instrumentation diagrammatically.

Liquid level is measured at three locations in the machine: kettle liquid level, low pressure column liquid level, and product liquid level. The kettle liquid level is monitored by a 0-50 psi range differential pressure transducer, (1 in Figure 99). The high pressure port of the transducer is submerged beneath the liquid and the low pressure port is referenced to the vapor above the liquid. The liquid level is controlled by valves (8) as discussed in Section 5.2.9.

The liquid level in the low pressure column is also sensed by a 0-50 psi range differential pressure transducer, (2). The peripheral seal installation on the outer faces of the column prevents mounting of the transducer adjacent to the liquid level as was done at the kettle. Since the transducer was moved radially inward, inside of the seal inner radius, a purge system from a high pressure gas source as shown is required to counterbalance the hydrostatic head created by the liquid level. Control of the low pressure column liquid level is performed by an automatic valve external to the separator which receives a signal from the transducer.

The product liquid level is monitored by a system identical to that on the low pressure column. The transducer (3) provides the signal for the external automatic valve.

Pressure drops across the stripping section and enriching section of the low pressure column are measured by two 0-25 psi range differential pressure transducers. A 0-50 psi range differential pressure transducer is provided to measure the pressure drop across the high pressure column. The pressure difference between the boiling side and the condensing side of the reboiler-condenser is measured by a 0-200 psi range differential pressure transducer.

Unbalance is monitored by measuring the transverse strain which results from the shaft deflection. The measurements are made with SR-4 strain gauges mounted on strain-multiplying tensile bars. Each bar is furnished with a strain measuring gauge on each side and two temperature compensating gauges. Two such bars are mounted inside the inlet air manifold at diametrically opposed locations.

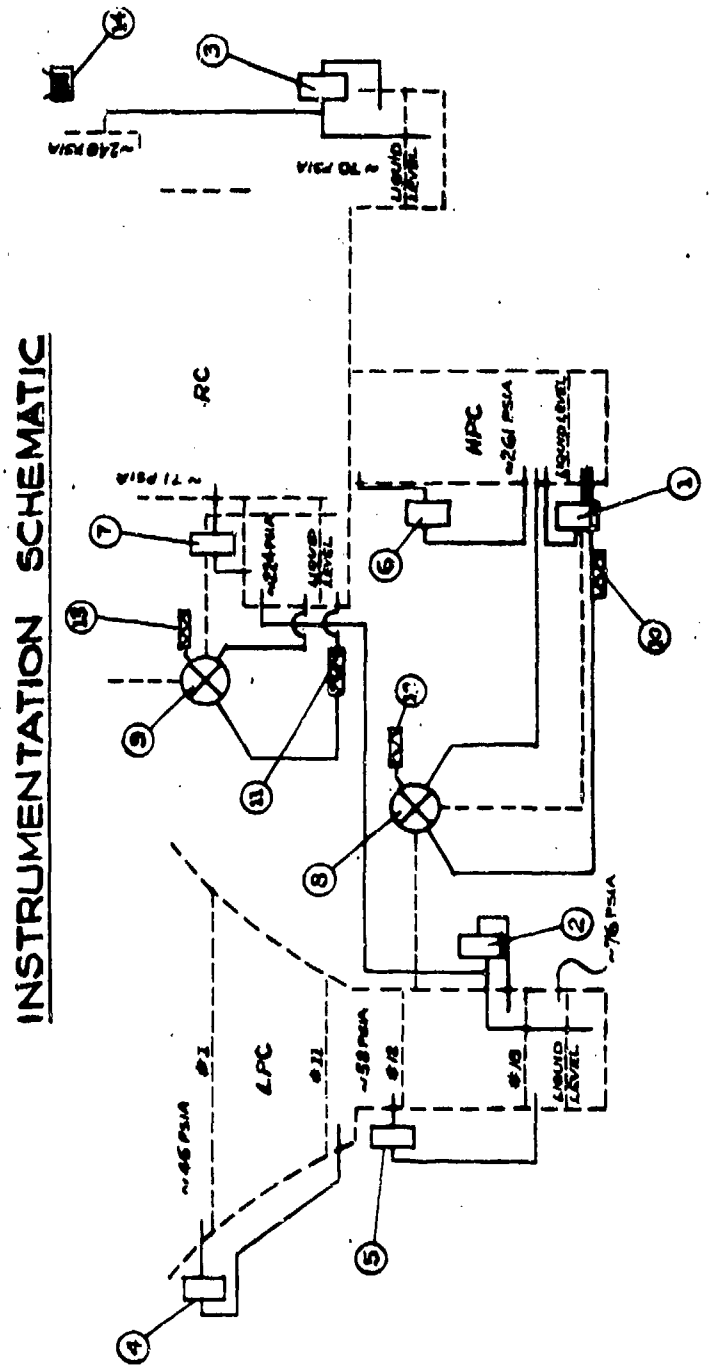

ITEM	QUAN	DESCRIPTION
1	1	PACE P7D 0-50 PSI RANGE
2	1	PACE P7D 0-50 PSI RANGE
3	1	PACE P7D 0-50 PSI RANGE
4	1	PACE P7D 0-25 PSI RANGE
5	1	PACE P7D 0-25 PSI RANGE
6	1	PACE P7D 0-50 PSI RANGE
7	1	PACE P7D 0-200 PSI RANGE
8	4	KETTLE TRANSFER CONTROL VALVE
9	2	SHELF TRANSFER CONTROL VALVE
10	2	500 W
11	1	500 W
12	6	125W IN VALVE SIGNAL VOLUME
13	4	126W IN VALVE SIGNAL VOLUME
14	6	UNBALANCE MONITOR W/ TEMPERATURE COMPENSATION

FIG. 99

The instrument leads are channeled through a central tube within the hollow shaft to the drive end where the electrical signals are withdrawn through a system of rotating slip rings.

Power input for the heater system of the control valves and their associated vapor signal system is accomplished through the same slip ring assembly. The two circuits associated with the control system heater elements will take up only four slip rings. The transducer and strain gauge circuits will take up an additional 32 slip rings.

The use of two, 30 ring each, slip ring modules leaves a number of rings available to accommodate added instrumentation if the need arises.

5.2.13 Power Requirements

5.2.13.1 Introduction

The power requirements of the boilerplate model air separator may be conveniently grouped into three areas: power to overcome mechanical friction losses which are proportional to the first power of the speed, power for fluid pumping work which is proportional to the square of the speed, and power to overcome windage losses which are proportional to the cube of the speed. The mechanical losses are caused by friction in the shaft seals and bearings. Pumping work is required to transport fluids from the center to the periphery of the machine and windage losses occur in the peripheral seals, which are immersed in liquid, as well as around the other rotating components which are turning in a vapor envirnonment. The power requirements as generated by these sources dictate the selection of a suitable drive train and power source. The power required by the machine at various speeds for a casing pressure of 60 psia is shown in Figure 100. For an established design speed of 60 rad./sec. power requirement is approximately 655 horsepower.

5.2.13.2 Discussion

The total power requirement for the boilerplate model air separator as plotted in Figure 95 is expressed by:

$$HP_T = \left[\pi f_f b_s \Sigma n P D_{so}^2 + f_b \Sigma n Fn D_{bb}\right] \frac{\omega}{12(550)} + \frac{\omega^2}{2 g_c 550} \Sigma WR_o^2 + \frac{Cm}{2 g_c 550} \Sigma \rho \left[\frac{R_o}{12}^5 - \frac{r_i}{12}^5\right] \omega^3 \quad (55)$$

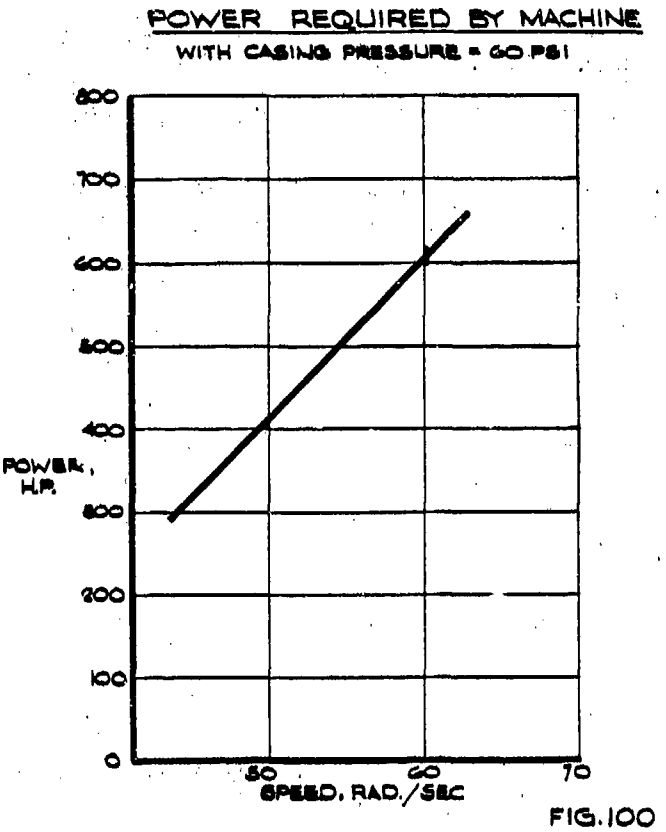

FIG. 100

The first grouping on the right hand side of the equation represents total power dissipation due to friction torque generated in mechanical elements. A single element contribution is expressed in the basic form:

$$HP_f = \frac{f_f F_n \pi d \omega}{12\ (550)} \qquad (56)$$

Two contributing basic elements have been considered in the group, namely the shaft seals and the bearings. Five different diameter seal sets sealing against various pressures and two bearing sets of different diameters are included.

The second grouping considers internal pumping requirements, expressed as:

$$HP_p = \frac{W (R_o \omega)^2}{2\ g_c\ 550} \qquad (57)$$

Two separate fluid streams, introduced at the shaft are withdrawn at appropriate peripheries. These include the low pressure column fluid and the product recirculation stream.

The third grouping takes into account disk friction and windage losses. The power dissipated due to these losses has been computed by the expression given by Daily and Nece (Ref. 18).

$$HP_{\omega} = \frac{Cm}{2} \frac{\rho}{g_c} \frac{\omega^3}{550} \left[\left(\frac{R_o}{12}\right)^5 - \left(\frac{R_i}{12}\right)^5 \right] \qquad (58)$$

The power consumption data recorded during the tests of the centrifugal type peripheral seal show good correlation with these expressions. As can be seen windage is very sensitive to environmental fluid density (ρ) and the radial dimensions of the wetted areas involved. On this basis the peripheral seal areas are responsible for the major part of windage loss. The magnitude of the windage loss is then a function of the active peripheral seal depth which is directly dependent on the casing pressure. Peripheral seal characteristics have been considered in detail in Ref. 1, Appendix X. The sources of windage loss considered include:

a. The liquid immersion windage loss at the low pressure column peripheral seal and at the product discharge peripheral seal.

b. The vapor immersion windage loss around the rotor.

(THIS PAGE IS INTENTIONALLY BLANK.)

APPENDIX I

BOILERPLATE DESIGN COMPUTER PROGRAM

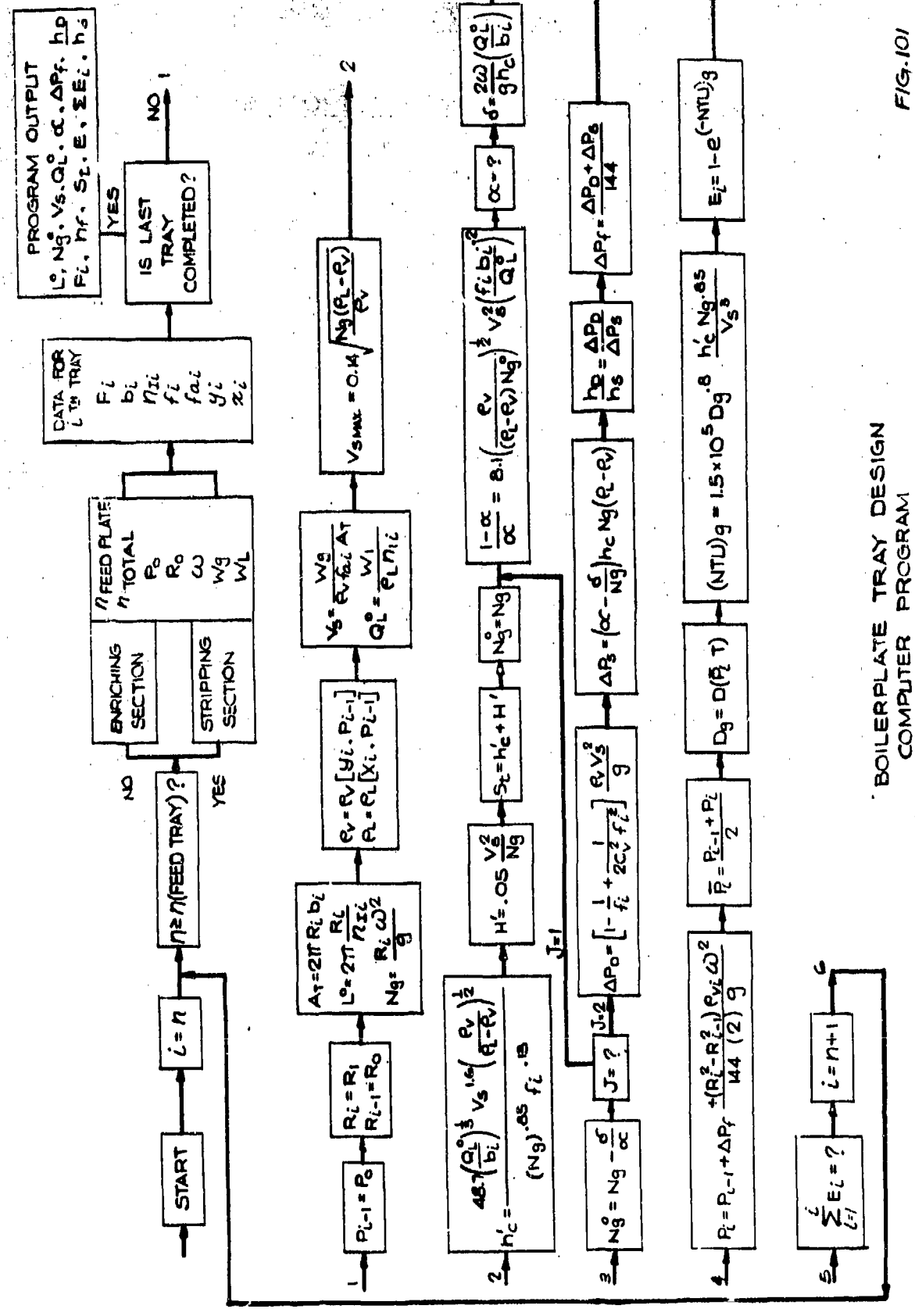

BOILERPLATE TRAY DESIGN
COMPUTER PROGRAM

FIG. 101

APPENDIX II

SHAFT FLANGE DESIGN

The disssimilar metal flange connections can be sources of high local bending stresses due to the differential thermal contraction at the steel-aluminum interface during shaft cooldown. The following analysis yields the levels of stresses encountered.

The radial differential contraction between the two mating dissimilar metal flanges is:

$$\Delta_r = r\,\Delta T\,(\alpha_{AL} - \alpha_S) \tag{59}$$

If the shaft is regarded as a thin-walled cylinder, rigid at the ends and subject to loading which produces the deflection Δ_r then the local bending stresses can be determined. Considering the unit strip beam, the deflection for which is radial

$$F^*_s = 4\,\Delta_r\,\beta^3 D \tag{60}$$

$$M^*_B = 2\,\Delta_r\,\beta^2 D \tag{61}$$

where: $\beta = \sqrt[4]{\dfrac{3\,(1-\mu_p^2)}{r^2\,t_s^2}}$

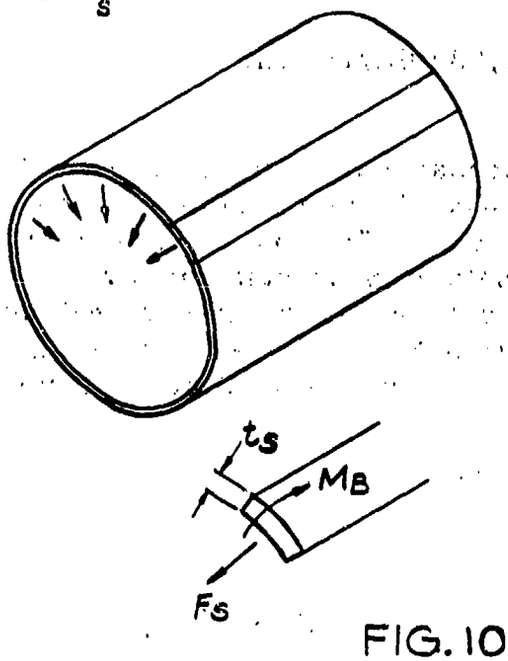

FIG. 102

and $$D = \frac{E_y t_s^3}{12(1-\mu_p^2)}$$

thus:

$$M_B^* = 2r\,\Delta T\,(\alpha_{AL} - \alpha_S)\left[\sqrt{\frac{3(1-\mu_p^2)}{r^2 t_s^2}}\right]\frac{E_y t_s^3}{12(1-\mu_p^2)} \qquad (62)$$

and:

$$S_1 = \frac{M_B t_s}{2I}\quad\frac{6M_B}{t_s^2} \qquad (63)$$

If this stress is excessive it is necessary to allow the aluminum flange to slide on the nineper cent nickel steel flange as the shaft cools. If no sliding took place for a representative flange, Δ, is computed as .0157", then

$$M_B = 6800 \text{ in.-lb. and } S_1 = 40,800 \text{ lb./in.}^2$$

The bending moments caused by the shaft loading and the torque transmitted by the shaft are additive to those caused by differential contraction. Between the columns the maximum stress due to bending moment is $\approx$ 775 lb./in.^{2} and outside the columns it is 1180 lb./in.^{2}. At this point the shearing stress is 280 lb./in.^{2}. This gives a combined stress of:

$$S_{total} = 41,980 \text{ lb./sq. in.}$$

Since this is an excessive value the flanges must be allowed to slide. As the aluminum flange slides on the nine per cent nickel steel flange the loading is as shown. The force F_T is the tension in the bolts and consists of three major components: the bolt load required to seal the flange gasket, the bolt preload required to maintain the seal when the shaft deflects, and the bolt load created when the aluminum bolt contracts more than the nine per cent nickel steel flange. The first component is:

$$F_{t_1} = C_g\,(2\pi r) = 2\pi C_g r \qquad (64)$$

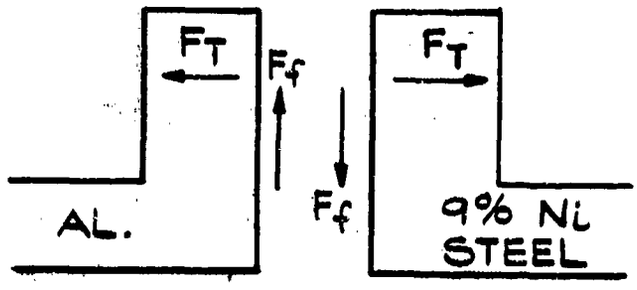

FIG. 103

The second component depends upon the position of the bolt under consideration and is a maximum when the bolt is directly beneath the shaft centerline. Thus all of the bolts must be prestressed this constant amount. For a shaft deflection of Δ_S the shaft length between fixed points on the centerline is, by Huygen's approximation, Ref. 19.

$$L_s = 1/3\ (8C'-C) \qquad (65)$$

Since:

$$C' = \sqrt{C^2/4 + \Delta_s{}^2}, \text{ then}$$

$$L_s = 1/3\ (8\sqrt{C^2/4+\Delta_s^2} - C)$$

and the change in shaft length is:

$$\Delta L_s = L_s - C = 1/3\ (8\sqrt{C^2/4 + \Delta_s^2} - C) - C \qquad (66)$$

The shaft geometry is now approximately as shown in Figure 104 and

$$\Delta_B = \frac{2R_B \Delta L_s}{R_B} = 2\,\Delta L_s = \frac{16}{3}\sqrt{C^2/4 + \Delta_s{}^2} - \frac{8}{3}\,C \qquad (67)$$

THIS
PAGE
IS
MISSING
IN
ORIGINAL
DOCUMENT

172

Thus the total bolt load is:

$$F_{total} = 2\pi C_g r + \frac{\pi N E_y D_B^2}{4L_B}\left[16/3\sqrt{\frac{C^2}{4} + \Delta_s^2} - \frac{8C}{3} + \Delta T\ (\alpha_{AL} L_B - \alpha_s b_F)\right] \quad (73)$$

If the coefficient of friction of the flange face is f_f, then

$$F_f = f_f F_{total}$$

Using representative values for the parameters

$$F_f \approx 8600 \text{ lb.} \quad (74)$$

The contact stress is

$$S_1 < \frac{F_f}{f_f A} = \frac{f_f F_{total}}{\pi (R_o^2 - R_i^2)} \quad (75)$$

which is approximately $S_1 > \approx 658$ lb./in.^{2} for a representative flange. Using the same representative value as above for Δ_r and letting $t_s = 3/4$ in. $F_s = 4290$ lb./in. which is the force acting if no sliding took place. However, since $F_f/2\pi r = 169.6$ lb./in. representing the force required to start sliding is considerably smaller than F_s, sliding will take place.

(THIS PAGE IS INTENTIONALLY BLANK.)

APPENDIX III

LIQUID UNBALANCE

The unbalance may be estimated by considering a percentage of the rotating liquid at each point as being maldistributed. The liquid holdup consists of:

1. Oxygen reflux holdup: 1.5 sec., 150 lb., at a mean radius of 4 in. If five per cent of this holdup was maldistributed and the shaft was rotating at 58 rad./sec. the resulting unbalance force would be:

$$F_{u1} = \frac{W'_{coll}}{g_c} \omega^2 r = 258 \text{ lb.} \qquad (76)$$

2. Nitrogen liquid at top of high pressure column:

$t = 3$ sec., $W_{coll} = 189$ lb., $r = 30$ in.

$F_{u2} = 2430$ lb.

3. Kettle liquid at bottom of high pressure column:

$t = 3.0$ sec., $W_{coll} = 189$ lb., $r = 50$ in.

$F_{u3} = 4060$ lb.

4. Kettle liquid at introduction to low pressure column:

$t = 3.0$ sec., $W_{coll} = 126$ lb., $r = 32$ in.

$F_{u4} = 1730$ lb.

5. Column liquid: $t = 3.0$ sec., $W = 262$ lb., $r = 50$ in.

$F_{u5} = 5620$ lb.

6. Nitrogen reflux and shelf-transfer holdup:

$t = 1.5$ sec., $W_{coll} = 68$ lb., $r = 4$ in.

$F_{u6} = 118$ lb.

7. Product discharge: $t = 3.0$ sec., $W_{coll} = 60$ lb. $r = 32$ in.

$F_{u7} = 824$ lb.

8. Fluid on the trays: If the average foam height on the trays is h'_f and the fluid density is ρ_f lb./in.^{3}, the unbalance force, assuming five per cent of the weight on each tray maldistributed, is given by the following approximate tray hydraulic relationships:

$$\Delta P = \left(\frac{\rho_f}{20736\,\rho_L}\right) \rho_L h_f N_g \qquad (77)$$

or

$$\rho_f = \frac{\Delta P}{h_f N_g} \quad (20736)$$

Hence:

$$W_f = \frac{2\pi r h_f b \rho_f}{1728} = \frac{2\pi r h_f b}{1728}\left(\frac{\Delta P}{h_f N_g}\right)(20736)$$

But

$$N_g = \frac{\omega^2 r}{g_c}$$

therefore

$$W_f = \frac{24\pi b \Delta P g_c}{\omega^2} \qquad (78)$$

and

$$F_{u8} = 0.05 \frac{W_f}{g_c}\left(\frac{r\omega^2}{12}\right) = (.05)\left(\frac{24\pi b \Delta P g_c}{\omega^2 g_c}\right)\left(\frac{r\omega^2}{12}\right) \qquad (79)$$

$$F_{u8} = 0.1\pi br\Delta P$$

Using this approximate relationship the unbalance force on each tray may be estimated. The total of all of these unbalance forces as calculated is 18,085 lb. equivalent to a 30 lb. weight in a force field of 600 Ng.

APPENDIX IV

SAMPLE STRESS AND DEFLECTION CALCULATIONS

Wall Thickness from Maximum Shearing Stress Theory

From the vertical shear diagram of Figure 37 it is found that the maximum bending moment occurs at the flange of the reboiler-condenser outward of which the high pressure column is located. On the funicular polygon (Figure 37) the distance at (de) measures 1.72 in. Since the moment scale for this polygon is 240,000 in. lb./in. the maximum bending moment is:

$$M_{Bmax} = 1.72\ (240,000) = 413,000\ \text{in.-lb.}$$

At (de) the shaft is carrying a torque of 76,242 in.lb. Thus from Equation (30)

$$D_o^{\,3} = \frac{16}{\pi S_s \left(1 - \frac{D_i^{\,4}}{D_o^{\,4}}\right)} \left[M_T^{\,2} + M_B^{\,2}\right]^{1/2}$$

$$D_i^{\,4} = (16)^4 - \frac{(16)^2}{\pi\ (13.33)} \sqrt{(76,242)^2 + (413,000)^2}$$

Thus

$$D_i = 15.79\ \text{in. and } t_s = 1/2\ (16 - 15.79) \approx 0.10\ \text{in.}$$

Graphical Shaft Deflections

After the bending moment diagram is constructed as shown in Figure 40, the areas are calculated as, for example:

$$A_{hj} = 1/2\ (15.5\ \text{in.})\ 168,000\ \text{in.lb.}) = 1,300,000\ \text{units.}$$

This area is represented by an imaginary force passing through the centroid of the triangular bending moment area as shown in Figure 40. The force polygon of Figure 39 constructed using these imaginary forces is used to construct the deflection funicular polygon shown in Figure 40. The scale of the deflection polygon is the product

of the space scale, the imaginary force scale, and the pole distance of the force polygon:

$$20(4{,}000{,}000)\ 3 = 24 \times 10^7/\text{in.}$$

A deflection can be obtained at any point by selecting a moment of inertia (I) and measuring the distance on the deflection polygon. For example, for a 16 in. O. D. shaft with a 3/4 in. wall thickness

$$I = \pi/64\ \left[(16)^2 - (14.5)^2\right] = 1{,}050\ \text{in.}^4$$

The deflection is given by

$$\Delta = Y\,(x)/EI \qquad (80)$$

where Y is the deflection polygon scale and x is the distance measured on the deflection polygon. For example, if the columns are not tied together by supports at the periphery, the deflection at (ef) is

$$\Delta = \frac{24 \times 10^7\ (1.47)}{10 \times 10^6\ (1050)} = 0.0359\ \text{in.}$$

Since deflections of this magnitude are obviously too large, the value of I is increased and the same polygon utilized. By adding 6 schedule 80 2-1/2 in. aluminum pipes between the columns at a radius of 55-1/2 in., the moment of inertia is increased to

$$I_\omega = I_o + Ad_y^2 = 42{,}650\ \text{in.}^4$$

This greatly decreased the shaft deflection. For example, at (ef) in Figure 40,

$$\Delta_{ef} = \frac{24 \times 10^7\ (1.47)}{10 \times 10^6\ (42{,}650)} = 0.000884\ \text{in.}$$

APPENDIX V

LOAD RATING, BEARINGS

The load and life of a ball bearing are empirically related by the previously stated equation (32):

$$L_N = \left(\frac{C_{sp}}{F_b}\right)^3$$

If a load acts for a certain fraction of that number of revolutions at which the bearing can function under this load, the same fraction of the ability of the bearing to endure load under rotation is consumed.

If the life is L_1 for the radial load F_{b1} then

$$L_1 = \left(\frac{C_{sp}}{F_{b1}}\right)^3$$

if f_L is the fraction of life during which this load acts, $f_L L_1$ is the number of revolutions during which F_{b1} acts, let:

$$f_L L_1 = n_1 = f_L \left(\frac{C_{sp}}{F_{b1}}\right)^3$$

or

$$F_{b1}^3 n_1 = f_{L1} C_{sp}^3$$

$$\vdots$$

$$F_n{}^3 n_n = f_{Ln} C^3{}_{sp}$$

$$\Sigma (F_b{}^3 n) = \Sigma f_L C^3{}_{sp}$$

$$\Sigma f_L = 1$$

$$\therefore \quad \Sigma (F_b{}^3 n) = C^3_{sp}$$

$$L_N = \frac{C^3_{sp}}{\Sigma (F^3_b\, n)/L_N}$$

$$F_m = \left[\frac{\Sigma (F^3_b n)}{L_N} \right]^{1/3} \tag{81}$$

$$L_N = \left(\frac{C}{F_m} \right)^3 \tag{82}$$

where F_m is the cubic mean load (mean effective load) which gives the same life as the actual variable load.

The radial loading on the bearing supports for the 100 lb./sec. rotary air separator is made up of two components:

a. A static load (Fs) due to the weight of the rotor.

b. A dynamic load (Fu) due to the rotor unbalance.

The resultant load vector is:

$$F = [Fu^2 - 2\, Fs\, Fu \sin \Theta + Fs^2]$$

It represents a rotating vector lagging Fu by $\cos^{-1} =$

$$\frac{Fu^2 + F^2 - Fs^2}{2\, Fu\, F}$$

A loading diagram for each bearing support is shown in Figure 105.

Approximate integration of the polar load diagram to calculate the cubic mean load (F_m), the effective load which gives an equivalent life for the actual variable load, was carried out by considering three constant load periods within each load cycle (1 revolution) as shown in Figure 106.

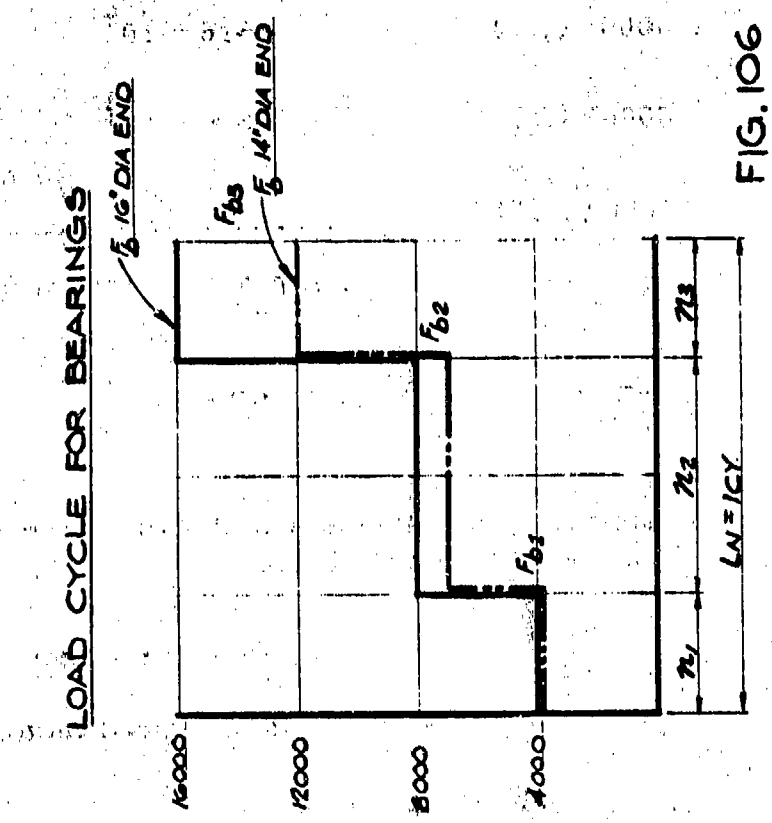

FIG. 106

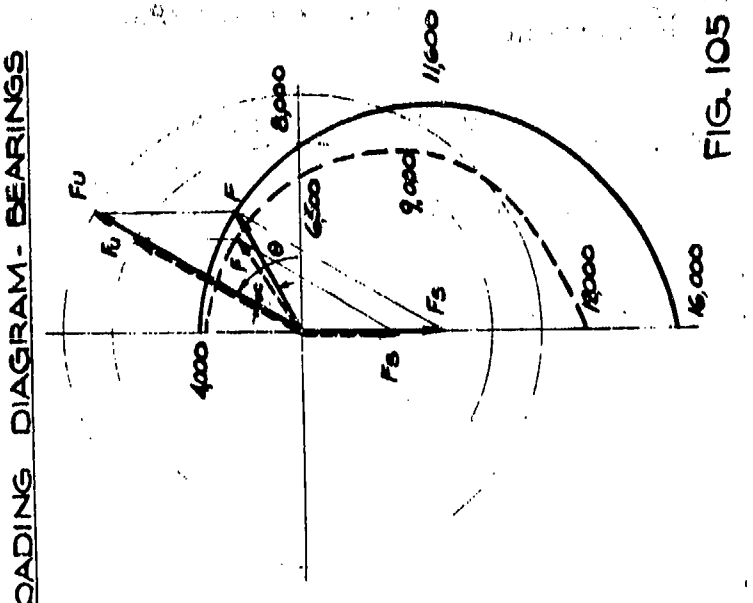

FIG. 105

Taking the 16" diameter bearing as an example:

$F_1^3 n_1$	4000^3 (.25)	16×10^9
$F_2^3 n_2$	8000^3 (.5)	256×10^9
$F_3^3 n_3$	16000^3 (.25)	1024×10^9
		$\Sigma(F_b 3n) = 1296 \times 10^9$

$$F_m = \left[\frac{\Sigma (F_b^3 n)}{L_N} \right]^{1/3} = 11000 \text{ lbs.}$$

Kaydon bearings are rated for 100 RPM and 3000 hrs. average life equivalent to 600 hrs. for 90% of group.

Then $C_{sp} = F_m \times \frac{\rho}{s}$

ρ - life factor

s - speed factor

for an average life of 3000 hrs. $\rho = 1$

for any speed other than 100 RPM from Ref. 20

$$S = \sqrt[3]{\frac{100}{N_{\text{operating}}}} = .54 \text{ for 640 RPM}$$

$$C_{sp} = F_m \frac{1}{.54} = 20,400 \text{ lbs. 16" diameter end}$$

Capacity KG - 160 100 RPM 7140 lbs.

$\frac{20,400}{7140} = 2.85$ ∴ use 4 bearings.

APPENDIX VI

LIMITING CONDITIONS CONTACT TYPE SEALS

With any type of contact seal the surface temperature developed is a limiting factor.

An available relation for the temperature generated during sliding is Equation (35).

$$\Delta T = \frac{f_f F_n V}{4.24\, l_s J^*} \quad \frac{1}{(K_m + K_p)}$$

For metal-plastic contact:

$$K_m >> K_p$$

$$\Delta T = \frac{f_f F_n V}{4.24\, l_s J^* K_p}$$

For the area of junction determined by the yield pressure of the plastic seal material (Py)

$$4 l_s^2 = \frac{F_n}{P_y} \quad l_s = 1/2 \frac{\sqrt{F_n}}{P_y}$$

$$\Delta T = \frac{f_f V \sqrt{F_n} P_y}{2.12\, J^* K_p}$$

For a seal surface speed of:

$$V = \frac{\omega D_{so}}{2} = \frac{\pi N D_{so}}{60}$$

$$\Delta T = \frac{f_f \pi N D_{so} \sqrt{F_n} P_y}{60\,(2.12)\, J^* K_p}$$

For a seal loading of:

$$F_n = pA = p\pi D b_s$$

$$\Delta T = \frac{f_f \pi^{3/2} N D_{so}^{3/2} b_s^{1/2} 144\sqrt{p}\, P_y}{60\ (2.12)\ J^* K_p} \qquad (84)$$

For a given rotational speed (N) and a given seal material so that P_y, K_p are fixed:

$$\Delta T = C D^{3/2} p^{1/2} . \qquad (85)$$

APPENDIX VII

ALUMINUM SHEET REQUIREMENTS - CIRCUMFERENTIAL TRAYS, 100 LB./SEC. UNIT

On the assumption that each tray ring in the low pressure column and high pressure column rotors behaves like a cylindrical shell with fixed edges under the action of internal pressure, an analysis was carried out to determine the maximum stresses developed (which occur at the fixed edges).

Under normal operating conditions the cylindrical shell considered experiences:

a. a radial load due to

1. centrifugal force
2. radial pressure gradients in rotors

b. an axial tension due to the pressure acting on the rotor sides.

By considering a section of the tray it is seen that the effect of the liquid on the tray is balanced by the hydraulic ΔP (ΔP_H).

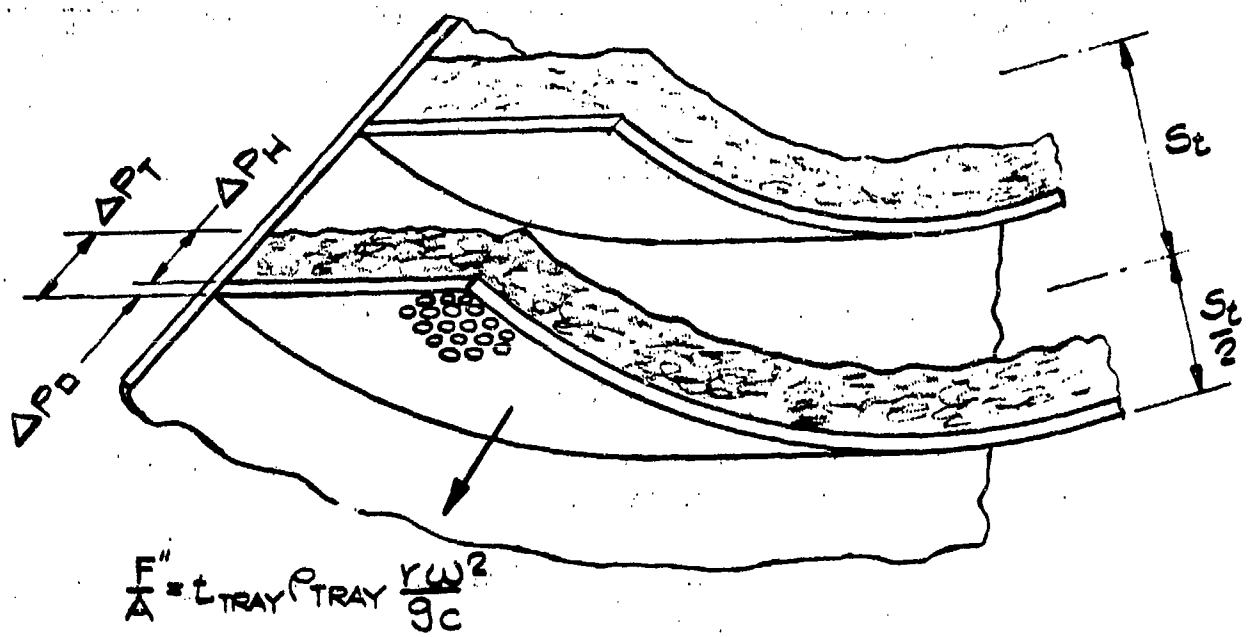

FIG. 107

The net radial load on the tray is:

$$P_{tray} = t_{tray}\, \rho_{tray}\, \frac{r\omega^2}{g} - \Delta P_D - \Delta P_s \qquad (86)$$

with the resulting hoop stress being :

$$S_1 = \frac{P_{tray}\, r}{t_{tray}}$$

The axial stress is:

$$S_2 = \frac{F_n}{A} = \frac{p \cdot 2\pi r \cdot s_t}{2\pi r \cdot t_{tray}} = \frac{p \cdot s_t}{t_{tray}}$$

The above loading condition results in a radial displacement of the shell:

$$\Delta_{shell} = \frac{r}{E_y} (S_1 - \mu_p P s_t) \qquad (87)$$

The radial displacement of the rotor sides, considering a disk with a hole at the center rotating and acted on by a pressure (P_o) at the O.D. can be expressed as:

$$\Delta_{disk} = \left[\frac{(1-\mu_p^2)}{g_c E_y 8} \rho \omega^2 \left(-r^3 + \frac{3+\mu_p}{1+\mu_p} (R_i^2 + R_o^2) r + \frac{3+\mu_p}{1+\mu_p} \frac{R_i^2 R_o^2}{r} \right) \right.$$

$$\left. + \frac{P_o}{E_y r} \left[(1-\mu_p) \frac{R_o^2 r^2 + (1-\mu_p) R_i^2 R_o^2}{R_o^2 - R_i^2} \right] \right] \qquad (88)$$

The net displacement at the edge would then be:

$$\Delta_{net} = \Delta_{shell} \sim \Delta_{disk} \qquad (89)$$

The discontinuity stress due to the bending moment at the clamped edge of the rings is expressed by

$$S_{bending} = \frac{\sqrt{3}\, E_y}{(1-\mu_p^2)^{1/2}} \frac{\Delta_{net}}{r} = 21.5 \times 10^{-6}\, \Delta/r \text{ for Aluminum} \qquad (90)$$

The total stress on the ring is:

$$S_{Total} = S_{bend} + S_{tension} \qquad (91)$$

$$= C \frac{\Delta}{r} + \frac{p.s_t}{t_{tray}}$$

(THIS PAGE IS INTENTIONALLY BLANK.)

APPENDIX VIII

CONTROL SYSTEM HEATER REQUIREMENTS

Assuming a constant vapor pressure (P_v) above the liquid reservoir and using the following notation:

P_1 - initial heater chamber pressure

P_t - heater chamber pressure after a time increment

V_{vl} - initial vapor in control system

V_{vt} - vapor in control system after a time increment

$V_{co.sy.}$ volume of control system

$$\frac{P_1}{P_{t'}} = \frac{V_{vl}}{V_{vt}} = \frac{\rho_{vl} V_{co.sy.}}{V_{vt}} \qquad (92)$$

Expressing in terms of incremental changes of P and V:

$$\frac{P_1}{P_1 + dP} = \frac{\rho_{vl} V_{co.sy.}}{\rho_{vl} V_{co.sy.} + d V_v}$$

then:

$$P_1 \, d V_v = \rho_{vl} V_{co.sy.} \, dP$$

also, if $Q_{ELECTRICAL}$ is taken as the capacity of the electric heater and λ as the latent heat of vaporization

$$\frac{dV_v}{dt_1} = \frac{Q_{EL}}{\lambda} \qquad (93)$$

and therefore:

$$\frac{dP}{dt'} = \frac{P_1 Q_{EL}}{\lambda \rho_{vl} V_{co.sy.}}$$

For instant response to a change in liquid level h_L^o

$$\frac{dP}{dt'} = Ng\,\rho_L \frac{dh_L^o}{dt'}$$

Letting $\frac{dh_L^o}{dt'} = K^* =$ a magnitude of liquid level variation

$$\frac{dP}{dt'} = K^* Ng\,\rho_L$$

or

$$\frac{P_1 Q_{EL}}{\lambda\,\rho_{vl} V_{co.sy.}} = K^* Ng\,\rho_L$$

and

$$Q_{EL} = \frac{K^* \rho_L \rho_v Ng V_{co.sy.} \lambda}{P_1} \qquad (94)$$

Inserting the proper values for the kettle conditions and letting $K^* = .75$ in./sec. a heater rating of 500 watts is obtained.

Liquid level building at the rate $K^* = .75$ in./sec. is equivalent to an increase of the liquid rate by 75 lb./sec.

APPENDIX IX

COOLDOWN OF BOILERPLATE MODEL SEPARATOR

Introduction

Operation of the boilerplate model air separator at cryogenic temperatures requires that the machine be precooled sufficiently to allow the metal to be brought to operating temperature without being subjected to thermal stresses of such a magnitude to cause yielding or failure. The most satisfactory method of achieving this cooldown appears to be passage of a cold nitrogen gas stream over the metal surfaces. A large mass of metal must be cooled from ambient (room) temperature to cryogenic temperatures in a minimum amount of time with a minimum amount of refrigeration. The amount of heat which must be removed is:

$$Q_{Tot.} = W_{bs} C_p \Delta T \tag{95}$$

The rate at which refrigeration, q, can be provided by the cold gas stream depends upon the available heat transfer coefficient, h,

$$q = hA\Delta T_f \tag{96}$$

The magnitude of the convection coefficient is dependent upon the mode of heat transfer. If free convection is the controlling mode, the convection coefficient is given by the equation of Weise and Saunders:

$$\frac{hL^\circ}{k} = 0.13L^\circ \Delta T^{1/3} \left(\frac{\rho^2 g \beta C_p}{\mu_k} \right)^{1/3} \tag{97}$$

If forced convection is induced, the coefficient is given by the Hottel equation

$$\frac{hD}{k} = 0.023 \left(\frac{VD\rho}{\mu} \right)^{0.8} \left(\frac{\mu \rho_p}{k} \right)^{0.3} \tag{98}$$

The time required for cooldown depends on the magnitude of the convection coefficient, the difference between the metal temperature and the bulk temperature of the coolant, and the rate and method of coolant supply.

An investigation into the nature of the heat transfer during cooldown indicates that free convection will be the dominant method of cooling. Large coolant flow rates are required to obtain reasonable forced convection coefficients. The cooldown time based on the free convection heat transfer coefficients and obtained by numerical integration was found to be approximately 4-1/2 hours. This is the time required to cool the metal from a temperature of 520°R to a temperature of 210 °R maintaining a metal-coolant temperature difference between 80°R and 10°R. Because of the upper limit of this temperature difference, dictated by resulting thermal stresses, only 17.5 Btu of refrigeration is utilized per pound of coolant. This points out the major advantage of a closed cooldown system consisting of a recirculated volume of nitrogen gas with the required refrigeration being provided by injecting liquid nitrogen into the gas at a controlled rate. Three methods of cooldown considered are listed as follows:

COOLDOWN METHODS

Method	Time Required	Liquid Nitrogen Required	Flow Rates
Once Thru Cold Nitrogen Vapor Supplied by Vaporization of Liquid	4-1/2 hrs.	~70,000 Lb.	Vapor 27,000 ACFH Liquid - 3.3 Lb./sec. @ Warm End -8 Lb./sec. @ Cold End
Closed Circuit Gas System With Liquid Injection	4-1/2 hrs.	~14,000 Lb.	As Above
Liquid Injection Thru Nozzles	4-1/2 hrs.	~14,400 Lb.	-

The reduced liquid requirement of the closed system makes it the most attractive of the three. Such a system is illustrated schematically in Figure 108.

The total refrigeration requirement for cooldown is approximately 1,225,000 Btu and is independent of the method employed. For free convection the cooldown time is also independent of the method if refrigeration is provided at a rate sufficient to maintain the desired range of ΔT_f.

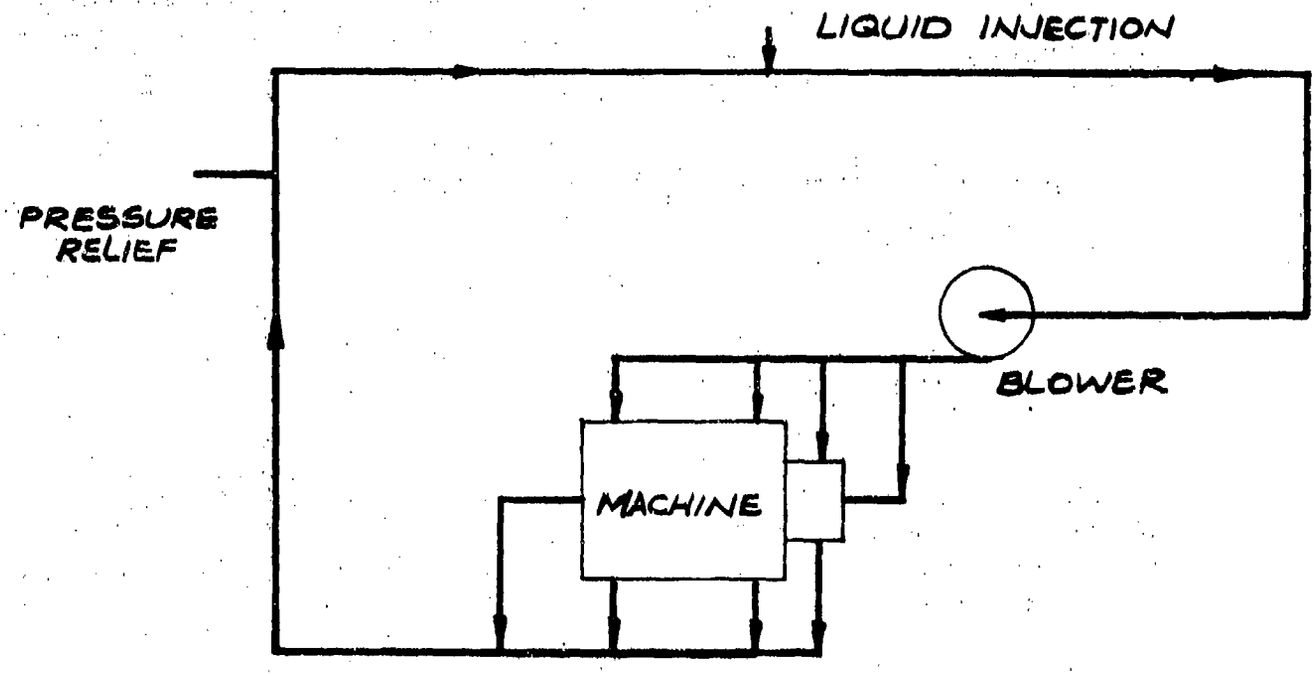

CLOSED CIRCUIT COOLDOWN SYSTEM

FIG. 108

Forced Convection

A stream of nitrogen gas being forced over the surface of the machine components will cool the surfaces at the rate

$$q = hA\,\Delta T_f \text{ Btu/hr.}$$

The forced convection heat transfer coefficient may be computed from the equation (98).

Using the hydraulic radius for the characteristic dimension D in equation (98):

$$D = \frac{\text{flow area}}{\text{wetted perimeter}} = \frac{A_f}{L_W} \text{ ft.} \qquad (99)$$

Thus, since $V = W/A_f \rho$

$$h = \frac{0.023\, k}{(A_f/L_W)^{0.2}} \left(\frac{W}{A_f \mu}\right)^{0.8} \left(\frac{\mu C_p}{k}\right)^{0.3}$$

$$= \frac{0.023\, k\, L_W^{0.2}}{A_f} \left(\frac{W}{\mu}\right)^{0.8} \left(\frac{\mu C_p}{k}\right)^{0.3} \qquad (100)$$

In cooling the metal from 520°R to 210°R, the total temperature drop is 310°R and the arithmetic mean temperature is 365°R. Evaluating the fluid properties at this temperature and a pressure of 60 psi and substituting into equation (100)

$$h = 2.68 \frac{L_W^{0.2}\, W^{0.8}}{A_f} \qquad (101)$$

Since this is a function of the component geometry as well as the flow rate, the forced convection coefficient will be different for each component. Most of the major components have large flow areas, which, for a given flow rate, produce relatively small flow velocities. As a result, the component Reynolds numbers tend to be low yielding small values for the forced convection coefficient.

The amount of heat which must be withdrawn from a component in lowering its temperature from 520°R to 210°R is

$$Q = W_{comp.}\, C_p\, \Delta T_m$$

where ΔT is the total temperature drop of the metal (310°R). This must be equivalent to the refrigeration provided in time, t_1, or

$$Q = hA\, \Delta T_f\, t_1 \qquad (102)$$

where ΔT_f is the difference between the temperature of the metal surface and the bulk fluid temperature. Since some small parts will cool very rapidly when they come into contact with the cold gas, thermal stresses will develop where these small parts are attached to larger parts which cool much more slowly. For example, a cold gas stream introduced into the columns will cool the trays to very near the gas temperature in a short time, resulting in a thermal contraction of the trays. The column walls to

which the trays are attached will not contract as rapidly. As a result, thermal stresses will be set up in the trays. Therefore, it is necessary to keep ΔT_f sufficiently low that the thermal stresses will not cause fracture of the small parts. These stresses are given by

$$S_1 = \alpha E_y \Delta T_f \qquad S = \alpha_{metal} E_y \Delta T_f \qquad (103)$$

For aluminum at the temperatures under consideration , the thermal stress for $\Delta T_f = 80°R$ is $\sim$ 9600 psi. This should be considered a limiting value since the components will also be subjected to pressure forces during cooldown.

Because of the high flow rates required to obtain satisfactory values of the forced convection coefficient, the temperature rise of the gas as it passes through a component is small. For example, the temperature rise of cold nitrogen gas passing through the high pressure column at a rate of 1 pound per second at an initial ΔT_f of 80°R is only 4°R. Thus, if higher flow rates are used and several gas inlet passages are provided, it is reasonably accurate, although somewhat optimistic to assume that a constant ΔT_f of 80°R can be maintained. If such is the case, the forced convection cooldown time as a function of the coolant flow rate for each component is

$$t_1 = \frac{W_{comp} C_p \Delta T_m}{hA \Delta T_f} = 0.275 \frac{W_{comp} A_f}{A L_w^{\circ 2}} \text{ hr.} \qquad (104)$$

Free Convection

If holes are placed in the windage shroud and gas is introduced into the machine, natural or free convection will take place at the metal surfaces. The heat transfer rate is according to equation (96) and the convection coefficient is given by equation (97).

In the latter expression the fluid properties on the right hand side are grouped and designated by:

$$Z = \frac{\rho^2 g_c \beta C_p}{\mu k} \qquad (105)$$

The variation of this term with fluid temperature has a greater effect on the heat transfer characteristics than do the fluid properties in the Hottel equation (98). The temperature dependence of the grouping is plotted in Figure 109 for nitrogen vapor at 60 psi. The product of the Grashof number and the Prandtl number always exceeds 10^9 placing the

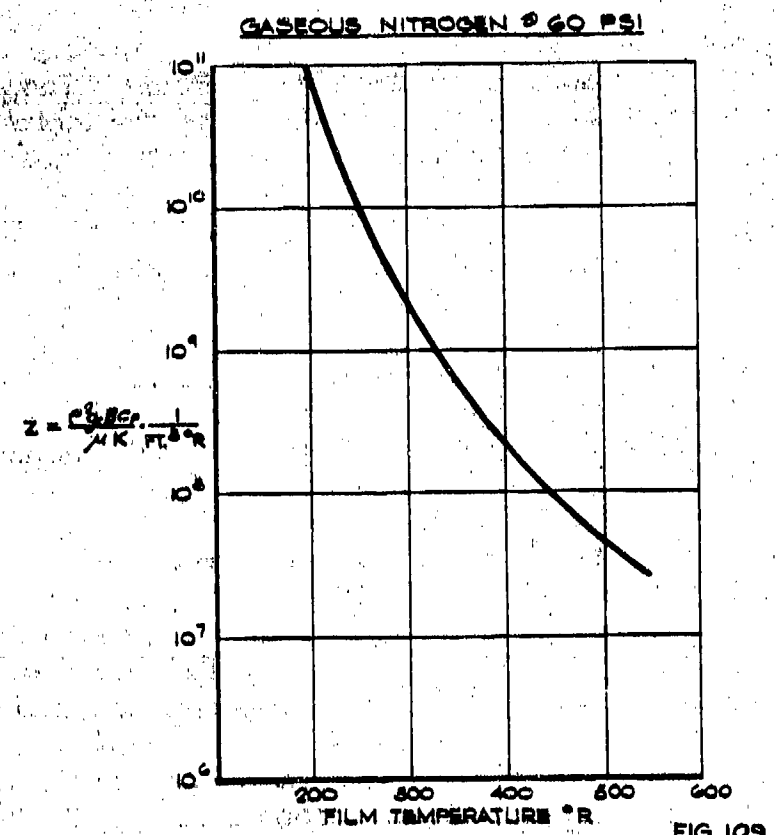

FIG. 109

convection process in the turbulent region and justifying the use of the exponent, 1/3, as used in equation (9). This makes the convection coefficient independent of geometry or, in more compact form,

$$h = 0.13\, K\, \Delta T_f^{1/3}\, Z^{1/3} \tag{106}$$

Figure 110 shows the free convection coefficient as a function of film temperature for several temperature differences.

If a metal surface is visualized as surrounded by nitrogen gas at a temperature 80° below that of the metal surface, the gas will begin to warm up and the metal will begin to cool down. In a small interval of time, ΔT_1, the temperature of the metal will decrease by an amount:

$$\Delta T_m = \frac{hA\Delta T_f\, \Delta t}{W\,(C_p)_m} \tag{107}$$

and the temperature of the gas will rise an amount:

$$\Delta T_g = \frac{hA\Delta T_f\, \Delta t_1}{V\,(C_p)_g} \tag{108}$$

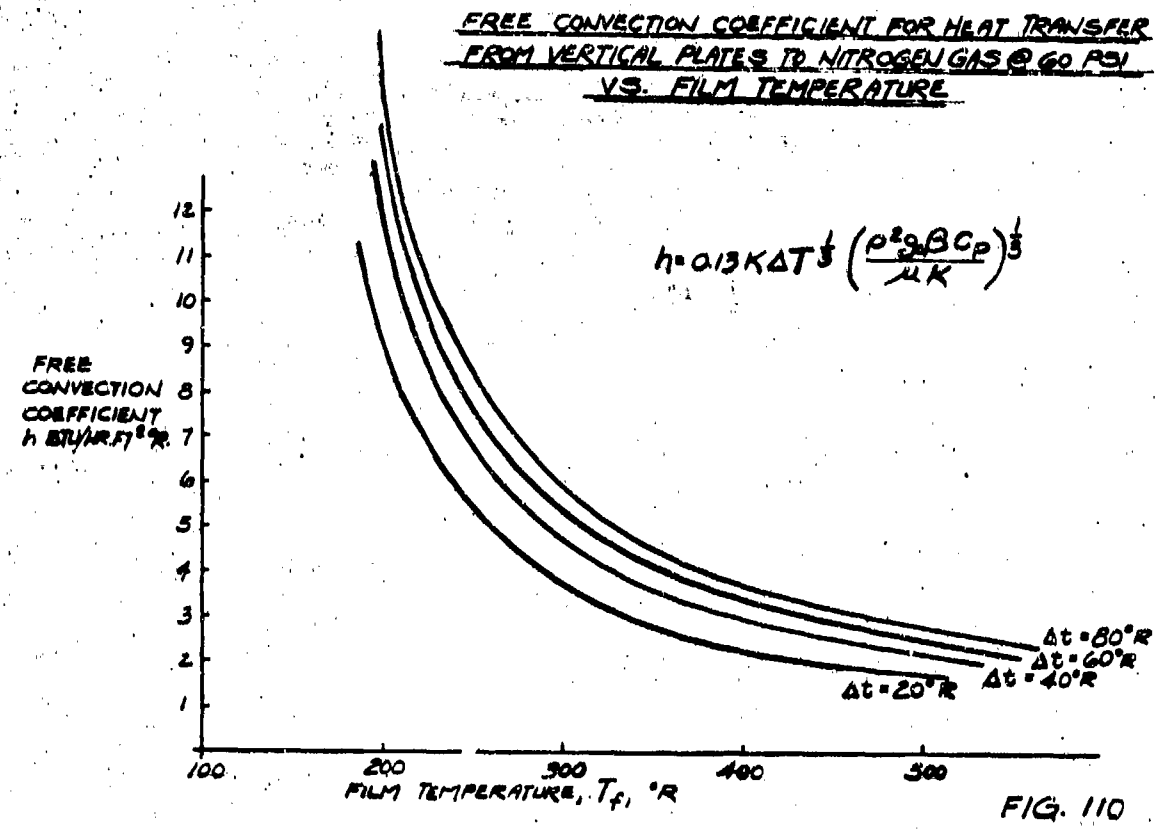

FIG. 110

This reduces the available temperature difference by

$$\Delta(\Delta T_f) = \Delta T_m + \Delta T_g$$

After a time the temperature difference between the metal surface and the gas will reduce to the point where very little heat transfer is taking place. Then a fresh supply of gas is introduced at a temperature 80° below the new metal temperature; or, more practically, a continuous gas flow is provided which maintains ΔT_f between 80°R and 10°R. If very small time intervals are considered, equations (107) and (108) may be integrated numerically taking into account the temperature dependence of all parameters.

With the exception of the reboiler-condenser, which cools very rapidly, most of the major components have similar surface area-to-weight and surface area-to-volume ratios and can, therefore, be considered as a composite whole. The weight less reboiler-condenser is 17,000 pounds, the surface area less reboiler-condenser is 1600 square feet, and the volume less reboiler-condenser is 360 cubic feet. Performing the numerical integration using these values gives the approximate cooldown curve shown in Figure 111. The total cooldown time by this method is approximately 4-1/2 hours.

APPROX. BOILER PLATE COOLDOWN MAINTAINING $\Delta T > 10^\circ R.$

P = 60 PSI.
W = 17,000 LBS.
A = 1600 FT^2
V = 360 FT^3
C = f(t)
h = f(t)

TOTAL N_2 SUPPLIED = 14,400 LB.
REFRIG. USED PER LB. OF CIRCULATING VAPOR : 17.5 BTU/LB.
NTP FLOW RATE @ T_H = 800 °R.: 149,000 CFH.
NTP FLOW RATE @ T_H = 800° R. 838,000 CFH.

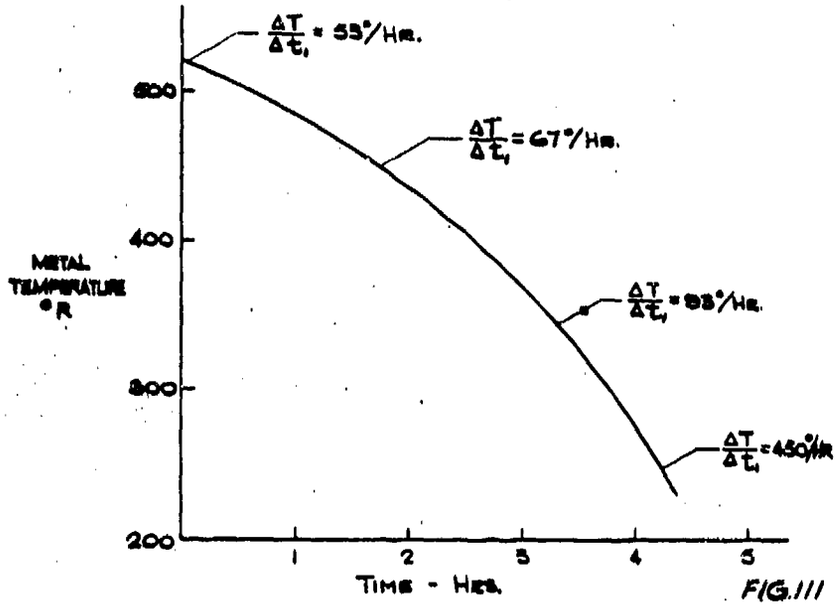

FIG. III

Cooldown System

The machine may be cooled by vaporizing liquid nitrogen and passing the cold gas over the metal surfaces. Since the temperature of the gas can be no more than 80° less than the metal temperature, the gas must be allowed to warm up by an amount depending upon the metal temperature and thus the stage of cooldown. This, of course, results in the loss of a large percentage of the available refrigeration and requires a large amount of liquid (~70,000 pounds).

To overcome the refrigeration losses inherent with the open circuit nitrogen vaporization system, the closed system of Figure 103 will be used to cool the boilerplate model air separator. A volume of nitrogen gas will be continuously passing over the metal surfaces with liquid being sprayed into the stream at a controlled rate to provide the necessary refrigeration. To insure even distribution of the cooling gas, four inlet ports and four outlet ports will be provided in the casing, one set in each head and two on the cylindrical center section of the casing. To maintain the gas temperature at the machine inlets 80° below the constantly lowering metal temperature requires a gradually increasing liquid injection rate. This is because refrigeration is required at a higher rate at the cold end of the cooldown period than at the warm end due to the increase of the heat transfer coefficient with decreasing film temperature. The liquid injection rate provides a positive control of the cooldown rate.

APPENDIX X

PROCEDURE FOR ASSEMBLY OF BOILERPLATE

MODEL AIR SEPARATOR

To affect a single element rotary air separator the various process components have to be assembled on a common shaft. The boilerplate model (100 lb./sec.) air separator includes a low pressure column, a high pressure column and the reboiler-condenser mounted on a continuous shaft and rotating within a single enclosure or casing.

Although the boilerplate model air separator design comprises a multirotor assembly on a horizontal shaft, the stack-up of the individual elements on the shaft and within the housing is best accomplished in a vertical position and the entire assembly then tilted to its horizontal position.

On the basis that both of the column rotors are subassembled as shown in Figures 55 and 56 and that the reboiler-condenser tube disks are sub-assembled in two, three, and five-disk modules as indicated in Figure 70 the established assembly procedure is as follows:

1. Insert the shaft section spanning the inner width of the low pressure column (1) and attach to the column (2) at the inner flanges.

2. Attach the 16" diameter end shaft section (3) to the adjacent section within the low pressure column.

3. With the 108" diameter head (4) supported horizontally the 16" diameter bearings (5) are inserted in the retaining housing.

4. The low pressure column ensemble from steps 1 and 2 is lowered within the 108" diameter head and appropriately supported to hold the proper spacing at the peripheral seal face fixed to the casing.

5. The mating seal ring (6) is positioned at the periphery of the exposed face of the low pressure column.

6. The spacer shaft section between the two column rotors (7) with the shelf liquid manifold (8) bolted to it is attached to the adjacent shaft section within the low pressure column.

7. Attach the high pressure column rotor (9) to the corresponding face of the shelf liquid manifold.

8. With the two column rotors in place proceed with assembly of the following:

a. Kettle liquid control valves.
b. Shelf liquid control valves.
c. Appropriate signal lines to the control valves.
d. All interconnecting piping between the column rotors.
e. Appropriate instrumentation.
f. Spacer rods at the periphery between the column rotors.

Having installed items (a) through (f), shroud the space between the two columns.

9. The shaft section spanning the reboiler-condenser (10) is attached by bolting to the adjacent short spacer section.

10. The reboiler-condenser disk modules (11) are stacked appropriately spaced (Fig. 66) around the shaft section of step 9.

11. The reboiler-condenser casing (12) is positioned around the stacked disk modules and attached to the high pressure column rotor.

12. The reboiler-condenser casing cover (13) is positioned to match the nitrogen vapor and air-inlet piping (14) and attached to the casing and the shaft section spanning the reboiler-condenser casing.

13. Couple the nitrogen vapor and air-inlet piping and install end shroud over piping.

14. The center section of the casing (15) is suspended around the rotating assembly until the seal face plate laying on the periphery of the low pressure column (step 5) is attached to it by bolting, then position mating flanges of the two casing sections.

15. Attach the stationary peripheral seal plate (16) to the 70" diameter flange of the casing center section.

16. Assemble product discharge manifold (17) on the periphery of the reboiler-condenser casing.

17. Attach short shaft section comprising the entrance to the air inlet manifold (18) to the adjacent shaft section traversing the reboiler-condenser.

18. The air inlet manifold (19) and the liquid oxygen duct (20) are assembled by bolting to the shaft section of step 17.

19. The shaft section supported on the drive end bearings (21) is attached to the adjacent section of step 17.

20. With one set of bearings (22) housed, the 70" diameter casing cover is positioned by guiding around the shaft.

21. Insert bearing spacer to position the second set of 14" diameter bearings and install lock nut (23).

At this point the rotating assembly is axially positioned within the casing.

22. Assemble the segmental seal rings (24) between the air inlet and the casing, around the shaft.

23. Insert the air inlet housing (25) around the seals and bolt to the casing inner diameter flange.

24. Install the segmental seal rings (26) in the open end of the air inlet housing.

25. Attach the drive end of the shaft (27) to the adjacent shaft section of step 19.

26. Install the segmental seal rings (28) adjacent to the liquid oxygen inlet, around the shaft.

27. Insert the liquid oxygen inlet housing (29) around the seals and bolt to the air-inlet housing.

28. Install the segmental seal rings (30) in the open end of the liquid oxygen inlet housing and enclose with cover plate (31).

29. Attach the cylindrical skirt (32) to the flange ring on the casing cover and to the cover plate of step 28.

30. Install slip ring assembly (33) and make all connections.

31. Install cylindrical skirt cover plate (34) and house drive shaft guide bearings.

32. Tilt entire assembly to horizontal position and set on support structure.

33. Install on the shaft the segmental seal rings (35) between the waste nitrogen discharge and the casing.

34. Attach end section of the liquid nitrogen reflux rotating duct (36).

35. Insert the waste nitrogen discharge housing (37) guiding it on the section of step 34 and attach by bolting to the casing cover inner diameter.

36. Install the segmental seal rings (38) between the liquid nitrogen reflux and waste nitrogen streams.

37. Attach liquid nitrogen reflux inlet housing (39) by bolting to the waste nitrogen discharge housing.

38. Install casing windows (40) and window spacers.

39. Make all piping connections.

40. Couple drive shaft to drive motor.

It is noted that appropriate instrumentation as shown schematically in Fig. 94 must be installed as assembly of the unit proceeds. All instrument leads are directed for connection to the slip rings via the inner duct (41) of the shaft drive end.

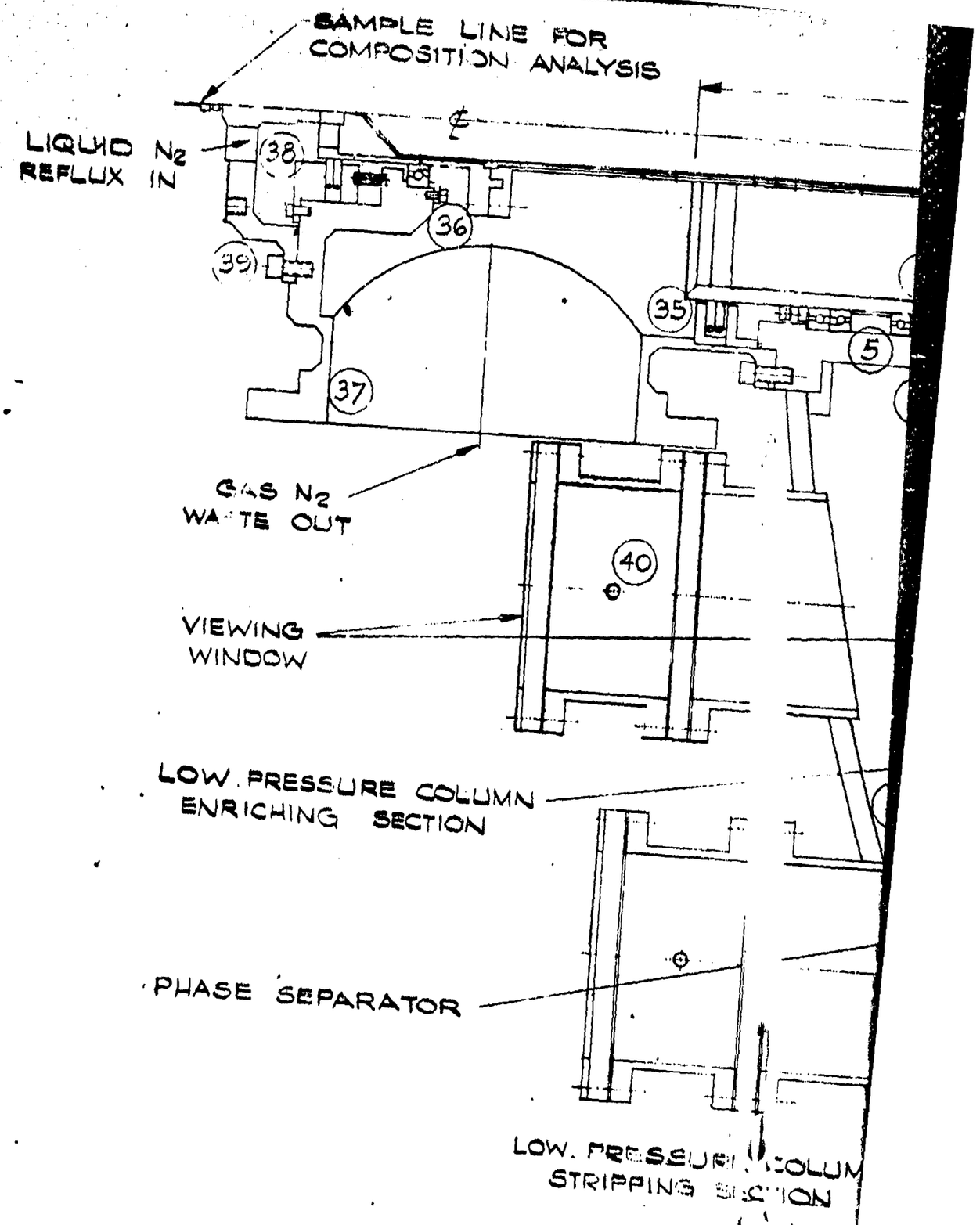

4-554428

19 6

STATIONA

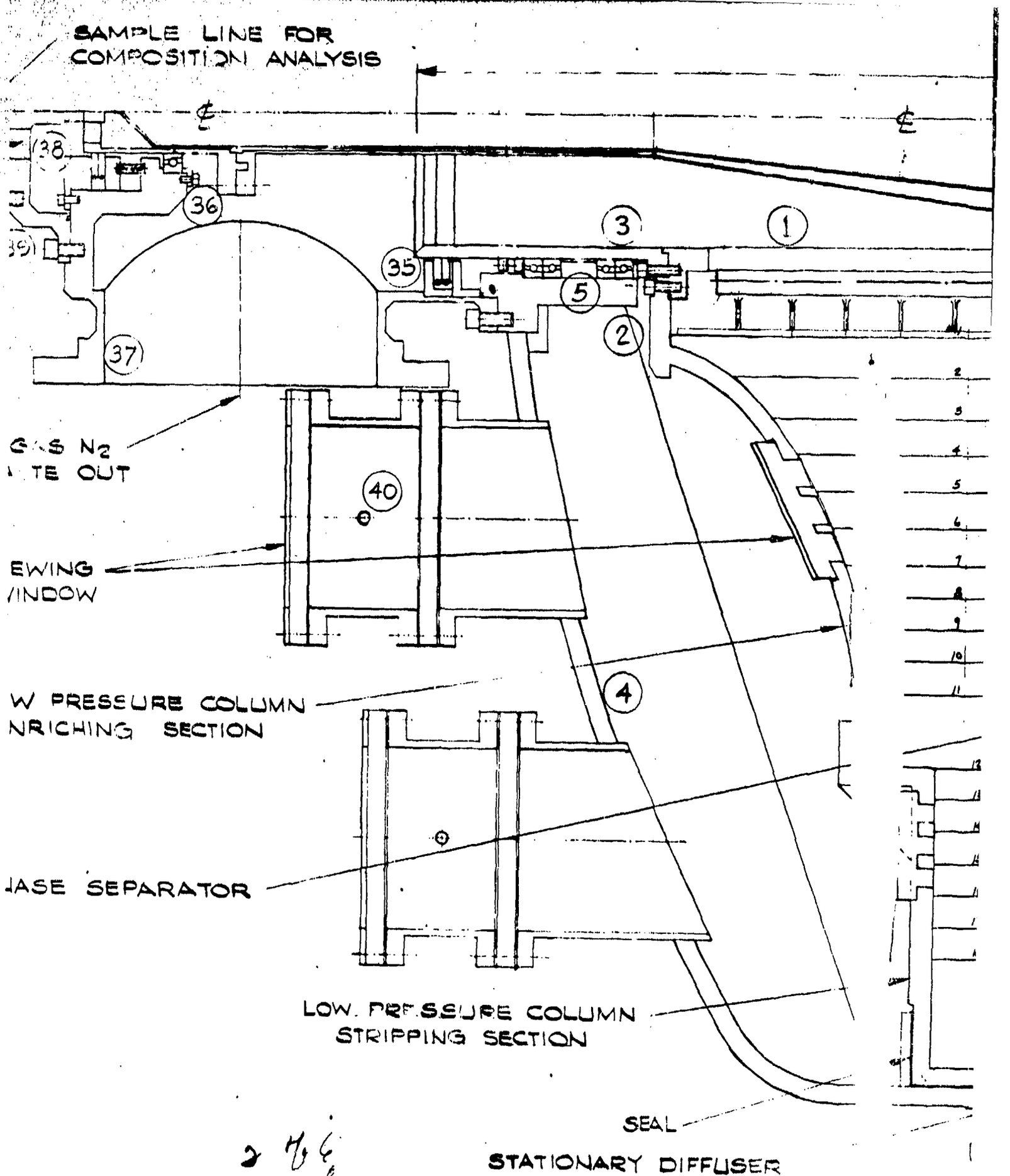
SAMPLE LINE FOR
COMPOSITION ANALYSIS
38
36
39
35
3
1
5
2
37
40
4
EWING
/INDOW
W PRESSURE COLUMN
NRICHING SECTION
JASE SEPARATOR
LOW. PRESSURE COLUMN
STRIPPING SECTION
SEAL
STATIONARY DIFFUSER
LIQUID O2

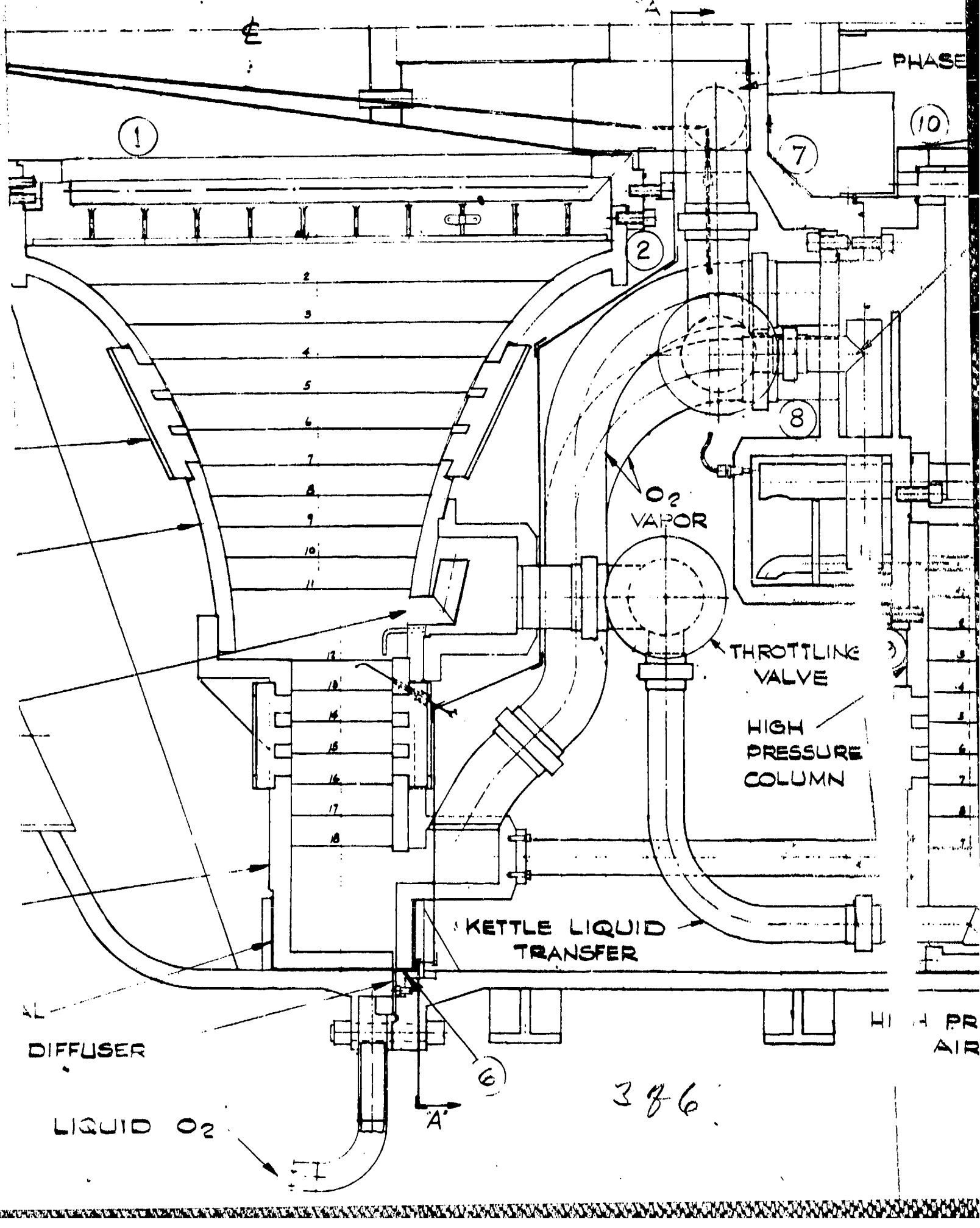
PHASE
1
10
7
2
8
O_2 VAPOR
THROTTLING VALVE
HIGH PRESSURE COLUMN
KETTLE LIQUID TRANSFER
DIFFUSER
LIQUID O_2
6
A
A
386

ROTOR LENGTH: APPROX 13'-11½"

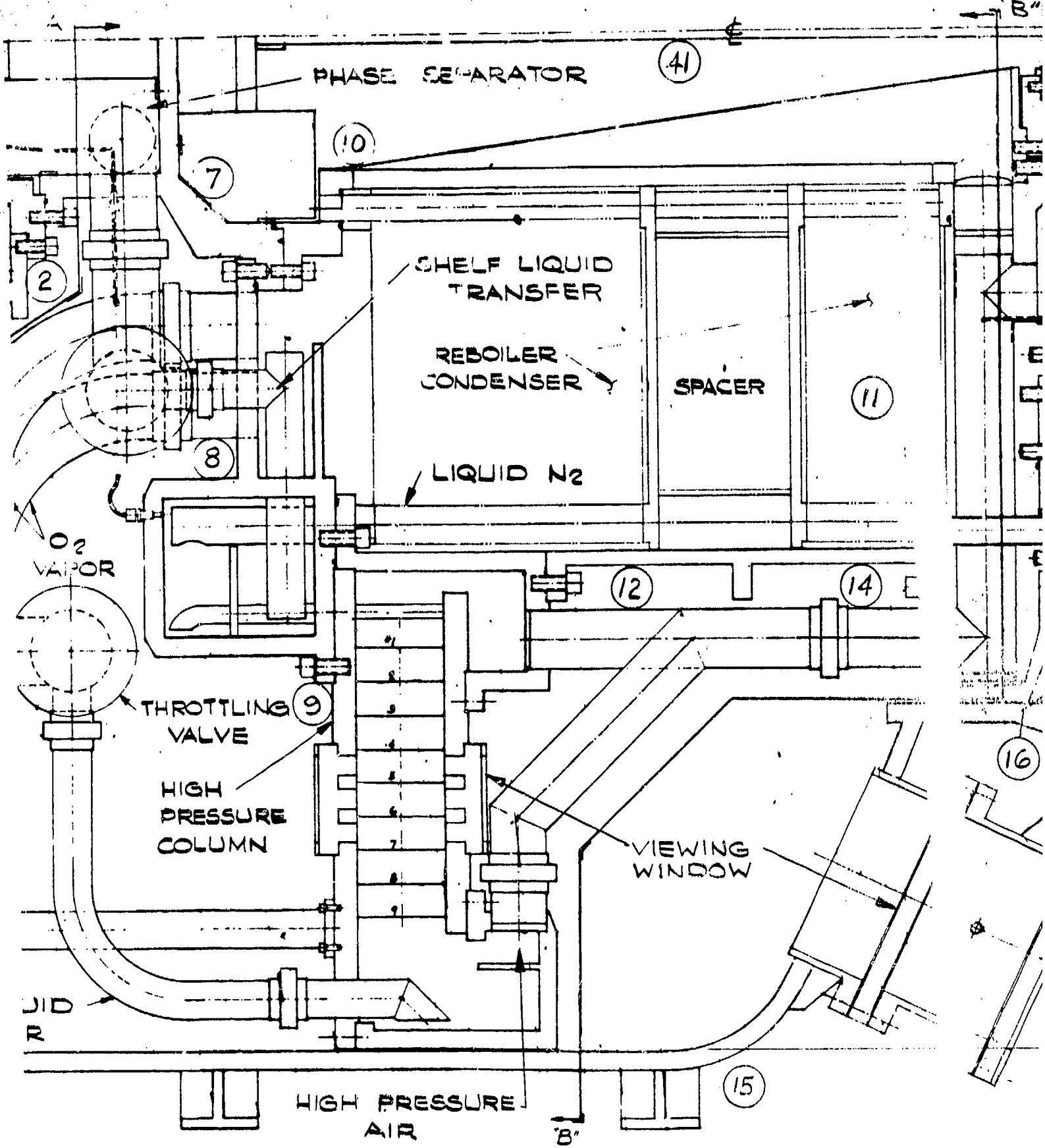

4 of 6

1 - 11 1/2"

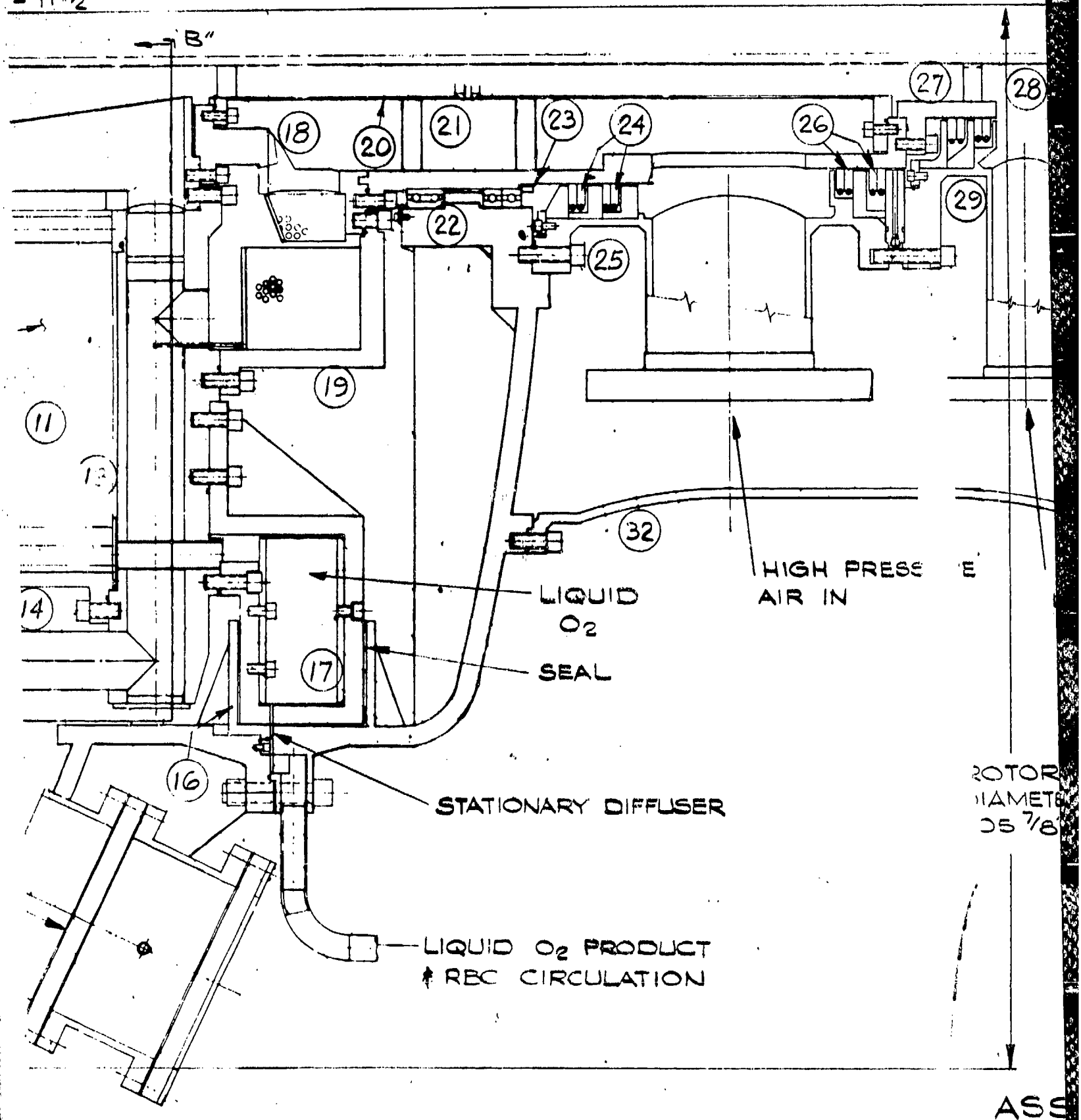
B"
18
20
21
23
24
26
27
28
29
22
25
19
11
13
14
17
16
32
LIQUID
O2
SEAL
HIGH PRESSE E
AIR IN
STATIONARY DIFFUSER
ROTOR
IAMET
05 7/8
LIQUID O2 PRODUCT
RBC CIRCULATION

ASS

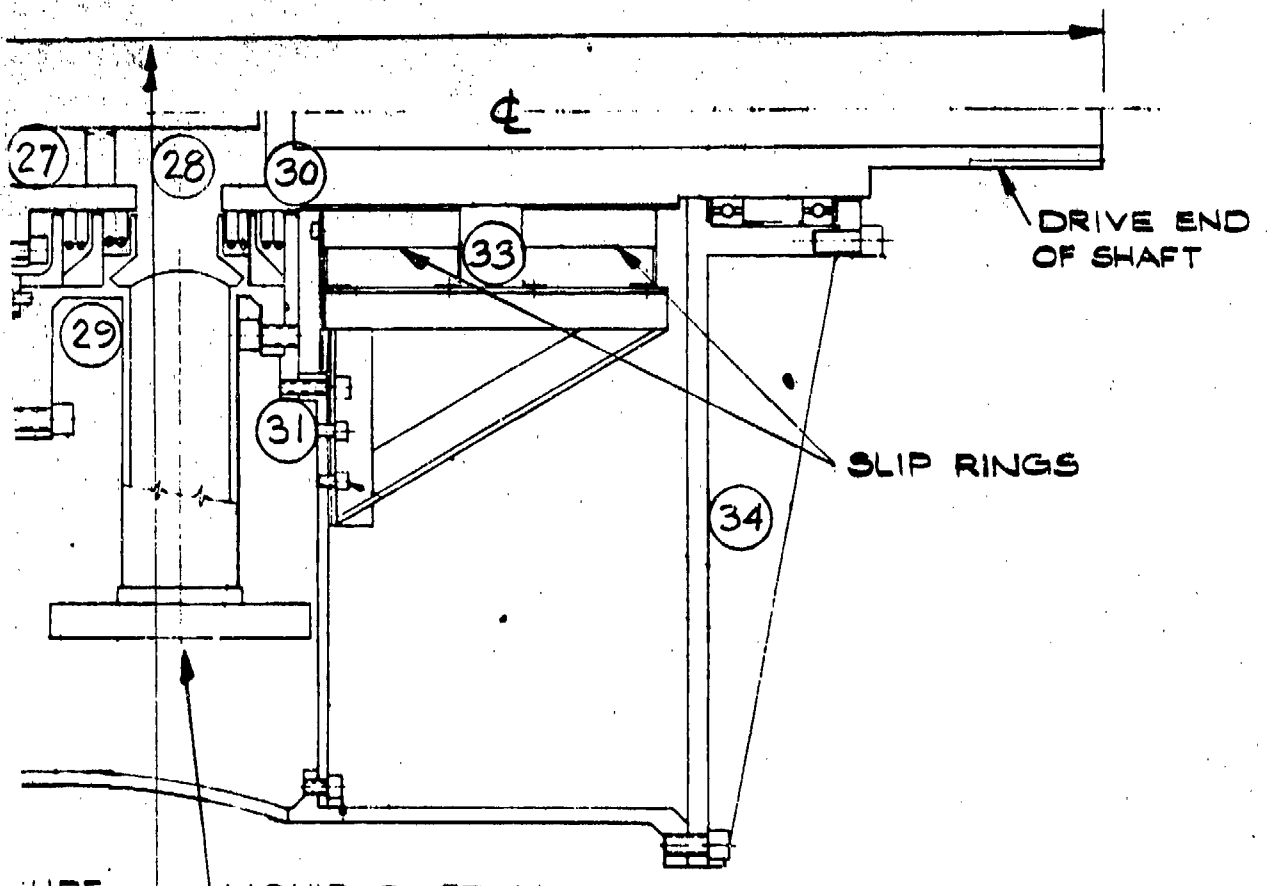

:URE

ROTOR DIAMETER 105 7/8"

12"

SCALE

ASSEMBLY - "BOILERPLATE" AIR SEPARATOR

6 of 6

FIG 11

(THIS PAGE IS INTENTIONALLY BLANK.)

LIST OF REFERENCES

1 Feasibility Study of a High Capacity Distillation Separator for an Air Enrichment System,

Technical Documentary Report ASD-TDR-63-665, Part I November, 1963

2 Study of an Airborne Air Enrichment Unit,

ASD Technical Report 61-411

3 Unit Operations of Chemical Engineering,

McCabe and Smith, McGraw-Hill Publishing Company, 1956, p. 397

4 Heat Transmission, McAdams, W. H., McGraw-Hill Book Company, Inc. 1954, p. 330

5 Saturation Properties of Oxygen Nitrogen Mixtures, Yendall, E. F. and Olzewski, W. J. ASD Technical Report 61-536 September, 1961

6 International Critical Tables, Vol. 4

7 Unfired Pressure Vessels, ASME Boiler and Pressure Vessel Code, Section VIII, 1962

8 ALCOA ALUMINUM HANDBOOK, Aluminum Company of America, 1962

9 Formulas for Stress and Strain, Roark, R.J. McGraw-Hill Book Company, Inc. 1954

10 Testing of Ball Bearings with Five Different Separator Materials at 9200 RPM in Liquid Nitrogen, Wilson, A.W. etal ASME Paper N°61-LUBS-18

11 Ball and Roller Bearing Engineering, Palmgren A. S.H. Burbank and Company Inc. Philadelphia, 1945

12 Evaluation of Ball Bearing Separator Materials Operating Submerged in Liquid Nitrogen, Wilson, A.W. etal. ASLE Paper No 60LC-4

13 "Flow of Compressible Fluid through a Series of Identical Orifices", Robinson, C.S.L. Journal of Applied Mechanics, Dec. 1948, pg. 308

14 "Labyrinth-Seal Leakage Analysis", Zabriskie, W., Sternlicht, B. Transactions of the ASME, Journal of basic Engineering, Sept. 1959 pg. 332

15 "A Review of Plastic Bearings", Pinchbeck, P.H. Wear, March/April 1962

16 Strength of Materials - Part II Advanced Theory and Problems, Timoshenko, S. D. Van Nostrand Company, Inc. 1952

17 "Flow of Steam-Water Mixtures in a Heated Annulas and through Orifices" Hoopes, J. Jr., A.I. Ch. E. Journal, 3, June 1957 pg. 268

18 "Chamber Dimensions Effects on Induced Flow and Frictional Resistance of Enclosed Rotating Disks" Daily, J.W. and Nece, R.E.

19 Mechanical Engineers Handbook, Marks, L.S. McGraw Hill Co.

20 Kaydon Bearings Catalog - Kaydon Engineering Co.

21 Centrifugal and Axial Flow Pumps, Stepanoff, A.J. John Wiley & Sons Inc. 1948

END

10-86

DTIC